



Climate Change and Arctic Browning: Understanding the Role of Extreme Winter Weather Events

Murk Komal Memon

PhD Thesis

A thesis submitted in partial fulfilment of the requirement for the
degree of Doctor of Philosophy

The University of Sheffield
Faculty of Social Sciences
Department of Geography

January 2023

Abstract

Vegetation browning is the decline in plant biomass and productivity arising from climate change, biotic interactions and disturbance. It is now considered one of the major disruptions in a rapidly changing Arctic landscape. Damaged Arctic vegetation due to extreme winter weather events such as warming events and frost drought conditions, has been shown to change from a sink to a net CO₂ source at the peak of the growing season. It is crucial to understand the satellite-based signature of browning events due to the challenging nature of field work in the Arctic and the sporadic nature of such events. It is important to understand how browning events can unfold in the future in response to projections of increased frequency, magnitude and severity of extreme winter weather events in the Arctic. This research is the first to provide a remote sensing and climate modelling based framework to examine Arctic browning. Northern Norway was selected as the study area for this PhD research. The first research objective of this PhD thesis was to understand the satellite-based signature of browning events caused by extreme winter weather conditions. This was achieved through examining the effectiveness of two different MODIS vegetation indices at quantifying the on-record ground observations of vegetation decline in the Norwegian Arctic and sub-Arctic areas. The indices included the Chlorophyll Carotenoid Index (CCI) and the Normalized Difference Vegetation Index (NDVI). The CCI and NDVI were extracted for early, peak and end of the growing season (July-September). Moreover, the average growing season CCI and NDVI were calculated as well. These calculations were conducted for three case study sites in northern Norway. The NDVI presented a more robust signal compared to CCI for detecting decreases in the Gross Primary Productivity (GPP) of dwarf shrub vegetation across different Arctic landscapes. This was concluded to be mainly due to the higher spatial resolution of NDVI (0.25 km) compared to that of CCI (1 km). The second research objective of this work was to determine the main meteorological drivers of satellite-based observations of vegetation decline in the Norwegian Arctic and sub-Arctic. Currently there is a substantial research gap with regards to the understanding of relationships between the variability of individual meteorological variables in winter and the summer

NDVI. For this, a regional climate model, the Weather Research and Forecasting Model (WRF), was used to produce high-resolution (1 – 10 km) simulations for the winter months November – April, over the time period 2000 – 2020, for northern Norway. The driving dataset for WRF here was ERA5. WRF's skill at reproducing the extreme winter weather conditions, which lead to recorded browning events at the three case study sites was examined, considering variables including 2m near-surface temperature, snow depth and precipitation. WRF was able to simulate extreme winter warming and low snow depth conditions at the case study sites after bias-corrections were applied. Following this, correlations between the different winter month-based meteorological variables and mean summer NDVI were examined. The correlations identified the most important winter meteorological variables with regards to summer NDVI, for the study area. These variables were used in multivariate regression analysis against summer NDVI to develop statistical models for projecting summer NDVI at the end of this century under different emission scenarios.

This leads to the third research objective of this thesis, which was to assess the changes in frequency and intensity of climatic drivers of Arctic browning at the end of this century in the Norwegian Arctic and sub-Arctic. Therefore, WRF was forced with the Community Earth System Model (CESM1) under three Representative Concentration Pathways (RCPs) 4.5, 6.0 and 8.5, for 2090 – 2100. The future simulations were compared with a historical baseline, 1990 – 2000, to assess the changes in the frequency and spatial extent of the different winter meteorological drivers of NDVI. The findings of this work can be viewed in a threefold-perspective; spatial context, seasonal winter meteorology and climate change scenario based. In the spatial context the main findings included; the vegetation most at risk of damage is projected to be in Trøndelag County, based on the strongest increases in frequency and intensity of winter warming events, low snow depth conditions and ROS occurrence. This research's projections about increased exposure of Norway's coastal areas to higher intensity warming events (duration-based), as compared to the inland regions, agrees with previous studies. Large spatial variability was found across the study domain with regards to the meteorological parameters and extreme weather indices of different winter months affecting the summer NDVI. The projections of

browning frequency at one of the case study sites (Storfjord), located well inside the Arctic Circle, are reflective of the pronounced negative impacts arising from multiple extreme winter weather events and conditions. At this site the maximum duration of winter warming events index (MDW) in December and the mean January temperature best explained the variance in the NDVI. In context of the three RCPs studied here, major findings with regards to overall impacts on vegetation included projections of mean December, January and March temperatures staying above 0°C for most of the study area. These temperature projections imply an increased probability of ROS in these peak winter months as precipitation would likely fall as rain rather than snowfall. Moreover, as vegetation can get damaged under low-snow conditions, it is concerning that under RCP 8.5, the average number of days with snow depth < 20 cm (SC20), per winter season, is projected to increase by 80-100 days, in Trøndelag County, compared with the 1990 – 2000 time period. In general, this study predicts large scale vegetation disturbance in response to changes in the overall winter meteorology in northern Norway.

Acknowledgements

First and foremost, I would like to thank my lead supervisor Dr. Julie Jones for her excellent scientific advice, endless support and patience throughout my PhD. I cannot thank her enough for the tremendous guidance she has provided, which allowed me to grow as a researcher. I am sincerely grateful for the invaluable expertise provided by my second supervisors Dr. Gareth Marshall, Dr. Rob Bryant and Professor Gareth Phoenix. They always found time for discussions and feedback. I could not have had better PhD supervisors.

I would like to thank The Grantham Centre for Sustainable Futures for funding this research. I am also thankful to Dr. Holly Croft for the ideas and discussions which helped to enhance parts of this research.

Many thanks must go to all my friends and colleagues at the University of Sheffield, who have always been happy to discuss ideas, python problems and climate model whimsies! I would also take this opportunity to thank the HPC team at the University of Sheffield, especially James Moore, for the amazing technical support.

I would like to mention how the lovely city of Sheffield, with its green spaces and friendly environment, helped me to accomplish my PhD research. Norfolk Heritage Park, the Botanical Gardens, Endcliffe Park and Weston Park provided fantastic spaces for quite a few thoughtful walks. I can't help saying thanks to McVitie's Digestives for bearing with me over the past couple years!

I am thankful to Aunt Fawzia for her unwavering encouragement in completion of this PhD project. I am deeply grateful to my partner Ameen, my Mum and Dad, and my cat Daisy! Their love and kindness has been immensely helpful in achieving this work. I think Ameen and Daisy are both knowledgeable now on the topic of Arctic browning! I dedicate this thesis to Ameen.

Table of contents

Chapter 1.....	1
Climate change and Arctic browning: An Introduction.....	1
1.1. Research context and aims.....	2
1.2. Past browning events and associated climatic drivers	5
1.3. Extreme winter weather events in the context of Arctic Browning	6
1.3.1 Winter warming.....	6
1.3.2 Rain-on-snow (ROS).....	10
1.4 Regional climate change studies for Norway	12
1.5 Application of satellite vegetation indices to examine Arctic browning.....	17
1.6 Projected changes in Arctic vegetation in the light of climate change	24
1.7 Summary	25
Chapter 2.....	28
Understanding Arctic Browning using spectral vegetation indices	28
2.1 Introduction.....	29
2.1.1 Chapter Aims and Objectives.....	30
2.2 Research Methods.....	30
2.2.1 Study sites	30
2.2.1.2 Extreme winter weather conditions at the study sites	33
2.2.2 Data	34
2.2.3 Methodology	36
2.4 Results	39
2.4.1 Flatanger.....	39
2.4.1.1 Satellite-based detection of browning events.....	39
Wilcoxon signed-rank test results	42
Spectral vegetation recovery trends	43
2.4.1.2 Phenology.....	44
2.4.2 Storfjord	48
2.4.2.1 Satellite-based detection of browning events.....	48
Wilcoxon signed-rank test results	51
Spectral vegetation recovery trends	52
2.4.2.2 Phenology.....	55
2.4.3 Lofoten	59
2.4.3.1 Satellite-based detection of browning events.....	59

<i>Wilcoxon signed-rank test results</i>	59
2.4.4 Comparison of the spectral browning event detection across the study sites.....	62
2.4.5 Summary of the findings	66
2.5 Discussion.....	67
2.5.1 Satellite-based phenological signature of browning events.....	67
2.5.2 The role of scale	69
2.5.3 Synergistic approaches to study Arctic browning events using remote sensing data	71
<i>A way forward</i>	72
2.6 Conclusion.....	74
Chapter 3.....	75
Understanding winter climate - summer NDVI relationships.....	75
3.1 Introduction.....	76
3.2 Methodology.....	77
3.2.1 Study area.....	77
3.2.2. Methods	77
3.2.3 WRF model compilation	78
3.2.3.1 WRF background	78
3.2.3.2 WRF compilation on the HPC	79
3.2.4 WRF validation simulations	80
3.2.4.1 CESM background	81
3.2.4.2 ERA5 background	82
3.2.4.3 Model domain setup for validation simulations	82
3.2.4.4 Model bias and RMSE calculation.....	83
3.2.5 WRF's reproducibility of meteorological conditions leading to past browning events	86
3.2.5.1 Model domain setup	86
3.2.5.2 Climate indices for quantifying extreme winter weather at browning sites.....	92
3.2.6 Analysing winter meteorological variables and satellite NDVI relationships	93
3.2.6.1 WRF setup and data pre-processing.....	93
3.2.6.2 Statistical Analysis.....	94
3.3 Results	97
3.3.1 WRF's reproducibility of climatic conditions associated with real browning events	97
3.3.1.1 Extreme winter warming event at Flatanger 2013/14.....	97
3.3.1.2 Frost drought conditions at Storfjord 2011/12	101
3.3.1.3 Winter warming and frost drought conditions at Lofoten 2013/14	109
3.3.2 Understanding winter climatology and growing season-NDVI relationships.....	115
3.3.2.1 Temperature and NDVI.....	115

3.3.2.2 Winter warming event (WWE) and NDVI	119
3.3.2.3 Maximum Duration Warming event (MDW) and NDVI	123
3.3.2.4 Snow depth and NDVI	126
3.3.2.5 Rainfall and NDVI.....	132
3.3.3.6 Rain-on-Snow (ROS) and NDVI.....	135
3.3.3 Multivariate regression analysis	139
3.3.3.1 Flatanger.....	139
3.3.3.2 Lofoten	141
3.3.3.3 Storfjord	142
3.4 Discussion.....	145
3.4.1 WRF's skill to reproduce winter meteorological conditions in northern Norway.....	145
3.4.2 Linking winter climate and growing-season NDVI	149
3.4.3 Linking winter climate and Arctic browning	153
3.4.4 Research limitations	157
3.5 Conclusions	158
3.6 Supplementary data	160
Appendix 3.1.....	160
Chapter 4.....	161
Climate change and Arctic Browning: Future Projections	161
4.1 Introduction.....	162
4.2 Methodology	163
4.2.1 Future climate simulations	163
4.2.2 Quantifying the meteorological drivers of Arctic Browning 2090 – 2100.....	165
4.2.3 Future NDVI projections	166
4.2.4.1 Limitations of the NDVI projections.....	168
4.3. Results	169
4.3.1. Extreme winter weather events under different RCPs	169
4.3.1.1 Winter warming event frequency (WWE)	169
Seasonal changes in future WWE.....	171
4.3.1.2 Maximum duration warm event (MDW)	172
4.3.1.3 Count of days with snow depth < 10 cm (SC10)	175
4.3.1.4 Count of days with snow depth < 20 cm (SC20)	176
4.3.1.5 ROS events.....	179
Seasonal changes in future ROS	181
4.3.2 Future change in winter meteorological variables under different RCPs	183
4.3.2.1 Temperature.....	183

Seasonal changes in future temperature	183
4.3.2.2 Snow depth	187
Seasonal changes in future snow depth.....	187
4.3.3 Future NDVI-change projections under different RCPs	190
4.3.3.1 Flatanger.....	190
4.3.3.2 Lofoten	192
4.3.3.3 Storfjord	194
4.4 Discussion.....	199
4.4.1 Extreme winter weather conditions under different RCPs.....	199
4.4.2 Future climate change and Arctic Browning.....	204
4.5 Conclusions	209
4.6 Supplemental material	211
Appendix 4.1.....	211
Appendix 4.2.....	212
Appendix 4.3.....	213
Appendix 4.4.....	214
Chapter 5.....	215
Conclusions and Future Recommendations	215
5.1 Conclusions	216
5.2 Future recommendations.....	220
References.....	222

List of Figures

<i>Figure 1.1 (a, b) Winter warming damage observed for E. Nigrum in Sub-Arctic Scandinavia (c) icing damage to Dryas octopetala in High Arctic Svalbard; (d, e) frost drought damage to Calluna vulgaris heathland in central Norway; and (f) fire on flammable, frost drought killed, Calluna heathland (Image source Phoenix and Bjerke, 2016, p.2961).....</i>	<i>3</i>
<i>Figure 1.2 Norway precipitation regions, with their respective mean precipitation in 1961 – 1990 (Source: Heikkilä et al., 2011)</i>	<i>14</i>
<i>Figure 1.3 Norway temperature regions with their respective mean temperature in 1961 – 1990 (Source: Heikkilä et al., 2011)</i>	<i>15</i>
<i>Figure 1.4 Freeze-thaw events in Norway over the time period 1961 – 2010 (Dyrrdal et al., 2015).....</i>	<i>16</i>
<i>Figure 1.5 Major geomorphic types on the Arctic Coastal Plain of northern Alaska (Lara et al., 2018, p.2)</i>	<i>19</i>
<i>Figure 1.6 Measurements of daily GPP (black lines), MODIS CCI (red circles, A, C and E) and NDVI (red circles, B, D and F), for three study sites of evergreen conifers (Figure 3 in Gamon et al., 2016).</i>	<i>21</i>
<i>Figure 1.7 Relationships between daily GPP and NDVI (a, b) for study sites E3 and E5; and daily GPP and CCI (e, f) for study sites E3 and E5. The open symbols indicate the senescence stage, whereas solid symbols show the green up stage. The fitted regression lines between the GPP and index is shown with the dashed line. (Wang et al., 2020, p.8).....</i>	<i>23</i>
<i>Figure 2.1 Map of Norway showing the point locations of case studies under this research. The left panel (inset maps) show the local study site characteristics. The insets correspond to (a) Flatanger, (b) Lofoten and (c) Storfjord. This map was produced in QGIS.....</i>	<i>32</i>
<i>Figure 2.2 Different leaf bio-physical status at the shoot level (a-c) and plot scale (e-g). (a) Green, (b, c) anthocyanin pigmentation, (d) mortality, (e) plots dominated by grey coloured Calluna vulgaris, (f) Dark red anthocyanin pigmentation and (g) green control plots (Photo adopted from Treharne (2018))</i>	<i>33</i>
<i>Figure 2.3 The main phenological stages in the annual growth cycle of vegetation, as represented by satellite VIs (Zhang et al., 2012)</i>	<i>38</i>
<i>Figure 2.4 Growing season distribution for (a) CCI and (b) NDVI at the Flatanger study site.</i>	<i>40</i>

Figure 2.5 Average growing season trajectory (2002 – 19), and the BY (2014) growing season trajectory for CCI at the Flatanger study site..... 41

Figure 2.6 Average growing season trajectory (2002 – 19), and the BY (2014) growing season trajectory for NDVI at the Flatanger study site 42

Figure 2.7 Maximum CCI and NDVI of each growing season 2002-19 at the Flatanger study site 43

Figure 2.8 Start of growing season VI observations for Flatanger. BY refers to browning year, meaning the year in which vegetation damage occurred; RY refers to recovery year, following the BY and DoY = Day of year 45

Figure 2.9 Peak of growing season VI observations for Flatanger. BY refers to browning year, meaning the year in which vegetation damage occurred; RY refers to recovery year, following the BY and DoY = Day of year 45

Figure 2.10 End of growing season VI observations for Flatanger. BY refers to browning year, meaning the year in which vegetation damage occurred; and RY refers to recovery year, following the BY. 46

Figure 2.11 Average and standard deviation of each stage of the growing season, for Flatanger study site. The vertical bars denote ± 1 standard deviation, and the circles within the bars denote the mean. 47

Figure 2.12 Growing season distribution for (a) CCI and (b) NDVI at the Storffjord study site respectively. Boxes show the median and interquartile range, whiskers present minimum and maximum values, and the circles denote outliers. 49

Figure 2.13 Average growing season trajectory (2002 – 19), and the BY (2012) growing season trajectory for CCI at the Storffjord study site 50

Figure 2.14 Average growing season trajectory (2002 – 19), and the BY (2012) growing season trajectory for NDVI at the Storffjord study site 50

Figure 2.15 Maximum CCI and NDVI of each growing season 2002-19 at Storffjord study site 52

Figure 2.16 Mean air temperature, snow depth and maximum air temperature for November 2015 – April 2016; as extracted from the meteorological station nearest to the Storffjord study site. The elevation of the station, SN 89350, was 76m a.s.l (Source: Norwegian Centre for Climate Services) 54

Figure 2.17 CCI and NDVI at the SOS, at the Storffjord study site. BY refers to the browning year, meaning the year in which vegetation damage occurred; RY refers to the recovery year, following the BY and DoY= Day of the year. The bubble value with a box outline represents the NDVI of the additional browning year 2016..... 55

Figure 2.18 CCI and NDVI at the POS, at the Storffjord study site. BY refers to browning year, meaning the year in which vegetation damage occurred; RY refers to recovery year, following the BY and DoY = Day of year. The bubble value with a box outline represents the NDVI of the additional browning year 2016. 56

Figure 2.19 CCI and NDVI at the EOS, at the Storffjord study site. BY refers to browning year, meaning the year in which vegetation damage occurred; RY refers to recovery year, following the BY and DoY = Day of year 57

Figure 2.20 Mean and standard deviation at each stage of the growing season, for the Storffjord site. The vertical bars denote ± 1 standard deviation, and the circles within the bars denote the mean. A=Start of season, B= Peak of season and C=End of season 58

Figure 2.21 Growing season distribution for (a) CCI and (b) NDVI at the Lofoten study site respectively. Boxes show the median and interquartile range, whiskers present minimum and maximum values, and the circles denote outliers. 59

Figure 2.22 Average growing season trajectory (2002 – 19), and the BY (2014) growing season trajectory for CCI at the Lofoten study site 60

Figure 2.23 Average growing season trajectory (2002 – 19), and the BY (2014) growing season trajectory for NDVI at the Lofoten study site 61

Figure 2.24 Maximum CCI and NDVI of each growing season 2002-19 at the Lofoten study site 62

Figure 3.1 Flow diagram of the steps to run WRF model..... 78

Figure 3.2 Domain setup for WRF validation simulations 83

Figure 3.3 WRF domain setup for the three case studies (a) Flatanger, (b) Lofoten and (c) Storffjord **Error! Bookmark not defined.**

Figure 3.4 Map of Norway with the Köppen climatic zones (Beck et al., 2018). 91

Figure 3.5 Domain setup for WRF winter simulations 2000-2020 94

<i>Figure 3.6 (a) Winter warming event frequency (WWE) index and (b) Maximum duration winter warming event (MDW) index for December 2013 at Flatanger, Norway (64.4° N, 10.6° E). Indices were estimated from the WRF high resolution (3km) simulations.</i>	98
<i>Figure 3.7 WRF daily 2m near-surface air temperature and nearest meteorological station (Buholmråsa Fyr, 71900) air temperature for December 2013 at the Flatanger study site</i>	98
<i>Figure 3.8 WRF mean snow depth for the Flatanger study site (64.4° N, 10.6° E) and surrounding areas (a) 1-10th December (b) 11th-20th December (c) 21st-31st December 2013 respectively</i>	100
<i>Figure 3.9 Daily mean snow depth observation from the meteorological station (71900) nearest to the Flatanger study area.</i>	100
<i>Figure 3.10 Maps showing the day count where snow depth < 5 cm at the Storffjord study site (69.3°N, 19.9 °E) for (a) December 2011 and (b) January 2012. Maps were produced using WRF simulations at a grid resolution of 5 km and daily time step.</i>	101
<i>Figure 3.11 WRF and the nearest meteorological station (Bardufoss 89350) snow depth for January 2012 at the Storffjord study site</i>	103
<i>Figure 3.12 WRF-based WWE index for the Storffjord site (69.3°N, 19.93 °E) for the time period December 2011 – January 2012. WRF’s grid resolution was 5 km.</i>	104
<i>Figure 3.13 Mean, maximum and minimum near-surface air temperature, snow depth (Meteorological station Bardufoss), mean wind speed and maximum wind gust observations (Meteorological station Skibotn), (top to bottom), from the meteorological stations nearest to the Storffjord study site, for the 2011/12 winter.</i>	105
<i>Figure 3.14 Standard deviation maps of WRF’s daily mean temperature for December 2011 and January 2012 at the Storffjord study site (69.3°N, 19.9 °E) . The WRF simulations were run at a 5 km grid resolution here.</i>	107
<i>Figure 3.15 WRF daily 2m near-surface air temperature and nearest meteorological station (Bardufoss 89350) air temperature for January 2012 at the Storffjord study site.</i>	108
<i>Figure 3.16 WRF 2m daily near-surface air temperature and nearest meteorological station near surface temperature for November 2013-April 2014 at the Lofoten study site</i>	109
<i>Figure 3.17 Maps of the Lofoten study site (68.1°N, 13.7°E) showing, (a) WWE and (b) MDW indices for December 2013 – March 2014. The indices were calculated using WRF simulations at a grid resolution of 1 km and daily time step.</i>	110

<i>Figure 3.18 WRF and nearest meteorological stations snow depth for Nov 2013 – April 2014 at the Lofoten study site. WRF simulations were run at a 1km grid resolution here. Meteorological stations (a) and (b) refer to the 87750 and 85540 stations.</i>	112
<i>Figure 3.19 Maps showing the total day count where snow depth < 5cm, for the 1 km grid WRF domain over the Lofoten area. The maps show the months (a) December 2013 (b) January 2014 (c) February 2014 and (d) March 2014.</i>	114
<i>Figure 3.20 (a) Maps showing correlations of mean summer NDVI with the mean temperature of November.</i>	116
<i>Figure 3.20 (b) Maps showing correlations of mean summer NDVI with the mean temperature of March</i>	117
<i>Figure 3.20 (c) Maps showing correlations of mean summer NDVI with the mean temperature of April</i>	118
<i>Figure 3.21(a) Maps showing correlations of mean summer NDVI with the WWE index for December</i>	120
<i>Figure 3.21 (b) Maps showing correlations of mean summer NDVI with the WWE index for March</i>	121
<i>Figure 3.21 (c) Maps showing correlations of mean summer NDVI with the WWE index for April</i>	122
<i>Figure 3.22 The total WWE for April 2001-2020.</i>	123
<i>Figure 3.23 (a) Maps showing correlations of mean summer NDVI with the MDW index for December</i>	124
<i>Figure 3.23 (b) Maps showing correlations of mean summer NDVI with the MDW index for January</i>	125
<i>Figure 3.23 (c) Maps showing correlations of mean summer NDVI with the MDW index for April.</i>	126
<i>Figure 3.24 (a) Maps showing correlations of mean summer NDVI with the mean snow depth of January</i>	127
<i>Figure 3.24 (b) Maps showing correlations of mean summer NDVI with the mean snow depth of February</i>	128

<i>Figure 3.24(c) Maps showing correlations of mean summer NDVI with the mean snow depth of April</i>	129
<i>Figure 3.25 (a) Maps showing the correlations for NDVI-snow depth < 10 cm</i>	131
<i>Figure 3.25 (b) Maps showing the correlations for NDVI-snow depth < 20 cm</i>	131
<i>Figure 3.26 (a) Maps showing correlations of mean summer NDVI with mean rainfall of December</i>	132
<i>Figure 3.26 (b) Maps showing correlations of mean summer NDVI with mean rainfall of January</i>	133
<i>Figure 3.26 (c) Maps showing correlations of mean summer NDVI with mean rainfall of April</i>	134
<i>Figure 3.27 (a) Maps showing correlations of mean summer NDVI with ROS day counts of December</i>	135
<i>Figure 3.27 (b) Maps showing correlations of mean summer NDVI with ROS day counts of January</i>	136
<i>Figure 3.27 (c) Maps showing correlations of mean summer NDVI with ROS day counts of April</i>	137
<i>Figure 3.28 (a) Scatter plot of NDVI against March MDW and at the Flatanger study site, over the 2001-2020 time period</i>	139
<i>Figure 3.28 (b) Maps showing the correlations of mean summer NDVI with March MDW over the time period 2001 – 2020</i>	140
<i>Figure 3.29 Scatter plot of summer NDVI against December SC20 at the Lofoten study site for the 2000-2020 time period</i>	141
<i>Figure 3.30 (a) Scatter plot of NDVI against mean January 2m surface temperature at the Storjford study site for the 2000-2020 time period</i>	143
<i>Figure 3.30 (b) Scatter plot of NDVI against December MDW at the Storjford study site for the 2000-2020 time period</i>	143
<i>Figure 3.31 Map showing Norway’s vegetation classification (Solberg et al., 2008)</i>	151
<i>Figure 4.1 Domain setup for future WRF simulations</i>	164

Figure 4.2 Average winter warming event frequency for (a) Historic baseline 1990-2000, (b) RCP 4.5, (c) RCP 6.0 and (d) RCP 8.5 2090-2100 respectively	169
Figure 4.3 Frequency of winter warming events under the different RCP emissions scenarios 2090-2100, as compared to the baseline time period 1990-2000. *The warm days grid box count refers to the total number of model grid boxes where near-surface air temperature > 0 °C, under each scenario respectively.....	170
Figure 4.4 Change in the mean monthly WWE index for the months of December, January and February (top to bottom row-wise), under three RCPs (a) 4.5, (b) 6.0 and (c) 8.5, over 2090-2100. The change was calculated w.r.t the baseline time period 1990-2000. The mean monthly WWE refers to the average number of warming events in the respective month for the time period 2090 – 2100. ...	172
Figure 4.5 Average ‘maximum duration winter warming event’ (MDW) per winter season for (a) Historic baseline 1990-2000, (b) RCP 4.5, (c) RCP 6.0 and (d) RCP 8.5 2090-2100 respectively.....	173
Figure 4.6 The years with the highest MDW under the baseline time period (1990-2000) and RCPs 4.5, 6.0 and 8.5.....	174
Figure 4.7 Maps showing the mean SC10 index under (a) the baseline time period (1990-2000), (b) RCP 4.5, (c) RCP 6.0 and (d) RCP 8.5	176
Figure 4.8 Maps showing the mean SC20 index under (a) the baseline time period (1990-2000), (b) RCP 4.5, (c) RCP 6.0 and (d) RCP 8.5	177
Figure 4.9 Maps showing the average number of days per month where snow depth < 10 cm and the near-surface temperature < 1 °C, for the months of (a) December, (b) January, (c) February and (d) March, over the time period 2090-2100, under RCP 8.5.	178
Figure 4.10 Average ROS days per winter season under (a) Historic baseline 1990-2000, (b) RCP 4.5, (c) RCP 6.0 and (d) RCP 8.5 (over 2090-2100 respectively).....	179
Figure 4.11 A comparison of ROS days for the different scenarios over the time period 2090 – 2100. The counts of model grid boxes with respect to the frequency of ROS. This count represents a general spatio-temporal view of ROS days.	180
Figure 4.12 Change in the mean monthly ROS, for the months of December, January, February and March (row-wise, top to bottom), under three RCPs,(a) 4.5, (b) 6.0 and (c) 8.5. The change is calculated for 2090 - 2100, w.r.t 1990 - 2000.	182

Figure 4.13 Maps showing the change in the mean winter temperature for 2090-2100; (a) RCP 4.5 (b) RCP 6.0 and (c) RCP 8.5. The change was calculated w.r.t the baseline time period 1990-2000. 183

Figure 4.14 Maps showing the change in the mean temperature for the months December, January and March (row wise top to bottom), 2090-2100; under the emissions scenarios (a) RCP 4.5 (b) RCP 6.0 and (c) RCP 8.5. Not the different scale for January. 184

Figure 4.15 Maps of the mean snow depth for the mid-winter months, January and February combined, for (a) baseline time period 1990-2000, (b) RCP 4.5, (c) RCP 6.0 and (d) RCP 8.5 188

Figure 4.16 Maps of the mean snow depth for the late winter month March, under (a) baseline time period 1990-2000, (b) RCP 4.5, (c) RCP 6.0 and (d) RCP 8.5 189

Figure 4.17 Projected change in NDVI at Flatanger for 2090-2100, w.r.t the average NDVI 2001-2020, under different RCPs 191

Figure 4.18 Projected change in NDVI at Lofoten for 2090-2100, w.r.t the average NDVI 2001-2020, under different RCPs 193

Figure 4.19 Projected change in NDVI at the Storfjord study site for 2090-2100, w.r.t the average NDVI 2001-2020, under different RCPs..... 195

Figure 4.20 Maps showing correlations of mean summer NDVI and mean January temperature for the 2001 – 2020 time period 214

List of Tables

<i>Table 1.1 Associated climatic drivers of various documented browning events across Norway</i>	5
<i>Table 1.2 Climate indices incorporated by Vikhamar-Schuler et al. (2016). P stands for total daily precipitation and T for daily average temperature.</i>	7
<i>Table 2.1 RO1 study site characteristics</i>	31
<i>Table 2.2 MODIS VIs used in this research</i>	35
<i>Table 2.3 A quick comparison of the vegetation damage related results of field-based studies and this research</i>	63
<i>Table 3.1 WRF validation simulations</i>	81
<i>Table 3.2 RMSE and bias estimates for WRF 2 m surface temperature against meteorological stations</i>	85
<i>Table 3.3 RMSE and bias estimates for WRF snow depth against meteorological stations</i>	86
<i>Table 3.4 Summary of the EWRf-BE simulations setup</i>	87
<i>Table 3.5 Summary of extreme winter weather conditions for the case study browning events</i>	91
<i>Table 3.6 Summary of climatological indices used within RO2</i>	92
<i>Table 3.7 Inputs for the climatological variables-NDVI analysis</i>	96
<i>Table 3.8 Standard deviation and mean of snow depth observations from the nearest meteorological station to the Storfjord site</i>	102
<i>Table 3.9 Standard deviation and mean of temperature observations from the nearest meteorological station (Bardufoss 89350) to the Storfjord site</i>	107
<i>Table 3.10 Mean temperature during the 2013/14 extreme winter season at the meteorological station closest to the Lofoten study site</i>	110

<i>Table 3.11 Mean snow depth during the 2013/14 extreme winter season at the meteorological station closest to the Lofoten study site</i>	<i>113</i>
<i>Table 3.12 A summary of the winter meteorological parameters which showed significant correlations with the average summer MODIS NDVI.....</i>	<i>138</i>
<i>Table 3.13 A summary of the vegetation types associated with different correlations. The numbers represent vegetation types based on the vegetation map (Figure 3.31)The colours red and blue represent positive and negative correlations, respectively.</i>	<i>152</i>
<i>Table 3.14 Details of the WRF trial runs for estimating real time vs model time for the simulations ..</i>	<i>160</i>
<i>Table 4.1 Summary of RCP scenarios (Source: Moss et al. (2010)</i>	<i>165</i>
<i>Table 4. 2 A summary of the meteorological indices used in this chapter</i>	<i>166</i>
<i>Table 4.3 A summary of the mean highest changes in ROS (month and area wise)</i>	<i>181</i>
<i>Table 4.4 A summary of the mean temperature change for various winter months under the RCPs over the study domain.....</i>	<i>186</i>
<i>Table 4.5 Mean of the projected percentage change in NDVI at Flatanger, for 2091 – 2100, under different RCPs. The change was calculated w.r.t the average summer NDVI 2001-2020.</i>	<i>191</i>
<i>Table 4.6 Mean of the projected change in NDVI and December SC20 at the Lofoten study site, under different RCPs.</i>	<i>193</i>
<i>Table 4.7 Mean of the projected change in NDVI, December MDW and January mean surface temperature at Stor fjord study site, under different RCPs.</i>	<i>194</i>
<i>Table 4.8 A simple summary of the NDVI change for each case study site, under each RCP scenario .</i>	<i>197</i>
<i>Table 4.9 Projected change in the SC20 index at Lofoten for 2090-2100, under different RCPs, w.r.t the average SC20 index (2001-2020).....</i>	<i>211</i>
<i>Table 4.10 Change in mean December MDW index (2090-2100) for the Stor fjord study site, under various RCPs, w.r.t the mean December MDW index (2000-2019).....</i>	<i>212</i>
<i>Table 4. 11 Change in the mean January temperature (2090-2100) for the Stor fjord study site, under various RCPs, w.r.t the mean January temperature (2001-2020)</i>	<i>213</i>

Chapter 1

Climate change and Arctic browning: An Introduction

1.1. Research context and aims

The frequency and magnitude of ecosystem-threatening extreme weather events continues to increase in the Arctic as a result of climate change (Callaghan et al., 2010; Landrum and Holland, 2020). Extreme weather events in terms of ecosystems can be defined as “an episode or occurrence in which a statistically rare or unusual climatic period alters ecosystem structure and/or function well outside the bounds of what is considered typical or normal variability” (Smith, 2011, p.658). Such events have been documented to inflict extensive damage on vegetation across numerous Arctic and boreal sites (Bjerke et al., 2014; Bokhorst et al., 2015; Treharne et al., 2020). For example, in December 2007, anomalous winter temperatures above 0 °C for over 12 days in Northern Scandinavia caused a notable decline in vegetation productivity, over an area of 1400 km², in the following growing season (Bokhorst et al., 2009). The term ‘Arctic browning’ refers to both gradual declines in biomass or productivity, as well as the aforementioned abrupt and short-term declines in vegetation productivity (Myers-Smith et al., 2020). Arctic browning has been attributed to climatic, biotic and physical drivers at various locations ranging from the Nordic Arctic Region (NAR) to Alaskan coastal sites. Potential climate-related causes of vegetation browning include extreme winter warming events (Bokhorst et al., 2008; Vikhamar-Schuler et al., 2016), heavier and extended snow cover (Bieniek et al., 2015), rain-on-snow events (ROS) (Bjerke et al., 2017), frost drought (Phoenix and Bjerke, 2016), reduced summer warmth index (Bhatt et al., 2013), increased standing water, late thawing of snow in spring (Bhatt et al., 2017) and thermokarst formation (Bieniek et al., 2015; Raynolds and Walker, 2016). Biotic drivers of vegetation damage could include increased herbivore activity, fungal pests and insect attacks (Bjerke et al., 2014). An example of a physical driver of vegetation browning is wildfires in the Arctic (Bret-Harte et al., 2013). Figure 1.1 shows what Arctic browning looks like in the aftermath of different types of extreme winter weather events.

Currently, Arctic vegetation accounts for 10% of the total carbon sequestered by land on Earth (McGuire et al., 2009). A single browning event has been shown to cause up to a 50% decline in the

plots-scale carbon absorption capacity of vegetation at a few sites in the Norwegian Arctic and boreal areas (Treharne et al., 2019). Moreover, phenological effects of extreme winter weather events on Arctic vegetation have been outlined in several studies. For example, multiple icing events caused an 83% reduction in *E. nigrum* berry production and an earlier leaf emergence in *V. vitis-idaea* (Preece and Phoenix, 2014). Repeated winter warming events lead to delayed spring bud burst in both *E. hermaphroditum* and *V. myrtillus*, 11-75% and 52-95% reduction in berry production of *E. hermaphroditum* and *V. myrtillus* respectively, and compensation growth as a recovery mechanism in *V. myrtillus* (Bokhorst et al., 2011). Although damaged vegetation recovers after a browning event, repeated occurrence of such browning events could cause irreversible damage and the Arctic ecosystem might not return to its equilibrium state (S. Bokhorst et al., 2012; Treharne et al., 2019). Thus, changes in the frequency and spatial distribution of Arctic browning raises huge uncertainties about whether the Arctic remains a net carbon sink in the long-term. Therefore, advanced analyses are required to improve the current efficiency of model projections regarding the potential causes, frequency and scale of browning events (Bjerke et al., 2017).

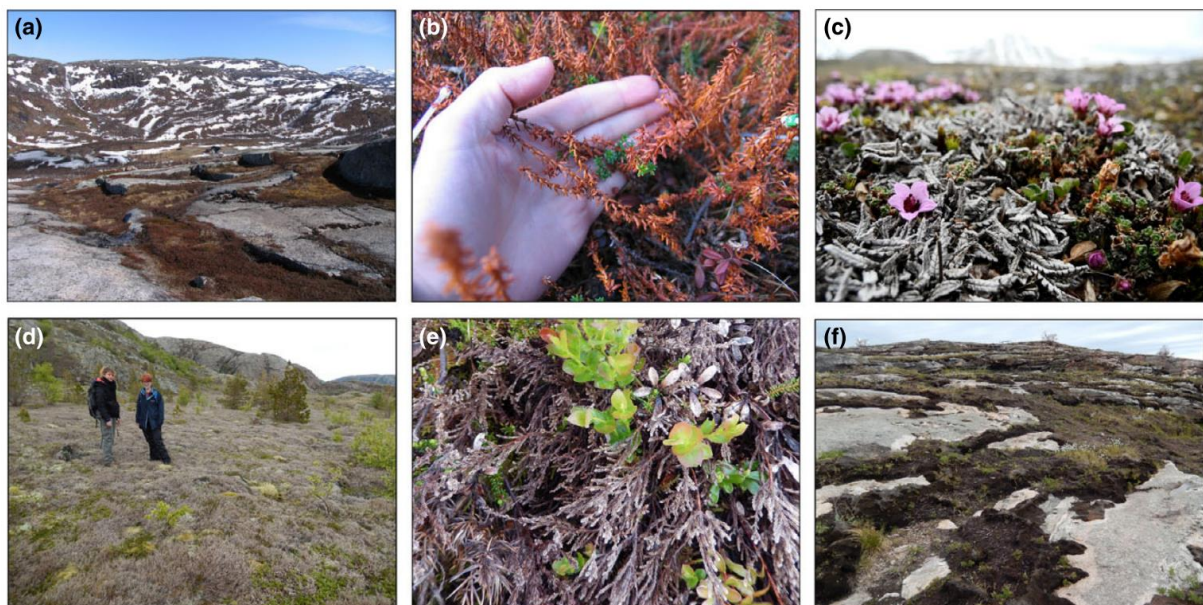


Figure 1.1 (a, b) Winter warming damage observed for *E. Nigrum* in Sub-Arctic Scandinavia (c) icing damage to *Dryas octopetala* in High Arctic Svalbard; (d, e) frost drought damage to *Calluna vulgaris* heathland in central Norway; and (f) fire on flammable, frost drought killed, *Calluna* heathland (Image source Phoenix and Bjerke, 2016, p.2961)

Vegetation is an integral component of Arctic ecosystems because it contributes to the carbon, water and nitrogen cycles, biodiversity, state of the cryosphere, surface energy equilibrium and soil stability (Bjerke et al., 2011; Johansson et al., 2013; Bjerke et al., 2017). Also, Arctic wildlife such as caribou, muskox, hares, lemmings and birds rely on vegetation for food. Vegetation in the Arctic has socioeconomic importance as well because indigenous Arctic communities such as Sami reindeer herders depend on vegetation for their herds (Horstkotte et al., 2017). Along with the essential ecosystem and socioeconomic roles of vegetation in the Arctic, it has become urgent to understand the causes of observed Arctic vegetation damage because most of the ecosystem and earth models have not predicted vegetation browning in the Arctic (Phoenix and Bjerke, 2016). The average decline of 8.7% in vegetation greenness (gradual browning) across the Arctic from 2011-2014 (Epstein et al., 2015), against a 33 year record of increasing Arctic greenness, has strongly challenged the earlier understandings of direct relationships between warming and greening in the Arctic.

The overarching research question of this PhD is, "how extreme winter weather could drive Arctic browning across spatiotemporal scales in the light of a changing climate?". To answer this question, the following research objectives are addressed within this thesis:

1. To understand the satellite-based signature of browning events caused by extreme winter weather conditions.
2. To determine the main meteorological drivers of satellite-based observations of vegetation decline in the Norwegian Arctic and sub-Arctic.
3. Assess the changes in frequency and intensity of climatic drivers of Arctic browning at the end of this century in the Norwegian Arctic and sub-Arctic.

As this PhD research is focused on exploring the role of extreme winter weather events in Arctic browning, climatological drivers of Arctic browning form the main theme of the literature review presented in this chapter.

1.2. Past browning events and associated climatic drivers

Vegetation damage due to extreme winter weather events has been reported across several regions in northern Norway. Therefore, northern Norway is selected as the study area under this PhD research.

Table 1.1 lists the few studies which have analysed browning events and their potential climatic drivers.

The drivers include extreme winter warming, ROS and frost drought. These climatic drivers are the focus of the literature review presented in section 1.3 ahead.

Table 1.1 Associated climatic drivers of various documented browning events across Norway

Location and year of browning events in Norway	Meteorological drivers	Research
1. Flatanger 2014	Extreme winter warming and frost drought	Bjerke et al. (2017), Treharne (2018)
2. Lofoten 2014, 2016	Frost Drought, winter warming	Treharne (2018)
3. Storfjord 2012	Extreme winter warming	Treharne (2018)
4. Lenvik 2014	Extreme winter warming and frost drought	Bjerke et al. (2017)
5. Tromsø 2014	Extreme winter warming and/or ROS lead frost drought	Bjerke et al. (2017)
6. Narvik 2008	Extreme winter warming	Bokhorst et al. (2011)
7. Magerøya 2012	Extreme winter warming and/or ROS lead frost drought	Bjerke et al. (2014)
8. Svalbard 2012	Winter warming and ROS	Bjerke et al. (2017), Treharne (2018)

1.3. Extreme winter weather events in the context of Arctic Browning

As this is an interdisciplinary PhD research, encompassing the fields of Arctic vegetation, ecology and climate change prediction, the following review considers how extreme winter weather events and the associated vegetation damage, have been analysed across the different disciplines.

1.3.1 Winter warming

The strongest Arctic warming has been observed over the winter season (Boisvert and Stroeve, 2015). The definition of a winter warming event varies significantly across studies. For example, Graham et al. (2017) have considered winter warming events as a time duration when the near-surface (1 - 2.5 m) air temperature increases beyond $-10\text{ }^{\circ}\text{C}$, in the Arctic Ocean's areas dominated by sea ice. Whether the definition of a winter warming event is based primarily on a meteorological threshold or an ecological context or both is dependent on the research question being asked. For example, Treharne et al. (2020) examined the mechanisms and effects of winter warming events in the context of vegetation productivity in the Scandinavian Arctic. Their definition of an extreme winter warming event is not limited to a simple temperature threshold, rather it is explained as an interaction between multiple meteorological conditions such as unseasonal snowmelt and accompanying ecosystem exposure, anomalous winter warmth to trigger dehardening of plants, followed by a return to freezing temperatures which then damage any buds and shoots that (due to de-hardening) are no longer freeze tolerant.

One of the approaches to study extreme winter weather events has been through the estimation of climatological indices. A range of indices have been used within studies, such as event related intensity, time duration, frequency and/or a combination of these. In this context, Vikhamar-Schuler et al. (2016) have quantified how frequent and intense winter warming events could get in the Nordic Arctic Region (NAR) across the 21st Century (2000 – 2100). The indices used within their study are summarized in Table 1.2. Based on the frequency of these five climate indices in climate models, the authors suggest a doubled rate of extreme winter warming events for the 21st Century, with reference to the 1985-

2014 period, for Northern Scandinavia. It is worth observing that despite the projections for an increased frequency of extreme events in the Arctic, regional Arctic climate studies scarcely focus on analysing the patterns of future extreme events (Ibid). While Vikhamar-Schuler et al. (2016) employed winter warming indices and comment on their possible effects on vegetation, their research doesn't actually link the indices with browning events.

Table 1.2 Climate indices incorporated by Vikhamar-Schuler et al. (2016). P stands for total daily precipitation and T for daily average temperature.

Number	Abbreviation	Name	Description	Type
1	WD	Warm day	$T > T_{90\text{percentile}}$	Frequency
2	MD	Melt day	$T > 0^{\circ}\text{C}$	Frequency
3	PDD	Positive degree-day sum	$\sum_{\text{days}=1}^n (T > 0^{\circ}\text{C})$	Intensity
4	MPD	Melt and precipitation day	$T > 0^{\circ}\text{C}$ and $P > 0\text{ mm}$	Frequency
5	MPD _{sum}	Precipitation sum for MPDs	$\sum_{\text{days}=1}^n (T > 0^{\circ}\text{C}$ and $P > 0\text{ mm})$	Intensity

Teharne et al. (2020) have also estimated a suite of climatological indices to quantify winter warming events at study sites in Norway. It is important to note that their work is one of the very few on the topic of Arctic browning and hence forms the foundation for ways and methods to explore the relationship between extreme winter weather and subsequent growing season vegetation productivity. Their indices include exposure events, where snow depth is equal to zero, and warming duration and intensity events, where surface temperature $> 2^{\circ}\text{C}$. Their selection of a 2°C surface temperature threshold was based on temperature observations during winter warming events known to have resulted in browning. Treharne et al. (2020) have explained how these climatological indices were conceptualised in the context of the physio-chemical effects that winter warming and/or frost drought can inflict on plants. For example, the intensity metric, i.e., air temperature \times duration, reflects “exposure to temperatures of sufficient warmth and duration to (a) melt snow and expose vegetation, and then (b) initiate bud burst and pre-mature loss of freeze tolerance” (Treharne et al., 2020, p.4). The results of Treharne et al. (2020) demonstrated significant positive correlations of the intensity of warming events and mean snow cover during the warming event with change in the time integrated

¹Normalized Difference Vegetation Index (TI-NDVI) respectively. These relationships have been explained in their study as “cooler and shorter warming events with shallower snow cover resulted in greater negative change in TI-NDVI” (Treharne et al (2020), p.6). Their results also included a negative correlation between the start day of an exposure event and change in the TI-NDVI (exposure events refer to vegetation being exposed to freezing temperatures following snow melt). This relationship is explained as longer lasting exposure events in later winter cause greater negative change in TI-NDVI (ibid). Based on these results Treharne et al. (2020) have concluded that vegetation browning on a regional scale can be well-associated with process-based climate indices.

Further evidence of the increased frequency and magnitude of winter related damage to Arctic vegetation is provided by Bjerke et al. (2017). Their work focused on measuring the damage ratio of various plant species, across 52 field sites in Svalbard, Norway. The sites were known to have experienced vegetation browning. Their research concluded that higher than average temperature and precipitation rates in mid-winter 2011-2012 resulted in lesser snow cover and increased ground-ice formation, respectively, causing plant dieback. In this case of vegetation browning, two distinct extreme climatic phenomena affected the vegetation simultaneously; i.e., winter warming and rain-on-snow. Bjerke et al. (2017) were unable to determine which phenomenon caused most damage to plants.

In the context of extreme climatic events damaging Arctic vegetation, various studies have examined the timescale and mechanisms of vegetation recovery. This leads to another research approach used to investigate browning events in the Arctic, i.e., in-field experiments based on simulations of extreme winter weather events. Though with limited scope across spatiotemporal scales, plot-level experimental setups provide necessary well-controlled and strong evidence of various kinds of plant damage resulting from simulated extreme weather (Bokhorst et al., 2015). The recorded observations from simulations could act as a unique signature of a specific type of extreme event, thus, assisting ecologists by providing ground evidence for remote sensing methods to assess vegetation damage on

¹ NDVI is explained ahead in section 1.5

larger scales in the aftermath of an actual extreme event. Moreover, findings of field simulations could also help to identify whether vegetation in a region was exposed to single or multiple extreme events (Bokhorst et al., 2012). Ultimately, the information about frequency of extreme climate events derived through previously known observations of simulation studies in the Arctic could strongly assist in developing future projections about frequency and severity of browning events.

An example of research using simulations is the study of Bokhorst et al. (2012), who have focused on a comparative assessment of the effects of naturally occurring and experimentally simulated extreme winter warming event on Arctic vegetation. They analysed the recovery of vegetation exposed to a seven-day experimental winter warming event in Abisko, Sweden. Additionally, they also analysed the impacts of an actual 12-day episode of anomalously high winter temperatures during December 2007 in higher latitudes of Scandinavia. Through in-field plot scale investigations of both the simulation and real winter warming events Bokhorst et al. (2012) have suggested that multiple winter warming events can lead to cumulative disturbance in the carbon sink capacity of Arctic vegetation.

A few previous studies have explained how winter warming events have often led to frost drought (Bjerke et al., 2011; Bjerke et al., 2017; Treharne et al., 2020), which is another important mechanism of extreme event-driven Arctic browning. Frost drought happens due to low or absent snow cover in winter, which can expose vegetation to freezing temperatures, wind and irradiance. Such conditions can cause plant transpiration at a time in winter when the soil water is frozen or near-frozen and unavailable for plant uptake (Sakai and Larcher, 1987). High winter transpiration rates have been known to cause plant desiccation and mortality at a landscape scale. Overall, it is the mid-winter thaw which is a typical and common feature of both extreme winter warming and frost drought.

The 2015-2016 winter was recorded as the warmest since 1950 on a pan-Arctic scale (Overland and Wang, 2016; Cullather et al., 2016), and there is a general agreement within the climate change literature about winter projected to be the most severely affected season in the Arctic in terms of frequency, scale and intensity of extreme weather events (Vikhamar-Schuler et al., 2016). Hence one

of the component analyses of this PhD is to detect and quantify potential vegetation browning with regard to both current (2000 – 2020) and future (2090 – 2100) winter warming events.

1.3.2 Rain-on-snow (ROS)

As mentioned in section 1.2, along with winter warming events, ROS events have also been linked with vegetation browning damage in the Arctic. The following sections review Arctic ROS studies in the overall climatological context, and not necessarily analysing ROS as a climatic driver of vegetation browning.

ROS events are one of the many types of extreme climate events in the Arctic. Assessing ROS is demanding due to difficulties in quantifying rain and snow in the Arctic and in modelling ROS events using GCMs (Rennert et al., 2009). Generally, ROS events are linked with short-term warm spells, lasting for hours to days, in autumn and winter (Hansen et al., 2014). Though ROS events are generally short lived, they can critically damage high Arctic ecosystems with far reaching and long term impacts (Rennert et al., 2009; Hansen et al., 2014; Christensen et al., 2021). For example, ROS events can lead to the formation of ice layers within the snowpack through a thaw-freeze cycle of the combination of snow on-ground and falling liquid precipitation. The ground ice then makes the underlying vegetation inaccessible for ungulates to forage. An ROS event across the Yamal Peninsula in November 2013 has been linked with the death of 61000 animals between November 2013 and 2014 (Serreze et al., 2021). Moreover, ground-ice causes damage to both vascular plants and lichens (Bjerke, 2011). When vegetation gets encapsulated in ice layers, it not only loses the insulation provided by snow against freezing temperatures, but also undergoes damaging effects such as hypoxia and CO₂ accumulation (G.K. Phoenix and Lee, 2004). Along with damaging ecological effects, ROS events also have significant socio-economic impacts such as slush avalanches leading to road and airport closures, major disruptions to services and the local tourism industry (Serreze et al., 2021).

An example of an ROS event resulting from extreme weather conditions, occurred in Svalbard over the 2011-12 winter season (Hansen et al., 2014). A temperature anomaly of up to 20° C above the daily

normal, was recorded at the Svalbard Airport meteorological station. Moreover, 8th February saw the highest February temperature record of Svalbard of 7.8° C. These extreme high winter temperatures were then followed by a 10° C plunge. Along with record high winter temperatures for two weeks across late January-early February 2011-12, a number of heavy rainfall events were observed as well. The most extreme rainfall event was recorded on 30th January with 25% of the mean annual precipitation falling in one day. The authors found a positive correlation for winter temperatures and seasonal ROS ($r=0.37$, $p<0.05$).

In the context of ROS events in Norway, Pall et al. (2019) have developed a first-time climatology of ROS for mainland Norway through examining the correlations between ROS events and atmospheric circulation indices. They defined an ROS event as a day with at least 3 mm of snow water equivalent (SWE) and 5mm of rain. Their variables of interest were temperature, precipitation, SWE, and atmospheric circulation indices; the North Atlantic Oscillation (NAO), the Arctic Oscillation (AO) and the Scandinavian pattern (SCA). An ROS event was defined as a day with at least 3 mm of SWE and 5mm of rain. The correlations were studied for the seasons with the most active ROS frequency, which were winter and spring. Pall et al. (2019), similar to Rennert et al. (2014), discussed the role of the Atlantic frontal systems that play a major role in shaping western Norway's weather and hence driving the winter ROS. The NAO was found to be most strongly correlated with ROS in southern-west Norway areas, up to 68 °N. For their North region, the correlation between the AO and ROS was higher as compared to the NAO due to the AO's centre of action being over the Arctic. As compared to the positive correlations of ROS with both NAO and AO, Pall et al. (2019) found a negative correlation between ROS and the SCA for winter.

The above review of ROS studies reveals that although a number of ROS events have been analysed within the Arctic climatology and ecosystems literature over the past 15 years, a significant research gap is seen for future ROS projection in general and especially in terms of future ROS affecting Arctic vegetation. Therefore, this PhD aims to understand the relationship between ROS and summer

vegetation productivity and also provide projections of future ROS occurrence under different emissions scenarios.

To summarise the literature review of extreme winter weather events in the context of Arctic browning, interestingly only a few of the studies have examined extreme weather events as climatological drivers of vegetation browning. Many have analysed winter warming and ROS events in a pure climatological context. Moreover, limited studies were found on the topics of projecting the potential frequency and severity of these browning drivers for the 21st Century and these studies were drawn principally from the atmospheric literature. There were no studies found that link satellite vegetation data with extreme winter weather events, using future climate change scenarios.

1.4 Regional climate change studies for Norway

General Circulation Models (GCMs) provide meteorological simulations on spatial scales around 100 km, e.g., the typical model resolution of The Coupled Model Intercomparison Project (CMIP6) is approximately 250 km in the atmosphere and 100 km over the ocean (Liang-Liang et al., 2022). In order to provide more accurate predictions over a geographical area of interest, the output of GCMs are often downscaled. Downscaling refers to the process of refining GCM outputs to a higher spatial resolution, so it is adequate for use in impact studies. This downscaling is carried out either dynamically through Regional Climate Models (RCMs) or by applying Empirical Statistical Downscaling (ESD) methods (Ibid). The output of RCMs, which usually covers a limited area such as country level, offer detailed and high-resolution meteorological simulations. Such simulations are generally well-suited for robust impact and adaptation assessments, as compared to the output from GCMs (Ibid).

To address the second and third research objectives of this PhD research (outlined in section 1.1) regional climate model simulations are required (explained in detail in chapter 3). For this the Weather Research and Forecasting model (WRF) is selected to generate simulations for Norway. Therefore, it is important to understand WRF's performance over Norway overall. An example of previous work running WRF over Norway is the study by Heikkilä et al. (2011). They ran WRF with ERA-40 reanalysis

as the input, at 30 and 10 km horizontal resolutions, for the time period 1961 to 1990. ERA-40 is an example of reanalysis datasets, which assimilate atmospheric observations into an numerical weather prediction (NWP) model, based on a variety of sources including satellite data, radiosondes and meteorological stations (Marshall et al., 2018). Heikkilä et al. (2011) evaluated a range of surface climatological variables from the WRF output against those from multiple meteorological stations, ENSEMBLES (Ensembles-based predictions of climate changes and their impacts) models and ERA-40. Their variables of interest, precipitation and 2m surface temperature, coincide with two of the primary climatological parameters in this PhD research, and hence their performance is reviewed here.

WRF's precipitation over Norway's coastal areas was well simulated overall, with a reduced bias as compared to ERA-40. The highest bias was observed inland on the leeward side of the mountains. This was attributed to a too small orographic uplift resulting in excessive precipitation falling on the lee side of the mountains. A large non-seasonal positive bias was also observed for northern Norway. A key measure for assessing a model's performance is its capacity to reproduce precipitation events in terms of frequency and the intensity (Heikkilä et al., 2011). WRF run at 30-km and especially at a refined 10-km grid, significantly outperformed ERA-40 in simulating extreme precipitation events (>50 mm/day), however could not simulate the highest extremes.

Norway being long, narrow and having a complex terrain has large regional variations in precipitation. Heikkilä et al. (2011) evaluated WRF's skill at representing these regional differences in precipitation. They have concluded that WRF's precipitation along the coastal western regions (2,4, 6-9 in Figure 1.2) is well simulated, however is exaggerated for the drier regions (3,10 and 12 in Figure 1.2).

Precipitation regions (1-13)

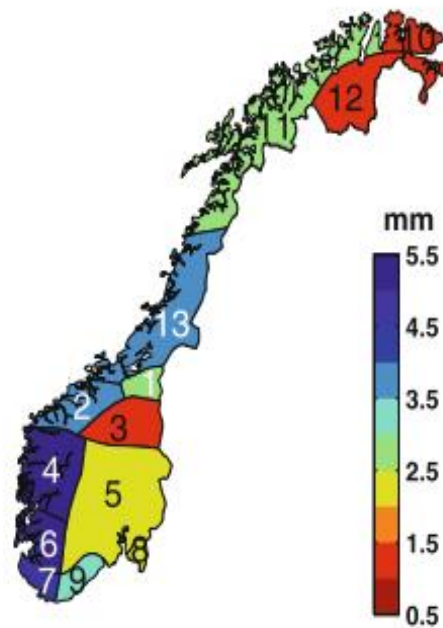


Figure 1.2 Norway precipitation regions, with their respective mean precipitation in 1961 – 1990
(Source: Heikkilä et al., 2011)

In the context of WRF's temperature output for Norway, Heikkilä et al. (2011) found that WRF's simulations performed better than the ENSEMBLES models in terms of the mean regional temperature bias. The regional temperature differences are well represented by WRF, with regions 4 and 6 exhibiting the strongest agreement and regions 1 and 2 the weakest as compared with the meteorological stations. An overall cold bias of 0.7-0.8°C over Norway was observed for both ERA-40 and WRF. Interestingly, the temperature simulations at the 30-km WRF grid outperformed the 10 km grid across all regions. Regarding extreme cold temperatures, WRF's performance was found to be slightly poor compared to the meteorological observations. On the other hand, extremely high temperatures were found to be well simulated, and the same for the 10 and 30 km grids.

Temperature regions (1-6)

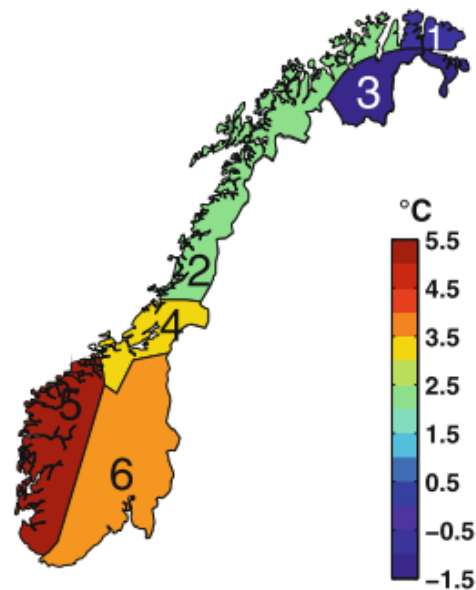


Figure 1.3 Norway temperature regions with their respective mean temperature in 1961 – 1990
(Source: Heikkilä et al., 2011)

Heikkilä et al. (2011) concluded that overall WRF reproduced Norway's meteorological conditions quite well even using the default physics parameterizations. The default settings helped with an economic runtime, while generating results similar to the more advanced WRF setups.

In the context of climatic change in Norway a number of studies have analysed historical trends in air temperature. For example, Dyrddal et al. (2011) analysed the trends of freeze-thaw events based on observed daily mean temperature, which were in the range $-1.5 - 1^{\circ}\text{C}$, over the time period 1961 – 2010. The results of their study showed that the highest number of days with freeze-thaw events occurred over the coastal areas across Norway. However, the strongest and positive, statistically significant trends in such events were mostly found over the colder, inland regions of Norway, and coastal areas in the northernmost Troms og Finnmark region (Figure 1.4).

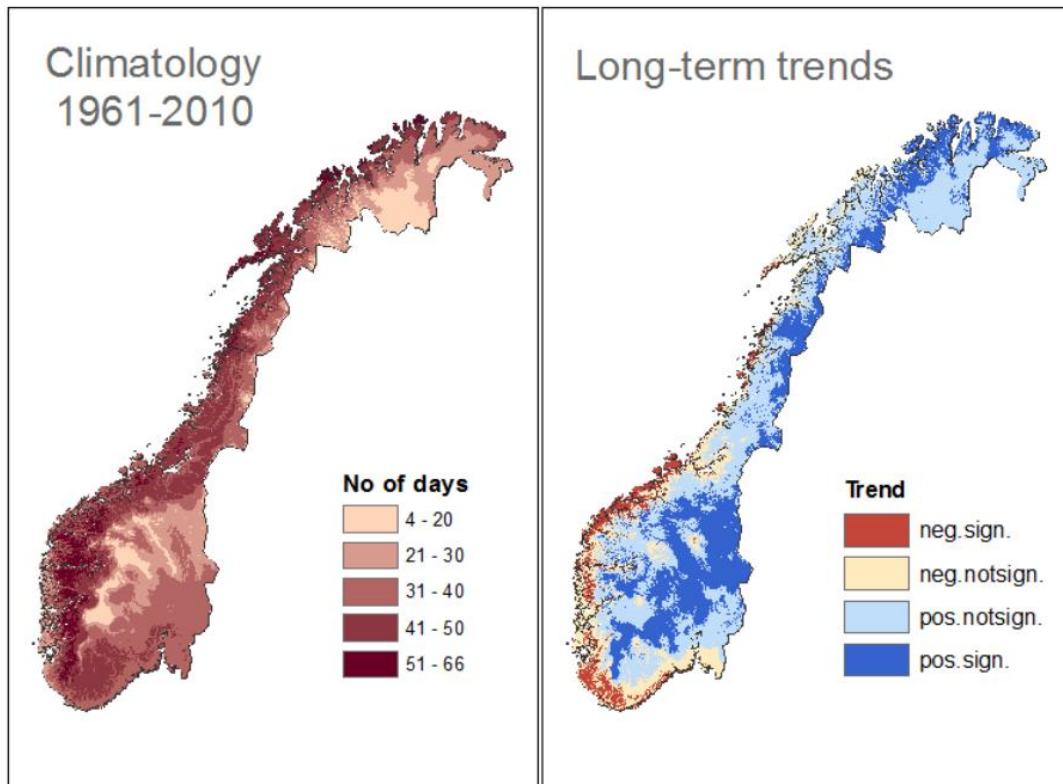


Figure 1.4 Freeze-thaw events in Norway over the time period 1961 – 2010 (Dyrrdal et al., 2011). *Neg. and pos. sign (legend) refers to the statistically significant trends in freeze-thaw events. Whereas the neg. notsign. and pos. notsign. refer to the trends which are not statistically significant.*

Kerguillec (2015) analysed trends and variability in the number of days where observed temperature crossed the 0° C threshold, on both annual and seasonal scales, for the 1950 – 2013 time period. The main results of their study were that factors such as altitude, latitude and distance from the coast determined the average number of days and decadal trends where temperatures crossed the 0° C threshold. In the context of temperature changes in Norway, another study is by Nilsen et al. (2021). Their work examined both the historical trends and future projections, in annual and seasonal frequency of days with zero-crossings (DZCs). Their study used the high-resolution (1 × 1 km) gridded output of the Coordinated Regional Climate Downscaling Experiment for the European domain (EURO-CORDEX) ensemble. Their main findings were that the frequency of DZCs has generally increased in winter over the time period 1971 – 2016. Interestingly future projections of DZCs showed a decrease for the lowlands and increases otherwise, especially in the northernmost county, Troms og Finnmark.

The strongest rise in DZCs is projected for the winter season under both Representative Concentration Pathways (RCPs) 4.5 and 8.5 over 2071 – 2100. RCPs 4.5 and 8.5 represent low and high greenhouse gas emissions trajectories, respectively, under the Fifth Assessment Report (AR5) by the Intergovernmental Panel on Climate Change (IPCC).

1.5 Application of satellite vegetation indices to examine Arctic browning

Numerous analyses based on satellite observations and field studies have reported a continuous increase in vegetation productivity and biomass overall in the Arctic starting in the 1980s. This increase has been attributed to both, warming releasing cold temperature constraints on photosynthetic activity and growth (including both warming and longer growing seasons) (Fensholt et al., 2012) and the CO₂ fertilization effect (Gustafson et al., 2021). The Normalized Difference Vegetation Index (NDVI) is the most widely applied satellite index to assess Arctic vegetation dynamics e.g. Karlsen et al. (2018), May et al. (2018), Lara et al. (2018), Bhatt et al. (2017), Vickers et al. (2016), Bienek et al. (2015), Bjerke et al. (2014), Epstein et al. (2013), Gamon et al. (2013), Bokhorst et al. (2012), Bhatt et al. (2010), and Tucker et al. (2001). It is commonly incorporated due to its straightforward calculation and historically available selection of bands (Myers-Smith et al., 2020). NDVI uses the difference between near infrared (NIR) and red spectral bands as the algorithm. The red spectral region is selected due to the maximum absorption of radiation by chlorophyll pigments in this band. The maximum reflection of radiation by vegetation occurs within the NIR region of the spectrum. NDVI (Tucker, 1979) is calculated as,

$$\text{NDVI} = (\rho_{\text{NIR}} - \rho_{\text{R}}) / (\rho_{\text{NIR}} + \rho_{\text{R}}), \text{ (where } \rho \text{ are reflectance values)}$$

Satellite NDVI is mainly applied to study vegetation phenology and productivity over a typical growing season (Gamon et al. 1995). While satellite-based analysis of browning events is limited, the few studies that exist have mainly applied NDVI to investigate the vegetation productivity decrease observed on the ground. For instance, Bokhorst et al. (2009) studied vegetation damage at five different sites across Scandinavia, resulting from an extreme winter warming event in December 2007. It is important to note

that they used both, satellite data and meteorological station observations to examine the browning event. The meteorological data included temperature and snow depth. For the satellite data they used Moderate Resolution Imaging Spectroradiometer (MODIS) NDVI, during mid-July, at a 250m spatial resolution, to compare the vegetation productivity in 2007 (the year before the browning event) and 2008 (the year following the browning event). Their results showed a 26% reduction in mid-July NDVI for the growing season in 2008, as compared to the growing season of 2007. Their study also used ground observations of a simulated warming event to validate the attribution of the level and type of vegetation damage observed in 2008, based on small plots (60 × 60 cm), over which the ratio of live to dead shoots was measured and compared with the nearby undamaged vegetation. The results of their ground observations confirmed that the satellite NDVI decrease was in fact a result of the winter warming event in December 2007. The different types of data and methods used by Bokhorst et al. (2009) underscores the importance of a multi-disciplinary approach to accurately identify browning events, examine them and assess the level of damage resulting from such events. Moreover, their work highlights issues of spatial scale discrepancies in comparing ground and satellite data related to vegetation damage; since the on-ground observations were at 60 × 60 cm plots, and one MODIS NDVI pixel covers 250 × 250 m area. For example, one of the drawbacks of medium-coarse resolution satellite data is that the type of vegetation most affected by a winter warming event cannot be identified. On the other hand, field observations are limited in understanding the spatial extent of vegetation damage. Despite the widespread application of satellite NDVI, it has been argued that the broadband NDVI algorithms are insensitive to the effects of continuously changing environmental stressors on plants in the short-term (Gamon et al., 2015). NDVI can have other problematic areas as well such as the effect of under canopy bare soil and saturation from dense vegetation cover (Huete et al., 2002). Hence research has strongly argued the potential of complementary techniques i.e., integrated or combined structural and physiological vegetation indices for analysing canopy scale vegetation state and photosynthetic performance (Gamon et al., 2016).

Lara et al. (2018) explored the role of landscape characteristics to explain climate vegetation interactions in detail. Their study is related to vegetation productivity changes in Alaskan coastal tundra and has incorporated a novel methodology for analysing the dynamics between climatic parameters and decadal vegetation productivity variations, based on 15 unique categories of tundra landscape features across their case study. Examples of landform categories are shown in Figure 1.5. Through evaluating the past and current interplay between climatic change and vegetation across distinct geomorphological spatial units, they statistically modelled which landform types could be most affected by future vegetation declines. Although differences between landform types occurred, Lara et al. (2018) concluded that increasing temperature and precipitation anomalies are likely to be the potential major climatic drivers of browning across coastal tundra. These findings agree with the results of Bjerke et al. (2017), as they have also attributed vegetation damage to warmer than usual temperatures and higher precipitation in the Norwegian Arctic.

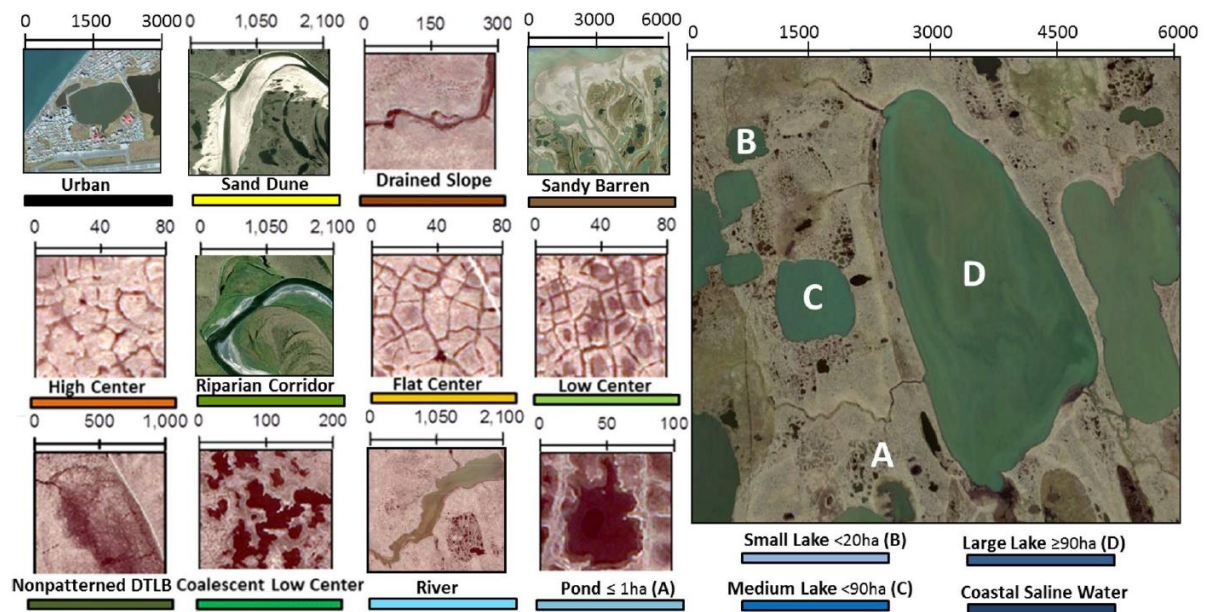


Figure 1.5 Major geomorphic types on the Arctic Coastal Plain of northern Alaska (Lara et al., 2018, p.2)

When investigating the bio-physical status of vegetation, various researchers have advocated the use of vegetation indices which are responsive to photosynthetic pigments, such as chlorophyll and carotenoids in leaves, to detect changes in photosynthetic activity and phenology (Goerner et al., 2011;

Gamon et al., 2015; Beamish et al., 2018; Wong et al., 2019). Levels of photosynthetic pigments in plant leaves can be strongly affected by biotic and abiotic stressors. One of the photosynthetic pigments are carotenoids. Carotenoids are a range of pigments which include lutein, beta-carotene, xanthophyll, (Gamon et al., 2016). The composition of the carotenoid pigment pool varies on a seasonal and sub-seasonal scale depending on various factors such as environmental stressors, light conditions and subsequent photosynthetic activity. Changes in the pool sizes of these pigments reflect how plants respond to a variety of evolving environmental states all through the start, peak and end of season vegetation stages (Filella et al., 2009; Gamon et al., 2016). For example, vegetation carotenoid pigments can increase due to exposure to various stress inducing forces such as extreme temperatures, low soil-moisture levels, and nutrients (Gamon et al., 2015). The photochemical reflectance index (PRI) is linked with the carotenoid concentrations and hence has been applied as a reliable indicator of photosynthetic activity and phenology (Gamon et al., 1997; Goerner et al., 2009). It has also been used to estimate stress associated spectral responses of plants (Hernández-Clemente et al., 2019). PRI (Gamon et al., 1997) is defined as,

$$PRI = (R_{531} - R_{570}) / (R_{531} + R_{570}), \text{ (R indicates reflectance at respective wavelengths (nm))}$$

Initially PRI was developed to monitor the xanthophyll cycle on a circadian timescale (Gamon et al., 1997). In the short-term, the xanthophyll cycle fluctuates as plants dissipate excess light energy from the photosynthetic complex via the xanthophyll cycle (Wong and Gamon, 2015). The cycle's alterations influence spectral reflectance at the wavelength 531 nm, thus offering a metric to study how the photosynthetic light-use efficiency (LUE) varies in the short-term (Gamon et al. 2015). In the context of annual time scale, and on landscape scales, however, PRI has been linked with the seasonally changing chlorophyll carotenoid ratios (Filella et al., 2009). In the context of a vegetation pigments-based satellite index, MODIS offers two spectral bands, B1 and B11, which are closest to the theoretical PRI. This leads to the chlorophyll/carotenoid index (CCI), which is an amended version of the PRI (Wang et al., 2020).

The CCI captures the changes in the carotenoids and chlorophyll pool sizes, and not the xanthophyll cycle.

Gamon et al. (2016) studied the performance of MODIS-derived CCI (1 km spatial resolution) in tracking photosynthetic phenology in evergreen conifers, in Canada. They evaluated MODIS CCI against a number of empirical measurements at the leaf and canopy scale. These included laboratory-based measurements of chlorophyll and carotenoids, in-field foliar gas exchange and daily Gross Primary Productivity (GPP). The results of Gamon et al. (2016) showed that MODIS CCI closely followed the seasonal changes in the canopy-scale flux-tower GPP, across the three study sites. Whereas NDVI stayed elevated at quite a few instances despite the decline in GPP in autumn and winter (Figure 1.6).

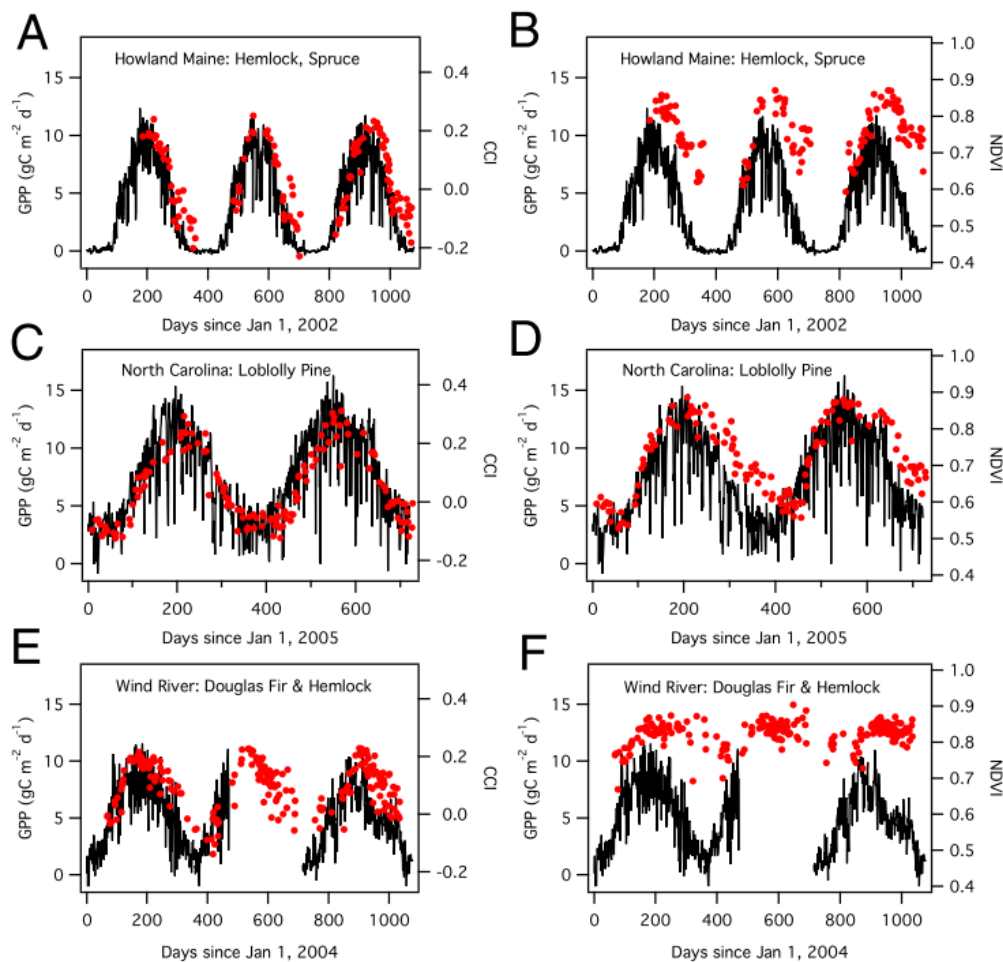


Figure 1.6 Measurements of daily GPP (black lines), MODIS CCI (red circles, A, C and E) and NDVI (red circles, B, D and F), for three study sites of evergreen conifers (Figure 3 in Gamon et al., 2016).

In the context of pigments-based approaches for remotely monitoring photosynthetic activity, Wang et al. (2020) have also examined the relationship between MODIS CCI and flux tower GPP. In addition to CCI, they studied NDVI's performance as well at tracking the seasonal GPP. Both indices were at a spatial resolution of 1 km. Their study was focused on native prairie vegetation, comprising of uniform grasslands, in Southern Alberta. The main findings of Wang et al. (2020) were that NDVI was more responsive to leaf emergence early in the growing season. Whereas CCI was better at capturing the subtle changes in canopy colour arising from variations in the chlorophyll and carotenoid concentrations. Therefore, CCI was able to track a delay in the peak productivity and was not affected by hysteresis issues as NDVI was. Interestingly NDVI showed a stronger relationship with GPP when the growing season was separated into the greenup and senescence phases (Figure 1.7). The findings about NDVI and CCI in Wang et al. highlight the importance of complimentary approaches, i.e., integrating NDVI and CCI, to examine the vegetation productivity dynamics more accurately at different stages of the growing season.

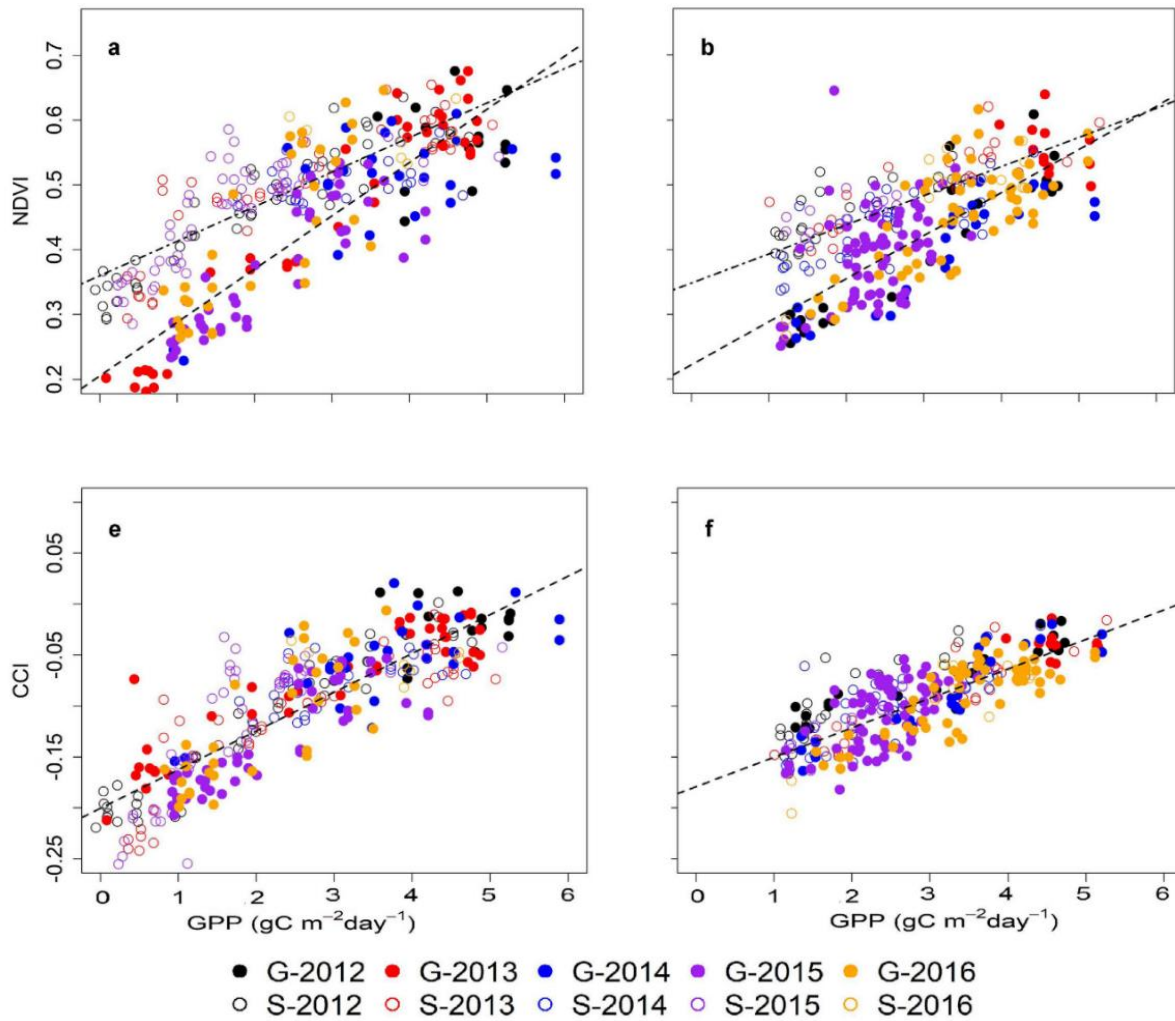


Figure 1.7 Relationships between daily GPP and NDVI (a, b) for study sites E3 and E5; and daily GPP and CCI (e, f) for study sites E3 and E5. **The sites E3 and E5 are pre-dominantly grasslands located within a working cattle ranch in southern Alberta, Canada.** The open symbols indicate the senescence stage, whereas solid symbols show the green up stage. The fitted regression lines between the GPP and index is shown with the dashed line. (Wang et al., 2020, p.8).

Despite the vital role of photosynthetic pigments in assessing vegetation productivity, limited research has been conducted in the context of GPP-CCI relationships of Arctic vegetation (Beamish et al., 2020). Moreover, no studies were found with regards to the application of satellite-based CCI to examine impacts of extreme weather events on the productivity of Arctic vegetation. Existing studies related to photosynthetic pigments of Arctic vegetation are mostly based on in-situ reflectance measurements. Studies that have used satellite-derived CCI have focused on applying the index to study phenological aspects in **evergreen** forests in the boreal or Arctic regions, (e.g., Gamon et al., 2016; Maguire et al., 2021). Therefore, application of a satellite-based CCI to examine dwarf shrub heathland in the Arctic,

in the aftermath of extreme weather events, provides a unique opportunity to explore the potential of pigment-based indices for assessing vegetation productivity.

1.6 Projected changes in Arctic vegetation in the light of climate change

As this PhD aims to quantify future vegetation browning under different climate change scenarios, a brief review is presented of studies focused on potential vegetation changes under climate change, as there have been few studies specifically on Arctic browning, it also considers browning studies in other regions.

The study of shifts in Arctic vegetation species range and distribution in response to environmental predictors such as CO₂ fertilisation, other nutrients, and climatic variables, is an active area of research. Vegetation responses to such evolving environmental conditions have been studied using Dynamic Global Vegetation Models (DGVMs) and Global Vegetation Models (GVMs). In this context, Friend et al. (2014) have simulated various types of vegetation responses, at a global scale, to future climate and carbon dioxide changes. While Friend et al., have performed their simulations on a global scale, here in this literature review it is most relevant to focus on the results of Friend et al., related to the Arctic because this PhD research is focused on the Norwegian Arctic Region. For the Arctic region, they have focused on boreal forests. Their results show a notable increase in the carbon storage across the majority of the boreal forest by 2100.

Niskanen et al. (2019) have studied how the biogeographical distribution of high latitude vegetation could alter in the time period 2070-2099, in response to a changing climate, under three CMIP5 based emissions scenarios. The scenarios were the RCPs 2.6, 4.5 and 8.5, which represent low, medium and high greenhouse gas emissions trajectories, respectively, under the Fifth Assessment Report (AR5) by the Intergovernmental Panel on Climate Change (IPCC). Niskanen et al. (2019) have applied a combination of environmental predictors representing climate, geology and topography at a high resolution of 1 km. The results of their study show varied responses of different types of vascular plants

to the suite of environmental predictors. One of their notable results was that most of the present high-latitude plant species could occupy higher slopes in order to continue their current range.

In addition to Friend et al. and Niskanen et al. , Gustafson et al. (2021) have similarly examined how major climatic and environmental drivers can affect vegetation distribution, particularly the treeline advancement into tundra, under different RCPs. Some of their major findings in the context of ground vegetation i.e. shrubs and grasses (the focus of this PhD), were that overall for both RCPs 2.5 and 8.5, CO₂ fertilisation strongly contributed to higher vegetation productivity (as seen in previous studies as well), higher air temperatures strongly drove tree productivity, whereas precipitation was weakly correlated with tree productivity, the nitrogen cycle dynamics have a key role in determining future treeline shifts in the Arctic; and that soil moisture had a major effect on vegetation composition, which in turn shapes the treeline progress.

1.7 Summary

While reviewing the studies presented in above sections, it was noted that literature around climate change impacts on Arctic vegetation comprises of studies incorporating different approaches and methodologies. These broadly include analyses based on one or a combination of the following approaches;

- i. Field observations of vegetation state in response to climatic conditions and events
- ii. Remote sensing techniques and satellite data related to vegetation characteristics
- iii. In-field experimental simulations of extreme weather events affecting vegetation
- iv. Land-cover typology based vegetation analyses
- v. Climatological and/or ecosystem modelling

It has been widely emphasised within the Arctic ecology and general climate change literature to consider stochastic extreme events to improve our understanding of how Arctic ecosystem processes

respond to environmental predictors in the light of climate change (Jentsch et al., 2007; Smith, 2011; Bokhorst et al., 2015). The literature review conducted for this thesis showed that very few studies have focused on simulating vegetation productivity changes, in the light of potential changes in the magnitude and frequency of extreme weather events which could occur under the different RCPs for the Arctic. Hence this PhD research addresses the research gap to understand possible vegetation browning events at the end of this century, by synthesizing previous field based browning observations with satellite vegetation indices, extreme weather events meteorology and different emission scenarios based climate model simulations.

The literature review of this thesis is followed by Chapter two which is aimed at addressing RO1 of this research. Chapter two outlines the case study browning events, provides the background of the ground data, related to these events, collected by previous research. This is followed by the hypotheses construction related to satellite-based examination of the browning events. The results of the analysis in chapter two are presented separately for each study site and hypothesis-wise. The results across the sites are subsequently compared. The discussion section of chapter two compares the performance of the different satellite vegetation indices in light of the on-ground observations, highlights the challenges faced in remote detection of browning events and explains the selection of the vegetation index proposed to be used ahead in chapters three and four.

Chapter three of this thesis addresses RO2 of this PhD research. This chapter provides the technical background of the RCM (i.e., WRF) used to produce the meteorological simulations. This is followed by description of the various datasets used to produce the simulations. Next, the statistical analysis used to understand the relationships between the vegetation productivity and meteorological variables, is explained. The results of chapter three are presented under two main themes. First, an assessment of WRF's simulations of extreme weather events and second, the results of the statistical relationships between summer vegetation productivity and winter metrics over the study area. These relationships inform the analysis in chapter four.

Chapter four of this thesis is focused on RO3 of this PhD research. It begins by providing the context of the future occurrence of browning in the light of climate change. The work presents the projections of changes in the frequency and intensity of different winter extreme weather events for northern Norway under three emissions scenarios. The discussion section of chapter four links the findings of chapters two and three in that the future projections of changes in vegetation productivity, are interpreted based on the findings of; the satellite-based signal of on-ground productivity decrease in chapter two and the statistical relationships between vegetation productivity and winter meteorology in chapter three.

Chapter five provides a summary of the major findings of this research, followed by recommendations for future research on the topic of Arctic browning.

Chapter 2

Understanding Arctic Browning using spectral vegetation indices

2.1 Introduction

Recent research has discussed the complexity involved in analysing browning events resulting from extreme winter weather conditions (Myers-Smith et al., 2020). For example, differences in the conceptual understandings of 'trend' vs 'event' browning, across spatio-temporal scales as well as within the remote sensing and ecology literatures. Most of the research related to impacts of vegetation browning resulting from extreme winter weather events in the Arctic has been conducted through field measurements (as discussed in chapter 1). However, field studies in the Arctic region are expensive, spatially restricted, challenging and time consuming (Beamish et al., 2020). Therefore, remote sensing-based approaches provide an opportunity to observe vegetation browning events in the Arctic. Moreover, there is a huge gap when it comes to the current understanding on how satellite vegetation indices (VI) characterise on-ground browning events. This is mainly because such events are comparatively recent, e.g. landscape-scale browning event reported first in 2008 (Bokhorst et al., 2009), and their spatial and temporal sporadic nature makes them hard to study .

'Spectral browning events' have been defined as, "Short-term decreases in the vegetation index that can be attributed to a disturbance such as permafrost thaw or plant dieback" (Myers-Smith et al., 2021, p.109). However, very limited research exists on the type of the satellite VI, e.g., structural or pigment based, most appropriate to quantify an acute decrease in vegetation productivity. Testing the effectiveness of a pigment-based satellite VI to examine browning events is important because in the ecological context vegetation browning has been discussed as an abrupt decline in the photosynthetically-active foliage as a result of vegetation exposure to extreme weather events (Myers-Smith et al., 2021). This explanation of vegetation browning motivates the examination of the impacts of extreme weather events on vegetation using pigment-based VIs, which is undertaken in this chapter.

2.1.1 Chapter Aims and Objectives

This chapter addresses RO1 of this PhD, which is to understand the satellite-based signature of browning events caused by extreme winter weather conditions. This chapter is focused on investigations of browning events observed in low lying Arctic vegetation such as dwarf shrub heathlands consisting of dominant species such as *Empetrum nigrum* and *Calluna vulgaris*. RO1 was achieved through examining the effectiveness of pigment-based and structural satellite VIs at capturing the vegetation disturbance observed on ground following extreme winter weather events. In doing so this research also offers in-depth insights into the potential of satellite VIs to independently identify browning events occurring at complex heterogeneous landscapes such as the Arctic region. Moreover, this research provides much needed insights on the potential of pigments-based satellite VIs in assessing dwarf shrub vegetation state in the Arctic.

2.2 Research Methods

2.2.1 Study sites

The study sites for RO1 make use of previous research on Arctic browning events (Bjerke et al., 2017; Treharne et al., 2020). Because this research is the first to provide in-depth satellite-based understanding of browning events in the Arctic, it was important to select areas where field data have provided clear evidence of vegetation disturbance because of extreme winter weather events. A varying percentage of damaged vegetation cover and intensity has been reported at the study sites by Treharne (2018). Table 2.1 provides study site details and relevant findings of Treharne (2018). Their observations were made in 2016, after a couple of growing seasons had already occurred following the browning events at these sites. Mean damage intensity in Table 2.1 refers to the mean fraction of the dominant vegetation species damaged at each site, relative to neighbouring undamaged vegetation. Figure 2.1 shows the location of the case study sites on the map of Norway, and the inset maps provide an overview of the landform heterogeneity at the study sites. Figure 2.2 provides an overview of

different vegetation bio-physical status at the plot level and helps to understand the spatial scale of the field measurements (50 cm × 50 cm plots).

Table 2.1 RO1 study site characteristics

Study site	² Climatology	Vegetation characteristics (Treharne, 2018)	Extreme winter weather events	Avg. GPP decrease for 2016 growing season (Treharne, 2018)	Mean damage intensity (Treharne, 2018)	Visual indicators of vegetation damage (Treharne, 2018)
1. Flatanger, Trøndelag County 64.4°N, 10.64°E	Dfc (Subarctic)	Evergreen shrubs (67%): <i>Calluna vulgaris</i> (dominant), <i>Vaccinium</i> species and <i>Erica tetralix</i> . Ground cover (30%): <i>Hylocomium splendens</i> and <i>Racomitrium</i> mosses Thin to no tree cover	2013/14 Extreme winter warming and frost drought	35%	66%	Shoot mortality and browned leaves
2. Storfjord, Troms og Finnmark County 69.3°N, 19.93°E	ET (Tundra)	Evergreen shrubs (79%): <i>Empetrum Nigrum</i> . Thin and sparse ground cover (45%): <i>Cladonia</i> lichens, and <i>Polytrichum</i> and <i>Hylocomium splendens</i> mosses	2011/12 Extreme winter warming and frost drought	41%	51%	Wilted and browned leaves
3. Lofoten, Nordland County 68.1°N, 13.76°E	Cfc (Subpolar oceanic)	Evergreen shrubs (75%): <i>Calluna vulgaris</i> and <i>Empetrum Nigrum</i> Ground cover: <i>Hylocomium splendens</i> and <i>Pleurozium schreberi</i> mosses No tree canopy	2013/14 Frost drought 2015/16 Extreme winter warming	37% 23%	NA	Shoot mortality Heavy anthocyanin pigmentation

² For details of the climatology classification see Beck et al. (2018)

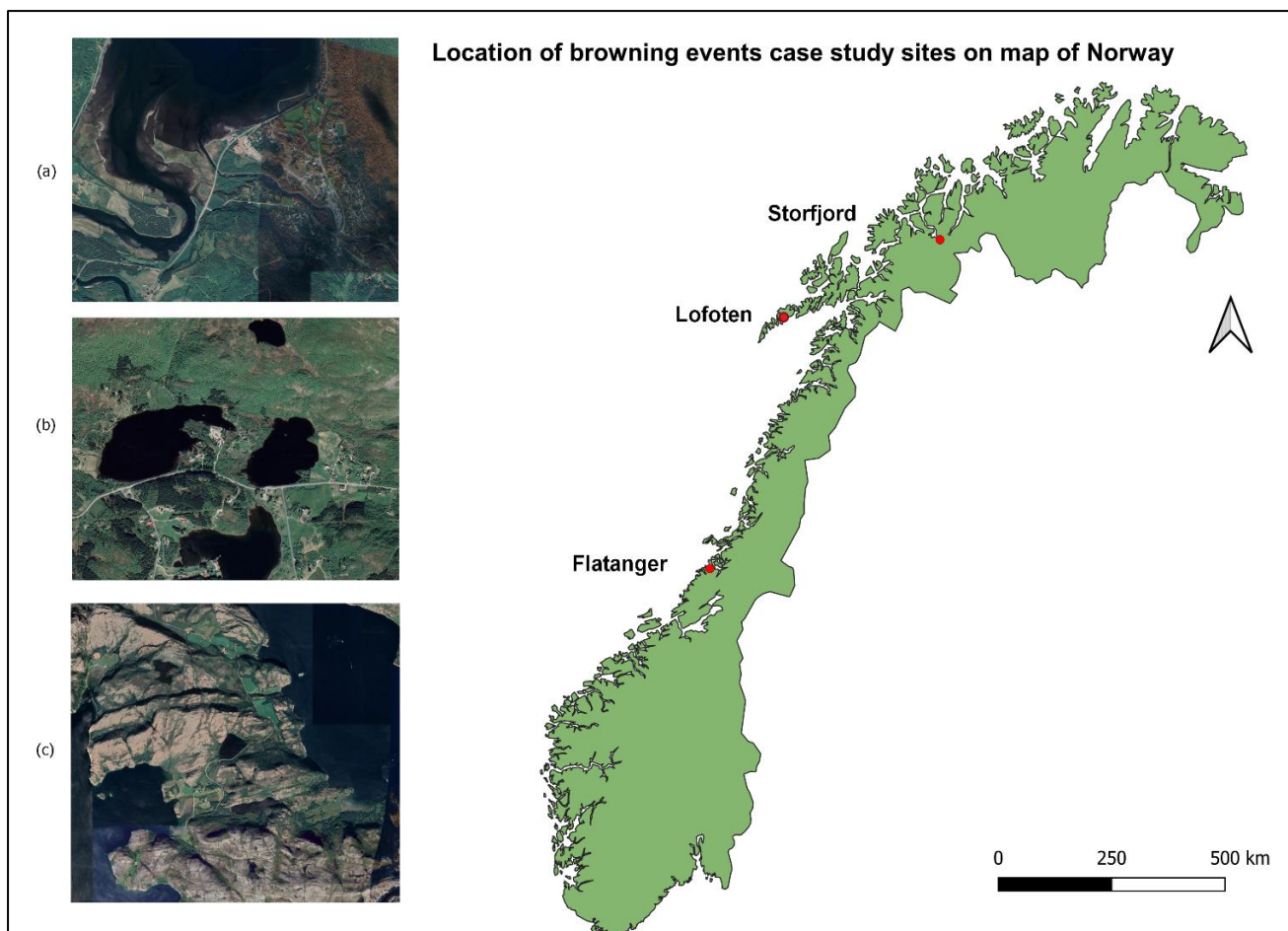


Figure 2.1. Map of Norway showing the point locations of case studies (Red circles) under this research. The left panel (inset maps) show the local study site characteristics. The insets correspond to (a) Storfjord, (b) Lofoten and (c) Flatanger. This map was produced in QGIS.

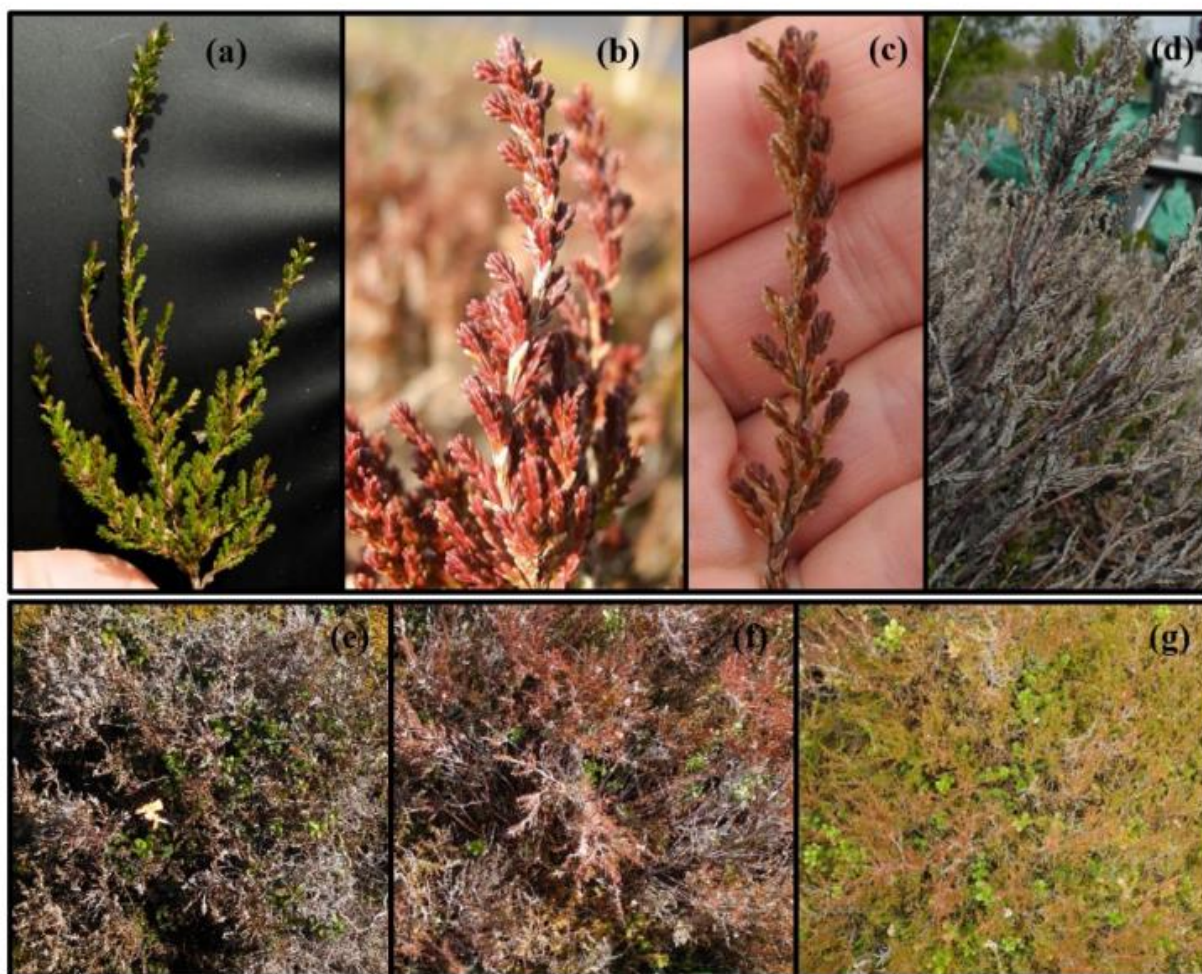


Figure 2.2 Different leaf bio-physical status at the shoot level (a-c) and plot scale (e-g). (a) Green, (b, c) anthocyanin pigmentation, (d) mortality, (e) plots dominated by grey coloured *Calluna vulgaris*, (f) Dark red anthocyanin pigmentation and (g) green control plots (Photo adopted from Treharne (2018))

2.2.1.2 Extreme winter weather conditions at the study sites

The three case study sites experienced different extreme winter weather conditions. These anomalous meteorological conditions are analysed and discussed in detail ahead in chapter 3 (section 3.3.1). A brief description is provided here. Vegetation at the southern maritime area of Flatanger experienced winter warming in December 2013, which resulted in elevated mid-December temperatures, rising up to 10 °C. The consecutive days of above-zero warm temperatures caused complete snowmelt over three weeks in December 2013. The snow melt exposed the vegetation at Flatanger to the return of freezing temperatures in January. The impacts resulting from such exposure have been discussed in chapter 1.

Vegetation damage at Storfjord was first observed in Spring 2012 (Bjerke et al., 2014). This has been attributed to high-temperature variability and frost drought conditions in December – January 2011/12 (Ibid).

The Lofoten study site experienced extensive shoot mortality following several episodes of warm conditions through December 2013 and severely dry conditions over January – March 2014. These conditions lead to desiccation of vegetation over the winter. It is worth noting that vegetation at this site made some recovery over the 2014 growing season (Treharne, 2018). Moreover, this site also experienced anomalous warm conditions in December 2015, with mean weekly temperatures of up to 4.2 °C, as compared to a December mean of -1.2 °C (Treharne, 2018). These warm conditions caused wide-spread loss of snow cover, which was followed by return to freezing temperatures over 1st – 3rd January 2016. These conditions caused strong anthocyanin pigmentation in the dominant species *Calluna vulgaris* at various locations across the Lofoten islands (Ibid).

It is important to note here that this chapter is focused on understanding the spectral signature of on-ground vegetation damage, rather than the analysis of the extreme winter weather events which caused the damage. The characteristics of the extreme weather conditions described in this chapter are based on previous research. Chapter 3 of this thesis provides in-depth analysis of the characteristics of the extreme winter weather conditions at each case study site.

2.2.2 Data

The satellite VIs used in this research were the Normalized Difference Vegetation Index (NDVI) and the Chlorophyll Carotenoid Index (CCI). Both were derived from the Moderate Resolution Imaging Spectroradiometer (MODIS), on-board Aqua and Terra satellites. MODIS is a medium to coarse spatial resolution satellite (250-1000 m pixels), offering daily observations on a global scale. All MODIS surface reflectance datasets have achieved a stage 3 validation which implies that these datasets are robust enough for scientific use (Wang et al., 2018). Although the spatial resolution of MODIS is coarser as compared to sensors such as Landsat and Sentinel, it has been argued to be one of the most viable

satellite data sources for the Arctic region (Karlsen et al., 2018). It enables the acquisition of higher amounts of imagery despite these regions being exposed to extensive cloud cover and fog all year round and especially during the growing season (Ibid). The NDVI dataset used in this chapter was MOD13Q1.006, which has a 250 m spatial resolution and 16-day temporal resolution. More details about this product can be found at [LP DAAC - MOD13Q1 \(usgs.gov\)](https://lpdaac.usgs.gov/products/mod13q1/).

One of the main advantages of using MODIS for this research was that it offers a band width i.e., Band 11 (526 - 536 nm), precisely centred at one of the wavelengths (531 nm) used in the CCI calculation. For CCI, the surface reflectance datasets were processed to obtain only cloud-free days. Following this a view zenith angle (VZA) correction was applied as well. This correction rectifies noise introduced by the bidirectional reflectance distribution function (BRDF). BRDF is a technical aspect of remote sensing related to effects arising from sensor view angle, sensor position and solar position. The VZA correction consisted of removal of observations with VZA < 45° (Wang et al., 2020). The resulting CCI algorithm was validated by calibrating values directly against locations and data used in Wang et al. (2020). Due to the nature of the wavelengths used (specifically Band 11), the final CCI product was calculated with a spatial resolution of 1000 m.

CCI was estimated as,

$$CCI = \frac{B_{11} - B_1}{B_{11} + B_1} \quad (\text{Gamon et al., 2016})$$

The CCI observations were then standardized, to be comparable with the NDVI (Rahman et al., 2004).

Hence the range for the CCI is 0 to 1, as is for the NDVI.

$$\text{Standardized CCI} = \frac{CCI+1}{2}$$

Table 2.2 MODIS VIs used in this research

Vegetation Index	Dataset	Spatial and temporal resolution
NDVI	MOD13Q1.006	250 m, 16 day
CCI	MYD09GA.006 MYDOCGA.006	1000 m, variable

It is worth noting that the spatial resolution of the NDVI and CCI datasets was different in this research, as explained above. The role of spatial resolution of VIs has been widely discussed within the remote sensing literature. For example Ji et al. (2010) studied varying resolutions of MODIS NDVI (0.25 – 10 km), of vegetation in Alaska, and have recommended NDVI at a 0.25 km resolution for examining vegetation changes at a local scale and 5 – 10 km resolution for regional and continental scales.

Both the NDVI and the CCI were obtained for the duration of the growing season at each of the study sites. The growing season for this research is considered as June – September, as per Treharne (2018). All datasets were accessed and processed using Google Earth Engine and RStudio.

2.2.3 Methodology

This section describes the steps followed to achieve RO1. This research assesses the effectiveness of two satellite VIs in detecting and quantifying on-ground reported vegetation disturbance in the aftermath of extreme winter weather events. Based on the findings of previous studies related to the impacts of extreme weather events on vegetation in the Arctic and sub-Arctic regions (see section 2.1), it was hypothesised that satellite VIs could present the spectral signal of a browning event in one or more of the following ways.

1. H1: Gross, anomalous changes to the whole growing season
2. H2: Changes to the start of the growing season [assumed that it may begin earlier or end later]
3. H3: Changes to the timing of peak productivity in a growing season
4. H4: Changes in photosynthetic activity at the peak of growing season
5. H5: Changes in productivity at the end of growing season, as a measure of compensation growth

To investigate H1, the first step was generating box plots of the NDVI and CCI timeseries for visual assessment of the full range of observations, e.g., median, maximum, minimum and outliers, of each growing season over 2002-2019, at the study sites. Following visual interpretations of the VI timeseries,

the next step in addressing H1 was to determine whether the VI distribution of the browning year-growing season (referred as BY here onwards), was statistically different from the historic average distribution, of the VI at each study site. The browning year here is considered as the year in which vegetation damage was observed. The distributions were compared through the Wilcoxon signed-rank test, a non-parametric test, used to determine whether the population distributions of two data samples, originating from repeated observations of the same subject, are different (Wilks, 2011). For the Wilcoxon signed-rank test, the null hypothesis was, H_0 = The VI distribution of a BY growing season is identical to the mean growing season. If $p < 0.05$ (the significance level), the null hypothesis is rejected.

With regard of H2 – H5, the next stages of the analysis consisted of understanding the potential effects of the extreme winter weather events on each phase of the phenological cycle of the disturbed vegetation at the study sites. Hence each stage of the phenological cycle of a BY was compared with that of the other years. For this the CCI and NDVI timeseries were categorized into three stages, Start of Season (SOS), Peak of Season (POS) and End of Season (EOS). Figure 2.3 presents a general depiction of distinct stages of the growing season in the Arctic. This temporal characterization is important because it helps to better understand the nuanced effects of a changing climate on vegetation productivity in context of the very short Arctic growing season. Quantifying the changes in phenology of vegetation in the Arctic has proved an effective way to understand vegetation's response to a changing climate (Wang et al., 2018). Therefore phenological transition dates were extracted separately for each case study site since these can significantly vary across different landscapes (Wang et al., 2018). The phenology transition dates were determined using TIMESAT, which is a tool widely used for deriving phenological parameters from VI timeseries (Jönsson and Eklundh, 2004). Different fitting methods/smoothing functions are available to use within the TIMESAT interface to extract phenological metrics. These include Asymmetric Gaussian (AG), Double Logistic (DL) and Savitzky-Golay (SG) functions. Details about these functions can be found in Eklundh and Jönsson (2017). All three functions have been found to be spatially consistent (Lara and Gandini, 2016). For this research

phenology metrics based on the AG function were selected after evaluating the three functions at one of the case study sites (Flatanger). Although the results of the three fitting methods were highly similar, the AG fitted timeseries best matched the case study VI. Moreover, a caveat to using the DL function was that it does not capture the changes in productivity due to extreme events (Ibid). The AG function is a semi-local method, which performs well even for timeseries with inter-annual variations (Eklundh and Jönsson, 2017).

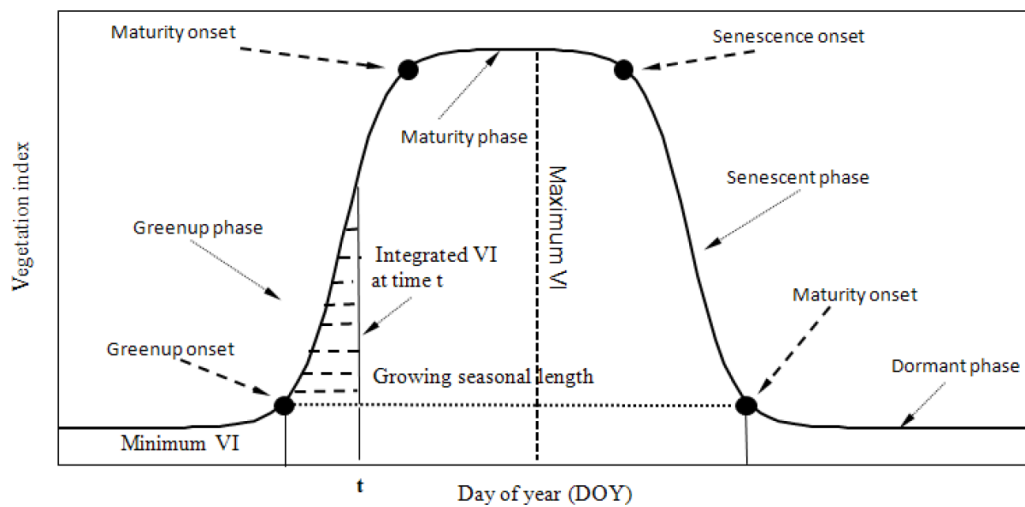


Figure 2.3 The main phenological stages in the annual growth cycle of vegetation, as represented by satellite VIs (Zhang et al., 2012)

Following the TIMESAT phenology extraction, mean and standard deviations of both NDVI and CCI, were estimated for each stage of the growing season for each study site. These steps helped to quantify the spectral signal for on-ground reported vegetation disturbance; and also assisted in characterising the shared and unique aspects of NDVI and CCI, which are important to consider in implementing a complementary, satellite-based approach to study Arctic browning events.

2.3 Results

This section first presents the results for the Flatanger study site, followed by the results for the Storfjord and Lofoten study sites. Next, a comparison of the results across the three sites is presented.

2.3.1 Flatanger

2.3.1.1 Satellite-based detection of browning events

A strong and clear decrease was seen in both CCI and NDVI for the full growing season observations in the browning year, 2014, at Flatanger.

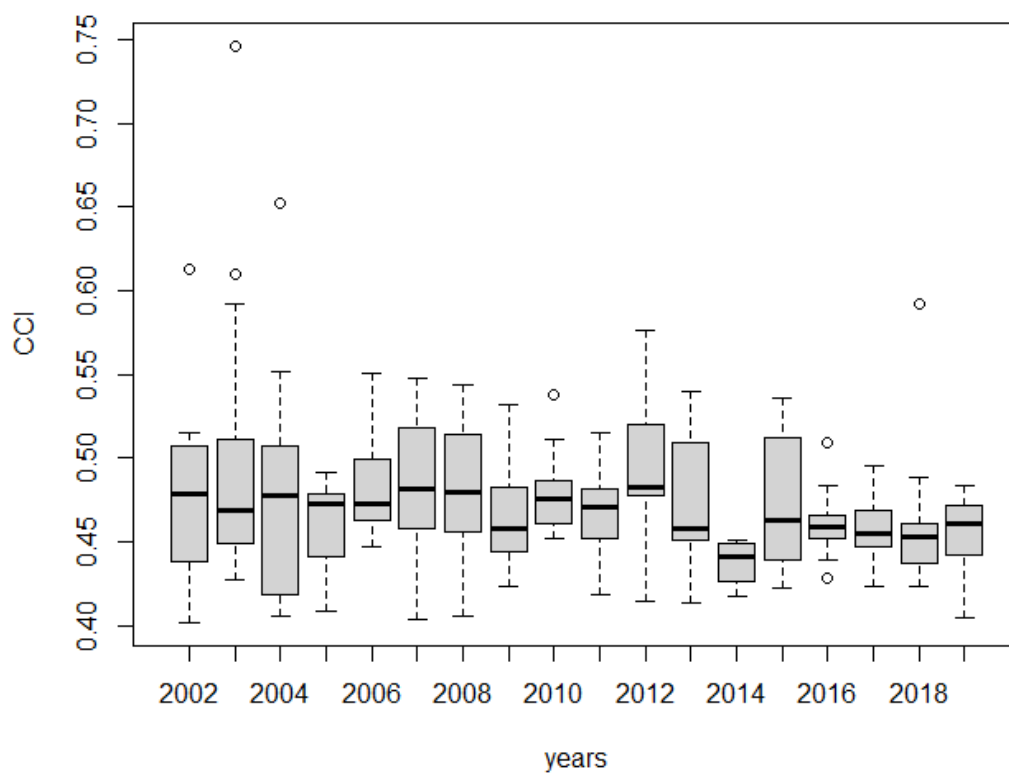


Figure 2.4 (a) Growing season distribution for CCI at the Flatanger study site. Boxes show the median and interquartile range, whiskers present minimum and maximum values, and the circles denote outliers.

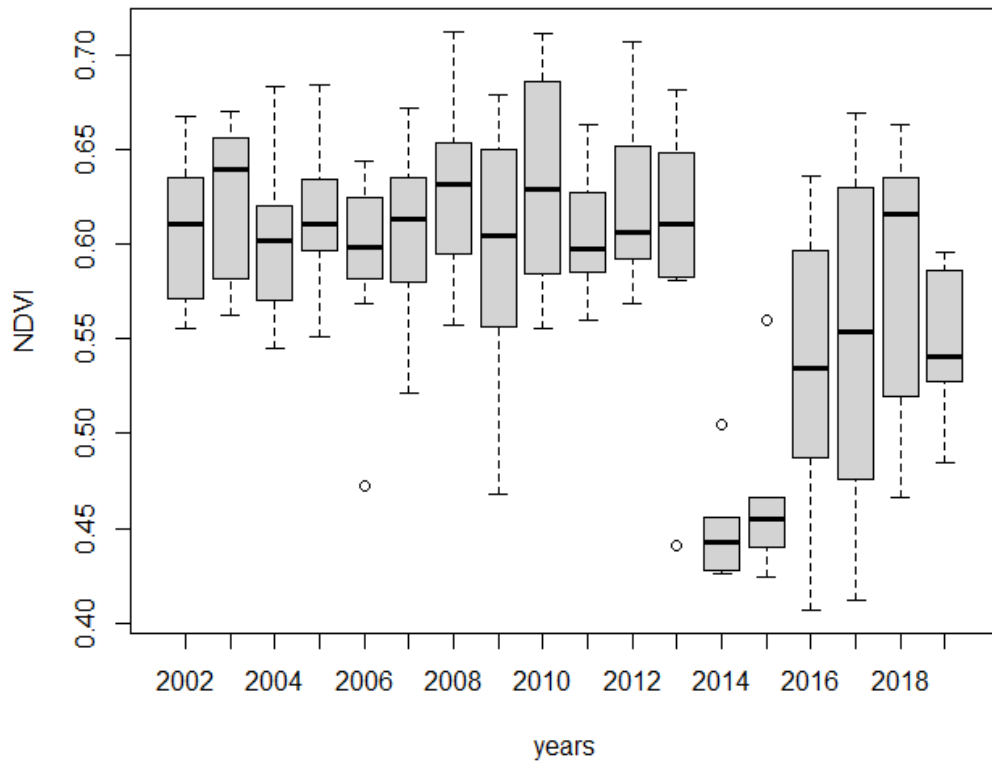


Figure 2.4 (b) Growing season distribution for NDVI at the Flatanger study site. Boxes show the median and interquartile range, whiskers present minimum and maximum values, and the circles denote outliers.

Figure 2.4 (a) and (b) present the growing season distribution of CCI and NDVI respectively, for the Flatanger study site. These figures address H1. Visual inspection of the VI timeseries showed a signal for the on-ground observed browning event in terms of a sudden, marked decrease in the VI timeseries. The box plots showed that for both CCI and NDVI, 2014's entire range of growing season observations were the lowest values over the time period of 2002-19.

Figure 2.5 presents the average growing season trajectory (2002 – 19), and the BY (2014) growing season trajectory for CCI at the Flatanger study site. Similarly Figure 2.6 presents these for NDVI. These diagrams were produced to address H1 of this chapter. Both figures showed that the BY trajectories were different from the average growing cycle of the VIs at this site. With regards to the BY CCI a distinct peak of the season was not observed as can be in the average trajectory. In context of the BY NDVI a steeper rate of growth and decline were observed, as compared to a stable and longer period of higher NDVI values of the average growth cycle. This altered pattern of the growth curve reflects

how more than 50% of the dominant species which were damaged at this site (Treharne, 2018), struggled to attain the normal annual maximum productivity levels.

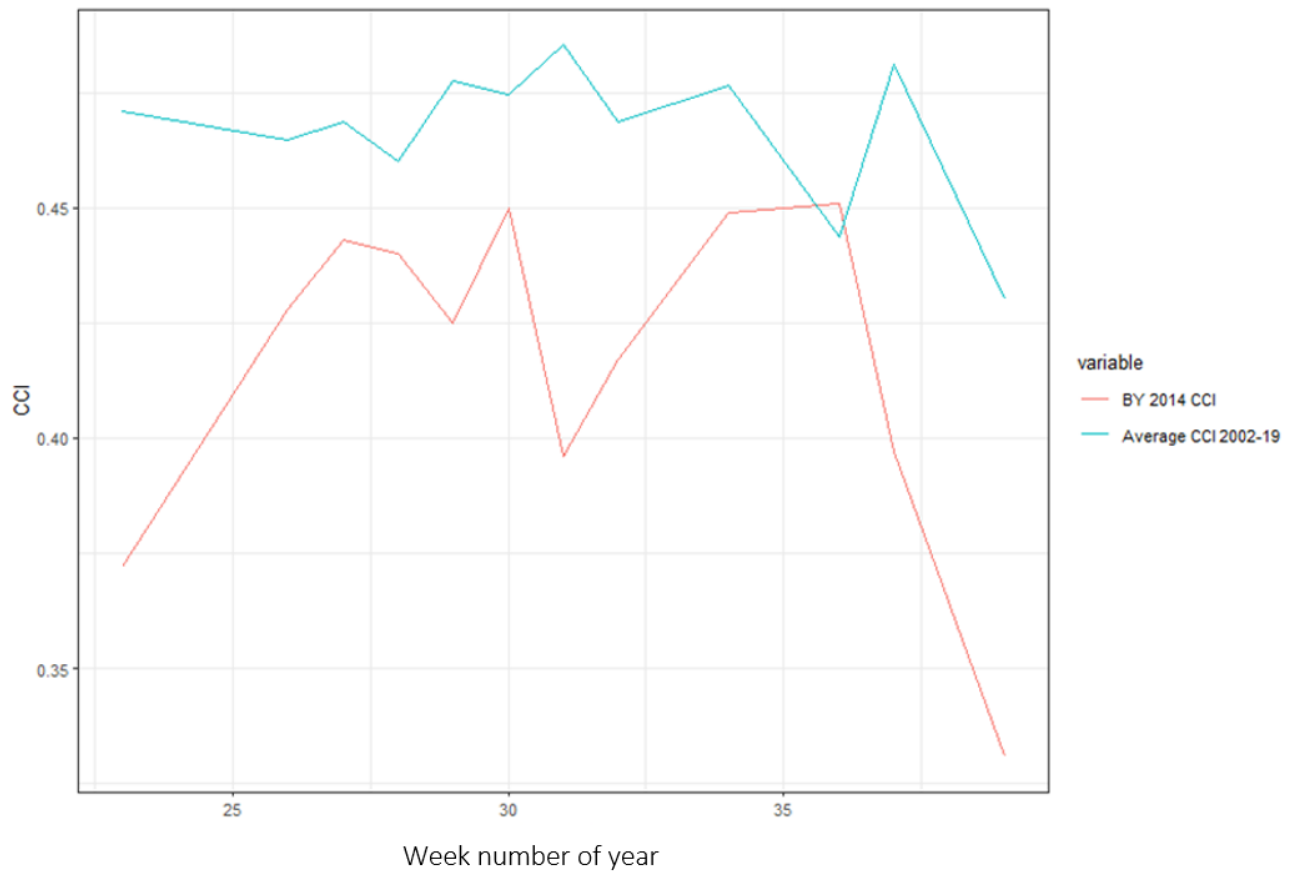


Figure 2.5 Average growing season trajectory (2002 – 19), and the BY (2014) growing season trajectory for CCI at the Flatanger study site

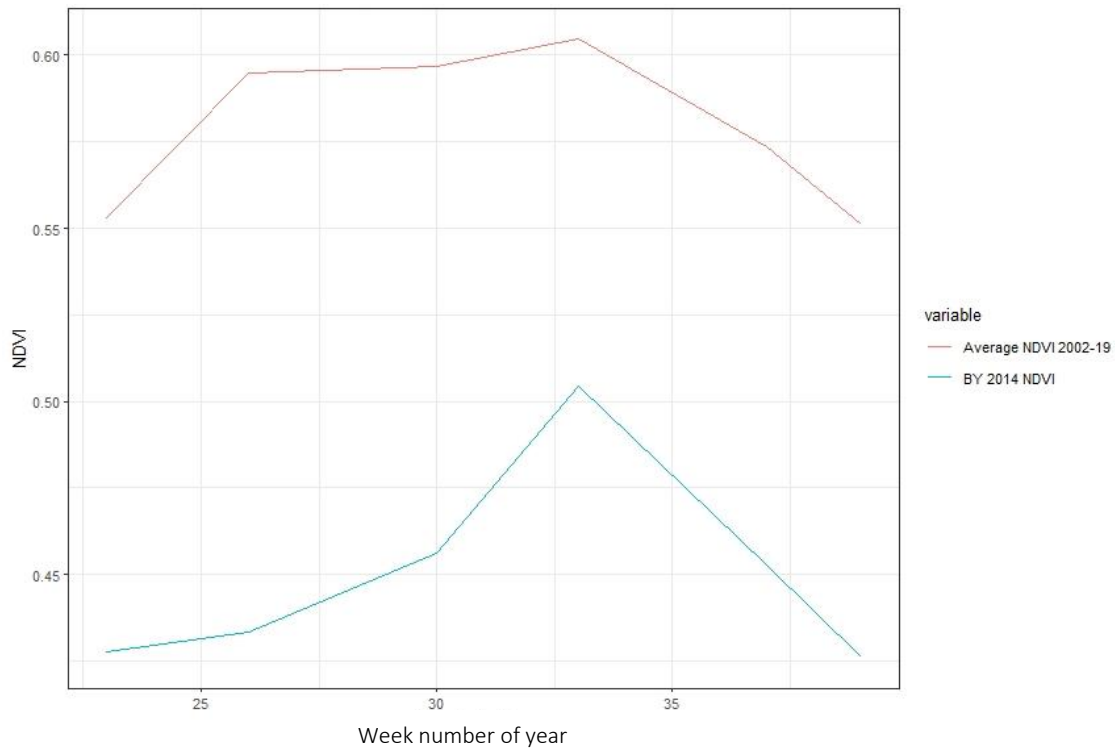


Figure 2.6 Average growing season trajectory (2002 – 19), and the BY (2014) growing season trajectory for NDVI at the Flatanger study site

Wilcoxon signed-rank test results

The Wilcoxon signed-rank test was also conducted to address H1 under this chapter. The results showed that the growing season NDVI distribution of both, BY 2014 and the recovery year 2015 were significantly different ($p < 0.05$) from the average growing season (2002-2019) at the Flatanger study site. On the other hand, for CCI, only 2014 was significantly different compared with the 2002 – 2019 average growing season CCI. These results reinforced the earlier visual interpretations of the VI timeseries in Figures 2.4 – 2.6.

Figure 2.7 presents the maximum CCI and NDVI for each growing season at Flatanger. Maximum NDVI has been widely used for Arctic vegetation assessment as it represents the annual peak photosynthesis activity (Bhatt et al., 2018). This figure is related to H4 of this chapter. A noticeable decrease was seen for 2014, which measured the lowest value in both VI timeseries over the time period 2002 - 2019.

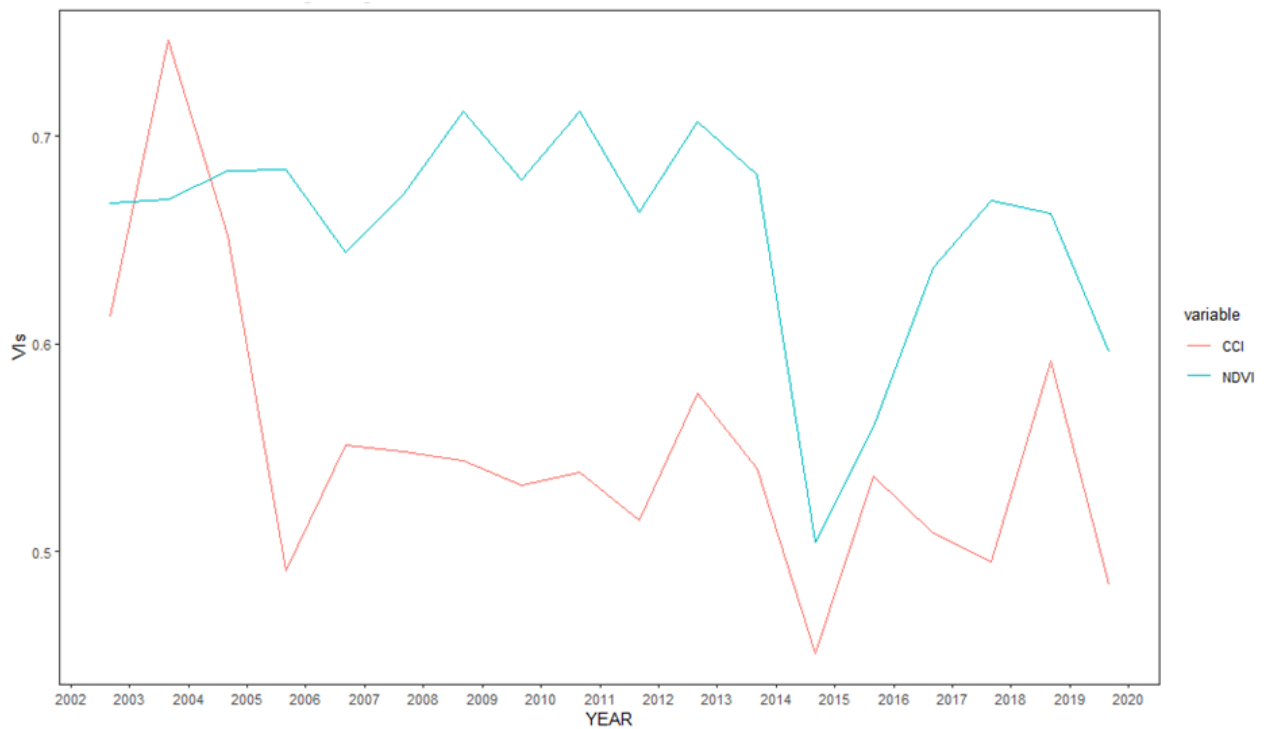


Figure 2.7 Maximum CCI and NDVI of each growing season 2002-19 at the Flatanger study site

Spectral vegetation recovery trends

Damaged Arctic vegetation, resulting from exposure to extreme winter weather events, has been shown to recover over the next couple of growing seasons (Bokhorst et al., 2012). However, the recovery trend is not necessarily a uniform, gradual increase in productivity of the damaged vegetation. It is dependent on multiple factors such as the severity of the damage, vegetation's natural tolerance of extreme weather and seasonal scale meteorology during the growing season. One of the aspects of robustly identifying a browning event within a long-term satellite VI timeseries was to check for a recovery trend following a sudden sharp decrease. Moreover, given the inherently different algorithms used for CCI and NDVI, it was hypothesised that the recovery trend might be different. While CCI showed a strong increase for the year following the browning event, i.e., 2015, however, NDVI showed a clear recovery trend over 2015-2016 in terms of gradual increase in the index values (Figures 2.4 (a) and (b)).

The VI timeseries behaviour in Figure 2.4 showed that CCI's spectral signal with regards to capturing the impacts of an extreme winter weather event was short-lived, appearing at a seasonal scale, with no discernible lowering of productivity in 2015. Whereas NDVI retained the continuing effects of the 2014 browning event at slightly longer, annual time scale, by being able to measure the lowered productivity in 2015. These results mean that the pigmentation-based response of vegetation to extreme winter weather event/s, in this case a combination of winter warming and frost drought conditions, can be monitored in the short-term only. Whereas the impacts on the overall green biomass of the canopy, arising from such meteorological conditions, are comparatively easier to monitor given that the structural impacts last longer.

2.3.1.2 Phenology

Figures 2.8 – 2.10 present a comparison of the different growing season stages of CCI and NDVI in 2014 (BY) with other years, for Flatanger. Figures 2.8, 2.9 and 2.10 address H2, H3 and H4 together, and H5, respectively. The overall objective of these figures was to examine whether the spectral browning signature was stronger and clearer at a particular stage of the growing season. The phenological metrics here were extracted using TIMESAT. The VI timeseries span in these figures is 2004 – 17. This is different compared to earlier figures due to TIMESAT's processing methods.

The BY NDVI was the lowest at every stage of the growing season. Moreover, a clear signal was seen for the recovery year (RY) NDVI as well, with its values being very similar to the BY NDVI. On the other hand, the BY CCI could not be differentiated from the other years through visual inspection, at any stage. In the context of H2, both NDVI and CCI in the BY occurred earlier, implying an earlier start to the growing season. With regards to H3 it was interesting to note the difference between TIMESAT suggested BY POS CCI and the BY MaxCCI based on the original CCI timeseries (Figure 2.7). While based on the original CCI timeseries, the BY MaxCCI was the lowest for 2002 – 19, however the BY POS CCI of the TIMESAT fitted POS stage was not the lowest (Figure 2.9). The difference between MaxCCI and TIMESAT POS CCI could be due to the inherent design of TIMESAT to detect seasonality parameters

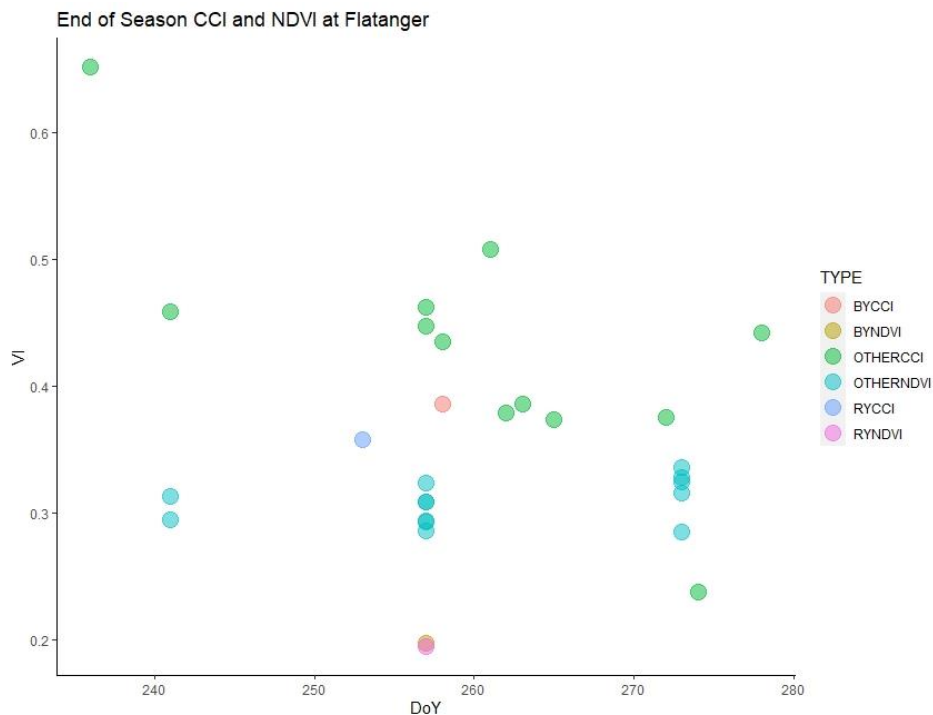


Figure 2.10 End of growing season VI observations for Flatanger. BY refers to browning year, meaning the year in which vegetation damage occurred; and RY refers to recovery year, following the BY.

It was worth noting that CCI showed a large variation in the annual phenology transition dates, as well as in the observed values at each stage. On the other hand, NDVI showed a rather compact distribution of the transition dates and values range at each stage. The larger seasonal variations in CCI, as compared to NDVI, are reflective of CCI's sensitivity to subtle changes in the carotenoid and chlorophyll pigments, and its capacity to track the changes in seasonal GPP more carefully than NDVI. These observations agreed with previous research. Wang et al. (2020) found that CCI more closely followed a delay in attaining the peak photosynthetic activity of a grassland as compared to NDVI and thus showed a more dynamic relationship with GPP.

The results presented here with regards to NDVI detecting reduced vegetation productivity at SOS (H2), POS (H3) and EOS (H5), agreed with (Zhang et al., 2018) in a way that they found NDVI to better represent the canopy's overall structural greenness across different sites in North America.

Visual inspections of the indices in Figures 2.8 – 2.10 were confirmed by comparing the BY VI observations against, the long-term average and standard deviation, estimated for each stage of the

growing season, respectively. Figure 2.11 shows the mean and standard deviation estimated for SoS, PoS and EoS at Flatanger. These calculations were based on the phenological transition dates extracted by TIMESAT. The BY NDVI at each stage was lower than the mean, and well outside ± 1 standard deviation. Whereas the BY CCI lied within ± 1 standard deviation and closer to the mean at each stage respectively.

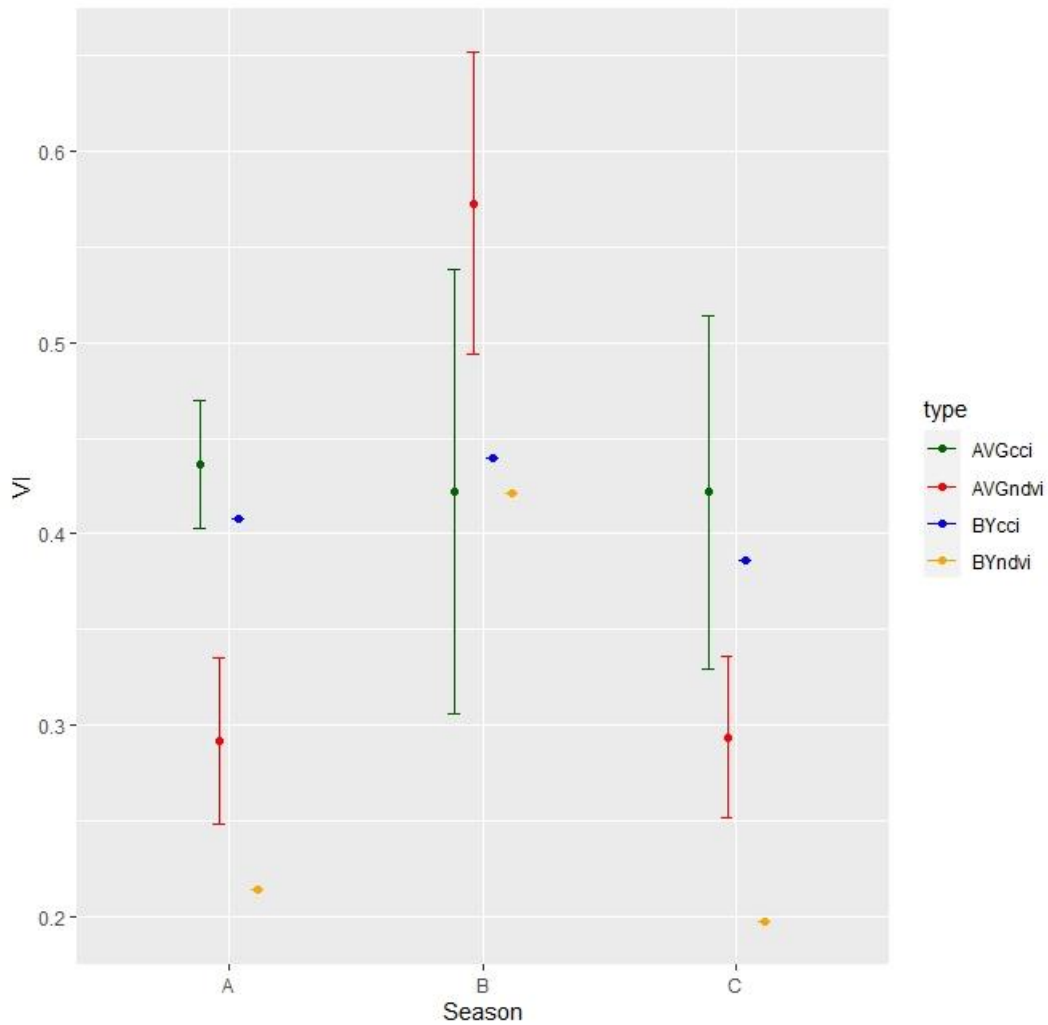


Figure 2.11 Mean and standard deviation of each stage of the growing season, for Flatanger study site. The vertical bars denote ± 1 standard deviation, and the circles within the bars denote the mean.

A=Start of growing season, B= Peak of growing season and C=End of growing season

2.3.2 Storfjord

2.3.2.1 Satellite-based detection of browning events

A robust spectral browning event signal was observed for the vegetation damage at Storfjord study site in the BY 2012 in the NDVI, but not in the CCI

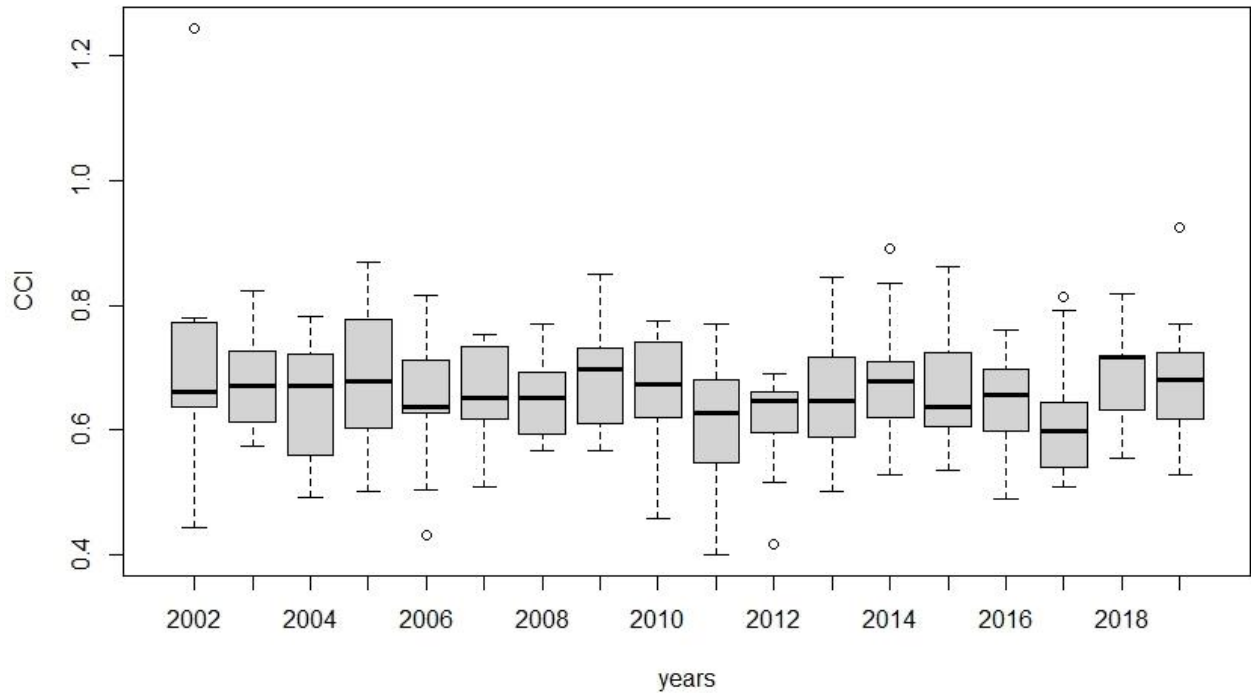


Figure 2.12 (a) Growing season distribution for CCI at the Storfjord study site respectively. Boxes show the median and interquartile range, whiskers present minimum and maximum values, and the circles denote outliers

Vegetation damage was observed at Storfjord after spring snowmelt in May 2012, following severely dry and high-temperature variability conditions in December and January 2011/12 (Bjerke et al., 2014).

Figure 2.12 shows the annual growing season CCI and NDVI range for the Storfjord study site, and addresses H1 under this chapter. The overall range of CCI for the 2012 growing season didn't visually stand out as particularly different or decreased. In contrast to CCI, NDVI presented a strong, clearly noticeable decrease for 2012.

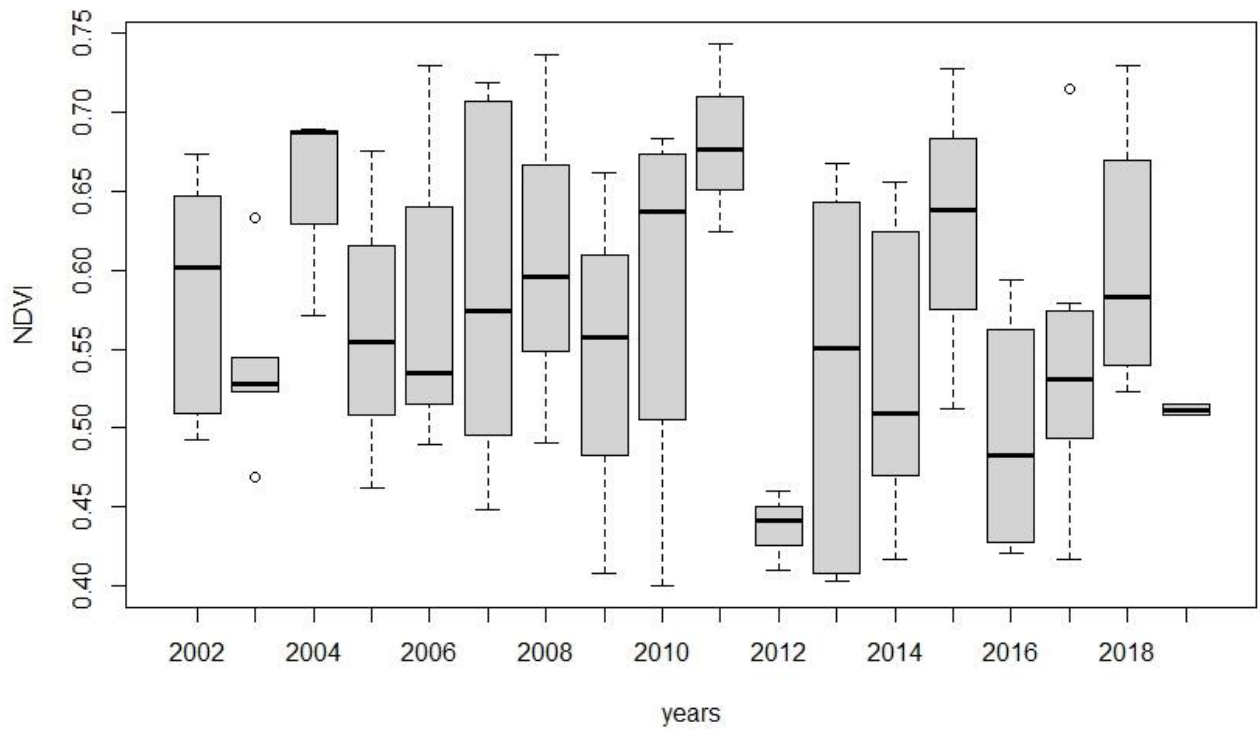


Figure 2.12 (b) Growing season distribution for NDVI at the Storfjord study site respectively. Boxes show the median and interquartile range, whiskers present minimum and maximum values, and the circles denote outliers.

Figure 2.13 presents the trajectories of the average growing season over 2002 – 19, and the BY (2012) growing season, for CCI at the Storfjord study site. Similarly Figure 2.14 presents these for NDVI. These diagrams were produced to address H1 of this chapter.

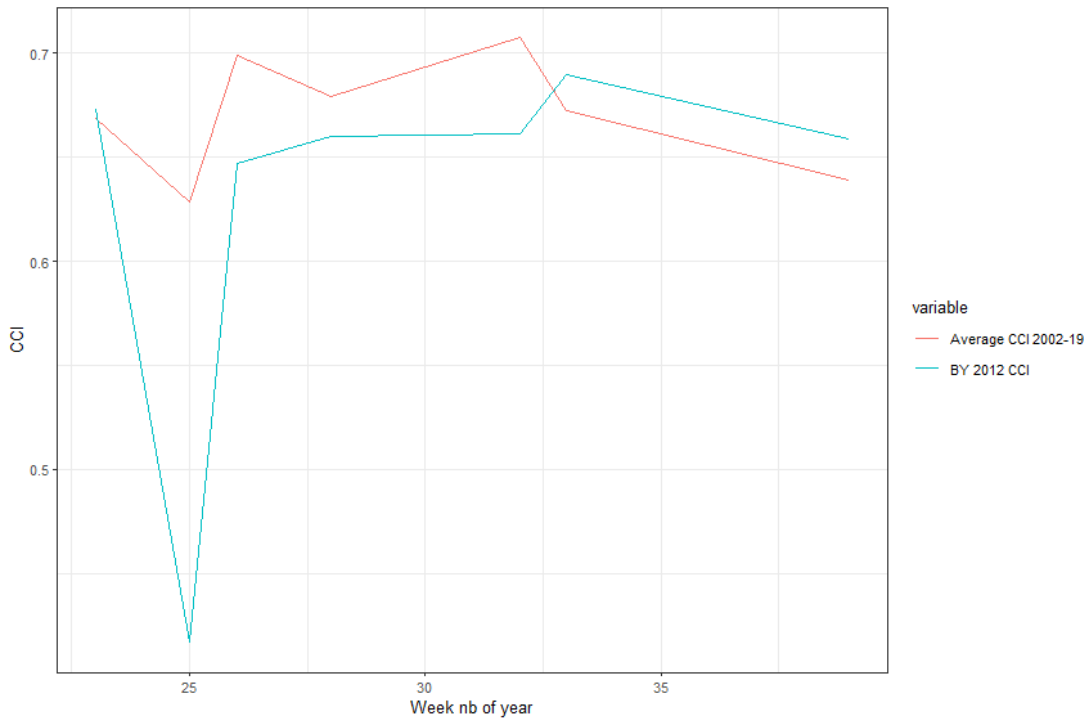


Figure 2.13 Average growing season trajectory (2002 – 19), and the BY (2012) growing season trajectory for CCI at the Storjord study site

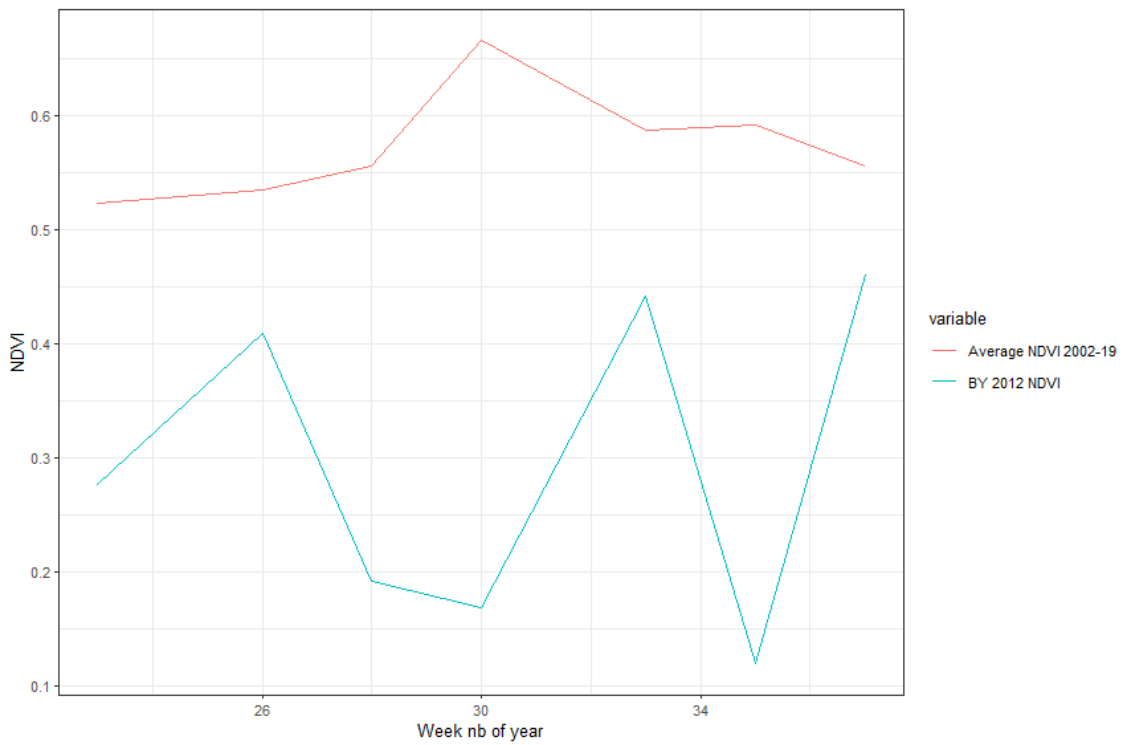


Figure 2.14 Average growing season trajectory (2002 – 19), and the BY (2012) growing season trajectory for NDVI at the Storjord study site

The BY CCI trajectory was quite similar to the average growing season cycle at Storfjord, other than a sharp decrease early in the season. Although the CCI timeseries were processed to remove cloud and low sun angle effects, it is still possible that this decrease might be related to spectral noise. On the other hand, the overall BY NDVI trajectory had lower values and did not have a distinct peak productivity stage compared to the average growing season trajectory of NDVI. It is worth noting that besides the vegetation being damaged at this site, there could be other factors as well associated with the large sub-seasonal fluctuations of NDVI in 2012 at Storfjord. These factors can include changes in meteorological conditions at the site level and/or role of the moss communities. Mosses are integral components in Arctic understories and community production (May et al., 2018). The presence of *Hylocomium splendens* mosses within the understory at Storfjord could have played a role in the seasonal NDVI fluctuations because there is evidence of strong links between rapid changes in moisture content of these species and changes in NDVI (Ibid). However, examining the role of such factors was beyond the scope of this research.

[Wilcoxon signed-rank test results](#)

The Wilcoxon signed-rank test was also conducted to address H1 under this chapter. The test results showed that the NDVI distribution of 2012 growing season was significantly different ($p < 0.05$) from the average growing season (2002-2019) at the Storfjord study site. However, the 2012 growing season measured through CCI was not statistically different compared to the average CCI. This reinforces the visual interpretations of the VI timeseries in Figures 2.12 – 2.14.

One of the potential reasons for the BY growing season CCI not being statistically different from the average at Storfjord, could be due to limited number of observations. The number of observations at a site can get reduced significantly as result of corrections applied to account for cloud contamination and view zenith angle (VZA) processing, which were applied to the CCI timeseries here, before conducting the analysis. MODIS derived CCI timeseries have previously been shown to be reduced by up to 46% as a result of VZA filtering (Wang et al., 2020). In the case of Storfjord CCI timeseries, the

cloud and VZA combined corrections resulted in removal of 70% of the data. Hence data limitations influenced the results of CCI at Storfjord.

Figure 2.15 shows the maximum CCI and maximum NDVI values, which denote the peak photosynthesis, of each growing season, for the Storfjord site. This figure was produced under H4 of this chapter. The 2012 maximum CCI and maximum NDVI values were the lowest for the 2002-19 time-period, indicating that changes in photosynthetic activity at the peak of the growing season are evident in both indices.

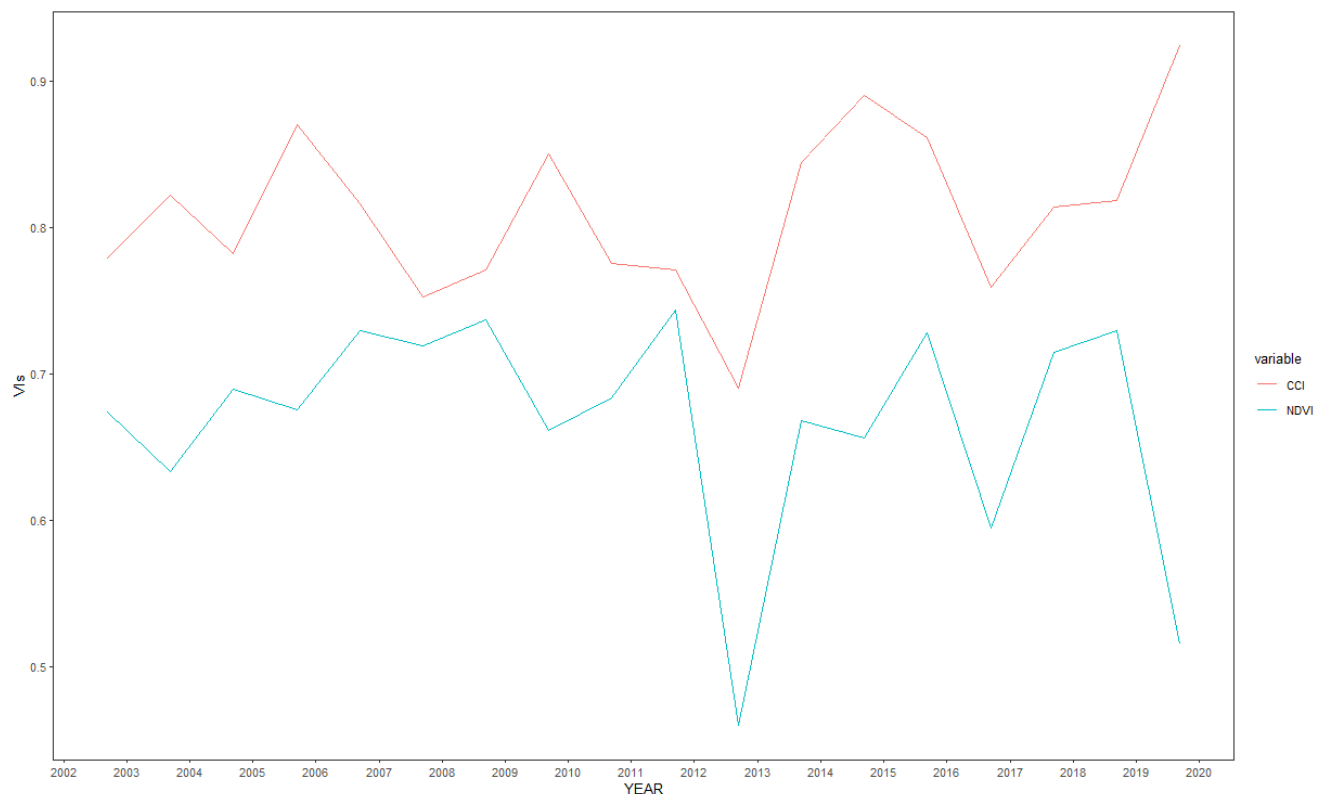


Figure 2.15 Maximum CCI and NDVI of each growing season 2002-19 at Storfjord study site

Spectral vegetation recovery trends

As also discussed for Flatanger, one of the factors in detecting a browning event within a long-term satellite VI timeseries was to examine the recovery trend following an anomalous decrease in the VI observations for a growing season. For Storfjord a rather peculiar trend was seen for the NDVI timeseries, in the context of a recovery trend. While a strong decrease was seen for 2012 growing

season, followed by a continuous recovery over the 2013-15 time period, a noticeable decrease was spotted again for 2016. While Treharne (2018) have attributed the vegetation disturbance at Storfjord, as studied in 2016, to the extreme winter weather events in 2011/12; the NDVI timeseries in this research showed contradicting observations. A review of literature on Arctic extreme weather highlighted that the 2015/16 winter was the warmest Arctic winter on-record and at a regional scale at that time (Cullather et al., 2016; Overland and Wang, 2016). To verify whether the abrupt decrease in the NDVI in 2016, was in fact due to an additional extreme winter weather event and not mainly due to the 2011/12 event, mean and maximum air temperature, and snow depth of the nearest meteorological station to the Storfjord study site were extracted. These meteorological variables are shown in Figure 2.16.

Based on these meteorological station observations, two winter warming events could have occurred in March 2016. First was in mid-March, where the mean air temperature stayed above 0°C for five consecutive days, then dropped to well under 0°C. The second possible winter warming event was at end of March with temperatures staying above 0°C for seven consecutive days. The snow depth observations have a time period of missing data between 9th Feb - 9th March. Moreover, this was not the time period when the winter warming events have occurred anyway. The snow depth observations in mid and end of March show a variable snow depth and instances of complete snow melt as well. This could have caused ground-icing, which is known to cause damage to vegetation. Keeping ahead the Storfjord study site NDVI timeseries, meteorological observations of the nearest station and published literature regarding the 2015/16 Arctic winter, it is most likely that the damage in 2016 growing season was caused by the variable high-temperature episodes in 2015/16 winter, and that the vegetation at this site had actually recovered from the 2011/12 damage.

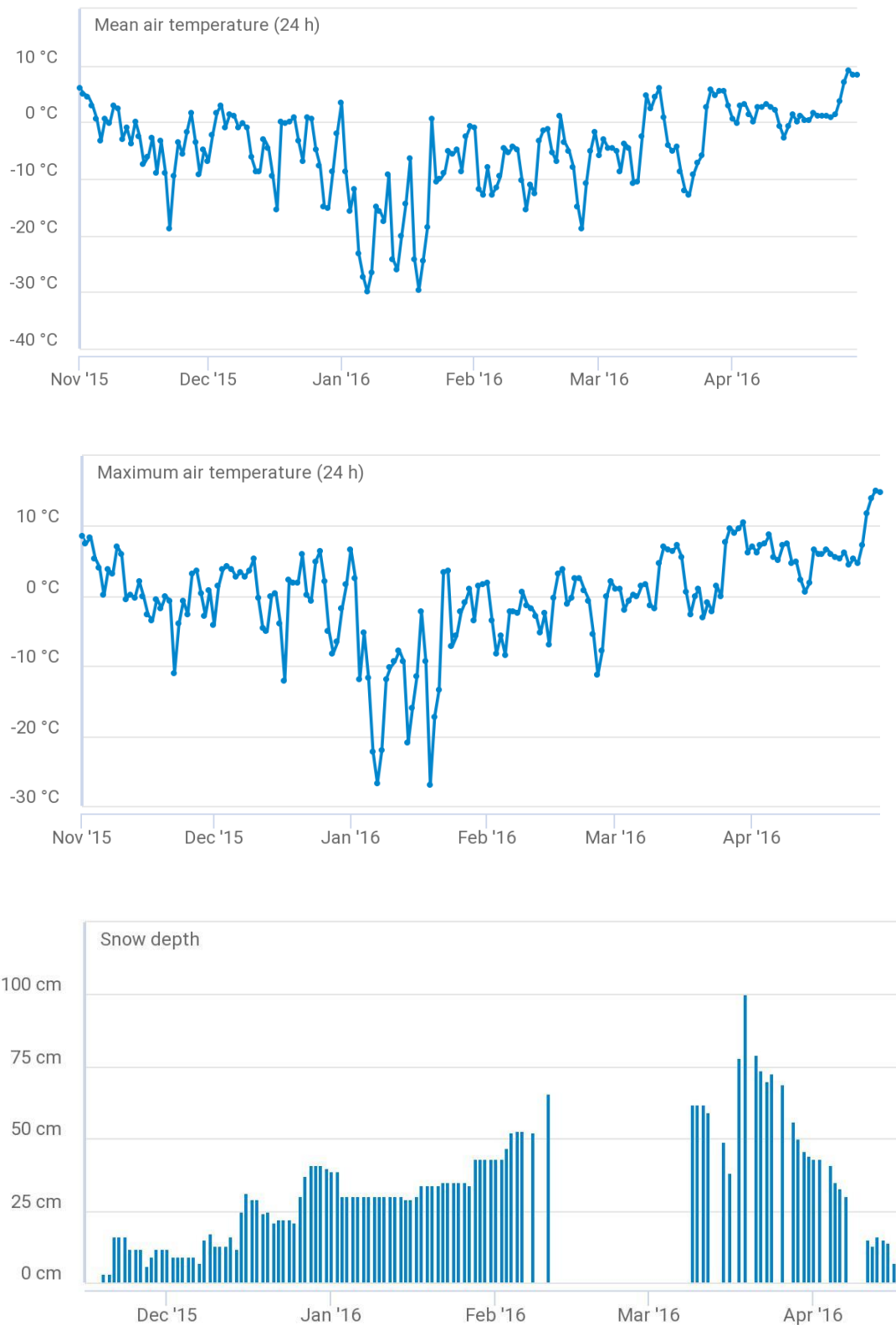


Figure 2.16 Mean air temperature, snow depth and maximum air temperature for November 2015 – April 2016; as extracted from the meteorological station nearest to the Storfjord study site. The elevation of the station, SN 89350, was 76m a.s.l (Source: Norwegian Centre for Climate Services)

2.3.2.2 Phenology

Figure 2.17 – 2.19 present a comparison of the BY CCI and NDVI with other years, at the three different stages of the growing season, for the Storfjord study site. Figures 2.17, 2.18 and 2.19 address H2, H3 and H4 together, and H5, respectively. These plots were produced based on phenological metrics extracted using the TIMESAT tool. The VI timeseries span is 2004 – 18. This is different compared to earlier figures due to TIMESAT's processing methods.

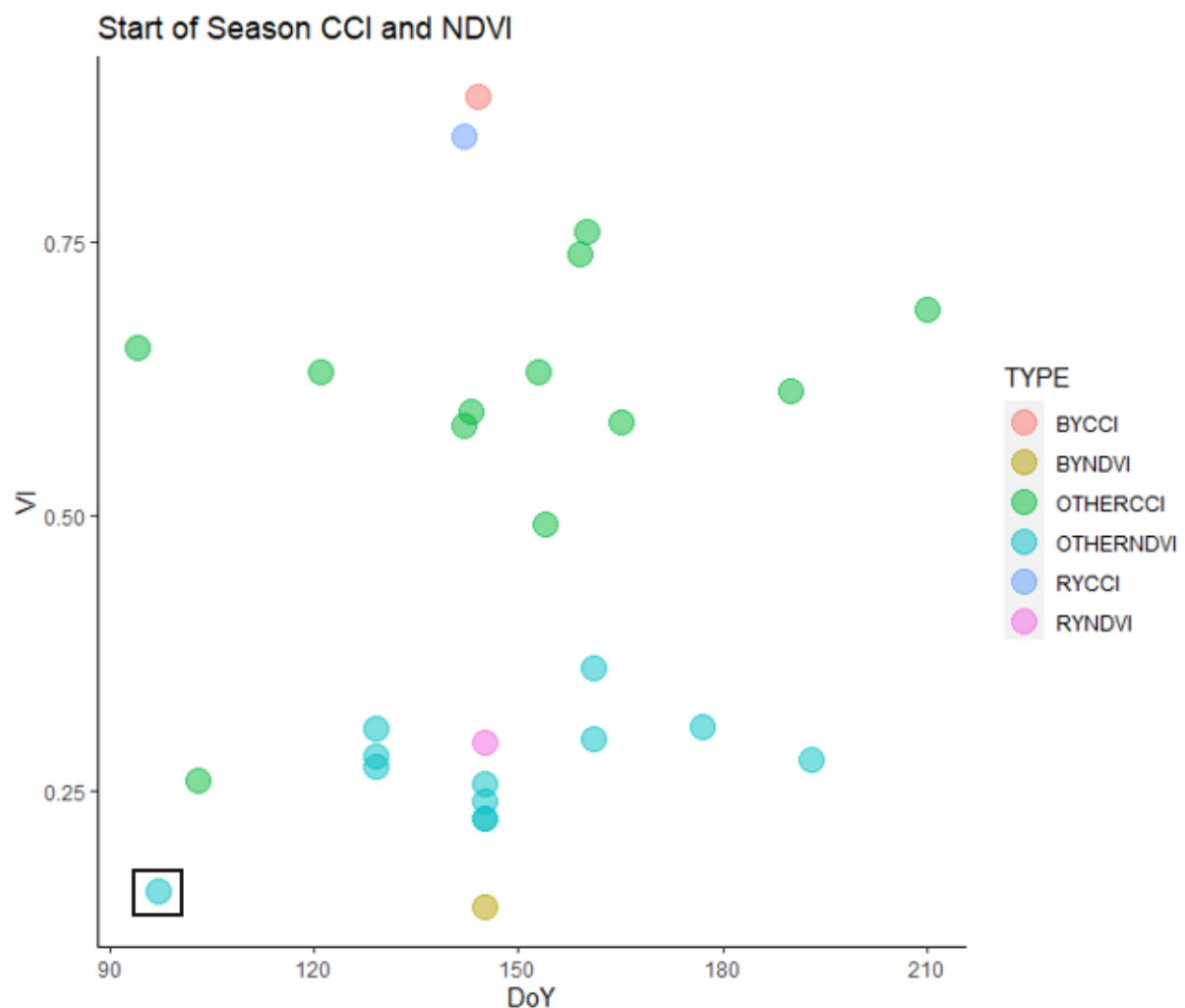


Figure 2.17 CCI and NDVI at the **start of season**, at the Storfjord study site. BY refers to the browning year, meaning the year in which vegetation damage occurred; RY refers to the recovery year, following the BY and DoY= Day of the year. The bubble value with a box outline represents the NDVI of the additional browning year 2016.

The BY NDVI was the lowest at every stage of the growing season. On the other hand, the BY CCI couldn't be differentiated from the other years CCI through visual inspection, at any stage. With regards to H2, it was interesting to note that the behaviour of the SOS NDVI in 2016 (the additional browning

year detected in this research) at Storfjord was similar to the on-record 2014 BY at Flatanger. The NDVI indicated an earlier start of the growing cycle in 2016 at Storfjord. In the context of H3 and H4, the BY (2012) NDVI as well as the 2016 NDVI values were lowest and shared the same occurrence timing, indicating changes to photosynthetic activity at the peak of the growing season. Thus, both the SOS and POS NDVI behaviour in 2016 reinforced the earlier interpretation of the results related to vegetation damage observed in 2016 at Storfjord.

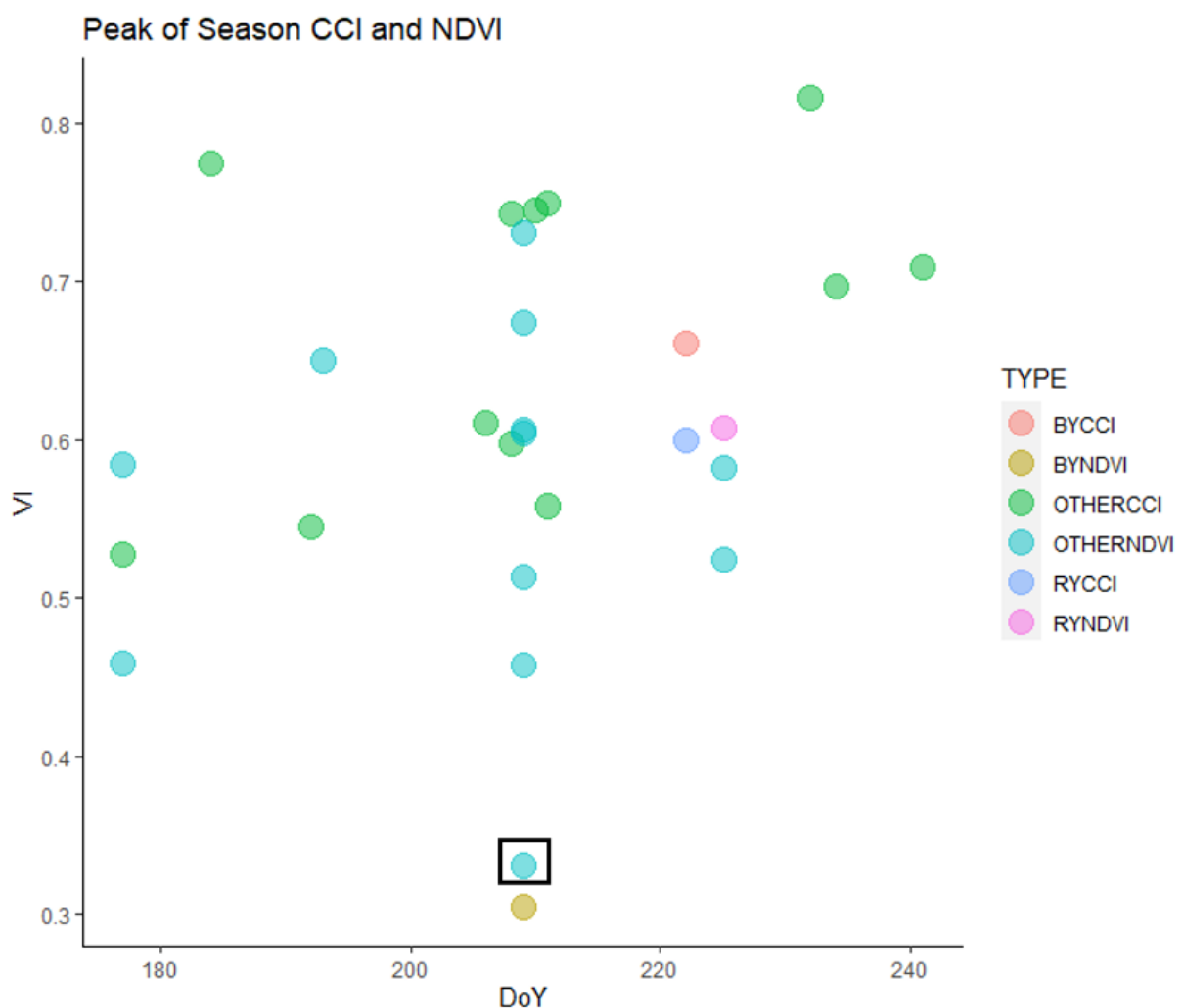


Figure 2.18 CCI and NDVI at the **Peak of Season**, at the Storfjord study site. BY refers to browning year, meaning the year in which vegetation damage occurred; RY refers to recovery year, following the BY and DoY = Day of year. The bubble value with a box outline represents the NDVI of the additional browning year 2016.

In the context of H4 (Figure 2.18), it was interesting to note the difference between the BY TIMESAT POS CCI and the original BY Maximum CCI. While based on the original CCI timeseries, the BY Maximum CCI was the lowest for 2002-19, however the BY Maximum CCI of the TIMESAT fitted POS stage was not the lowest. This was also observed for the Flatanger study site.

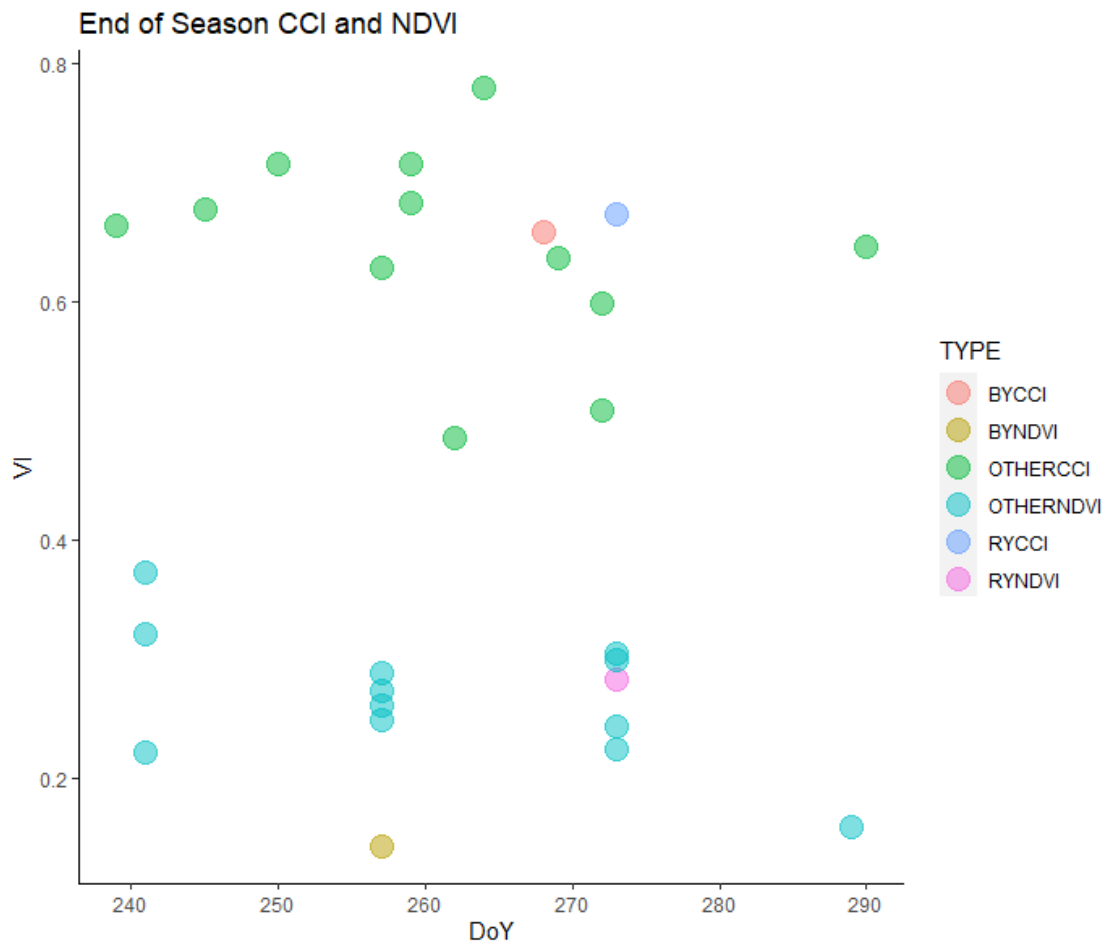


Figure 2.19 CCI and NDVI at the end of season, at the Storjford study site. BY refers to browning year, meaning the year in which vegetation damage occurred; RY refers to recovery year, following the BY and DoY = Day of year

With regards to H5, both the EOS NDVI and CCI measurements in the BY 2012 were not higher than the other years; the NDVI value was the lowest (Figure 2.19). This means that the dominant vegetation types at Storjford did not respond to an extreme winter weather-led decrease in GPP, by increased biomass at the EOS.

Visual interpretation of the indices in Figures 2.17 – 2.19 was reinforced by comparing the BY VI observations against the mean and standard deviation estimated for each stage respectively. Figure 2.20 presents the mean and standard deviation estimated for each of the three stages of the growing season at Stor fjord. The BY NDVI at each stage was lower than the mean, and outside ± 1 standard deviation. Whereas the BY CCI at SOS (H2) was surprisingly higher compared to the long-term mean CCI at SOS. CCI at POS (H3) and EOS (H5) were contained within ± 1 standard deviation as well as closer to the mean.

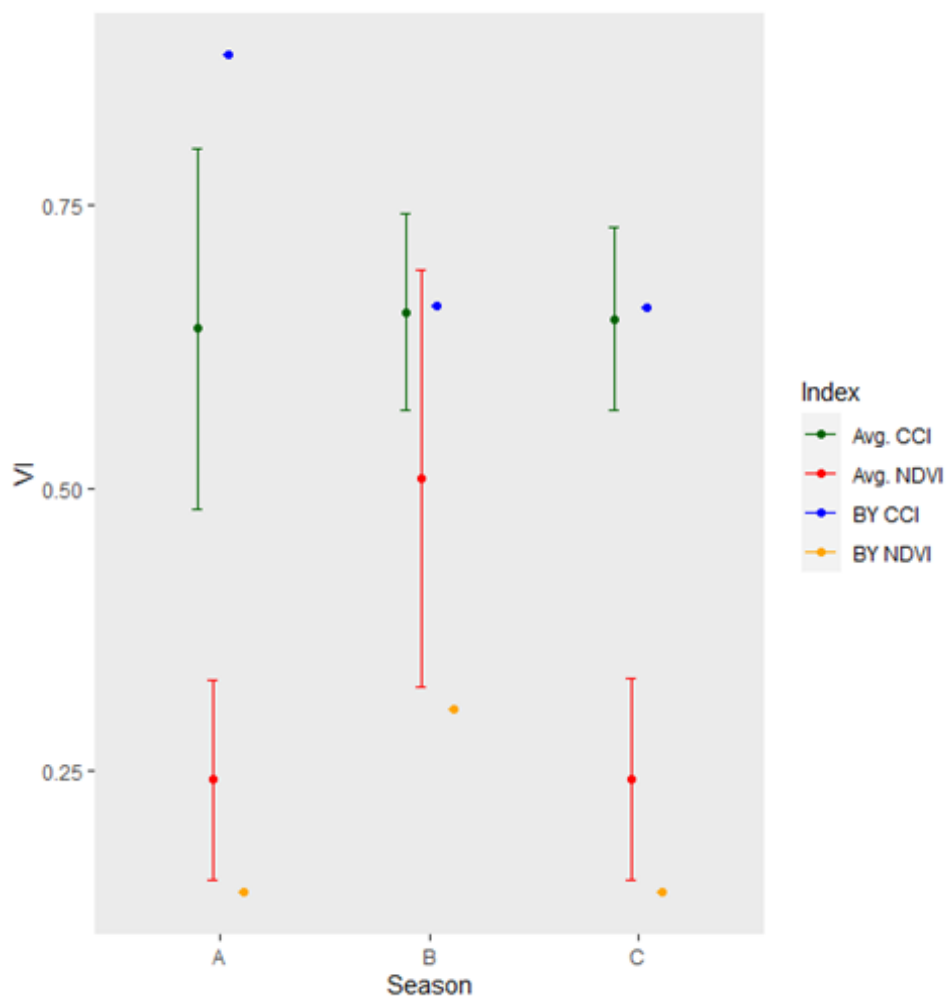


Figure 2.20 Mean and standard deviation at each stage of the growing season, for the Stor fjord site. The vertical bars denote ± 1 standard deviation, and the circles within the bars denote the mean. A=Start of season, B= Peak of season and C=End of season

2.3.3 Lofoten

2.3.3.1 Satellite-based detection of browning events

A noticeable/anomalous decrease was not observed for either the CCI or the NDVI for the browning year 2014, based on visual examination of the full growing season values (Figure 2.21).

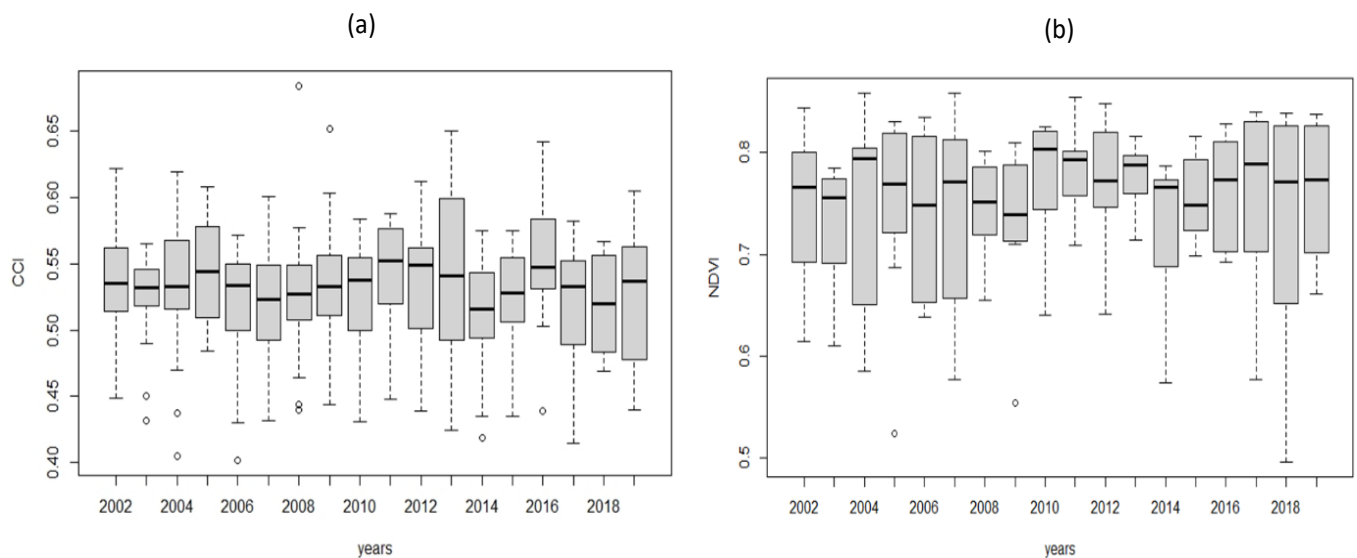


Figure 2.21 Growing season distribution for (a) CCI and (b) NDVI at the Lofoten study site respectively. Boxes show the median and interquartile range, whiskers present minimum and maximum values, and the circles denote outliers.

Widespread shoot mortality was observed at Lofoten on a landscape scale in 2014. The damage has been attributed to frost drought conditions linked to the unusually warm and dry conditions during the 2013/14 winter. Figure 2.21 (a) and (b) present the annual growing season CCI and NDVI range for the Lofoten study site, and address H1 under this chapter. The overall range of both CCI and NDVI for the 2014 growing season did not visually stand out as particularly different or decreased.

Wilcoxon signed-rank test results

The Wilcoxon signed-rank test was conducted to address H1 under this chapter. The results showed that both the CCI and NDVI distribution of 2014 growing season was not significantly different ($p < 0.05$) from the average growing season (2002 – 19) at the Lofoten study site. Figure 2.22 presents the average growing season trajectory (2002 – 19), and the BY (2014) growing season trajectory for CCI at the Lofoten study site. Similarly Figure 2.23 presents these for NDVI. Both figures show that the BY

trajectories were quite similar to the average behaviour of the VIs at this site. The Wilcoxon test results reinforced the visual interpretation of the absence of a spectral browning event in the VI timeseries based on Figures 2.21 – 2.23. The potential reasons for the poor detection of a spectral browning signal at this site for 2014, despite a 37% reduction in the GPP still evident in 2016 (field measurements by Treharne (2018)), are unclear. It is quite likely that spectral noise due to the site-level heterogeneity (seen in Figure 2.1 (b)) played a role here. However, such factors were also present at the Flatanger and Storfjord study sites.

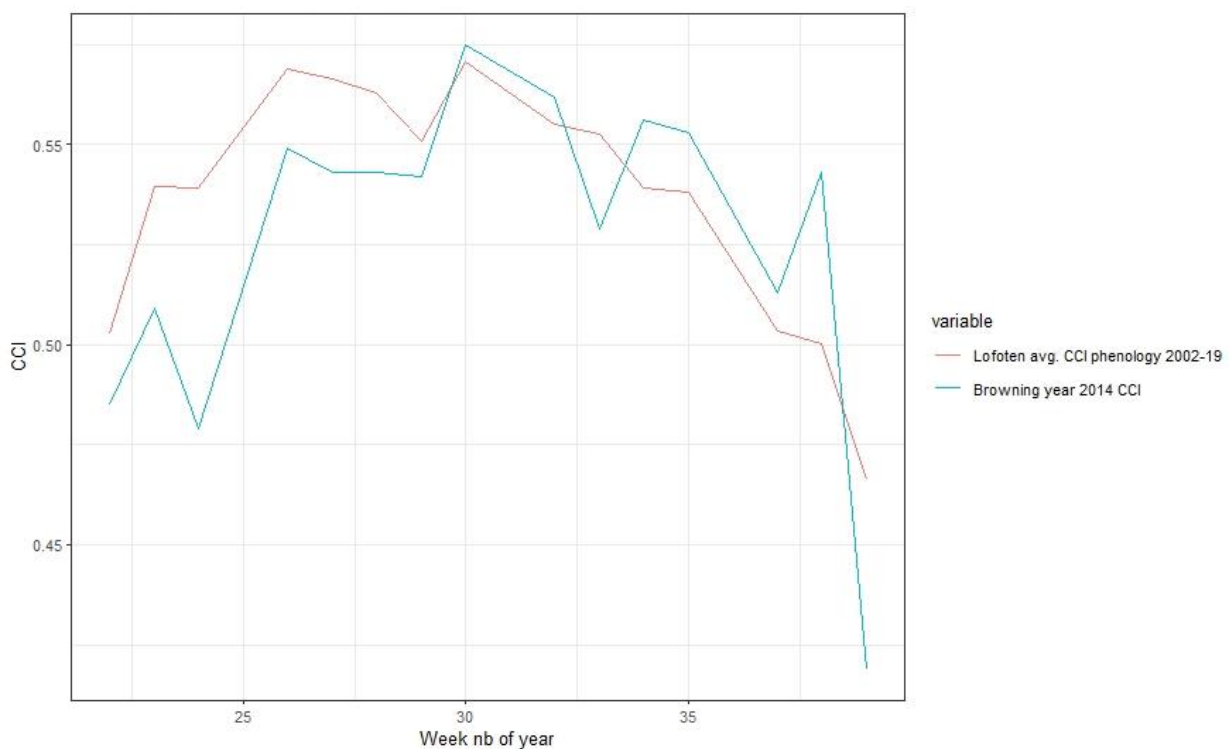


Figure 2.22 Average growing season trajectory (2002 – 19), and the BY (2014) growing season trajectory for CCI at the Lofoten study site

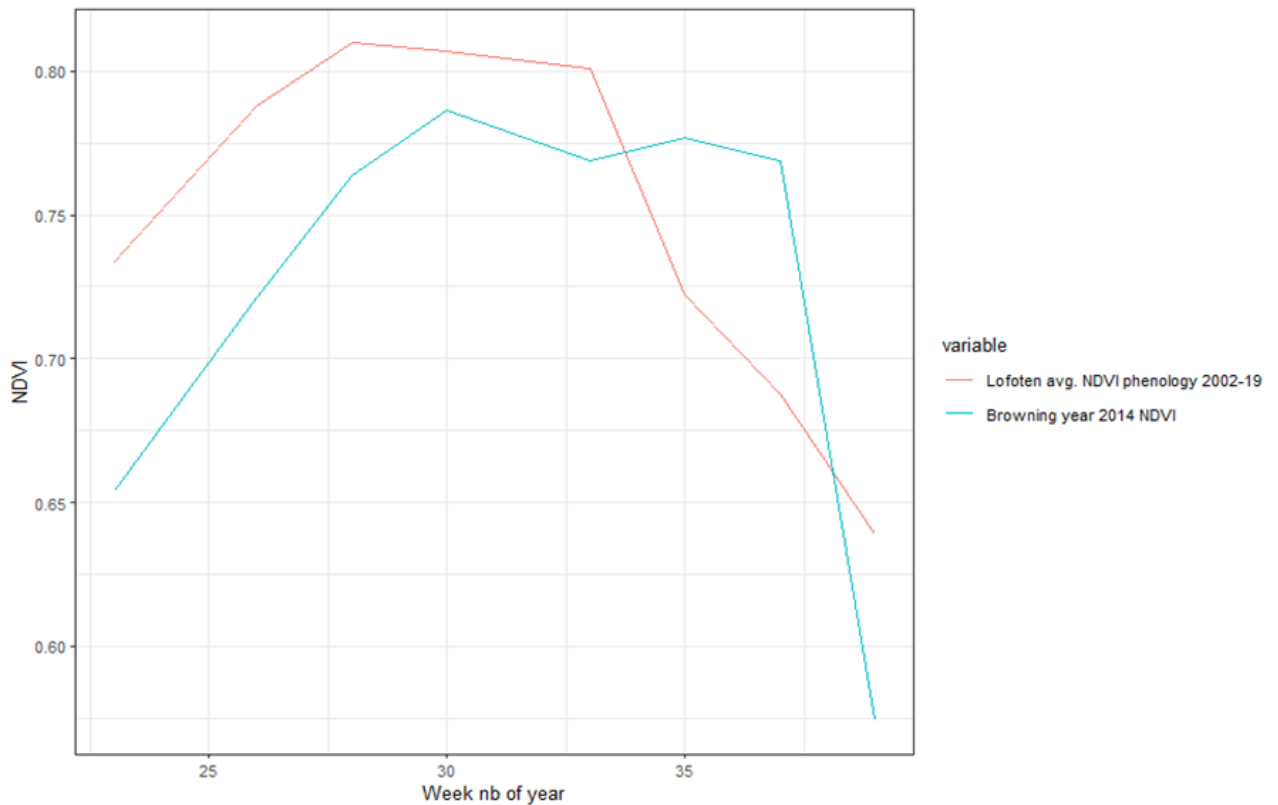


Figure 2.23 Average growing season trajectory (2002 – 19), and the BY (2014) growing season trajectory for NDVI at the Lofoten study site

Figure 2.24 presents the maximum CCI and maximum NDVI values for the Lofoten study site, which addresses H4 of this chapter. Both the 2014 maximum CCI and maximum NDVI values were amongst the lowest for the 2002-19 time-period. However, these did not stand out as anomalously lower in comparison to the overall maximum values over the study time period (2002 – 19).

Based on the lack of a detection of a spectral browning event signal at Lofoten, further examination of the 2014 growing season (as in the cases of Flatanger and Storfjord), was not conducted here.

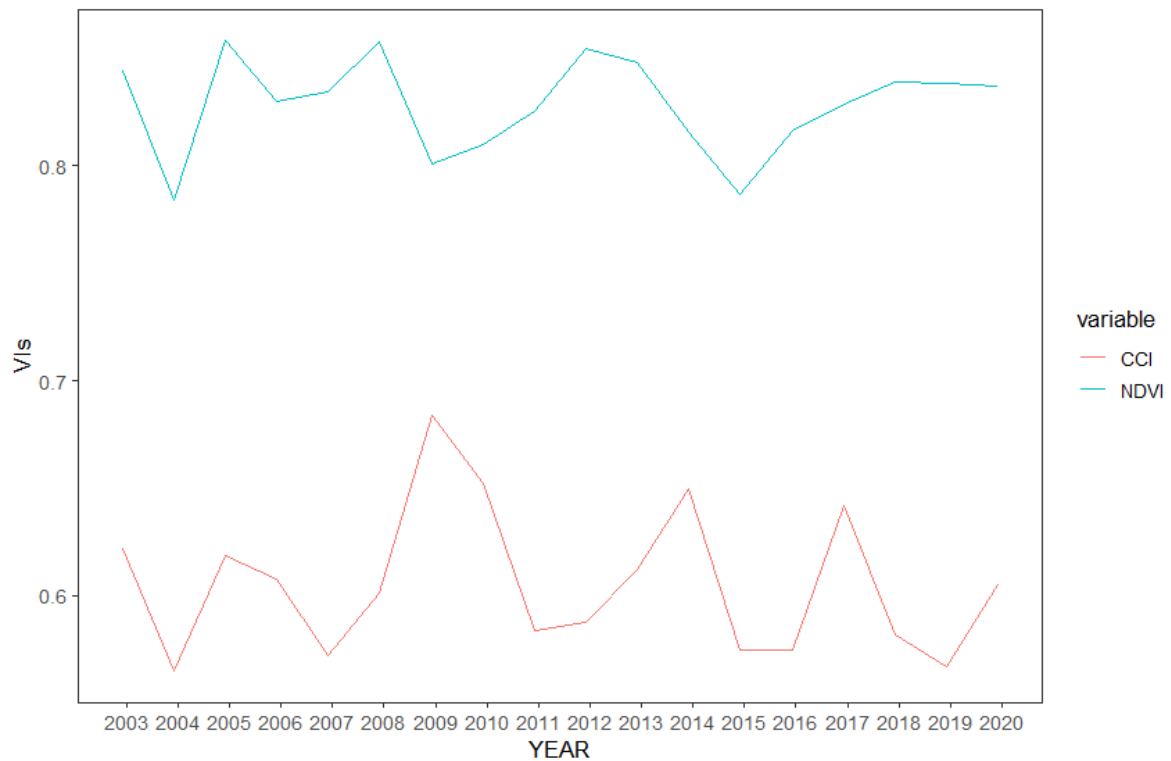


Figure 2.24 Maximum CCI and NDVI of each growing season 2002-19 at the Lofoten study site

2.3.4 Comparison of the spectral browning event detection across the study sites

The spectral browning event signal was stronger and clearer at Flatanger, as compared to Storffjord and Lofoten. Field measurements, of the browning events discussed in this chapter, were conducted by Treharne (2018) at the peak of season in 2016. These showed 66% and 51% of the dominant species were damaged, at the Flatanger and Storffjord study plots respectively, even after two to three growing seasons. Flatanger being below the Arctic Circle at 64°N, and coastal, is a more productive site compared to Storffjord at 69°N, which is also more inland. While the 41% mean GPP decrease at Storffjord was slightly higher than the 35% decrease at Flatanger, it is important to note that these reductions were calculated relative to the undamaged vegetation at the study sites. Flatanger was the most affected site in terms of damage severity (Treharne, 2018). Hence both the satellite CCI and NDVI, being more receptive to the vegetation damage at Flatanger was plausible.

Table 2.3 A quick comparison of the vegetation damage related results of field-based studies and this research

Study site	Avg. GPP decrease 2016 (Treharne, 2018)	% Damaged of overall vegetation	% Damaged of dominant species in 2016 (Treharne, 2018)	VI	Growing seasons significantly different from long-term avg. (Wilcoxon signed-rank test results, $p < 0.05$)
1. Flatanger	35%	43%	66%	NDVI	2014 and 2015
				CCI	2014
2. Storfjord	41%	42%	51%	NDVI	2012
				CCI	None
3. Lofoten	37%	NA	NA	None	None
				None	None

Although the three case study sites experienced slightly different types and sequence of extreme winter weather conditions (as described in section 2.2.1.2, and explored further in Chapter 3, section 3.3.1), vegetation damage resulting from both winter warming and frost drought conditions, as well as a combination of the two conditions, is more than often similar. It is evident as partial to complete shoot mortality (Treharne, 2018). Moreover, determining the exact cause of vegetation die-back in retrospect is quite challenging even at the ground-level. Therefore, distinguishing between the vegetation damage resulting from different types of extreme winter weather events was not an important factor in the interpretation of the results related to VI-based spectral browning signal, under this research.

The vegetation composition differed slightly across the three sites. Vegetation at Flatanger comprised of three types of evergreen shrubs, including *Calluna vulgaris* (dominant), *Vaccinium* species and *Erica tetralix*, and two type of mosses. Whereas at Storfjord the dominant shrub was *Empetrum nigrum*, and it had lichen and two types of mosses. The dominant species at Lofoten were *Calluna vulgaris* and *Empetrum nigrum*, with ground cover of two types of mosses. Species composition has been shown to

affect the productivity patterns at a site level, with the dominant species in the community having a major influence on growth timings (Thornton et al., 2009 cited in Wang et al., 2020). In the case of Storfjord, the BY CCI phenology not being statistically different from the average CCI growing season, might come down to multiple factors, including the differences in species composition and how that affects the CCI's signal. For example, *Calluna vulgaris* grows taller than *Empetrum nigrum* (Barkman, 1990), has spherical leaves with +90° to - 90° inclinations, as compared to *Empetrum nigrum*'s long, narrow leaves, which are mainly horizontal (Barkman (1979) in Barkman, 1990). Whether morphological differences, such as increased shrub height of *C. vulgaris* or its particular angular distribution of leaves, contributed to a stronger CCI signal at Flatanger, was beyond the scope of this research. In addition to structural differences between vegetation types, their inherently different seasonal variability could also have affected the overall VI patterns (Gillespie et al., 2018). Moreover, understanding the effects of vegetation composition and characteristics in spectral detection of browning events was made more challenging because vegetation composition at Lofoten was not drastically different compared with Flatanger and Storfjord; rather it was a mix of the vegetation species at both the sites. Therefore, it is unclear based on the results here, whether CCI and/or NDVI better represented damage in a particular species within a 250 m pixel.

CCI is highly sensitive to changes in chlorophyll and carotenoid pigments in plants, on a seasonal and on a sub-seasonal scale. In general an exponential relationship between CCI and GPP has been observed for a number of species and environmental conditions (Peñuelas et al., 2011). However, the variation in CCI's performance to remotely capture the different levels of on-ground observed GPP reduction, across the study sites, in this research has demonstrated the need to understand species-specific CCI-GPP links. For Arctic vegetation, the growth season considered in this research was 1st June to 30th September. *Empetrum nigrum* flowers soon after snow melt (May-June in this region), and being the dominant's species at Storfjord, it is likely that its flowers were already present when the CCI was measured for this research. The flowers range from pink to purple colours, and hence would mainly comprise of anthocyanins rather than carotenoids. Carotenoids based reflectance indices have not

been recommended to be applied to anthocyanin containing plant tissues (Merzlyak et al., 2003). Hence it is possible that a comparatively large proportion of the anthocyanin pigments in the satellite pixel, due to the presence of the *Empetrum nigrum* flowers, could have interfered with the CCI signal at Storfjord. Other factors differentiating the CCI's browning detection signal between Flatanger and Storfjord could be location-bound such as microtopography and landform type. Such factors were understood to be especially important with regards to the poor spectral detection of vegetation damage at Lofoten, considering the highly coastal location of the Lofoten islands. Based on the differences in spectral detection of vegetation damage at Lofoten compared to the other two sites, it is recommended that CCI and NDVI's performance with regards to vegetation in coastal areas with complex orography, should be evaluated in future studies.

While the spectral browning detection in this research builds upon the field observations of Treharne (2018), it is important to remember the inherently different spatio-temporal scales used within these analyses. A huge spatial scale mismatch is faced when attempting to compare the field measurements with the satellite-based VIs in this research. Treharne's ground-based measurements were conducted using 1m x 1m plots, whereas MODIS's VIs in this research were 250m x 250m pixel NDVI and 1000m x 1000m CCI. In terms of the temporal scale, it was challenging to compare results of Treharne (2018) with this research since their observations were conducted two to three years after the browning events and hence in some ways reflected the recovery trend of the damaged vegetation rather than the immediate productivity decrease following the winter warming events. It is fair then to assume that significantly larger reductions in the field-based GPP of damaged vegetation would be observed when measurements are conducted at the beginning of the first growing season following the extreme winter warming event. Bearing in mind the above factors it can be said that the overall satellite quantification of dead, damaged and stressed vegetation, across the study sites was weaker as compared to the ground observations. However, despite the spatial discrepancy, the MODIS CCI and NDVI, especially the maximum values, and the entire growing season's NDVI did offer a reliable signal of the vegetation damage at Flatanger and Storfjord, albeit at a pixel level.

2.3.5 Summary of the findings

The analysis here was aimed at quantitatively determining a spectral signature of vegetation browning, in the aftermath of extreme winter weather events in the Norwegian Arctic and sub-Arctic. The objective of the analysis was also to develop a definition for identifying spectral browning events in terms of a threshold-based reduction in a VI, on a pixel scale, which could then be applied at larger, landscape scales to monitor Norwegian vegetation. Based on the findings of previous studies related to impacts of extreme weather events on Arctic vegetation (section 2.1), it was hypothesised that satellite VIs could present a spectral signal for a browning event in one or more of the ways as described with H1 – H5 (section 2.2.3).

H1: Gross, anomalous changes to the whole growing season. The BY NDVI at both Flatanger and Storfjord were statistically different, whereas the BY CCI was only at Flatanger. Both the BY CCI and NDVI distributions at Lofoten were not different.

H2: Changes to the start of the growing season. Based on the TIMESAT phenological transitions dates, it was found that both, SOS NDVI and SOS CCI in the BY were not only the lowest but occurred earlier than the rest of the years as well at Flatanger. Whereas at Storfjord such behaviour was exhibited only for 2016 by NDVI. Changes to SOS were not observed for the 2012 growing season.

H3: Changes to the timing of peak productivity in a growing season and H4: changes in photosynthetic activity at the peak of a growing season. In the context of the POS attainment timings being altered due to the vegetation damage, a clear signal was not observed for any of the indices at any study sites. Whereas for the POS photosynthetic activity, only NDVI showed a clear decreased productivity signal for the Flatanger and Storfjord sites.

H5: Changes in productivity at the end of a growing season. The TIMESAT based EOS NDVI at both Flatanger and Storfjord was lowest as compared to the rest of years, which means that within the BY growing season, vegetation did not compensate for reduction in the POS growth by increased growth at the EOS. H5 was not investigated at Lofoten due to the lack of a signal identified in H1-H4.

2.4 Discussion

The importance of satellite VIs to detect a browning event and associated changes in vegetation phenology for remote regions such as the Arctic is crucial because field-based studies are expensive, challenging and time consuming (Bokhorst et al., 2009; Beamish et al., 2020). Large scale positive trends in remotely sensed VIs for the Arctic are widely understood to be indicators of increasing vegetation productivity and biomass. However, can the same indices be applied to assess vegetation stress, damage and mortality in the aftermath of extreme winter weather events in the Arctic? The results of this study have helped to identify the following themes, which are critical for examining browning events in the Arctic.

2.4.1 Satellite-based phenological signature of browning events

This research has helped to reduce uncertainties related to satellite VIs providing indications of a browning event in context of the various stages of the short Arctic growing season. Findings of this research show that effects of a browning event on vegetation phenology are reflected differently depending on the type of satellite VI. While both the CCI and the NDVI showed a noticeable decrease in the peak photosynthetic activity at one of the study sites (Flatanger), however overall NDVI outperformed CCI by exhibiting a clear and strong signal for decreased productivity at every stage of the growing season across two study sites (Flatanger and Storfjord). The CCI related findings of this research are difficult to compare since in the Arctic context the CCI has mainly been applied to examine productivity of evergreen forests, and no literature was found regarding low-lying dwarf vegetation, which were the prime focus of this study. Beamish et al., (2020) have similarly noted that photosynthetic pigments are one of the least understood characteristics of Arctic vegetation, so this research has contributed towards a better understanding of these pigments. While the different CCI results across the study sites in this research highlights the need for further investigation to understand satellite-derived pigmentation and biochemical impacts of extreme winter weather events. It is equally

important to understand what CCI would have signified in case of positive detection of the vegetation damage across all sites. Since this index represents seasonal changes in chlorophyll/carotenoid pigments and given the definition of browning as a sudden loss in the photosynthetically active foliage, it is highly likely that decreased chlorophyll (productivity related) and increased carotenoid (stress related) pigments would be measured by CCI right before the start of season before any sort of existing vegetation recovery or new vegetation growth occurs.

CCI is responsive to subtle pigment changes at shorter time intervals, whereas NDVI can capture long-term, annually accumulated canopy greenness (Wang et al., 2020). CCI in the case of Flatanger was able to track an earlier onset of the growing season as well as a lower-than-average SOS photosynthetic activity. Earlier leaf emergence in an Arctic vegetation species, *V. vitis-idaea*, has been reported as one of the responses to winter icing events (Preece and Phoenix, 2014). Both CCI and NDVI capturing an earlier SOS at Flatanger implied that this in fact could have been one of the phenological responses to winter warming and frost drought. Hence earlier in the SOS, following the spring snow melt, is suggested as the optimum growing stage to apply a pigment-based satellite VI for detecting vegetation damage and/or mortality following extreme winter weather events. However more research is required in this context due to the micro-scale spatial heterogeneity of Arctic landform and vegetation composition (Maguire et al., 2021)

The browning events discussed in this study exhibited different signs of vegetation damage and stress. These ranged from shoot mortality, wilted, browned and greyed leaves, to anthocyanin pigmentation in leaves. The focus of the analysis in this chapter was understanding how different satellite VIs exhibit a spectral browning event to capture the reduced vegetation productivity caused by extreme winter weather events in the Norwegian Arctic and sub-Arctic. Whether a particular index significantly excels at quantifying a specific type of damage could not be concretely concluded from this research. Non-obvious physiological effects such as reduced flowering and berry production can also not be captured by satellite indices such as NDVI and CCI, although such effects still have knock-on effects on the ecosystem, due to wild berries being a food source for wildlife in the Arctic.

As this PhD research is focused on the role of extreme weather events in Arctic browning, therefore, the case studies used here for evaluating the spectral signal, were of vegetation damage arising from climatic drivers. However, browning events caused by biological drivers such as defoliating insect outbreaks must also be considered for determining a holistic remote sensing approach to study on-ground vegetation disturbance. The resulting damage from insect outbreaks could be slightly different as compared to that from climatic drivers such as winter warming or frost drought. Vegetation damage from defoliating insects, in the form of loss of entire leaves and or reduced leaf area, is more structural/morphological as compared to climatic drivers induced effects such as anthocyanin pigmentation and the loss of photosynthetic capacity in dead leaves and shoots which are still physically intact and attached to the plants.

2.4.2 The role of scale

Examination of different types of vegetation disturbance (damaged, dead, stressed; as shown in Figure 2.2) is a challenging process, even at the plant shoot level (Treharne, 2018). By incorporating a pigment-based index, the CCI, this PhD research investigated the different types of disturbance on a landscape scale (1 km). The findings show that, as may be expected, the satellite detection of vegetation disturbance was weaker as compared to plot level ground observations. This is attributed to the fact that browning is occurring unevenly and at finer scales (Phoenix and Bjerke, 2016). The browning signal can also be weakened because a sensor's pixel is an aggregation of various ecological processes happening on the ground and as well as by undisturbed, healthy vegetation, occurring within the same pixel (Berner et al., 2020; Myers-Smith et al., 2020). One of the major reasons that NDVI outperformed CCI, at both the study sites, was because NDVI's spatial resolution was higher than CCI, 250 m NDVI compared to 1000 m CCI. Applying medium to coarse satellite VIs for the assessment of phenological processes, within the compact growing season in the Arctic, is a challenging task in itself (Wang et al., 2018), let alone applying these indices to study the sporadic damage in scattered vegetation cover at

complex landscapes such as the Norwegian coast and fjords. Despite these challenges, signals were detected, and useful insights and understanding of the browning signature at each site were obtained.

Defining a spectral browning event in terms of a threshold decrease, relative to a baseline average is made more challenging by the large variation in VI percent decrease across different locations, although the decrease results from the same winter warming event. For example, the largest reported browning event in the Scandinavian Arctic, in terms of land area, was for the 2008 growing season, which was attributed to the winter warming event in December 2007. A large range of 16% - 91% reduction in NDVI was observed for 2008 w.r.t to 2007, across five different sampling sites (Bokhorst et al., 2009). Such a large variation in the NDVI decrease, due to the same winter weather event, presents a challenge in determining a threshold-based definition for 'spectral browning events'. There is almost no evidence about the understanding of the equivalence of ground damage and satellite response. Across these five sites in Bokhorst et al. (2009), the field measurements showed that shoot growth had decreased by 87% in damaged plots as compared to nearby undamaged plots. The % decrease in vegetation productivity on ground is often measured relative to neighbouring undamaged vegetation, in study plots ranging from 1 to 60 m (Bokhorst et al., 2009; Treharne, 2018). In terms of medium-high satellite spatial resolution (250 m MODIS – 30 m Landsat), these nearby undamaged vegetation could possibly lie within the same pixel; hence it is difficult to translate % damage on ground to decrease in satellite VI.

Moreover, large variations in the damage intensity of vegetation such as shown in Bokhorst et al. (2009), and resulting from the same extreme winter weather event, could be an indication of how different vegetation species respond to such events. Different Arctic and sub-Arctic vegetation types have showed different responses to extreme winter weather events (Bokhorst et al., 2008). Field measurements of browning events enable vegetation classification. When comparing satellite-based VI decrease with field observations of vegetation damage, it is important to remember that the satellite decrease is representative of different levels and types of on-ground damage. Hence more research is

needed to develop a definition of spectral browning events which is representative of how extreme winter weather events can affect the dominant vegetation species in the Arctic. Such analyses can help identify vegetation species most at risk in the light of projections of increased frequency and intensity of extreme winter weather events, and thus lead to developing conservation strategies aimed at regionally dominant vegetation species.

2.4.3 Synergistic approaches to study Arctic browning events using remote sensing data

Complementary remote sensing approaches, which are based on joint application of two or more satellite VIs, can significantly help to improve the assessments of vegetation productivity status and phenological patterns (Gamon et al., 2015; Jeong et al., 2017). Hence this research applied two conceptually different satellite VIs to study on-ground reported vegetation disturbance. Moreover, it was hypothesised that the varied characteristics of vegetation disturbance (as observed on-ground), might be better represented by different VIs.

CCI and NDVI applied in conjunction has been shown to provide a more accurate interpretation of the satellite-VI and flux tower-GPP relationship (Wang et al., 2020). While CCI is overall more dynamic than NDVI at tracking the GPP fluctuations on a seasonal scale, however, NDVI is more responsive to the initial canopy green-up (Wang et al., 2018). Issues of seasonal hysteresis in the NDVI-GPP relationship can be managed by applying the CCI simultaneously, since it doesn't face saturation defects after attaining a certain productivity level (Rahman et al., 2004). Hence both the indices complement each other. It is also worth noting that NDVI-GPP hysteresis occurs once the peak NDVI within the growing season is attained. However, vegetation damage resulting from exposure to extreme winter weather events is more likely to be picked up by the satellite VIs at or before the peak of the season; as by the end of the season the vegetation might have recovered by a certain level, although that is strongly dependent on the severity of the damage. Hence NDVI related hysteresis issues should not be an impeding factor in applying it to examine browning events. Ideally comparing the NDVI and CCI simultaneously with the flux-tower GPP near a damaged vegetation site would best help to assess the

effectiveness of a complementary approach for studying effects such as, reduced peak season productivity, resulting from extreme winter weather events. However, such analyses was beyond the scope of this research due to time limitations.

Another factor to note for future application of CCI to study vegetation damage in the Arctic and sub-Arctic is the CCI algorithm. While this research used MODIS's band 1 as the reference band for calculating CCI at both study sites, other MODIS bands such as bands 4, 12 and 13, can also be applied as a reference band (Drolet et al., 2005). The choice of the reference band can significantly influence CCI's response to photosynthetic efficiency (Rossini et al., 2012). Site level characteristics and vegetation type have been shown to play a key role in for example the performance of CCI with regards to determining the light use efficiency (LUE) (Goerner et al., 2011). Because limited research using CCI in the context of Arctic vegetation has been undertaken, the band that showed promising results across most of the sites in Goerner et al. (2009) was used as the reference band here. Considering that there was a difference between the performance of CCI at Flatanger, Storfjord and Lofoten, it is likely that CCI estimated with different reference bands might be required for different vegetation cover and landform types in the Arctic and sub-Arctic regions. Hence more research is recommended to determine the optimum band for the application of CCI in assessing Arctic vegetation damage.

A way forward

The spatial setting of the Arctic browning events studied here, and their climatic drivers were known through previous research (Treharne et al., 2020). Despite this knowledge, the analysis performed during this research has shown how meticulous analysis is required to understand the spectral signature of various types of vegetation disturbance, and that so at a pixel scale. Hence it could be quite a tedious process to apply medium-coarse spatial resolution satellite VIs on their own, independently, to detect patchy damage in sparse, dwarf vegetation, at a landscape scale in the Arctic. On the other hand, a key challenge in applying higher resolution satellite data such as Sentinel-2 (10 m spatial resolution) to study browning events is that these are not available for the time period (2000 – 2015)

of the browning events reported here. Moreover, this means a lack of baseline for comparisons of the vegetation productivity in a browning year with normal growing seasons.

To facilitate and advance the approach taken in this research, it is suggested that meteorological data be incorporated to validate any NDVI and CCI decrease within a timeseries which is beyond the mean and/or ± 1 standard deviation. Previous studies related to Arctic browning events e.g., Bokhorst et al. (2009), Bokhorst et al. (2010) and Treharne et al. (2020), have as well linked both spectral and field measurements of vegetation damage, to meteorological observations. Meteorological data are often publicly accessible. Meteorological conditions associated with extreme winter weather events such as winter warming, frost drought and rain-on-snow, are often represented through climatic indices (Vikhamar-Schuler et al., 2016). Hence to increase the accuracy of spectral detection of browning events on a landscape scale, it is recommended that meteorological information be integrated with satellite VIs. The next chapter of this PhD research is thus aimed at understanding the relationship between satellite VIs and extreme winter weather conditions and events. Based on this understanding the analysis then progresses to project future occurrences of vegetation browning events under different climate change scenarios. With regards to the work ahead, the average growing season NDVI is selected as the most suitable satellite VI, based on its better spectral browning detection as compared to CCI. Moreover, the average rather than the Maximum NDVI is proposed because the clearest signal of browning impacts, as shown at Flatanger, consisted of changes to the full growing season trajectory. Additionally, the maximum NDVI is not always truly representative of vegetation peak productivity in the Arctic due to missed observations resulting from cloud cover processing.

2.5 Conclusion

This research is the first comprehensive application of satellite VIs to detect spectral browning events in the Arctic, and it has shown the complexities of the task. The effectiveness of CCI and NDVI was analysed in detecting the on-ground GPP decrease in the aftermath of extreme winter weather conditions. It was hypothesized that the spectral signal for browning events could be evident in one or more ways as described under H1 – H5. Overall, the results of both the indices varied across the three study sites, highlight the importance of spatial heterogeneity. Both CCI and NDVI exhibited a statistically significant browning signal at Flatanger in the context of H1. This was true for NDVI only at Storfjord. NDVI performed notably better than CCI with regards to H2 – H5 both at Flatanger and Storfjord. This was attributed to two main factors; first NDVI had a higher spatial resolution (250 m) as compared to CCI (1000 m). Second CCI is more sensitive to subtle changes in the pigment levels hence the browning signal is short-lived. The reasons for an absolute lack of detection of a spectral browning signal at Lofoten is unclear. Therefore, more research is recommended to determine the effectiveness of satellite VIs in assessing browning events, in dwarf shrub heathlands over complex landforms such as the Norwegian Arctic. Based on the results of this research it was concluded that NDVI better captured the on-ground decrease in GPP. Despite this it is highly challenging to apply medium-coarse satellite VIs independently to detect browning events in sparsely vegetated areas in the Arctic. Therefore, it is proposed to consider meteorological information about browning causing extreme winter weather events alongside NDVI to accurately detect the occurrence of browning events at a landscape scale.

Chapter 3

Understanding winter climate - summer NDVI relationships

3.1 Introduction

The Arctic is currently undergoing rapid climate change (AMAP, 2017). As discussed in section 1.3, extreme winter climatic events such as severe winter warming, Rain-on-Snow (ROS) and frost drought have been linked with various vegetation browning events at multiple Arctic and sub-Arctic locations (Bjerke et al., 2017; Treharne et al., 2020). Along with winter extreme weather events, the overall winter climatology plays an important role in determining Arctic vegetation productivity in the subsequent growing season (Bokhorst et al., 2012). Moreover, the timing and duration of extreme weather events can determine their overall impacts on the functioning of Arctic ecosystems (Christensen et al., 2021). Although recent work shows that simple climatological indices can explain the observed decrease in vegetation productivity related indices, such as NDVI, in the aftermath of a browning event (Treharne et al., 2020); the current understanding of the lagged relationship between individual meteorological parameters, at different times during the winter season, and summer NDVI of Arctic vegetation is quite limited. One of the reasons is that extreme events responsible for browning, such as winter warming and ROS, are a construction of multiple interacting meteorological parameters, and hence are very complex to quantify, compare or predict (Phoenix and Bjerke, 2016).

Recent work by Treharne et al. (2020) has discussed how mid to late winter warming events could be more damaging to vegetation as compared to early winter warming events. While their work is the first of its kind in understanding and quantifying the relationships between winter extreme weather related indices and both satellite and field-based NDVI, their analysis is based on a short time period (2011 – 15) and only two meteorological parameters (temperature and snow depth). This PhD research aims to advance such analyses by understanding the relationship of monthly winter meteorological parameters with summer NDVI, based on longer NDVI and climate datasets spanning the time period 2000 - 2020, and also by incorporating precipitation. Hence, this new analysis helps achieve RO2 of this PhD, which is to determine the main meteorological drivers of satellite-based observations of vegetation decline in the Norwegian Arctic and sub-Arctic. Subsequently, the statistical model developed through this analysis, will assist to inform and produce future browning projections (set out

in chapter 5). Thus, this analysis links RO2 and RO3 of this PhD, which is, to explore future extreme winter events and Arctic browning linkages.

3.2 Methodology

3.2.1 Study area

Numerous browning events in central and northern Norway have been reported previously (Bjerke et al., 2017). Hence the study area for RO2 was selected to include the Norwegian sub-Arctic and Arctic regions (covering latitudes from 63°N to 72°N). This area also includes the three case-study browning sites as discussed in Chapter 2. Details about Norway's overall climatology and landforms have previously been described in Chapter 2 section 2.2.1

3.2.2. Methods

To achieve RO2 of this PhD, multiple steps were followed, which broadly fall under three main categories; first, initialization and validation of the Weather Research and Forecasting Model (WRF); second, using WRF to reproduce past extreme weather events that lead to browning; and third, the development of statistical models linking the changes in vegetation NDVI to variations in WRF-derived meteorological parameters. WRF was run to produce regional high resolution (1-10 km) climate parameters, because output from global climate models (GCMs), and reanalysis products are usually too coarse (30 to 100 km horizontal resolution) to understand and analyse the meso-scale physical and atmospheric processes significant to Norwegian landscape and climate (NCCS, 2017). Also, as explained in Section 3.1, RO3 of this PhD builds upon the statistical model developed through RO2. For robust future browning projections under RO3, the statistical model developed between the meteorological parameters and the NDVI had to be based upon meteorological parameters simulated through WRF, which is used for the future projections as well (in Chapter 4). Therefore, to explore the relationship between meteorological parameters and satellite NDVI across Northern Norway, WRF was run on historical data to provide high resolution climatological variables.

The following sections, 3.2.3 – 3.2.6 explain in detail all the steps followed under RO2.

3.2.3 WRF model compilation

3.2.3.1 WRF background

WRF is developed and maintained by the National Center for Atmospheric Research (NCAR). WRF is one of the most widely used climate and weather prediction models (Powers et al., 2017), encompassing interdisciplinary research, such as hydrological, atmospheric and climate change simulations, and operational weather prediction services (Gadian et al., 2018). It is equipped for use across a varied range of scales i.e., metres to thousands of kilometres, offers various physical parameterization schemes and has 45 vertical pressure levels, with the top level at 50 mb.

Running WRF consists of two major components, first is the WRF Pre-processing System (WPS) and second, the Advanced Research WRF (ARW) dynamic solver. The program flow for WPS and WRF dynamic solver is shown in Figure 3.1. The details of each step can be found in the user guide of WRF (https://www2.mmm.ucar.edu/wrf/users/docs/user_guide_v4/v4.0/contents.html).

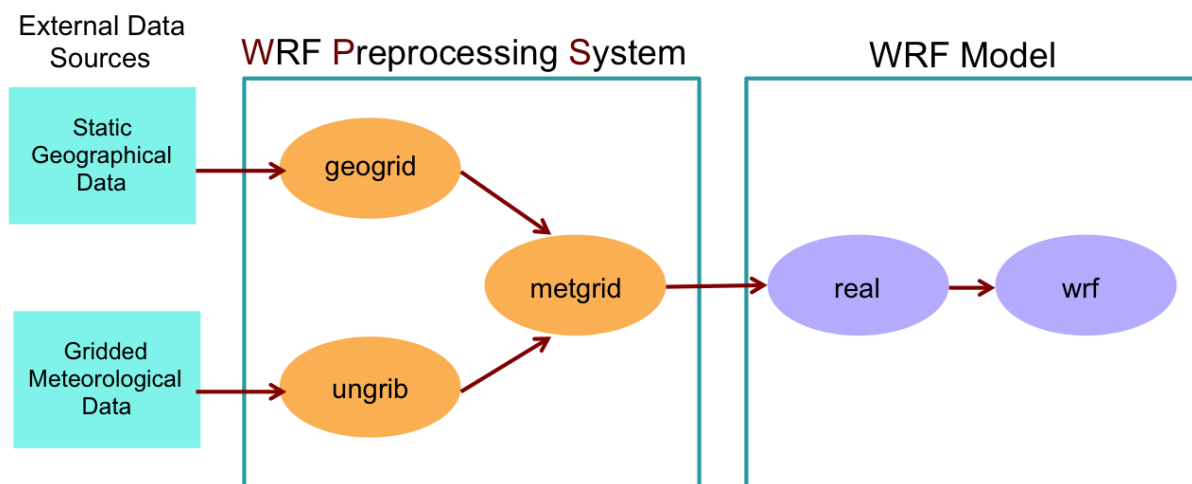


Figure 3.1 Flow diagram of the steps to run the WRF model

WRF enables simulations at varying horizontal grid-resolutions. This is carried out through the nesting procedure. Utilising the nesting technique in an NWP model means to run higher-resolution domain/s located within a larger domain, termed the parent domain, which is usually configured to run at a

coarser resolution. The nesting options in WRF consist of one-way and two-way nesting, and a moving nest. During one-way nesting, several domains, at varying grid resolutions, can be forced simultaneously but only the parent domain communicates with the nest (inner domain), providing boundary observations for the nest. The nest does not transfer its calculations back to the parent domain. Within the two-way nesting method, the inner domains feed their calculations back to their parent domains.

Both nesting methods have been used extensively within atmospheric and weather prediction studies using WRF. The selection of a nesting option is dependent on the research objective. For example, whether the objective is to methodologically evaluate WRF's performance and computational economy based on different settings or applying WRF to mainly study an atmospheric process or event. At the end it is a trade-off between model stability, computation resources and time, and the depth of analysis in context of the inner-outer nest dynamics (Skamarock et al., 2019).

3.2.3.2 WRF compilation on the HPC

Simulations for this PhD were run using Sheffield's High Performance Computer (HPC), Bessemer. Hence WRF was first compiled on Bessemer. Several trial simulations at varying horizontal grid resolutions, 1-30 km, were run for estimating the feasibility of computation resources before running the actual simulations. Thus, the spatial and temporal resolutions for the simulations were decided based on the estimates of model simulation times and model output storage capacities (Appendix 3.1). WRF's compilation on the HPC and all the simulations, trial and actual ones combined, took about 1.5 years to complete. Conventionally, the post-processing tool for WRF output has been the National Center for Atmospheric Research (NCAR) Command Language (NCL). However, Python is increasingly being used for the post-processing and analysis of WRF output. As WRF related Python resources are still in the process of developing, Python's use as a tool for post-processing of the WRF output was one of the challenges in this PhD.

All WRF simulations were run using the default physics parametrizations of WRF, which include the cloud microphysical scheme known as the 3-class scheme, the Kain-Fritsch option for convective processes, the Yonsei University planetary boundary layer scheme, the Monin-Obukhov surface layer parameterization and the 4-layer Noah land surface scheme. The output was produced on a daily temporal resolution. The 1-way nesting procedure was incorporated for the simulations throughout, because it helps keep computation times lower (Hawbecker, 2013), is the more widely used approach in climatological studies, and ensures greater model stability compared to 2-way nesting, which has been known to cause WRF destabilisation (Heikkilä et al., 2011). Conventionally, finer resolution, nested domains in NWP models, are run following the parent/outer domain's completion. However, WRF enables simultaneous execution of several nests, allowing dynamic information exchange between domains for every timestep, hence fewer spurious artefacts are generated over the inner domain boundaries (Skamarock et al., 2019).

NWP models usually require a certain time-period to attain their own climatology, and thus reduce the effects of the initial conditions on the model's internal variability. This time is called model spin-up time (Skamarock, 2004). WRF typically requires a 6-12 hour spin-up time, which is quite economic, and thus the driving models for WRF mainly provided the lateral boundary conditions and no artefacts were introduced that could have influenced WRF's internal variability.

3.2.4 WRF validation simulations

Model validation is an important step when running meteorological simulations. Hence WRF was validated over a recent time-period 1990-2000, against meteorological station observations. WRF output was validated against observational data from 10 meteorological stations, with the objective of covering the spatial breadth of various simulation domains. This is due to Norway being a very long country with significant regional climatological differences. Although it has a vast network of meteorological stations, they have been operational for quite different time periods (Heikkilä et al., 2011). As a consequence, the meteorological stations selected for validation did not share a common

operational time-period. WRF’s 2-m surface temperature and snow depth were extracted for the grid point nearest to the meteorological station locations. Bias and root mean square error (RMSE) measures were utilised to compare WRF output against the observed climate

Also, to note, validation was conducted of WRF simulations with two different driving datasets. These were The European Centre for Medium-Range Weather Forecasts (ECMWF) ERA5 reanalysis and Community Earth System Model version 1 (CESM1) GCM, respectively. ERA5 driven WRF (E-WRF herein onwards) was validated because E-WRF simulations were used to examine the relationship of meteorological parameters and satellite NDVI over the recent period (Table 3.1). Whereas validation of CESM driven WRF (C-WRF here onwards) was required as WRF was driven with CESM simulations for the future climate , under RO3 (discussed in Chapter 5 ahead).

Table 3.1 WRF validation simulations

Time period	Driving model	Domain resolution (km)
1990-2000	CESM1	d01 30, d02 10
1990-2000	ERA5	d01 30, d02 10

3.2.4.1 CESM background

CESM is developed and maintained by NCAR. It formed part of phase 5 of the Coupled Model Intercomparison Experiment project (CMIP5), supporting the Intergovernmental Panel on Climate Change Fifth Assessment Report (IPCC AR5) (Bruyere et al., 2015). WRF’s simulations forced with CESM’s ‘global bias-corrected twentieth century all-forcing simulation’ was used for model validation over the time period 1990 – 2000. CESM1 provides the entire set of variables required for the initial and boundary conditions for WRF simulations at a spatial resolution of 111 km and 26 pressure levels. The data are provided at six hourly frequency, which is also required by WRF. The CESM dataset is in the Intermediate File Format, a specialised format for quicker and more efficient WRF simulations. Data

for all the CESM1 driven WRF simulations were downloaded from the publicly available NCAR research data archive at <https://rda.ucar.edu/datasets/ds316.1/> (UCAR, 2022).

3.2.4.2 ERA5 background

ERA5 is one of the latest atmospheric reanalysis products (Serreze et al., 2021). Reanalyses datasets assimilate atmospheric observations into an NWP model, based on a variety of sources including satellite data, radiosondes and meteorological stations (Marshall et al., 2018). ERA5 serves as an advanced representation of weather conditions in retrospective, as noted by Hersbach et al. (2020, p.1999) “This new reanalysis replaces the ERA-Interim reanalysis (spanning 1979 onwards) which was started in 2006. ERA5 is based on the Integrated Forecasting System (IFS) Cy41r2 which was operational in 2016. ERA5 thus benefits from a decade of developments in model physics, core dynamics and data assimilation.” ERA5 has a spatial resolution of 31 km and consists of 137 pressure levels up to 1 Pa. For all the ERA5 driven WRF simulations within this PhD, the ERA5 6-hourly single levels and pressure levels data were downloaded using the Climate Data Store (CDS, 2021).

3.2.4.3 Model domain setup for validation simulations

Domain setup for the WRF validation simulations consisted of one outer (parent) domain, d01, at a 30 km grid, and an inner domain (nest) d02, at a higher 10 km resolution (Figure 3.2). The analyses in chapters three and four (ahead) mainly uses the 10 km-resolution simulations, if not stated otherwise.

WPS Domain Configuration

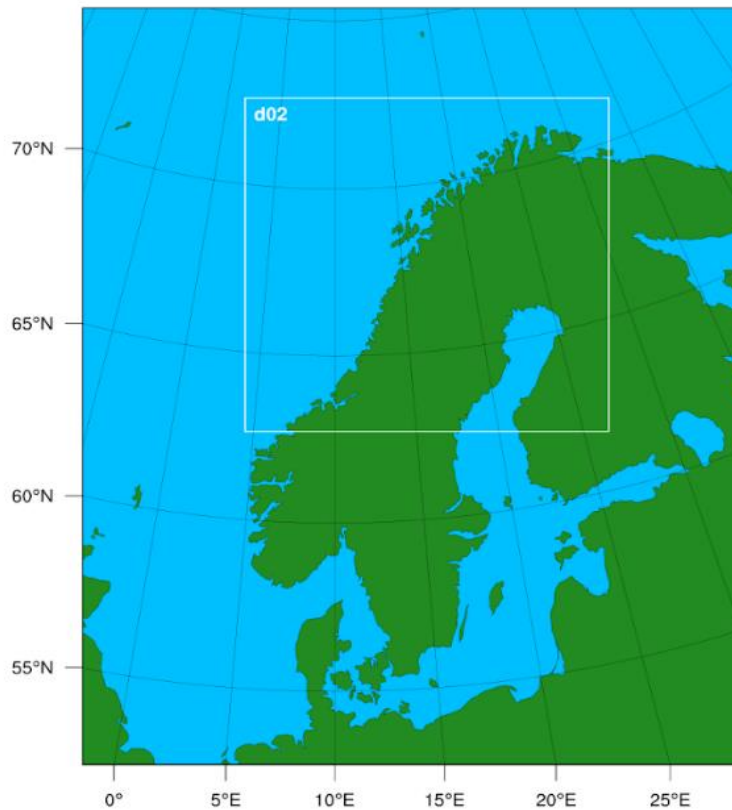


Figure 3.2 Domain setup for WRF validation simulations

3.2.4.4 Model bias and RMSE calculation

NWP predictions have significantly improved over the past two decades due to the development of computational resources, higher model grid resolutions and better representation of land surface-atmosphere dynamics within models. Despite such advances models can still have systematic biases (McDonnell et al., 2018). In the context of climate models, “A climate model bias can be defined as the systematic difference between a simulated climate statistic and the corresponding real-world climate statistic” (Maraun, 2016, p.211). Biases in models occur predominantly from errors in the quantification of energy flows at the land surface and atmosphere boundary layer (Salathe Jr. et al., 2008). Biases in NWP models are also introduced due to model grid design, that is an assimilated value of a meteorological parameter being equivalent of the parameter over an area (McDonnell et al., 2018). These grid box integrated values are validated against observations from meteorological stations .

Potential biases may come from the driving model as well; however, for the purposes of this research, the source of the bias is not important.

The bias in WRF's temperature and snow against meteorological observations was calculated as part of the model validation process, together with the RMSE. The RMSE helps determine the overall error in model simulations which could have been introduced by various sources, e.g., from WRF's initial and boundary conditions and the inherent errors in the datasets used to force the model, such as those arising from interpolation methods.

For the bias and RMSE calculations, WRF variables were extracted at the nearest meteorological station locations. The meteorological observations of temperature and snow data were downloaded from Norway's publicly accessible climate database (seklima.met.no). Both bias and RMSE were calculated for the winter months November-April 1990-2000.

Tables 3.2 and 3.3 present the RMSE and bias estimates of WRF's temperature and snow depth against the meteorological station observations, respectively.

a. Temperature

Overall, a cold bias was observed for both CWRF and EWRF simulations, as compared to the meteorological station observations.

Previous WRF simulations driven by ERA40 over Norway (Heikkilä et al., 2011) also had an overall cool bias, ranging from 0.7-0.8 °C. Both CWRF and EWRF contained an overall cold bias, with average values across the nine meteorological stations of -4.12 and -2.60 °C, respectively. It was not surprising that the EWRF simulations had a smaller bias and RMSE compared to the CWRF simulations, because the driving model for EWRF, ERA5, is a reanalysis product constrained by real meteorological observations.

Table 3.2 RMSE and bias estimates for WRF 2 m surface temperature against meteorological stations

Meteorological Station number	CWRF and station T2 RMSE	CWRF and station T2 bias (°C)	EWRf and station T2 RMSE	EWRf and station T2 bias (°C)
71990	7.10	-4.06	3.85	-2.5
72100	7.92	-3.6	3.96	-2.5
80700	8.94	-6.8	6.78	-6.23
87350	5.93	-2.8	3.32	2.05
88920	7.65	-2.44	4.03	-1.93
89350	8.14	-1.86	4.70	-1.41
91370	8.78	-5	5.72	-4.59
92350	5.57	-2	3.6	2.21
98400	11.17	-8.5	9.45	-8.28

b. Snow depth

Both sets of WRF simulations overestimated the snow depth at the majority of the meteorological stations. The CWRF simulated snow depth had slightly higher RMSE and bias values compared to the EWRf snow depth, fitting with the cold bias identified above. The RMSE values for CWRF snow depth, ranged from 21 to 123.6 and the bias ranged from -0.03 to 83 cm. Whereas the RMSE values for EWRf ranged from 9.7 to 83.6, and the bias ranged from -0.5 to 76.5 cm. The highest bias values observed for CWRF and EWRf were at different stations. For CWRF the highest bias was observed at comparatively southern station (at 65.4 °N), whereas for EWRf it was at a station above the Arctic Circle at 69 °N.

Table 3.3 RMSE and bias estimates for WRF snow depth against meteorological stations

Meteorological Station number	CWRF and station snow RMSE	CWRF and station snow bias (cm)	EWRF and station snow RMSE	EWRF and station snow bias (cm)
71810	52.26	-16.65	43.39	-26.11
71900	46.26	10.22	60.97	19.5
75020	20.93	-0.04	9.73	-0.55
77290	123.65	83.02	77.88	67.17
91110	55.97	31.84	52.75	47.22
97250	25.58	15.02	29.18	24.67
85410	43.94	11.45	18.92	8.5
85540	66.74	49.3	77.2	22.3
89800	79.12	66.19	83.55	76.53
76380	81.22	48.35	50.60	37.97

3.2.5 WRF's reproducibility of meteorological conditions leading to past browning events

3.2.5.1 Model domain setup

Three observed browning events were selected as case studies to validate WRF's reproduction of the extreme weather conditions, which lead to vegetation damage at the three different locations (Bjerke et al., 2017; Treharne, 2018). Here, WRF was forced with ERA5 as currently ERA5 is the latest reanalysis product and offers a robust representation of past meteorological conditions (Serreze et al., 2021). The browning event simulations are here onwards referred to as EWRF-BE for ease. Because these experiments were aimed at verifying WRF's performance in the context of simulating actual extreme events, and spanned a shorter time period, i.e., a single winter season for each site, it was computationally affordable to run these at a very high resolution, 1-3 km, as compared to the other decadal scale simulations (run at 10 km). While the initial aim was to run all the three browning sites at

the same spatial resolution i.e., 1 km, due to WRF becoming unstable at the Flatanger site when run at 1 km, it was forced at a lower 3 km spatial resolution here. Another issue with the high-resolution case-study simulations was during the post-processing of WRF output for the Storfjord study site. The d03 1 km WRF files turned out to be corrupted, and, therefore, the d02 (5km) simulations were assessed. Table 3.4 and Figure 3.3 summarise and show the domain setup and locations for these simulations. Table 3.5 summarizes the meteorological conditions attributed to the extreme winter weather events at the three case study sites (Treharne, 2018).

Table 3.4 Summary of the EWRf-BE simulations setup

Browning site	Time period	Driving model	Domain resolution (km)
Flatanger	Nov 2013-Apr 2014	ERA5	d01 30, d02 10, d03 3
Lofoten	Nov 2013-Apr 2014	ERA5	d01 25, d02 5, d03 1
Storfjord	Nov 2011-Apr 2012	ERA5	d01 25, d02 5, d03 1

WPS Domain Configuration



Figure 3.3 (a) WRF domain setup for the case study Flatanger

WPS Domain Configuration

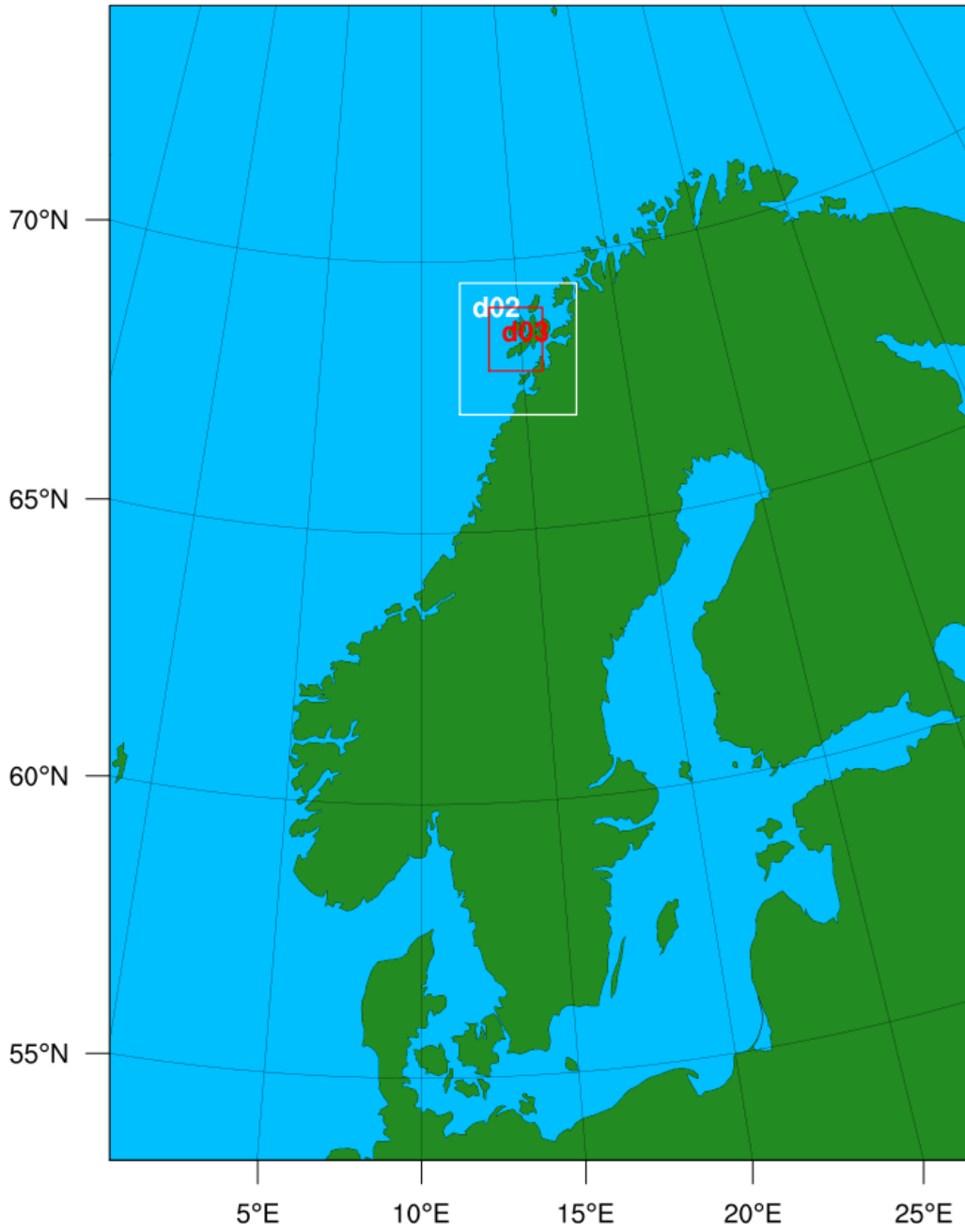


Figure 3.3 (b) WRF domain setup for the case study Lofoten

WPS Domain Configuration

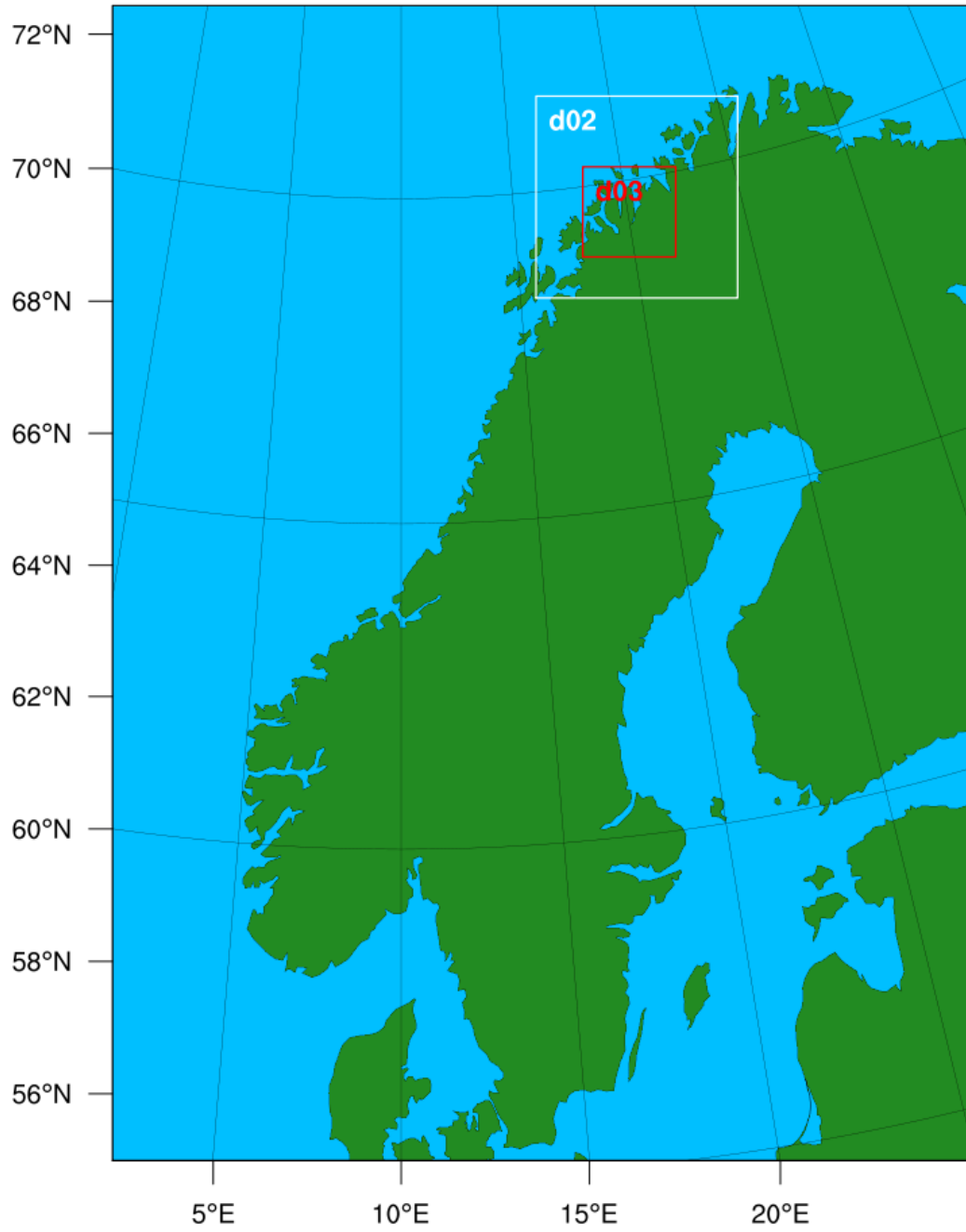


Figure 3.3 (c) WRF domain setup for the case study Storjford

Table 3. 5 Summary of extreme winter weather conditions for the case study browning events

Study site	³ Climatology (Fig 3.4)	Meteorological conditions during the extreme weather event (Treharne, 2018)
Flatanger, Trøndelag	Dfc (Subarctic)	2013/14 winter Extreme winter warming and frost drought conditions <ul style="list-style-type: none"> • Mid-December 10°C temperatures • 3 Dec weeks, complete snowmelt • 11.9°C temperature fall within 24 hours in early January
Lofoten, Nordland	Cfc (Subpolar oceanic)	2013/14 winter Frost drought <ul style="list-style-type: none"> • Anomalous mild December, • Severely dry conditions caused vegetation desiccation in January, February and early March 2014
Storfjord, Troms og Finnmark	ET (Tundra)	2011/12 winter Extreme winter warming and frost drought conditions <ul style="list-style-type: none"> • Extremely dry winter • Snow depth < 5cm or absent • Unusually large variations in temperature

Köppen climate types of Norway

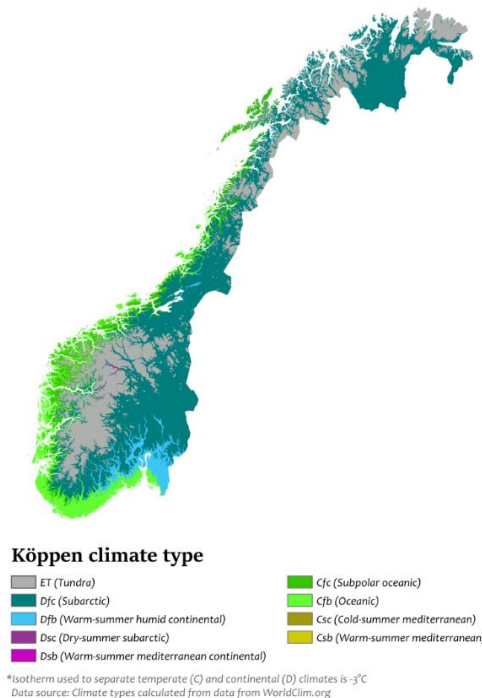


Figure 3.4 Map of Norway with the Köppen climatic zones (Beck et al., 2018).

³ For the climatology classification see Beck et al. (2018)

3.2.5.2 Climate indices for quantifying extreme winter weather at browning sites

Extreme weather events described by simple climate indices have been shown to explain vegetation browning induced change in both plot and satellite based NDVI in the subsequent growing seasons (Treharne et al., 2020). To assess WRF's performance with regard to reproducing the extreme meteorological conditions which lead to vegetation browning at Flatanger, Lofoten and Storfjord, different indices related to extreme winter weather were estimated for each site. The indices are summarised in Table 3.6.

Table 3.6 Summary of climatological indices used within RO2

Extreme weather event index	Definition
a. Warm event frequency (WWE)	Daily mean T2 > 2 °C, 3 consecutive days
b. Maximum duration warm event (MDW)	Maximum days where T2 > 2 °C
c. ROS	Liquid prec. > 1 mm, snow depth > 1 cm
d. Snow count (SC10)	Snow depth < 10 cm day count
e. Snow count (SC20)	Snow depth < 20 cm day count

The above indices were selected based on the literature review of past studies related to extreme winter weather events in the Arctic, presented in section 3.2. For example, ROS is known to damage Arctic vegetation through ice-encapsulation mechanisms (Bjerke et al., 2011). Liquid precipitation for estimating the ROS index was obtained by applying a temperature threshold of 1.5° C to the WRF precipitation output. This temperature threshold was applied to distinguish between snow and rain, as explained in detail by Jennings et al. (2018). Moreover, because this research strongly builds upon previous Arctic browning related studies, especially the field work conducted by Treharne (2018), who have defined winter warming in relevance to how it damages vegetation, this PhD research

incorporates their definition of a winter warming event i.e., surface temperature stays above 2°C for at least 3 consecutive days.

To further validate WRF's skill in reproducing the actual extreme weather events which caused browning, WRF's simulated near-surface temperature was compared against the nearest meteorological station observations for each browning site. For this, meteorological station temperature data was downloaded from Norway's publicly accessible climate database (seklima.met.no). WRF-temperature timeseries were extracted at the nearest grid-point to a meteorological station location for each case study site, respectively. Bias and RMSE between WRF-temperature and station temperatures were then calculated. In assessing WRF's reproduction of the real extreme winter weather conditions at the three case study sites, a simple bias correction was applied to the snow and temperature parameters. For example, in case of a cold bias in WRF temperature, the calculated bias figure was simply added to the WRF temperature.

3.2.6 Analysing winter meteorological variables and satellite NDVI relationships

As discussed in earlier sections, RO2 of this PhD is aimed at determining the most important winter meteorological parameters related to vegetation browning. This is done through understanding the relationship between satellite NDVI and winter climate. This understanding would then help achieve RO3 as well, which is focused on obtaining projections of future occurrence of browning events under different climate change scenarios.

3.2.6.1 WRF setup and data pre-processing

WRF was run to produce winter season, November-April, simulations for the time-period 2000-2020. The selection of the 2000-2020 time interval for the analysis was based on the availability of MODIS NDVI data. ERA5 reanalysis provided the input to drive WRF here. The domain setup for these simulations consisted of an outer domain at 30 km and the inner at 10 km grid. Figure 3.5 shows the domain setup for these simulations.

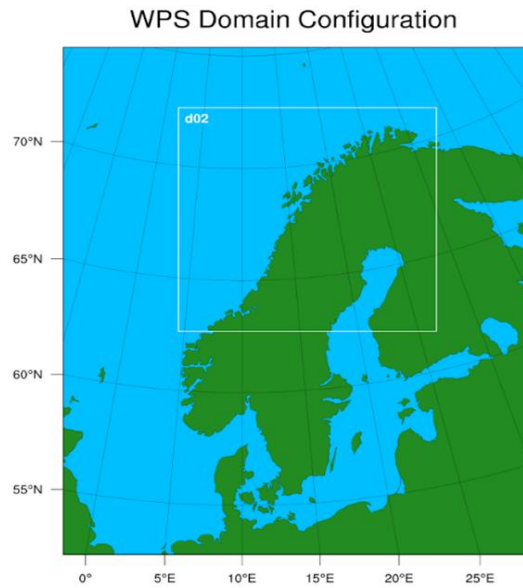


Figure 3.5 Domain setup for WRF winter simulations 2000-2020

The analysis conducted in Chapter 2 of this thesis provided evidence of MODIS NDVI being the most suitable satellite-based index to quantify on-ground observed vegetation damage in Norwegian Arctic and sub-Arctic areas. Therefore, the **mean of the** growing season MODIS NDVI was selected. The NDVI product used here is MOD13Q1, which has also been discussed and used in chapter 2. The NDVI product was pre-processed before carrying out the statistical analysis. The pre-processing steps for the NDVI consisted of estimating the average growing season NDVI for each year (2001-2020) and then reprojecting the NDVI timeseries onto WRF's projection system and simulation resolution. These pre-processing steps were performed in Google Earth Engine Code Editor and Python.

3.2.6.2 Statistical Analysis

The objective of the statistical analysis was to understand how different stages of the preceding winter climate impact the subsequent summer NDVI. Since the resolution of the NDVI dataset was 16 days and WRF'S output was on a daily interval, both the datasets were aggregated before performing the analysis. WRF variables were averaged (or summed for the indices in Table 3.6) for each winter month. This helped in producing an equal timeseries, i.e., 20-timesteps, for each climatological variable, for each winter month spanning 2000-2020, and 20-timesteps as well for NDVI, on a seasonal basis,

spanning 2001-2020. So, for example, mean November 2m surface temperature for each year starting 2000 up to 2019, is 20 time steps, correlated with each June – September averaged NDVI starting 2001 up to 2020, another 20 time steps. The significance of the correlations between climatological variables in different months and seasonal NDVI was tested at two significance values, $p < 0.05$ and $p < 0.01$. The calculation of the meteorological indices, monthly means and the correlations was on the model grid box scale (10 x 10 km), along the time dimension, unless stated otherwise.

The correlation analysis was followed by multivariate regression analysis. The objective of the multivariate regression analysis was to understand the role of different winter meteorological parameters in explaining the summer NDVI. The analysis was conducted separately for three case study sites, Flatanger, Lofoten and Storfjord. These are the same study sites as used for the high-resolution WRF simulations under section 3.2.5, as well as in chapter 2 for the remote sensing based analysis of actual browning events. The three study sites fall under three different counties of Norway, Trøndelag, Nordland and Troms og Finnmark (location shown in Chapter 2, Figure 2.1). The predictor variables used within the multivariate regression analysis at each site were based on the results of the correlation analysis. The winter meteorological parameters/indices which had shown significant correlations with summer NDVI at the county level were input to step-wise multivariate regressions.

Broadly it was assumed here that meteorological variables in their raw form, i.e., temperature, precipitation and snow depth, were likely to be related to ‘trend browning,’ whereas the indices which reflect extreme winter conditions and events were more likely to be linked with ‘event browning’ (Personal conversation with Prof. Gareth Phoenix, 2022).

The predictor variables for the regressions were tested for multicollinearity before conducting the analysis, using the Variance Inflation Factor test (Wilks, 2015). The analysis here was performed in Python and RStudio. Table 3.7 provides details of the variables used in the statistical analysis.

Table 3.7 Inputs for the climatological variables-NDVI analysis

Variables	Time period	Spatial resolution processing	Temporal resolution processing
Growing season NDVI (MOD13Q1)	June – September	250m to 10 km	16 days to seasonal average
WRF meteorological parameters	Preceding November - April	10 km	Daily to monthly Averaged and/or frequency

3.3 Results

3.3.1 WRF's reproducibility of climatic conditions associated with real browning events

3.3.1.1 Extreme winter warming event at Flatanger 2013/14

This section presents results of WRF's high-resolution, 3 km, simulations for reproducing the on-record December 2013 winter warming event at Flatanger, Norway (Treharne, 2018). Figure 3.6 shows (a) winter warming event frequency (WWE) and (b) maximum duration winter warming event (MDW) indices respectively, for Flatanger.

WRF's simulations showed at least one warming event had occurred throughout the domain area, whereas the areas nearest to the coast experienced more than two warming events during December 2013. With regards to duration of the warming events, Figure 3.6 (b) shows a noticeable variation over the domain for duration of the longest lasting warming event at each grid box. For example, the areas closest to the coast consisted of the longest warming events of 10-12 days, whereas at the more inland areas the longest warming event was of 2-6 days.

Comparing the two figures, it is evident that for most of the domain, although a single warming event had occurred, the duration was different for several 3x3 km grid boxes; thus, highlighting the significance of micro-scale meteorology that can influence vegetation exposure to damaging climatic events.

Plant responses to anomalous winter warming events have been shown to be both species dependent and event dependent (Bokhorst et al., 2011). Thus, because vegetation in the Arctic is quite heterogeneous there could be varied plant responses at a micro-scale to the varying duration and intensity of winter warming events at a 3x3 km grid. Therefore, there are resultant difficulties in predicting a browning event in terms of a homogenous, mean reduction in vegetation NDVI, at a regional scale.

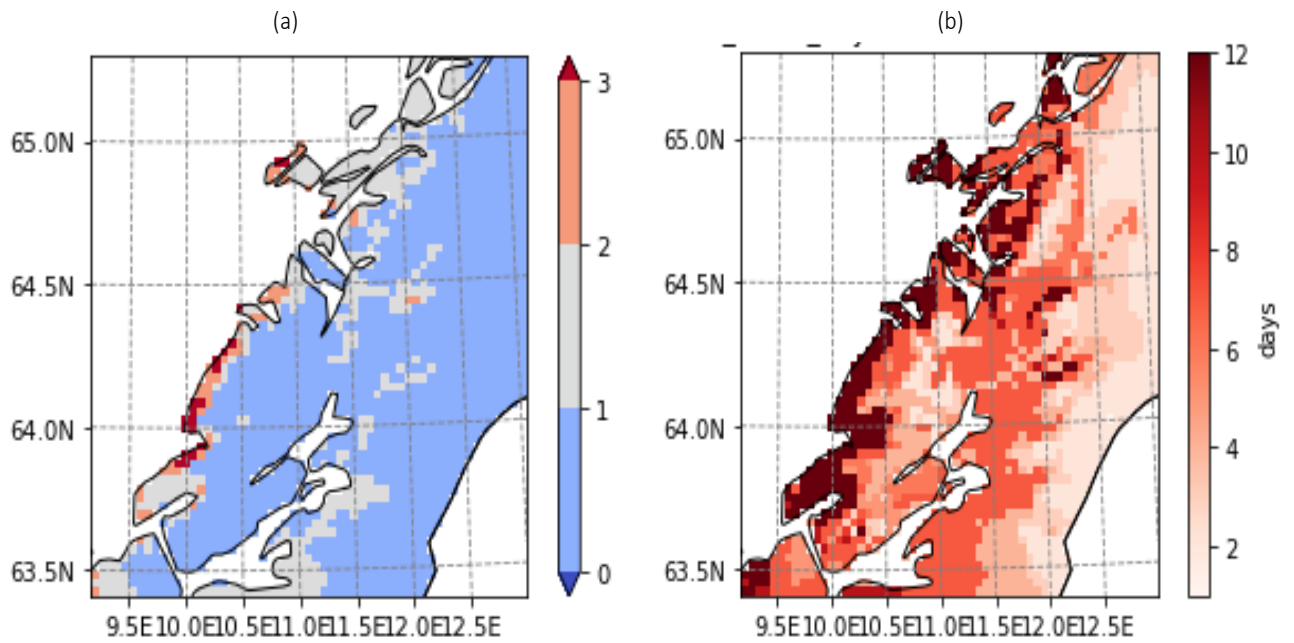


Figure 3.6 (a) Winter warming event frequency (WWE) index and (b) Maximum duration winter warming event (MDW) index for December 2013 at Flatanger, Norway (64.4° N, 10.6° E). Indices were estimated from the WRF high resolution (3km) simulations.

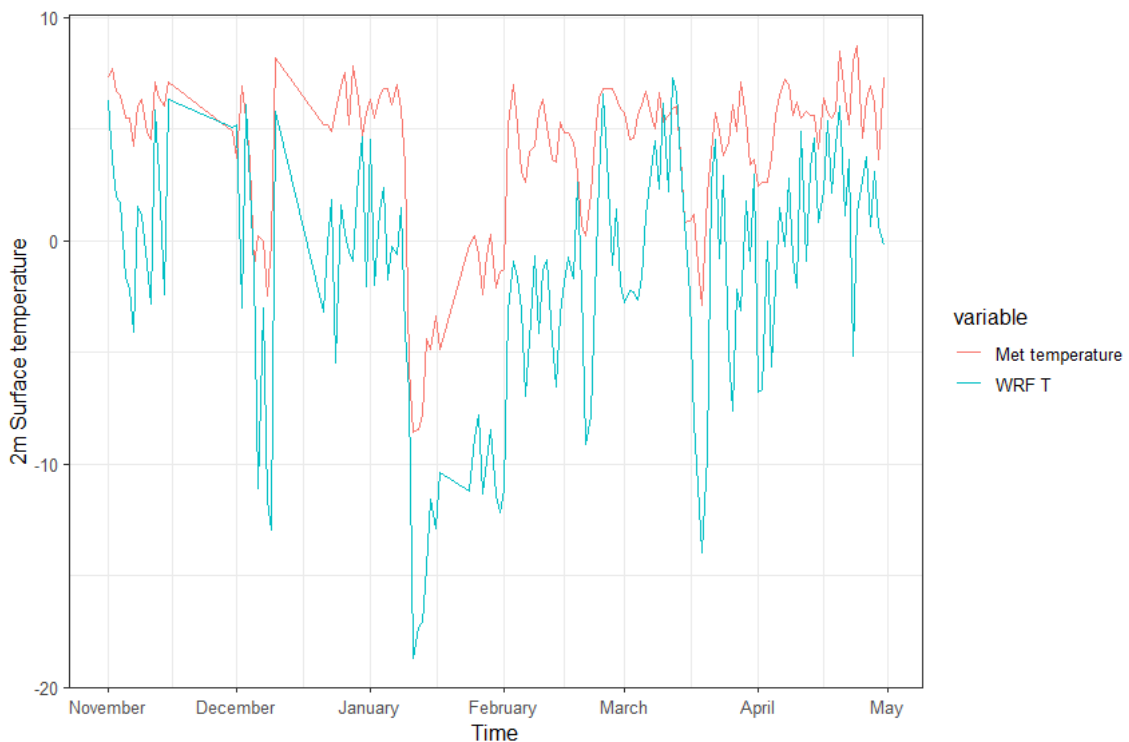


Figure 3.7 WRF daily 2m near-surface temperature and nearest meteorological station (Buholmråsa Fyr, 71900) air temperature for November 2013 – April 2014 at the Flatanger study site

Figure 3.7 shows the daily mean air temperature observations of the meteorological station nearest to the Flatanger browning site and 2m surface temperature simulated by WRF at the study site. The station observations showed that December 2013 experienced temperatures above 5°C for quite a few consecutive days. This was anomalous for December, when temperatures are usually well under 0°C (Hanssen-Bauer et al., 2017). It should be noted that although the temperature kept fluctuating above 0°C throughout the other winter months, it did not stay consecutively as warm (above 5°C), for as long as in December. Although WRF's temperature simulations at this site had a cold bias of 5.7 °C, overall, it followed the trajectory of the station temperature for most of the 2013/14 winter, with WRF capturing the timing of the temperature increases and decreases.

Comparing the WWE and MDW indices with the meteorological station observations, it can be concluded that WRF was able to reproduce a winter warming event signal for December 2013. It is important to note that due to WRF's cold bias of the near-surface temperature simulations over Norway, as explained in section 3.2.4.4 (a), the warming indices estimated here were quite likely underestimated.

In the context of the winter warming event at Flatanger, Treharne et al. (2018) have also discussed how the complete snowmelt that occurred over three weeks in December 2013, as a result of the winter warming, exposed vegetation to freezing temperatures in January. Hence to further validate WRF's reproducibility of the 2013/14 winter warming event, mean snow depth maps were produced for early, mid and late December 2013. Figures 3.8 (a), (b) and (c) show the mean snow depth at various stages in December. Figure 3.8 (b) shows that mid-December average snow depth across the study area was lower as compared to the early December mean snow depth.

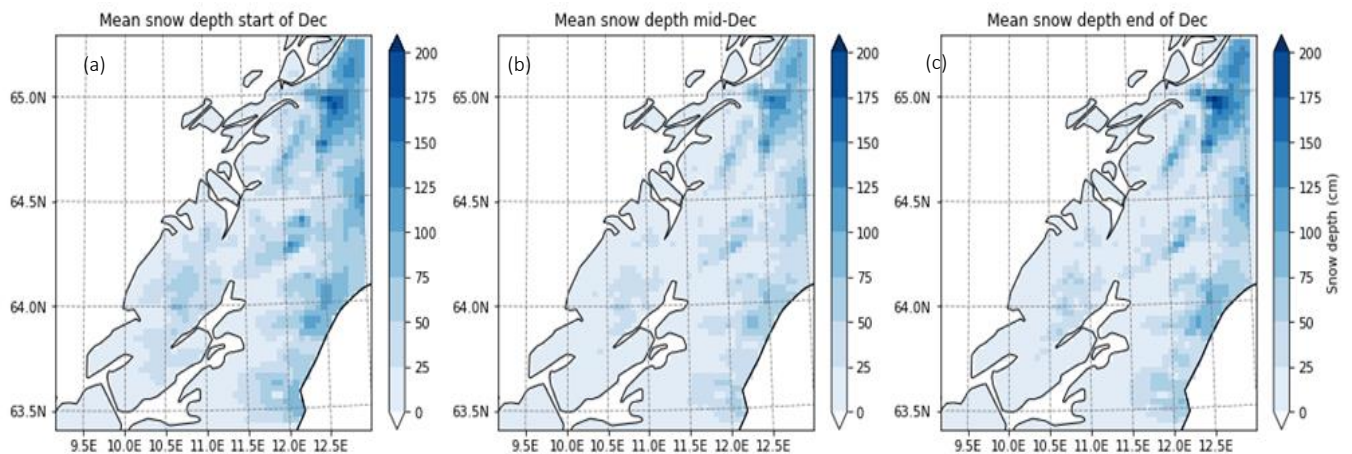


Figure 3.8 WRF mean snow depth for the Flatanger study site (64.4° N, 10.6° E) and surrounding areas (a) 1-10th December (b) 11th-20th December (c) 21st-31st December 2013 respectively

This mostly agrees with snow depth observations obtained from the nearest meteorological station, shown in figure 3.9. The meteorological observations show the absence of snow cover starting in mid-December 2013. However, very few grid boxes showed completely snow-free days, compared to the met station observations for December, 2013. This is because WRF tends to overestimate snow depth, as explained in section 3.2.4.4 (b).

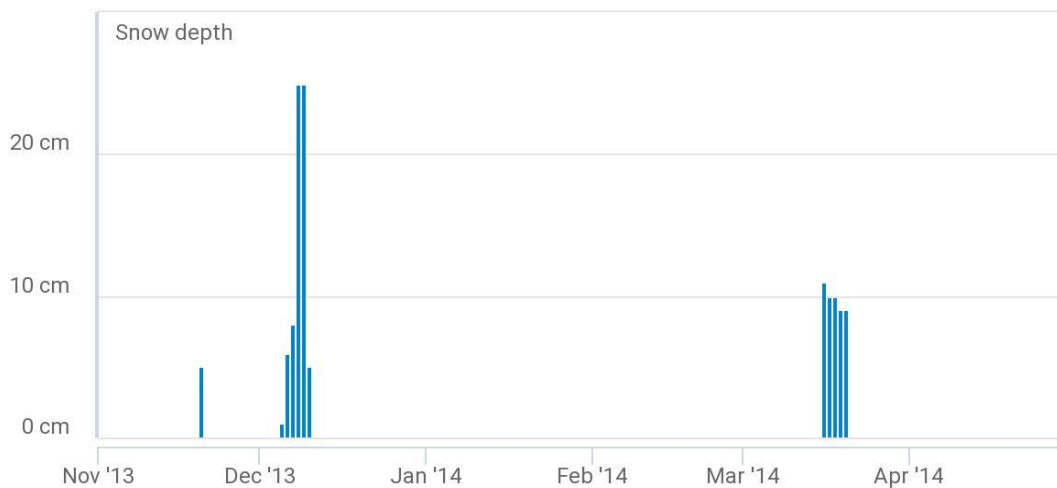


Figure 3.9 Daily mean snow depth observation from the meteorological station (71900) nearest to the Flatanger study area.

To summarise the findings of the Flatanger study site, the analysis conducted here showed that despite WRF's tendency to underestimate temperature (cold bias) and overestimate snow depth across Norway, it was able to reproduce the extreme winter warming event that led to snowmelt at this site. The WWE and MDW indices were able to show the extreme winter warming events at Flatanger.

3.3.1.2 Frost drought conditions at Storfjord 2011/12

This section presents results of the analysis conducted to evaluate WRF's capability of reproducing the 2011/12 extreme winter weather conditions at the Storfjord study site. Previous research (Bjerke et al., 2014) has attributed the vegetation damage observed at this site in Spring 2012 to high-temperature variability and frost drought conditions in December - January 2011/12.

Frost drought conditions can be damaging to vegetation. These usually consist of extreme cold spells with low or absent snow cover in winter, which can expose vegetation to freezing temperatures, wind and solar irradiance. Moreover, mid-winter thaw is also a typical and common feature of frost drought as well as winter warming events (Bjerke et al., 2014). WRF's overall ability to simulate frost drought conditions was examined based on both snow depth and surface temperature parameters.

Figure 3.10 presents the maps of count of days where snow depth < 5cm, at each model grid-box of the Storfjord study site, for December 2011 and January 2012. These maps were produced using WRF's 5km grid-resolution simulations and bias-corrected snow depth.

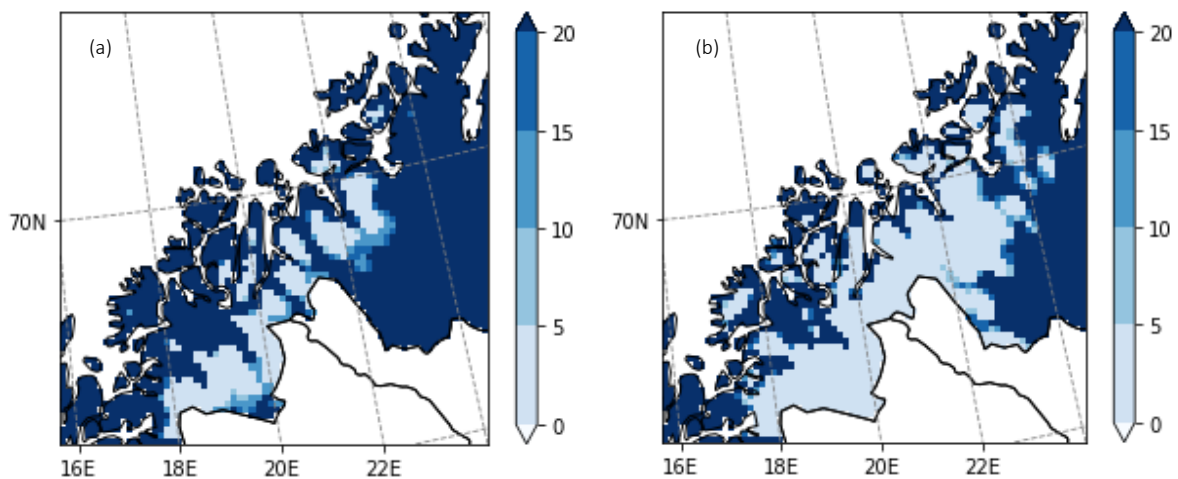


Figure 3.10 Maps showing the day count where snow depth < 5 cm at the Storfjord study site (69.3°N, 19.9°E) for (a) December 2011 and (b) January 2012. Maps were produced using WRF simulations at a grid resolution of 5 km and daily time step.

Figures 3.10 (a) and (b) showed that in both December and January there were several days where the snow depth < 5cm. The count of such days ranged from 5 to more than 20 per month, across the study

domain. Interestingly, the higher count of low snow depth days occurred at lower elevation areas. This is because the higher elevation and mountainous regions in Norway still continue to have winters with temperatures well below 0 °C, despite recent warming trends over most of Norway (Dyrrdal et al., 2013). Hence, snowfall accumulated in such areas is deeper compared to the low-lying areas and does not melt as quickly.

In the context of mid-winter thaw, which is a common feature of frost drought conditions, January was considered as the peak mid-winter month to analyse any snow melt events which could have occurred. Figure 3.11 presents the snow depth of the nearest meteorological station and WRF's snow depth (5km resolution) at the Storfjord study site for January 2012. The general trend of the WRF snow depth was found to be similar to that at the nearest meteorological station, other than that WRF overestimated the snow depth throughout January, despite the bias correction. Both WRF and observations showed that snow cover was unstable throughout January 2012, with WRF's snow depth simulations fluctuating more than those at the station. The WRF mean snow depth for January 2012 was 7.8 cm, slightly higher than the meteorological station, which was 5.8 cm (Table 3.8). Both means were significantly lower than the 1990 – 2020 January average, which was 34.7 cm. Overall, WRF was able to simulate the variable and reduced snow cover at the Storfjord site. Table 3.8 presents the mean and standard deviation of December and January snow depth, calculated from the nearest meteorological station observations.

Table 3.8 Standard deviation and mean of snow depth observations from the nearest meteorological station to the Storfjord site

Snow depth (cm) Met station (Bardufoss 89350)	Standard deviation (cm)	Mean (cm)
December 1990-2020	15.5	22.6
December 2011	5	6.8
January 1990-2020	20.17	34.7
January 2012	3.4	5.8



Figure 3.11 WRF and the nearest meteorological station (Bardufoss 89350) snow depth for January 2012 at the Storfjord study site

In combination with low snow cover, winter warming events can also lead to frost drought conditions (Bjerke et al., 2017). Therefore, following the analysis of snow depth at Storfjord, this section presents results of WRF's capacity to reproduce the temperature related parameters that could help explain whether winter warming events had a role in creating the frost drought conditions at Storfjord.

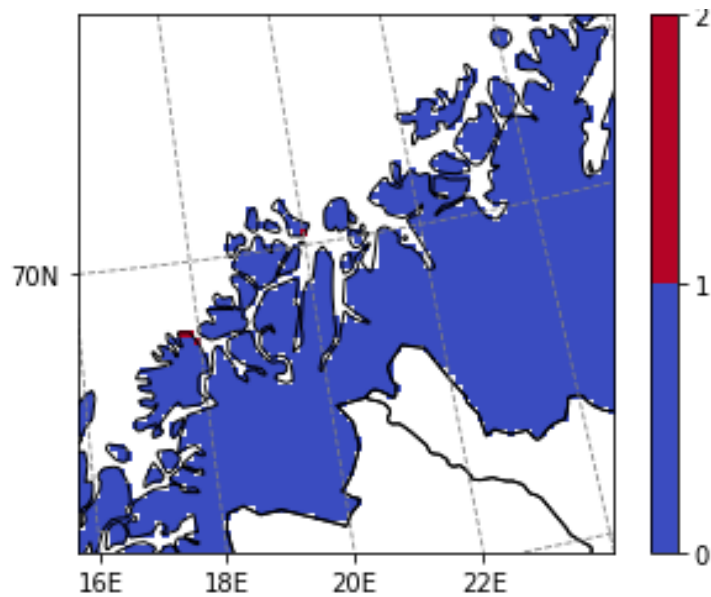


Figure 3.12 WRF-based WWE index for the Storfjord site (69.3°N , 19.93°E) for the time period December 2011 – January 2012. WRF's grid resolution was 5 km.

Figure 3.12 shows the WWE index map for December 2011 - January 2012. The WRF simulations did not show a winter warming event over this time period at the Storfjord study site, in agreement with the nearest meteorological station temperature observations, which also showed an absence of winter warming events in both December 2011 and January 2012. Figure 3.13 presents the nearest meteorological station's mean, maximum and minimum near-surface air temperature, and the snow depth observations for the 2011/12 winter. These show that the mean surface temperature stayed under zero throughout December and January. For February the temperature increased slightly above 0°C for a day or two, however that did not qualify as a winter warming event as defined in Table 3.6.

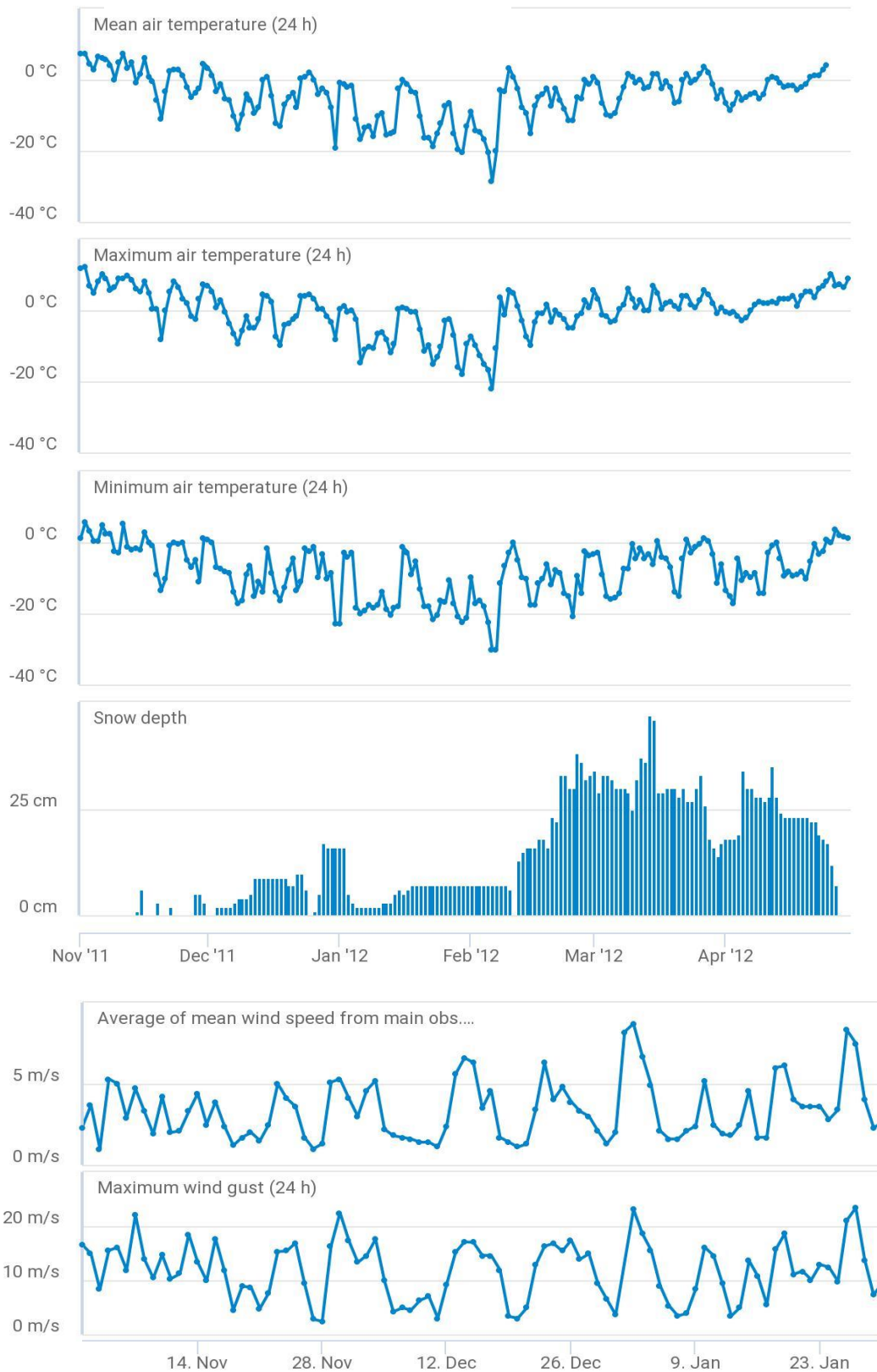


Figure 3.13 Mean, maximum and minimum near-surface air temperature, snow depth (Meteorological station Bardufoss), mean wind speed and maximum wind gust observations (Meteorological station Skibotn), (top to bottom), from the meteorological stations nearest to the Storfjord study site, for the 2011/12 winter.

Thinner initial snow depth results in more snow removed by warming events, high wind speed and ROS (Semenchuk et al., 2013). In the case of the Storfjord study site, the snow depth was quite low at the onset of winter in November 2011 (as shown in Figure 3.13). It is worth noting that the snow depth varied during late December and early January, although the mean air temperature stayed under 0 °C. Therefore, the wind speed observations of the nearest meteorological station were checked for potential wind redistribution of the snowpack at this site. In addition to the temperature and snow depth observations, Figure 3.13 shows the mean wind speed and maximum wind gust of the nearest station at Storfjord study site. The station's elevation was 20 m a.s.l. On average, dry snow can be blown away by a wind speed of 7.7 m/s (Li and Pomeroy, 1997). The wind charts showed that at the end of December/start of January, this area experienced mean wind speeds of above 5 m/s, which could have caused snow redistribution and thus, potentially, the snow depth to decrease at this time. Hence this evidence suggested that in cases where the existing snow cover was shallow, wind speed could be an important meteorological parameter in predicting vegetation damage resulting from exposure to freezing temperatures in low snow conditions.

In addition to low snow cover and winter warming events (as discussed above), high temperature variability in December and January 2011-12 has also been discussed as one of the possible meteorological conditions leading to the frost drought at Storfjord (Treharne, 2018). The analysis here, however, showed that the temperature variability for December 2011 and January 2012 was actually lower than the mean climatological variability observed for these months over the past 30 years, as shown in Table 3.9, which provides the standard deviation of daily temperature for December and January over the time period 1990 – 2020 and December and January 2011/12, based on the nearest meteorological station to the Storfjord study site.

Table 3.9 Standard deviation and mean of temperature observations from the nearest meteorological station (Bardufoss 89350) to the Storfjord site

Time period	Standard deviation of near surface air temperature (°C)	Mean near surface air temperature (°C)
December 1990-2020	7.6	-6.8
December 2011	5.3	-5.1
January 1990-2020	8.0	-8.4
January 2012	6.4	-10.4

Standard deviation maps of WRF's daily mean temperature were produced for the entire domain as well, for December 2011 and January 2012, as a measure of daily temperature variability (Figure 3.14). WRF did well in reproducing the variability in daily temperature at a few inland and coastal areas; however, it underestimated the variability across the majority of the Storfjord study domain grid boxes. The WRF standard deviation range at such grid boxes was 2.0 - 3.5 °C for both December and January, whereas the meteorological station values were 5.3 and 6.4 for December and January, respectively (Table 3.9).

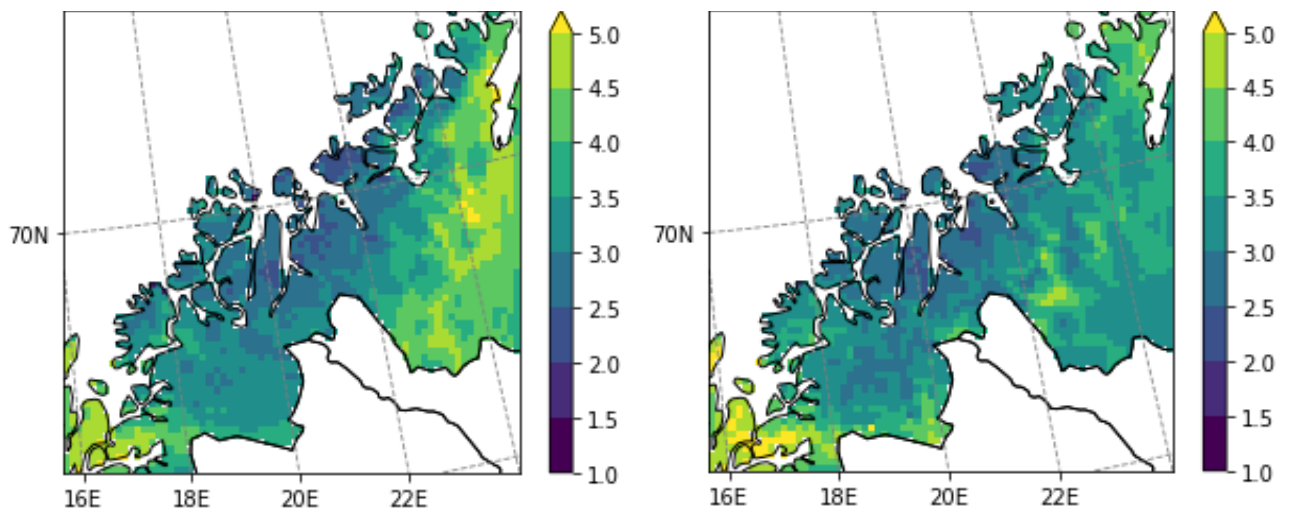


Figure 3.14 Standard deviation maps of WRF's daily mean temperature for December 2011 and January 2012 at the Storfjord study site (69.3°N, 19.9°E). The WRF simulations were run at a 5 km grid resolution here.

WRF's simulated temperature for mid-winter, January, at the vegetation damage site, was compared to the meteorological station temperature, shown in Figure 3.15. Although WRF's simulated temperature at Storfjord had a mean cold bias of 2.6 °C with regard to the nearest meteorological station, in general, WRF's temperature trajectory over January 2012 agreed with the observations. Although differences of up to 10 °C were observed for some dates at the beginning and end of January, despite the bias correction.

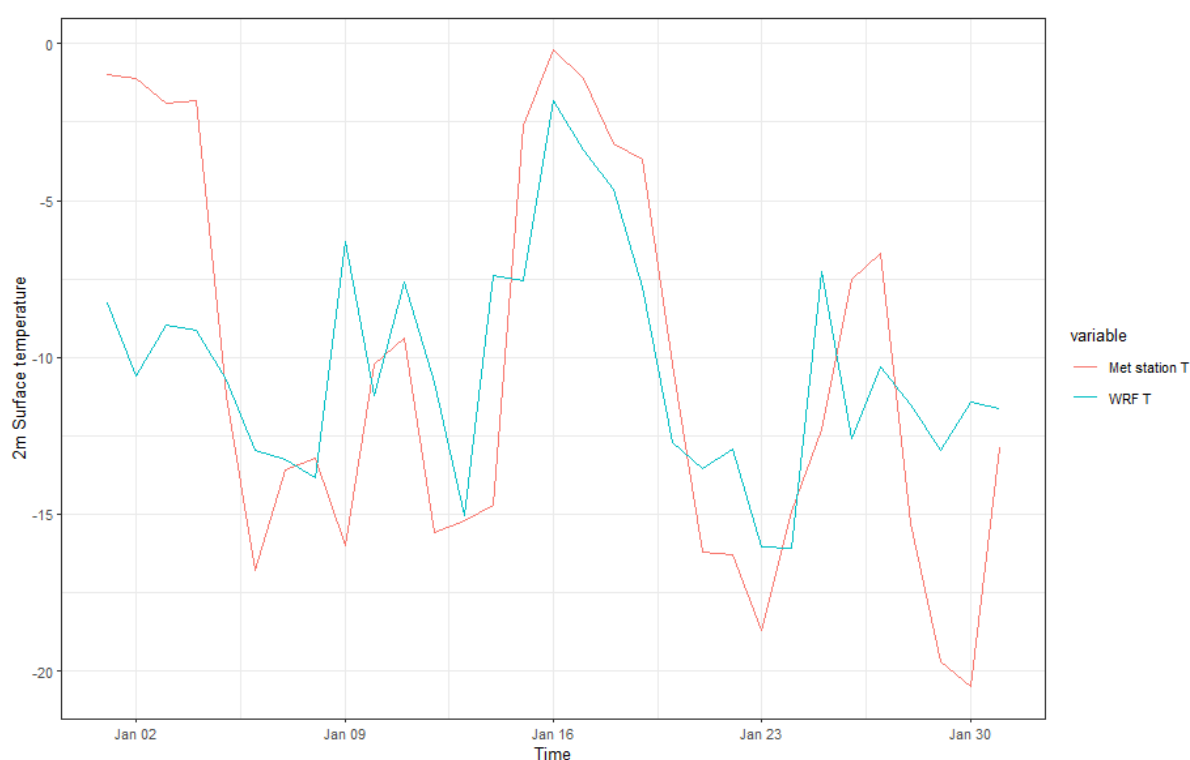


Figure 3.15 WRF daily 2m near-surface air temperature and nearest meteorological station (Bardufoss 89350) air temperature for January 2012 at the Storfjord study site.

To summarise the findings of the Storfjord site, the analysis conducted here showed that it was a combination of severely low snow conditions in early to mid-winter, and consequent exposure to freezing mid-winter temperatures, which caused the vegetation damage at this site.

3.3.1.3 Winter warming and frost drought conditions at Lofoten 2013/14

Vegetation damage and mortality at Lofoten was reported for the 2014 growing season. The disturbance has been attributed to winter warming events and frost drought conditions (Bjerke et al., 2014; Treharne, 2018). Results of the analysis conducted in this chapter mostly corroborates previous research.

Temperature observations from the nearest meteorological station showed that during the 2013/14 winter the Lofoten study site experienced recurring episodes of warm temperatures, ranging from 0 – 5 °C, with intermittent return to freezing temperatures (minimum of -5.0 to -7.5 °C), between the winter warming events. Surface temperatures from the nearest meteorological station (85560) and from WRF simulations at the study site, are shown in Figure 3.16. WRF's temperature simulations had a cold bias of 4.7 °C as compared to the met station. The bias-corrected WRF temperature closely followed the meteorological station temperature for most of the 2013/14 winter.

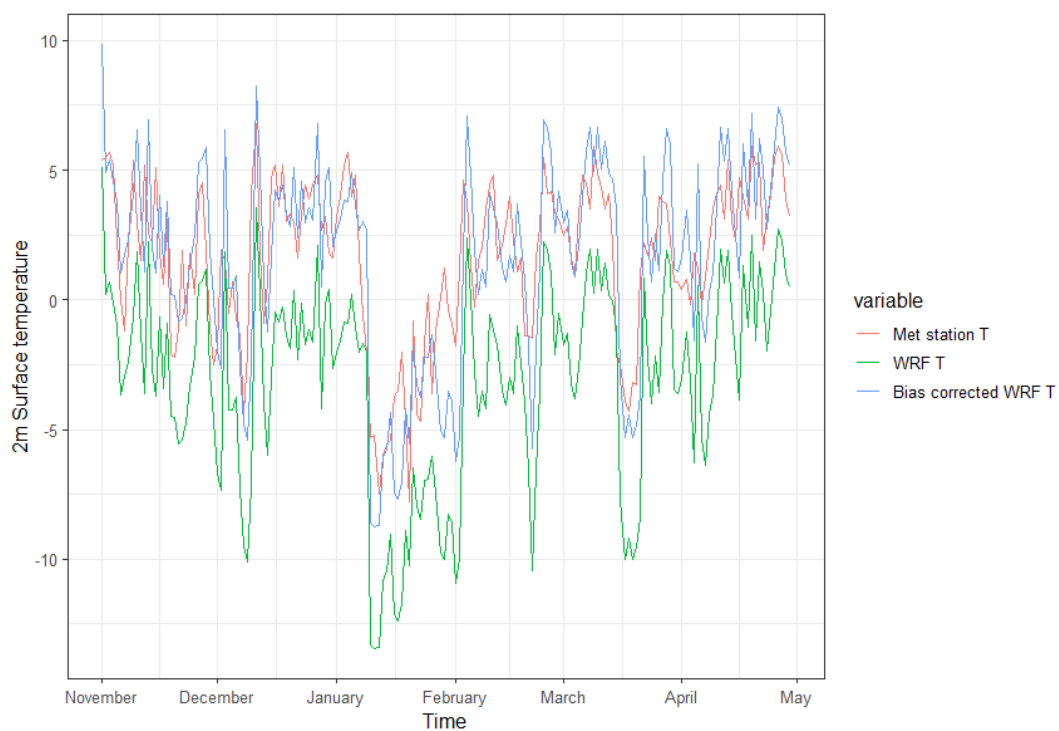


Figure 3.16 WRF 2m daily near-surface air temperature and nearest meteorological station near-surface air temperature for November 2013-April 2014 at the Lofoten study site

Table 3.10 Mean temperature during the 2013/14 extreme winter season at the meteorological station closest to the Lofoten study site

Winter month	Meteorological station (85560) mean temperature (°C) 2004 - 20	Met station (85560) mean temperature (°C) 2013/14
December	1.25	2.10
January	-0.17	-1.50
February	-0.50	2.17
March	0.19	1.73

To verify WRF's reproduction of the winter warming events at Lofoten, maps of the WWE and MDW indices were generated for the study domain. These maps are shown in Figure 3.17. The indices maps present the number of warming events and maximum duration warming event at each grid box, spanning December - March 2013/14. These are produced from the WRF simulations at a 1 km grid resolution. Figure 3.17 (a) shows that the majority of the land area experienced up to 8-12 warming events during December to March, where temperatures stayed above 2°C for at least three consecutive days. Figure 3.17 (b) shows that the longest warming event was in the range of 5-15 days across much of the study domain.

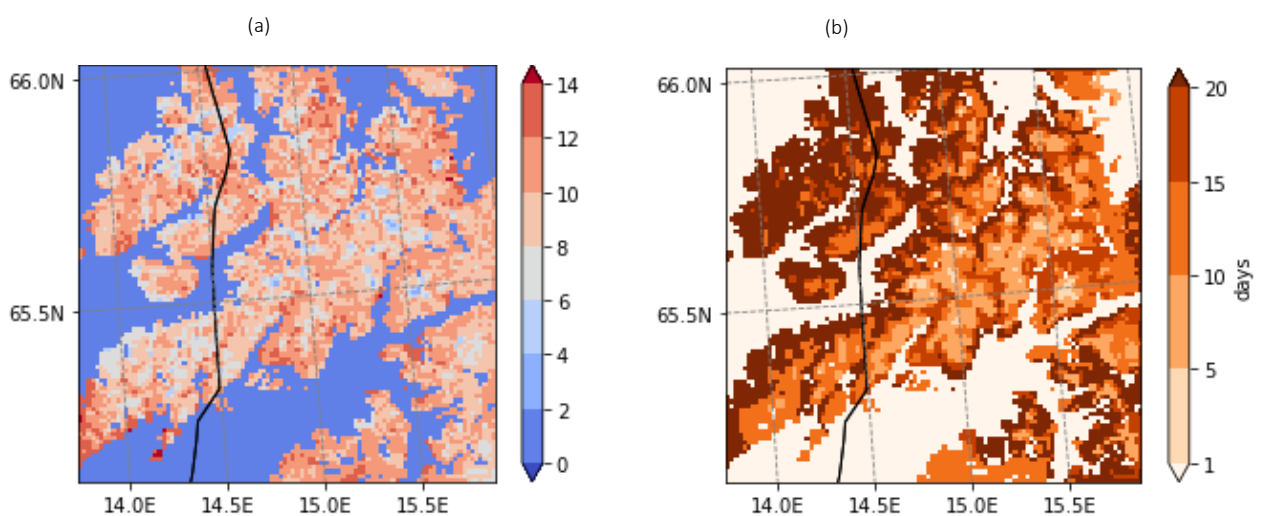


Figure 3.17 Maps of the Lofoten study site (68.1°N, 13.7°E) showing, (a) WWE and (b) MDW indices for December 2013 – March 2014. The indices were calculated using WRF simulations at a grid resolution of 1 km and daily time step.

After incorporation of the bias correction (adding the calculated bias, i.e., 4.7° C to the WRF temperature simulations), the WRF simulations captured the general temperature evolution and variability throughout the time period, with a 2.3 °C RMSE value. Overall, WRF's reproducibility of the mild temperature conditions in 2013/14 was good at a 1 km grid resolution. However, ideally the WRF simulations over this study domain should be validated against multiple meteorological stations located in this area so a more accurate assessment of the simulations could be carried out. Secondly, these high-resolution (1 km) simulations should be compared with coarser resolution simulations (10 km), to understand whether a higher resolution resulted in a significant reduction of model error in this region of Norway. However, such analyses were not possible given the time constraints of this PhD.

In addition to winter warming events, low and absent snow cover has also been attributed as a climatic driver that led to frost drought conditions at Lofoten (Treharne, 2018). Therefore, WRF's snow depth simulations were compared with snow depth observations from the two nearest meteorological stations (87750 and 85540). Figure 3.18 presents bias corrected WRF snow depth and meteorological station snow depth at the Lofoten study site, for the 2013/14 winter. The WRF snow depth had a 9 cm bias (w.r.t Meteorological station (87750), which is not large given the general uncertainty of NWP snow depth simulations. While WRF did reasonably well in capturing the overall trend of November - January snow depth, substantial differences were found between the WRF and observed snow depth values for the late winter months of March and April, even after the bias correction. WRF strongly overestimated the snow depth from mid-February to April.

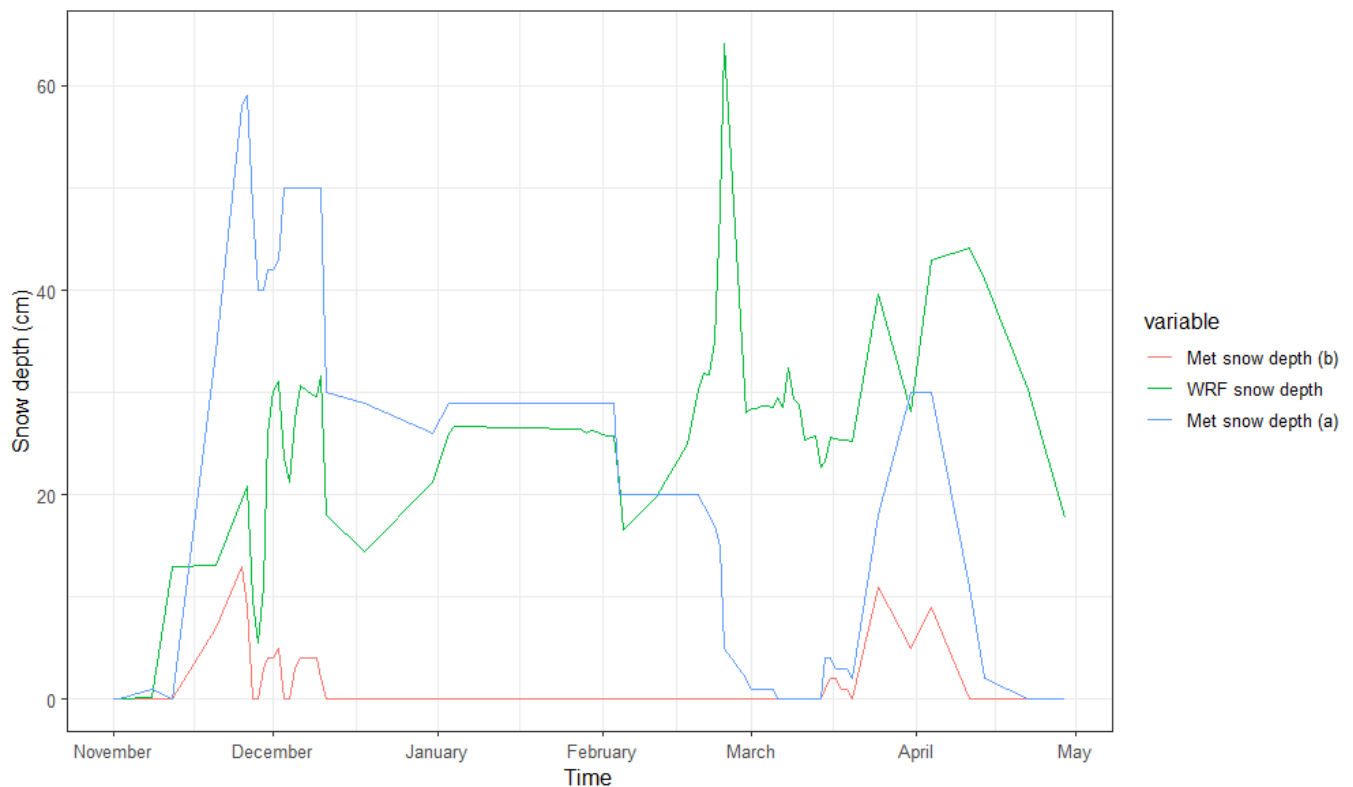


Figure 3.18 WRF and nearest meteorological stations snow depth for Nov 2013 – April 2014 at the Lofoten study site. WRF simulations were run at a 1km grid resolution here. Meteorological stations (a) and (b) refer to the 87750 and 85540 stations.

Table 3.11 presents the 30-year mean snow depth of different winter months and 2013/14 monthly mean snow depth at station 87750. While the December 2013 mean snow depth was significantly higher than the 30-year average, the mean values for February and especially March 2014, were much lower compared to the 30-year mean values. Although complete snowmelt did not occur in any month other than March for meteorological station (87750); another nearby station (85540) did show a complete snow melt time period starting mid-December up to mid-March, which is quite anomalous for a high Arctic region during winter months. The difference between the observations of these two meteorological stations highlights the substantial spatial variability of snow cover in coastal regions of Norway (Bokhorst et al., 2012). This implies that vegetation can get damaged even when snow melt occurs at a patch scale: for example, due to the influence of local temperature changes (Dyrrdal et al.,

2013) and that snow melt does not necessarily have to occur at a landscape scale (Bjerke et al., 2012) to cause vegetation disturbance.

Table 3.11 Mean snow depth during the 2013/14 extreme winter season at the meteorological station closest to the Lofoten study site

Winter month	Meteorological station (87750) mean snow depth (cm) 1990 – 2020	Meteorological station mean (87750) snow depth (cm) 2013/14
December	20.78	43.8
January	37	29
February	50	18.8
March	53.6	3.4

Another possible mechanism for vegetation damage at Lofoten could have been through ice-encapsulation of plants (Gareth K. Phoenix and Lee, 2004). The temperature and snow depth observations considered together i.e., the partial snow melt caused in mid-December due to winter warming, as indicated by meteorological station (a), and the return to freezing temperatures during January, suggest it is highly possible that ice layers would have formed within the snowpack, wherever snow still existed. One of the ways to estimate melted snow which exists as refrozen water (ice layers) could be through the snow water equivalent variable (SWE). An increase in SWE value after snowmelt could mean that either rainfall has been retained within the snowpack or melted snow has been refrozen. It can help explain the increase/decrease of water content within the snowpack (Dyrrdal et al., 2013). However due to time limitations of this PhD research, such analysis could not be conducted here.

In addition to the snow depth time series at the browning site, maps were produced of the total day count when snow depth < 5cm for the 1 km grid WRF domain over the Lofoten area. These maps were produced for different winter months and are shown in Figure 3.19.

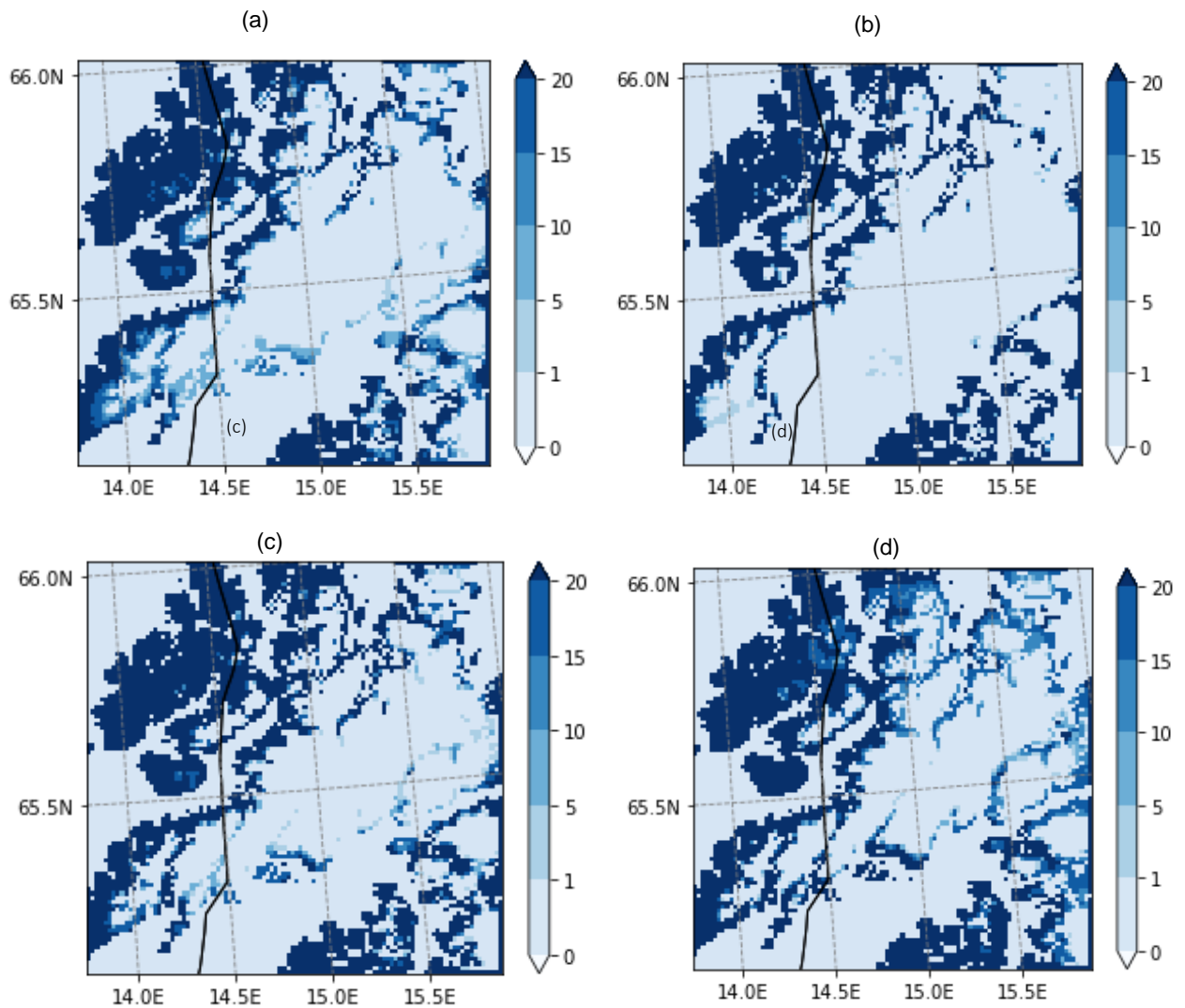


Figure 3.19 Maps showing the total day count where snow depth < 5cm, for the 1 km grid WRF domain over the Lofoten area. The maps show the months (a) December 2013 (b) January 2014 (c) February 2014 and (d) March 2014.

As discussed earlier, snow cover in coastal areas of Norway is highly variable (Bokhorst et al., 2012). WRF's simulations for the Lofoten islands, in this study, also showed noticeable differences in the snow depth within this comparatively small but highly dissected land area. The few grid boxes which experienced zero days where the snow depth < 5cm were predominantly the mountain peaks. In contrast, model grid boxes located over areas of lower elevation and the base of the mountains, had up to 15 - 20 such days in each winter month. Since low lying, dwarf vegetation tends to be at the foothills at many places across the Lofoten mountain range, this means that in the occurrence of snow-

melt, a lot of vegetation would be susceptible to the damaging effects of such events, as also reported for the 2013-14 growing season at Lofoten (Treharne, 2018).

In summary, the analysis of the Lofoten study site showed that the combination of recurring warming events with freezing winter temperatures occurring between the warming events, sporadic snow melt albeit at a landscape scale and potential ice-layer formation within the snowpack, caused vegetation damage and mortality at this study site. Overall, based on the analysis of WRF's simulated temperature and snow depth, it is concluded that bias-corrected WRF simulations were able to capture the anomalous winter conditions which led to vegetation damage at the Lofoten study site.

3.3.2 Understanding winter climatology and growing season-NDVI relationships

This section presents the results of correlation analysis between various climatological parameters, climatological indices and the NDVI. The correlations were calculated for the winter months (November – April) over the time period 2000 – 2020. The climatological variables included 2m near-surface temperature, winter warming event frequency (WWE), Maximum duration warming event (MDW), snow depth, rainfall and Rain-on-Snow (ROS) (as defined in Table 3.6). The parameters represent the mean/sum, estimated for each winter month, respectively. The NDVI here represents the average NDVI of each growing season (as explained in section 3.2.6.1). For the sake of conciseness, the results presented here are for three of the six winter months, those with the highest number of statistically significant correlation grid boxes over the study domain.

3.3.2.1 Temperature and NDVI

Temperature and NDVI were found to be moderately correlated ($r = 0.4 - 0.8, -0.4 - -0.6$) over most of the study area (Figures 3.20 (a)-(c)). Interestingly, the correlation varied depending on the winter month. While large homogenous areas of positive correlations were observed for NDVI with temperature, at both the start and end of winter i.e., November and April, for mid-winter temperatures in March, NDVI was negatively correlated across most of the study domain.

November

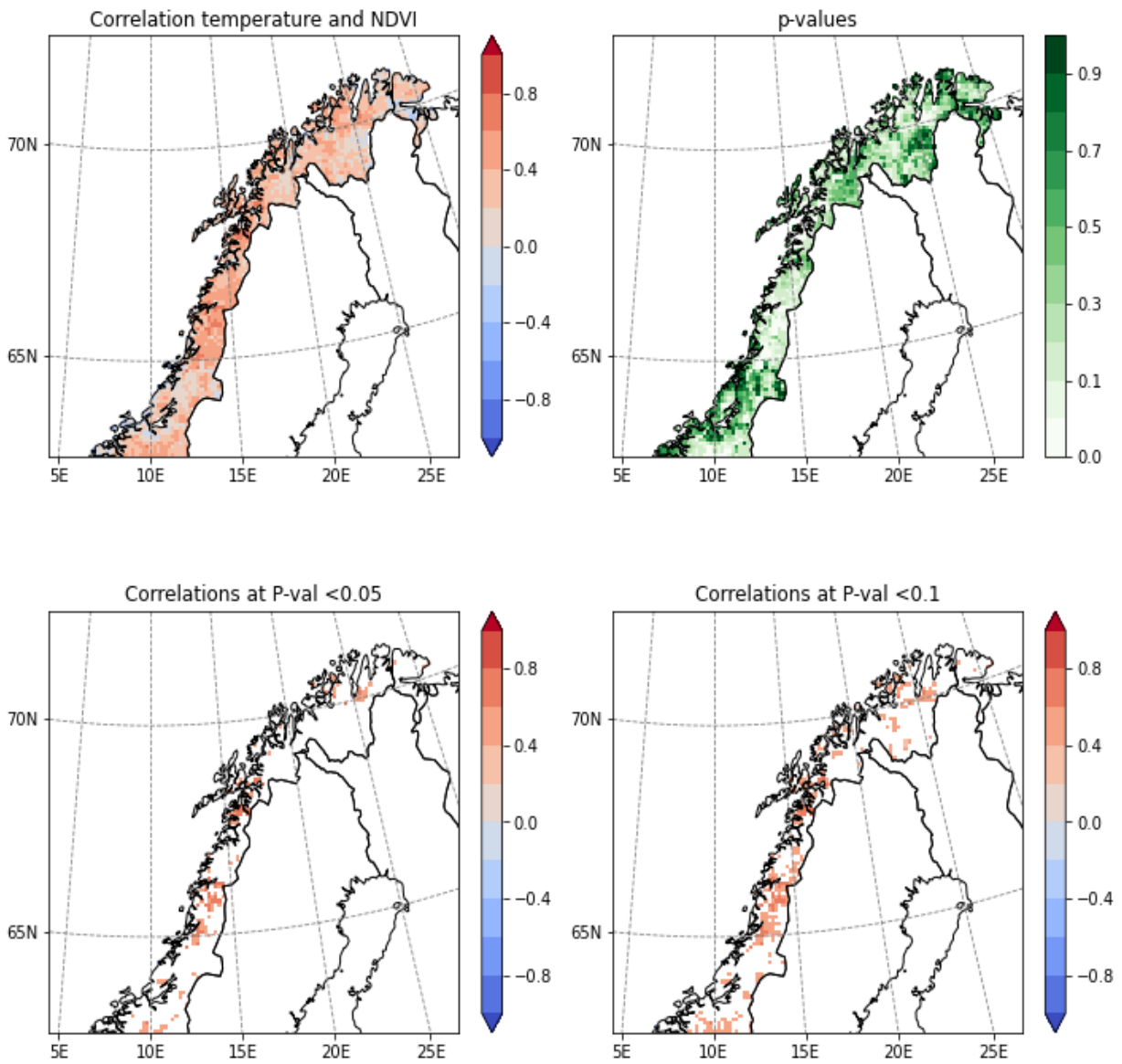


Figure 3.20 (a) Maps showing correlations of mean summer NDVI with the mean temperature of November.

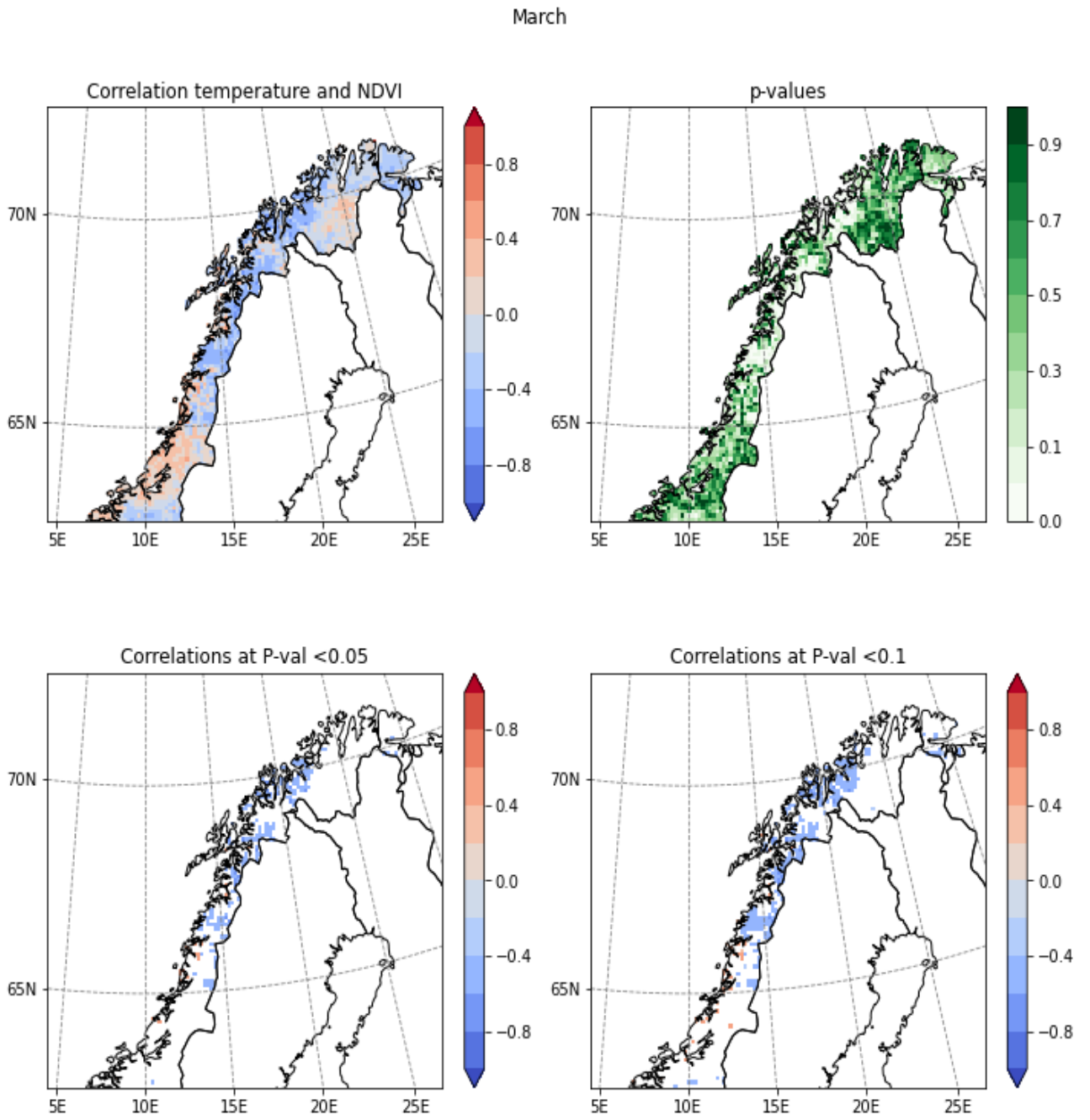


Figure 3.20 (b) Maps showing correlations of mean summer NDVI with the mean temperature of March

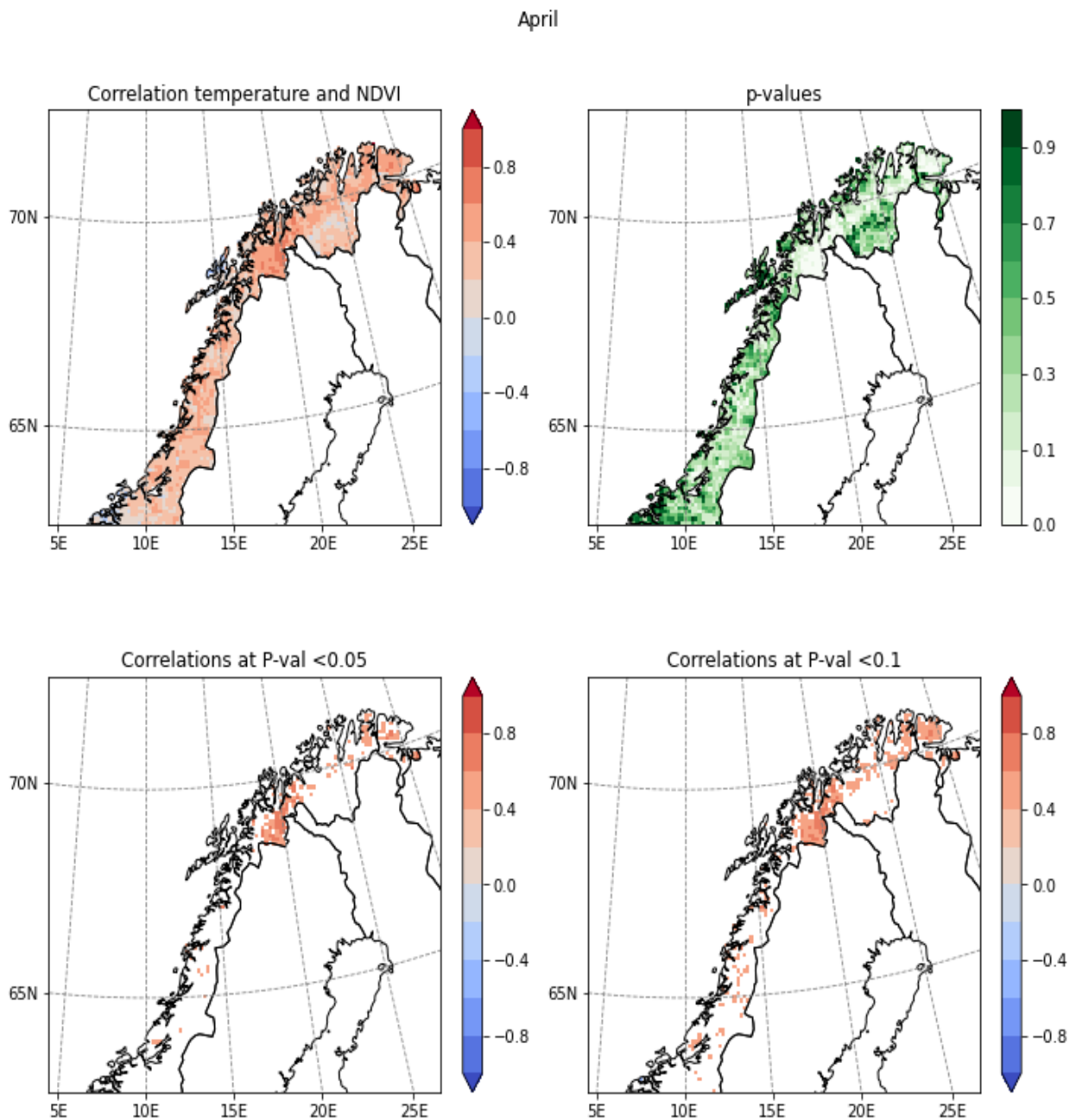


Figure 3.20 (c) Maps showing correlations of mean summer NDVI with the mean temperature of April

The correlation was significant ($p < 0.05$) at several locations and varied latitude-wise as Norway has high regional temperature variability (Heikkilä et al., 2011). NDVI in the northernmost county, Troms og Finnmark, was most strongly correlated with surface temperature in late winter, April, as compared to November, which is just the beginning of the winter season in Norway. However, NDVI in Nordland, between 65 and 68 °N, was most strongly correlated with temperature in March.

Vegetation located in the maritime areas of Norway, such as Flatanger, is generally more productive due to the milder winters in this region. Moreover, the vegetation in these areas also experiences comparatively longer growing seasons as compared to the northernmost areas of Norway, for example above 68°N. Therefore, within these maritime areas, November temperature and summer NDVI being significantly positively correlated, could mean that processes such as nutrient cycling are still on-going in November. This is especially likely during the years with delayed summer peak productivity and warmer than usual autumn temperatures.

Winter warming events cause vegetation damage due to the loss of freeze tolerance when subsequent severe cold temperatures return, and snow cover is absent. November is typically the beginning of winter in Norway, and hence it does not yet have the thickest snow cover. The vegetation is usually still undergoing freeze hardening processes during this time of the year. Hence winter warming events occurring in November might not severely impact the vegetation's resilience to colder temperatures ahead as the freeze tolerance process is still occurring. This is one of the plausible explanations for positive correlations between November temperatures and summer NDVI.

One of the possible reasons for positive correlations between April temperature and summer NDVI in the northernmost region of Norway (above 68 °N) is that higher temperatures in April could benefit the vegetation in these areas that have a thicker snow layer as compared to lower latitudes regions with a thinner snowpack. Spring snowmelt timing is a crucial environmental control of vegetation productivity, for many plant species, in higher snowfall regions of Norway because the melted snow provides essential nutrients right at the beginning of spring when days are starting to get longer and there is light for plants to utilize. If not for these warmer temperatures in April, the spring snow melt would be delayed resulting in a shorter growing season.

3.3.2.2 Winter warming event (WWE) and NDVI

WWE and NDVI correlations were of weak to moderate strength ($r = -0.2$ to -0.6 , 0.2 to 0.6) (Figure 3.21 (a)-(c)). The correlations were mostly negative for the early and mid-winter months (indicating a decrease in NDVI with an increase in WWE), and positive for the late winter month of April. For December a clear negative correlation occurred for the entire study domain and *vice versa* for April. The correlations were significant ($p < 0.05$) at a few model grid boxes. A distinct spatial pattern was observed for December and April. For December, several clusters of the significant correlation grid boxes were located in the northern areas of Norway (above 68°N), whereas for April these were in the southern county of Trøndelag.

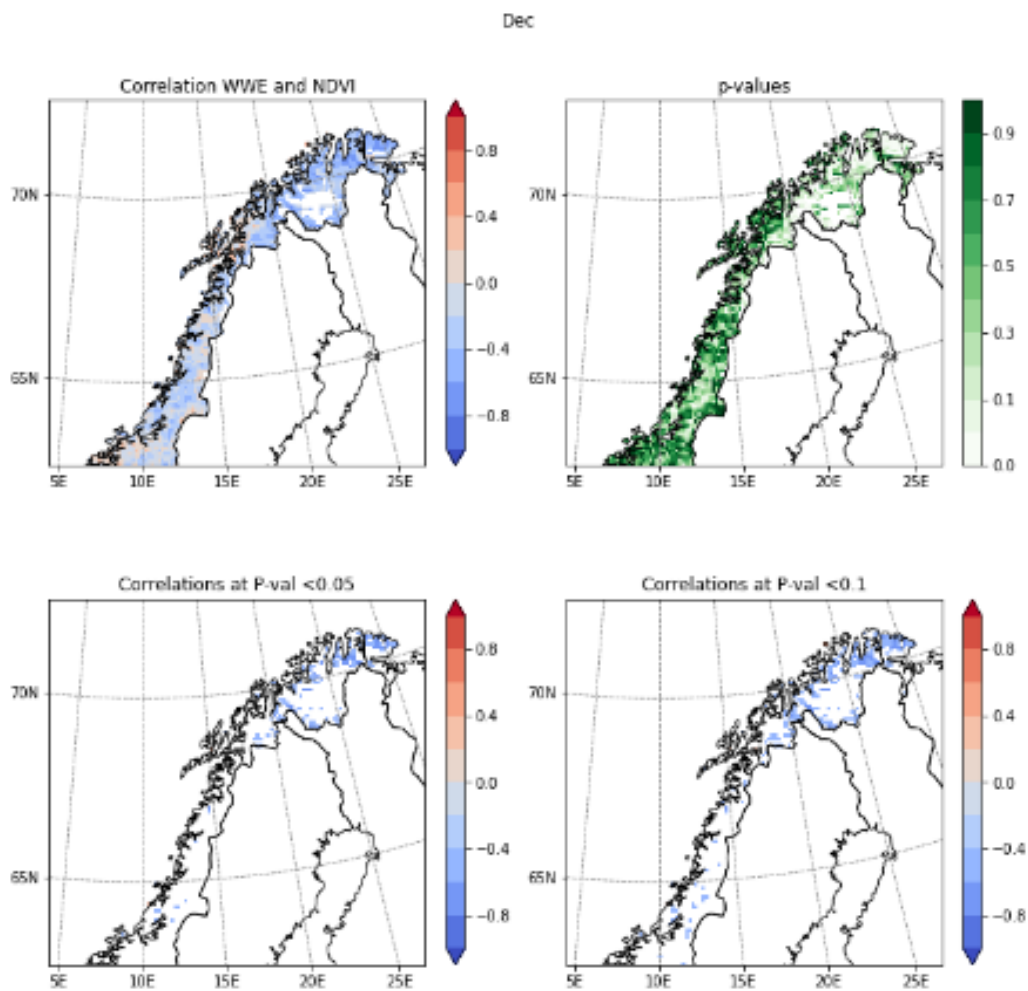


Figure 3.21 (a) Maps showing correlations of mean summer NDVI with the WWE index for December

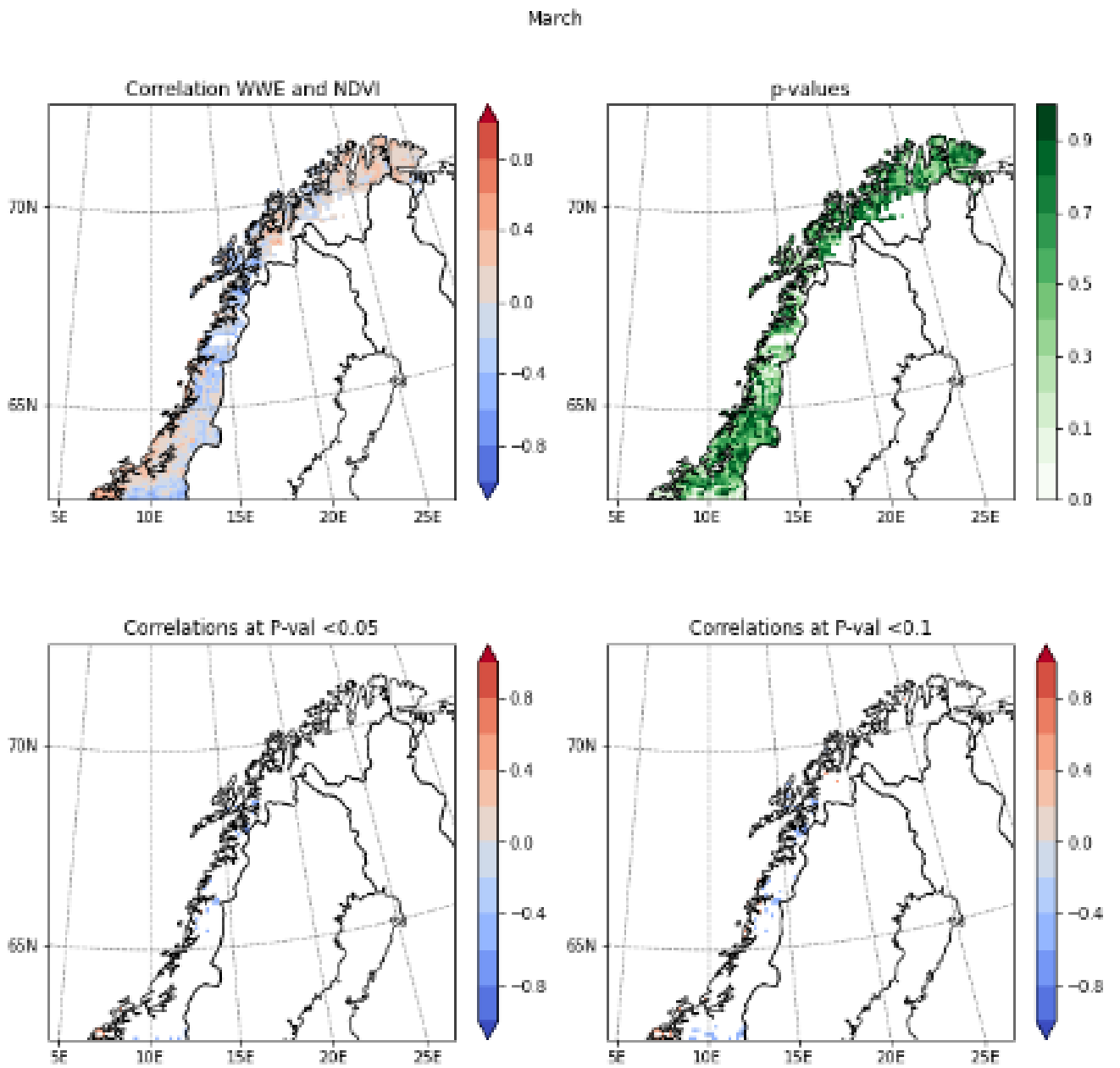


Figure 3.21 (b) Maps showing correlations of mean summer NDVI with the WWE index for March

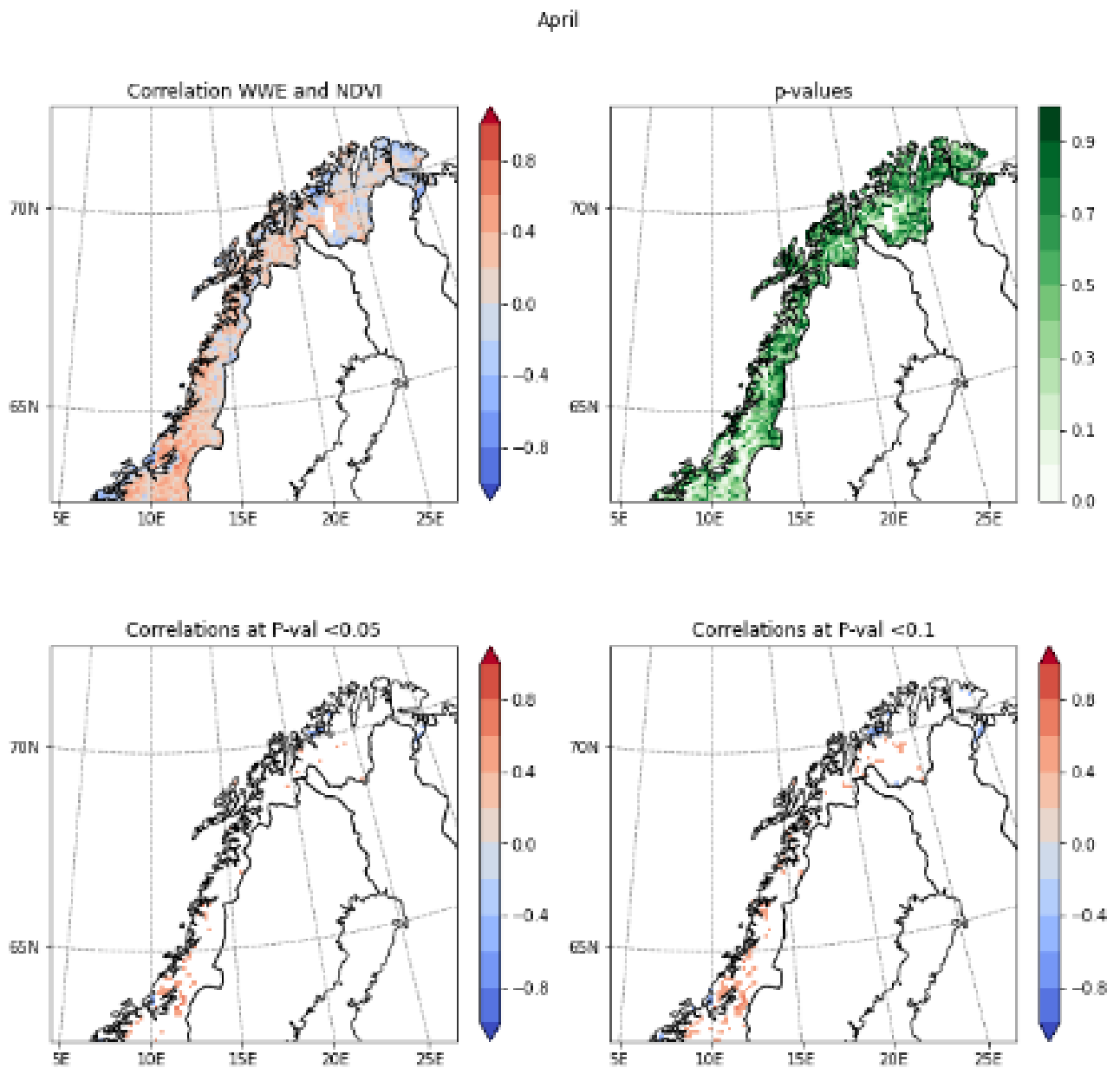


Figure 3.21 (c) Maps showing correlations of mean summer NDVI with the WWE index for April

Since the WWE index was constrained by the temperature parameter, it was interesting to note the differences in the spatial patterns of WWE-NDVI correlations and temperature-NDVI correlations, especially for April. Although NDVI was positively correlated with both temperature and WWE, most of the significant temperature-NDVI correlation grid boxes were in the northern areas and for WWE-NDVI these were in the southern areas. The most likely reason for this difference may be a lower frequency of winter warming events in the northern areas of Norway. Figure 3.22 presents the total number of the WWE, for April 2001-2020. The highest number of winter warming events, 35-45, was observed to

be in the south-western maritime areas and over the Lofoten Islands. Whereas the northern Troms og Finnmark county (above 68 °N) experienced just a few (1-5) winter warming events, in April over 2001-2020.

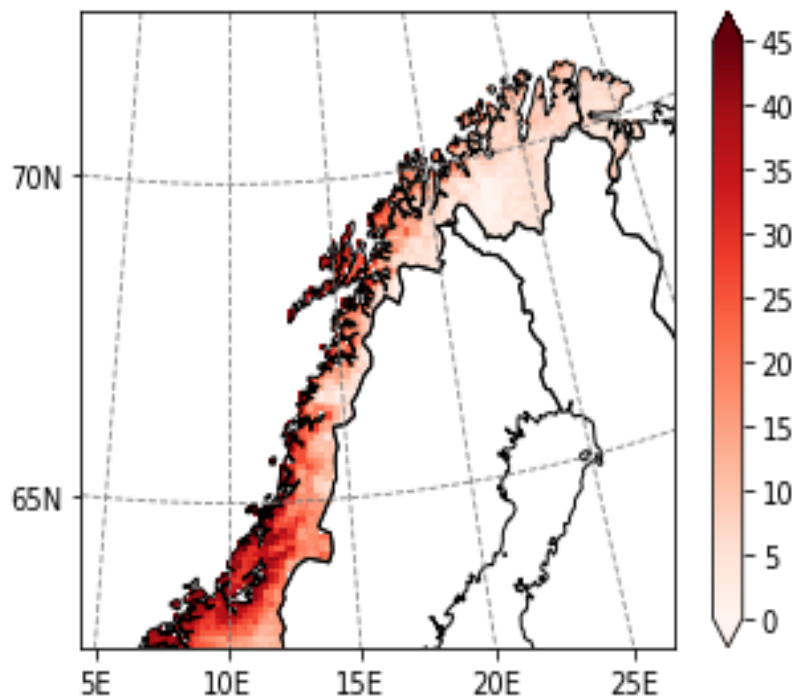


Figure 3.22 The total WWE for April 2001-2020.

3.3.2.3 Maximum Duration Warming event (MDW) and NDVI

The correlations between winter MDW and growing season NDVI varied on a monthly basis as well as across the study area, as shown in Figure 3.23 (a-c).

While a predominantly negative relationship was observed for December across the study area, it was mixed for January and mainly positive for April. The strength of these relationships were weak to moderate; $|r| = 0.4 - 0.6$. The highest number of model grid boxes with significant correlations ($p < 0.05$) were observed to be for December, which were spread out over the study domain.

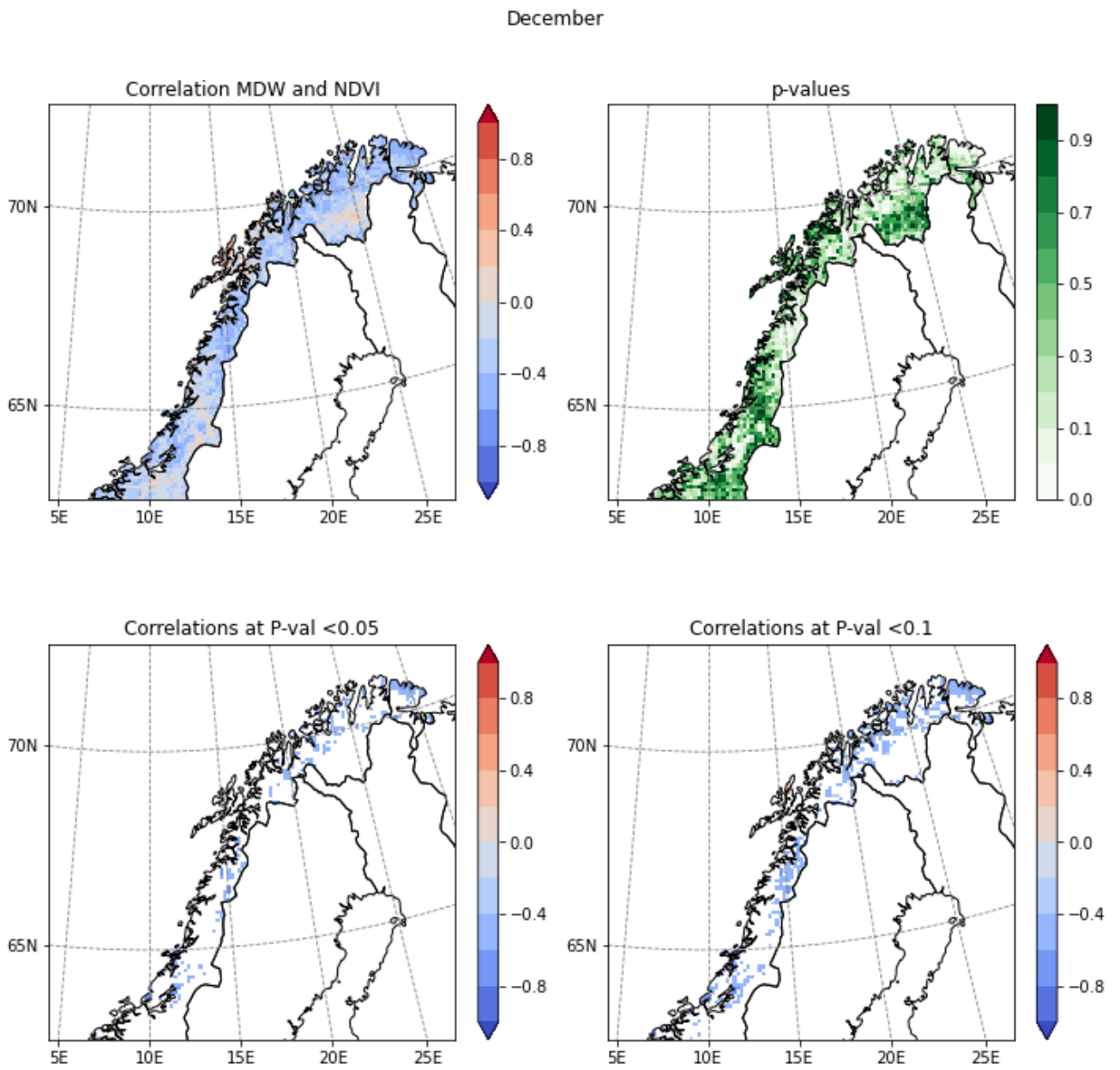


Figure 3.23 (a) Maps showing correlations of mean summer NDVI with the MDW index for December

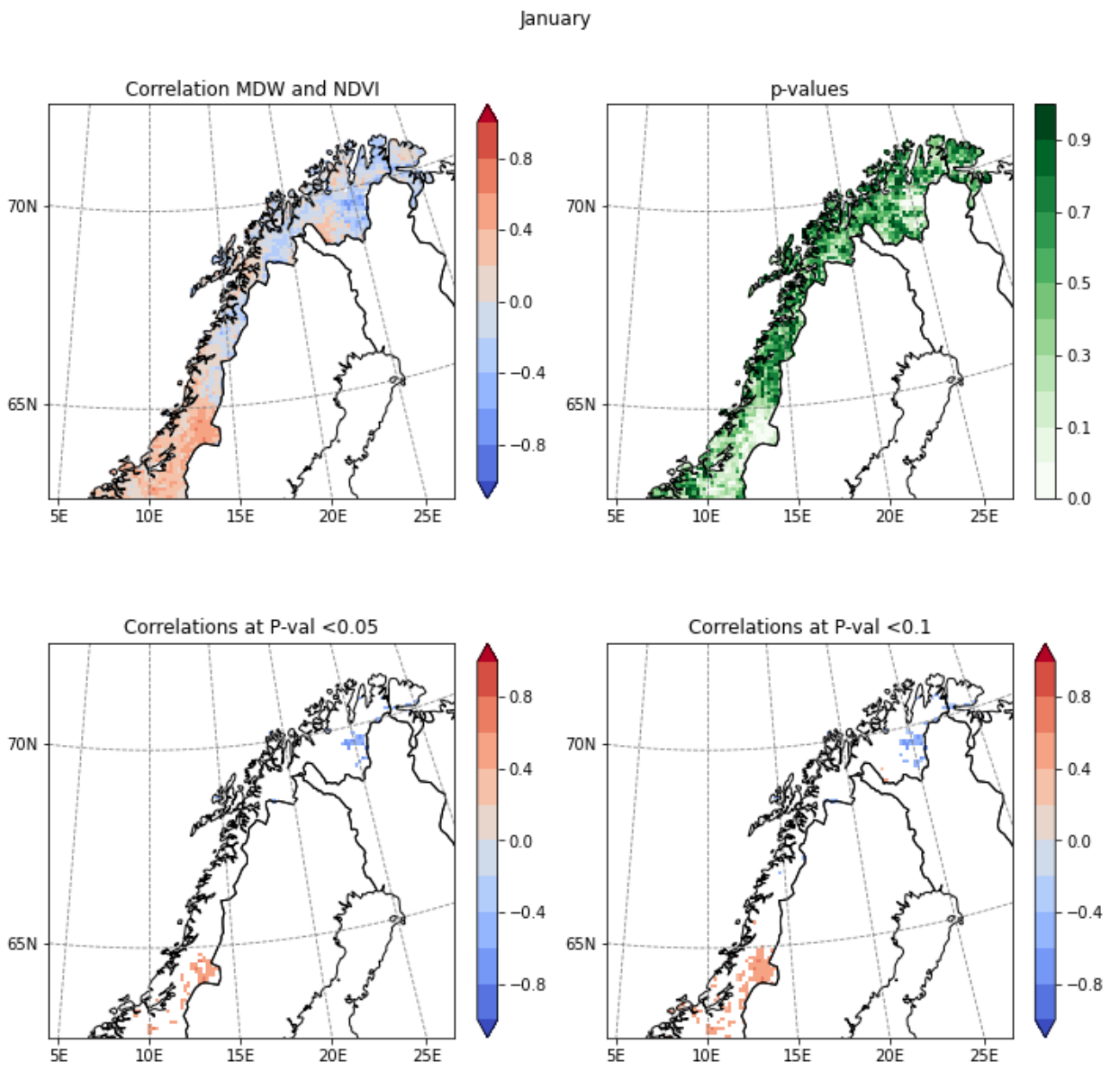


Figure 3.23 (b) Maps showing correlations of mean summer NDVI with the MDW index for January

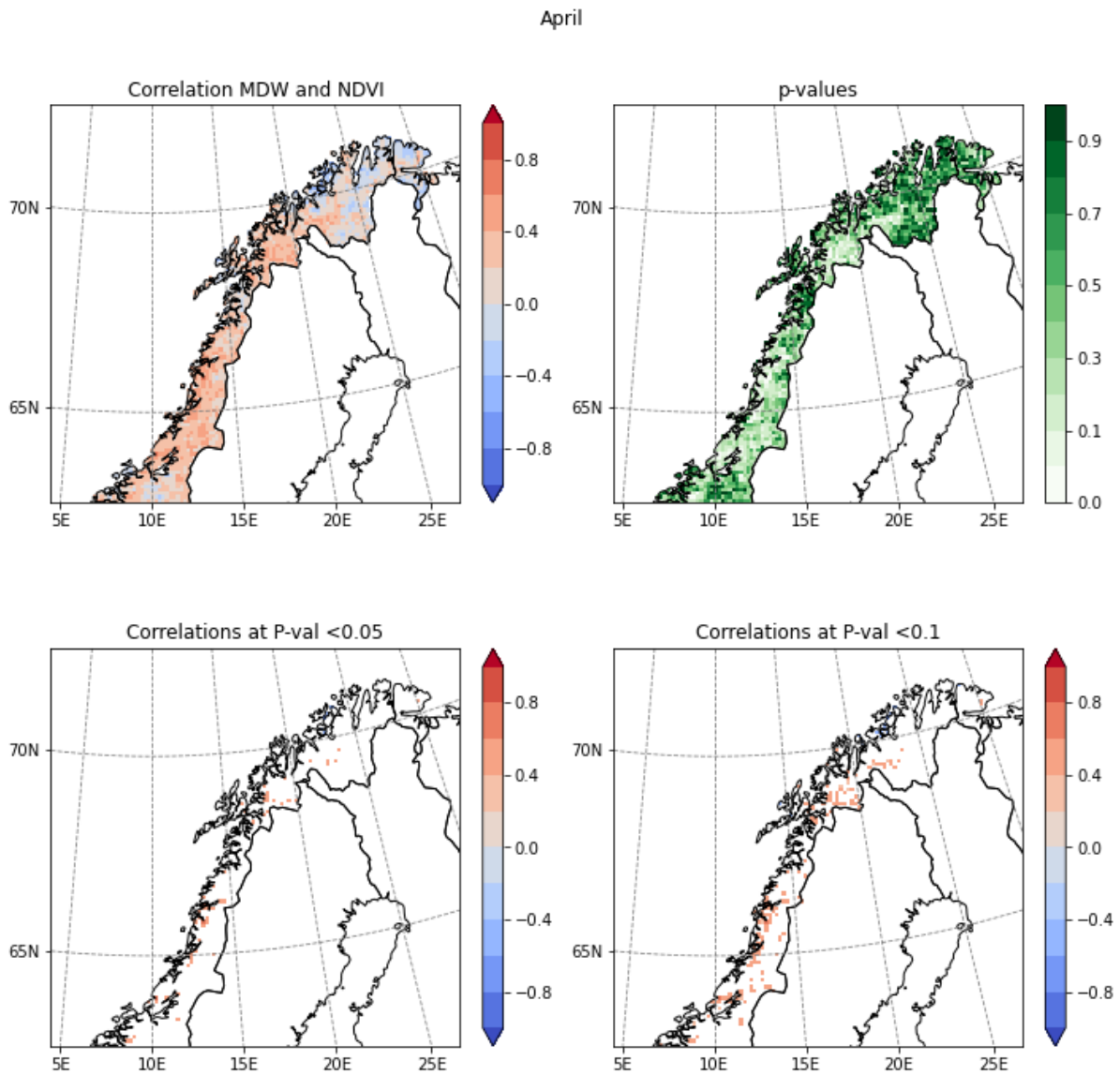


Figure 3.23 (c) Maps showing correlations of mean summer NDVI with the MDW index for April.

3.3.2.4 Snow depth and NDVI

The correlations between snow depth and summer NDVI varied across the study area (Figure 3.24(a)-(c)). The highest number of significant correlations were observed for mid and late winter months, i.e., January, February and April. While a clear pattern could not be observed for the Trøndelag, negative correlations were found over Nordland, across the winter months. Interestingly for the northernmost county, Troms og Finnmark, the nature of the NDVI and snow depth correlations varied depending on the month. The general variation in correlations across the study domain is likely due to a close

relationship between snow cover and vegetation species type (Evans et al.,1989, cited in Callaghan et al., 2011, p.35).

The NDVI-snow depth correlations were significant ($p < 0.05$) at a few locations, mainly above 65°N, in the Nordland and Troms og Finnmark. Somewhat expected, most of the significant correlations, were for the eastern, mainland Norway. The correlations over these areas were mostly of a negative nature. For January and February, the negative correlations were found over the Scandinavian mountains, indicating lower summer NDVI with higher snow depth in these months. This is likely due to heavy snowfall in these areas taking longer to melt during spring and thus reducing the length of the growing season in the mountainous areas.

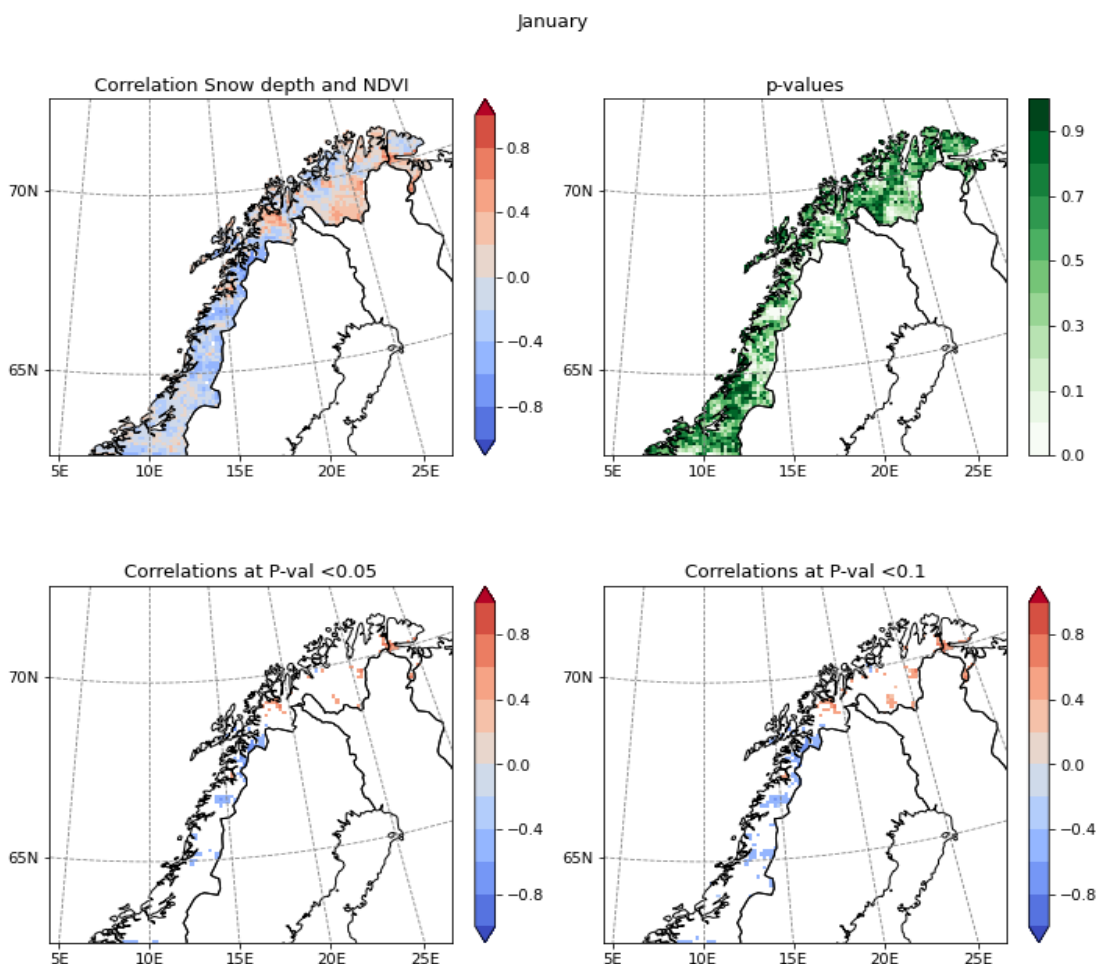


Figure 3.24 (a) Maps showing correlations of mean summer NDVI with the mean snow depth of January

February

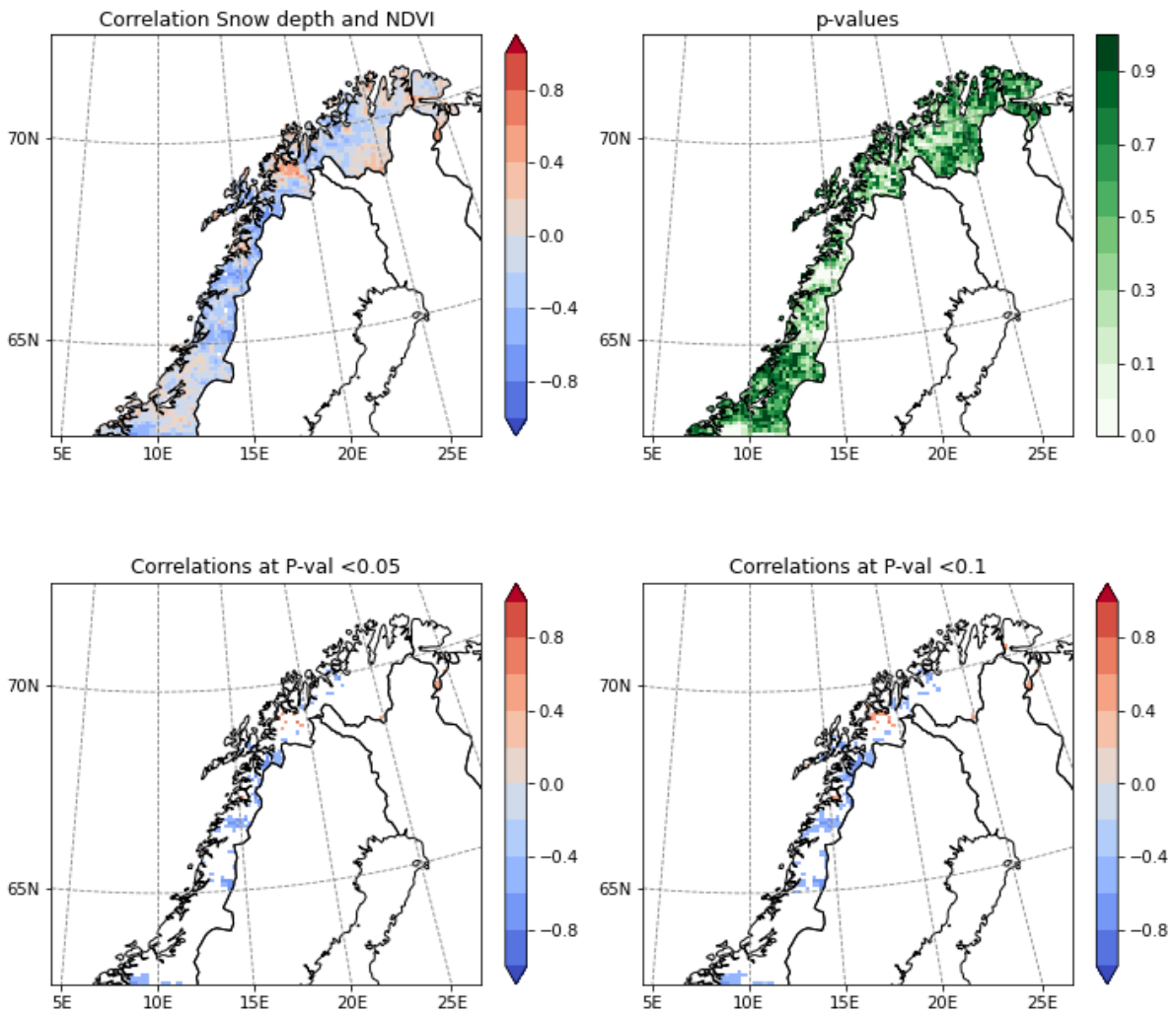


Figure 3.24 (b) Maps showing correlations of mean summer NDVI with the mean snow depth of February

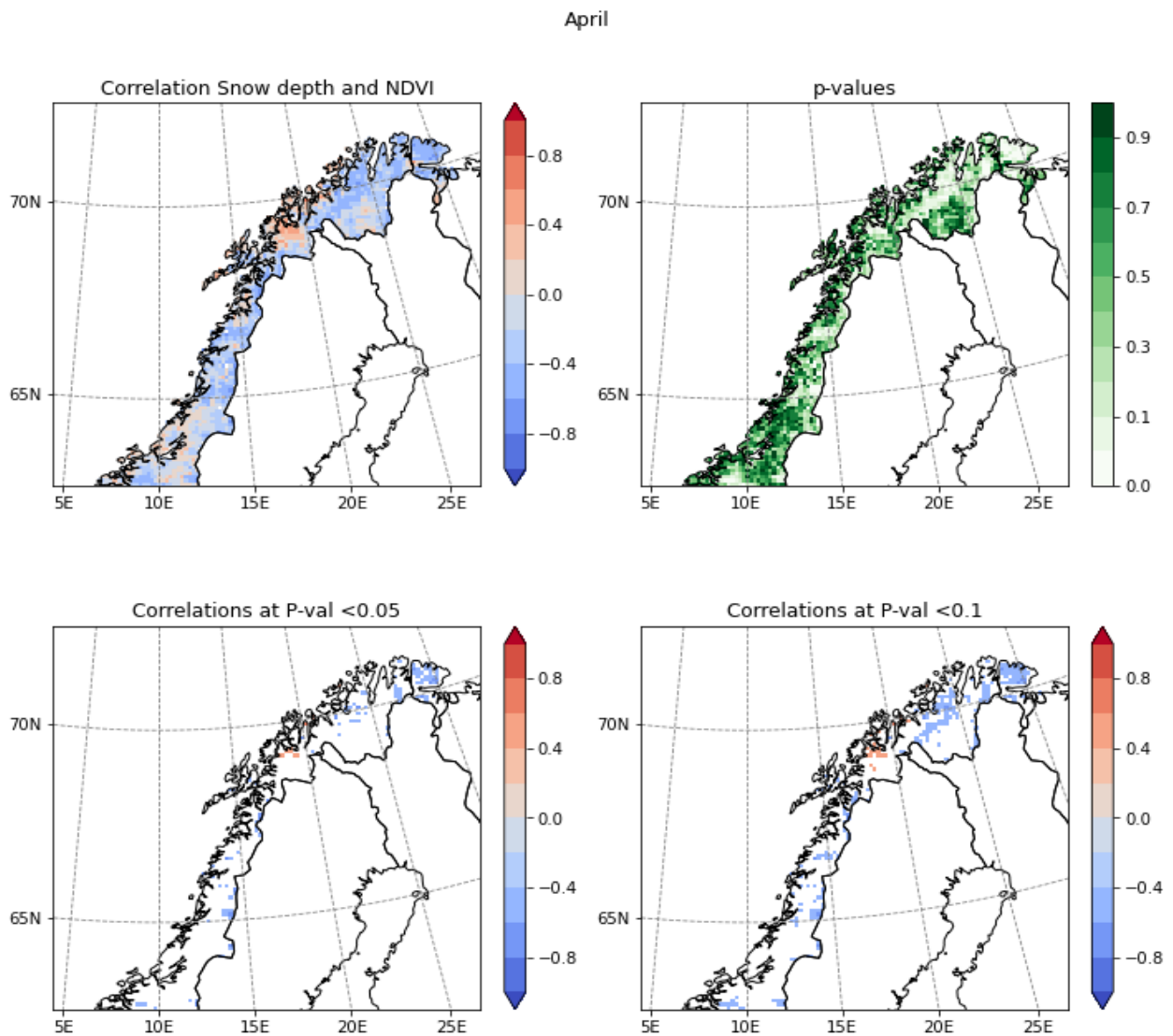


Figure 3.24 (c) Maps showing correlations of mean summer NDVI with the mean snow depth of April

It is worth noting that vegetation productivity in the coastal areas below the Arctic Circle, is generally comparatively higher than in the northern regions. Despite this the absence of significant correlations around these areas is likely due to either, the local vegetation's adaptability and resilience to both snow depth fluctuations and time periods of absent snow cover; or a non-linear relationship between the mean monthly snow depth in winter and summer NDVI. A caveat to the first explanation of the absence of significant correlations is that vegetation at Flatanger was damaged in the 2013/14 winter due to snow melt in early winter (December) and exposure to freezing temperatures in mid-winter due to the absence of snow cover. Thus, implying that the vegetation at Flatanger was not adapted to the level of variability in snow depth as was observed in the 2013/14 winter at this site. Therefore, it is not straight

forward to interpret the correlations between mean monthly snow depth (winter months) and summer NDVI across the study domain.

Snow depth is a crucial winter climatological parameter because it insulates vegetation from the damaging effects of freezing temperatures. Bokhorst et al. (2012) have highlighted the significance of snow depth < 10 - 20 cm, in the context of low-lying Arctic vegetation such as *Empetrum nigrum*, *Vaccinium myrtillus* and *Calluna vulgaris*. These plant species comprise a fair percentage of the vegetation cover and abundance in Arctic dwarf shrub heathlands. Hence, in addition to monthly mean snow depth, other measures of snow depth such as minimum monthly snow depth, snow depth < 10 cm days count (SC10) and snow depth < 20 cm days count (SC20), were also regressed with the NDVI. The correlations of NDVI and minimum monthly snow depth were similar to that for the mean monthly snow depth. However, for correlations of NDVI and SC10 and SC20 respectively, December was the only month with significant correlations at a few locations (Figures 3.25 (a) and (b)). NDVI and SC20 were negatively correlated, up to the northernmost municipality of Hammerfest at about 70 °N. Whereas for SC10, the significant correlations occurred mainly for areas below 68°N.

As explained in the model validation analysis (section 3.2.4.4 (b)), WRF markedly overestimated the snow depth throughout the study domain. Therefore, it is quite likely that days where snow depth < 10 - 20 cm are undercounted, and this would have influenced the correlations presented here. Due to time limitations of this PhD, a systematic bias correction technique could not be applied to the snow depth simulated by WRF.

SC10

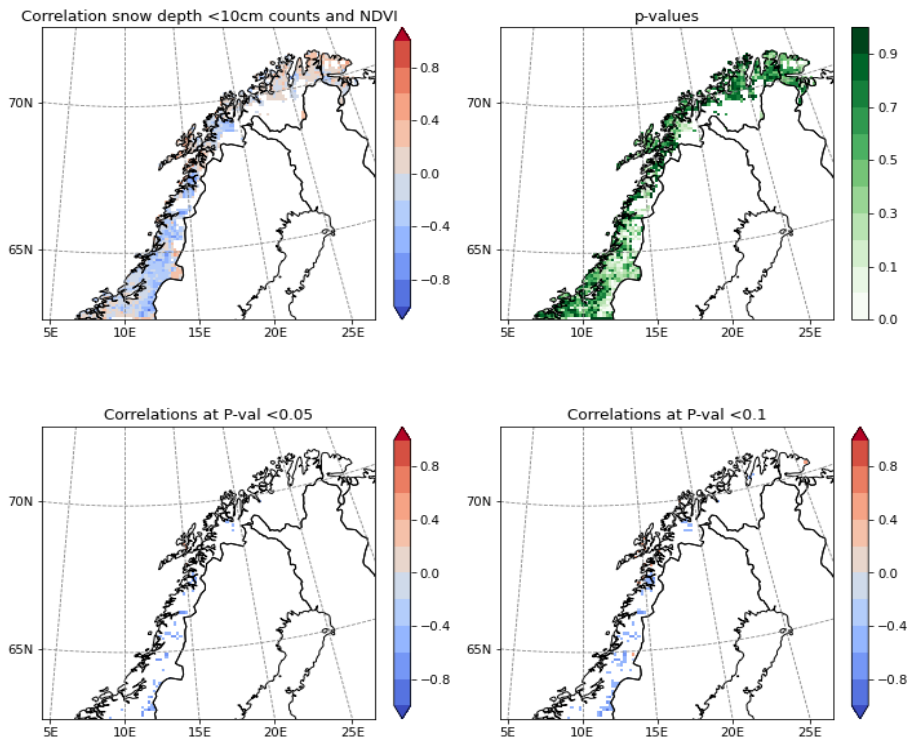


Figure 3.25 (a) Maps showing the correlations for NDVI-snow depth < 10 cm

SC20

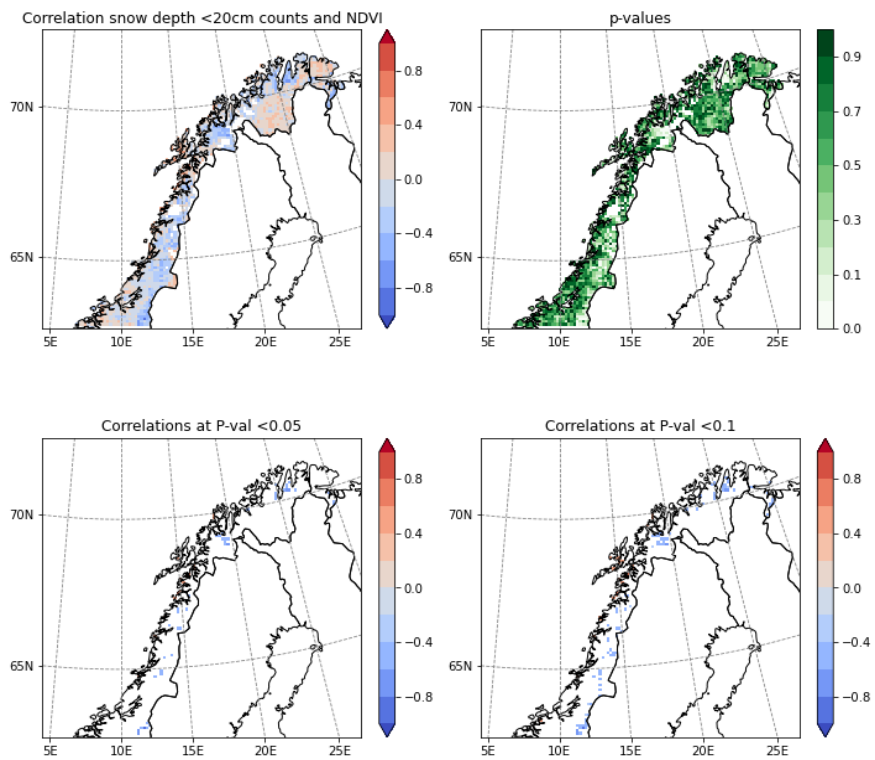


Figure 3.25 (b) Maps showing the correlations for NDVI-snow depth < 20 cm

3.3.2.5 Rainfall and NDVI

Correlations of NDVI and rainfall were found to be mixed overall. While mostly positive correlations, ($r = 0.2 - 0.4$), were observed for December, noticeable spatial variability in the sign of the correlation was seen in January and April. It was also noted that for all the maps in Figure 3.26 ((a) – (c)), a consistent absence of a correlation occurred for the most eastern parts of northern Norway (between 68 and 70 °N). This is understood to be primarily due to the absence of liquid precipitation in winter, due to the overall dry and cold continental climate found in these regions, despite the overall warming trends in Norway (Dyrrdal et al., 2013). Hence correlation coefficients could not be calculated at these grid boxes.

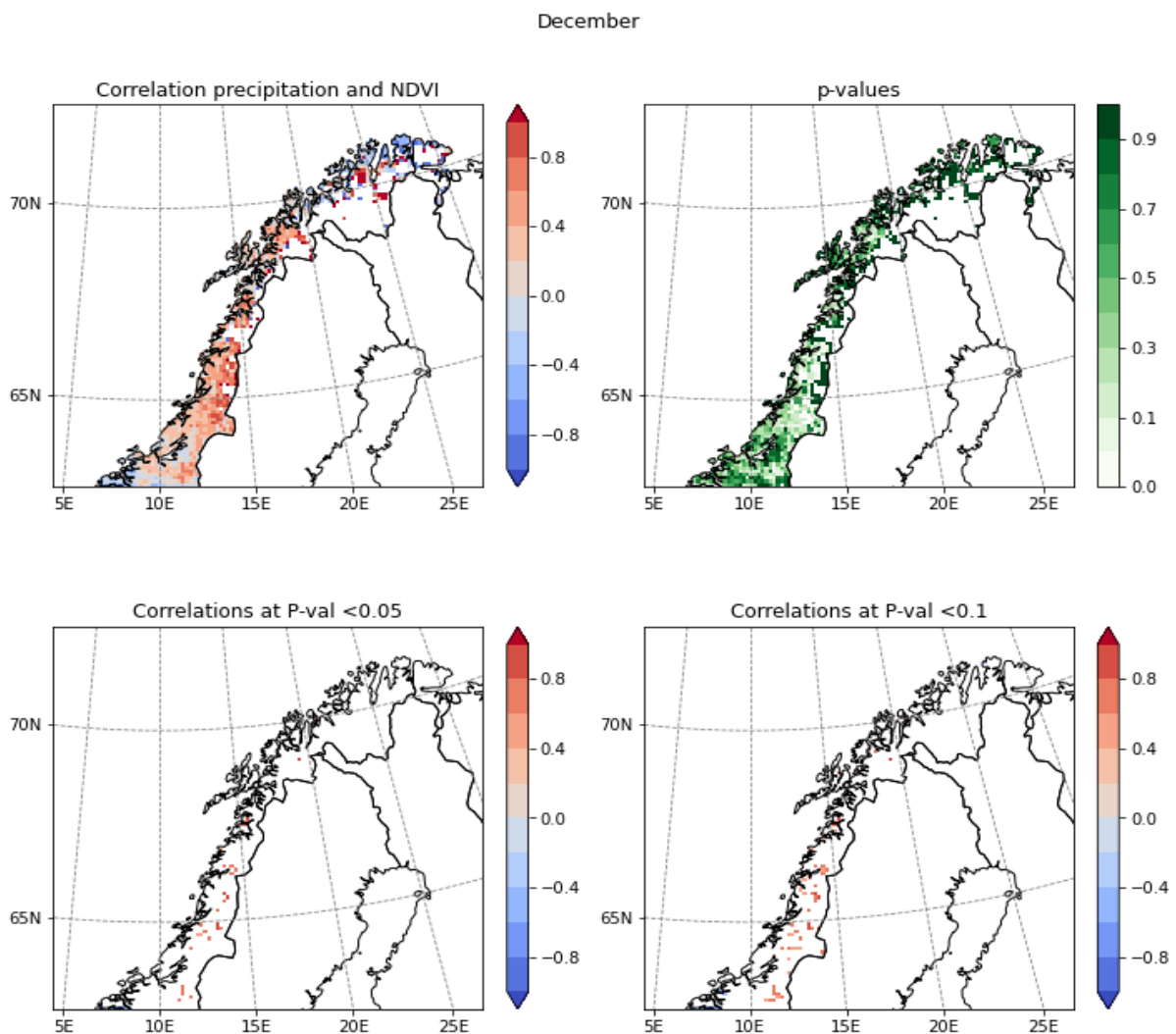


Figure 3.26 (a) Maps showing correlations of mean summer NDVI with mean rainfall of December

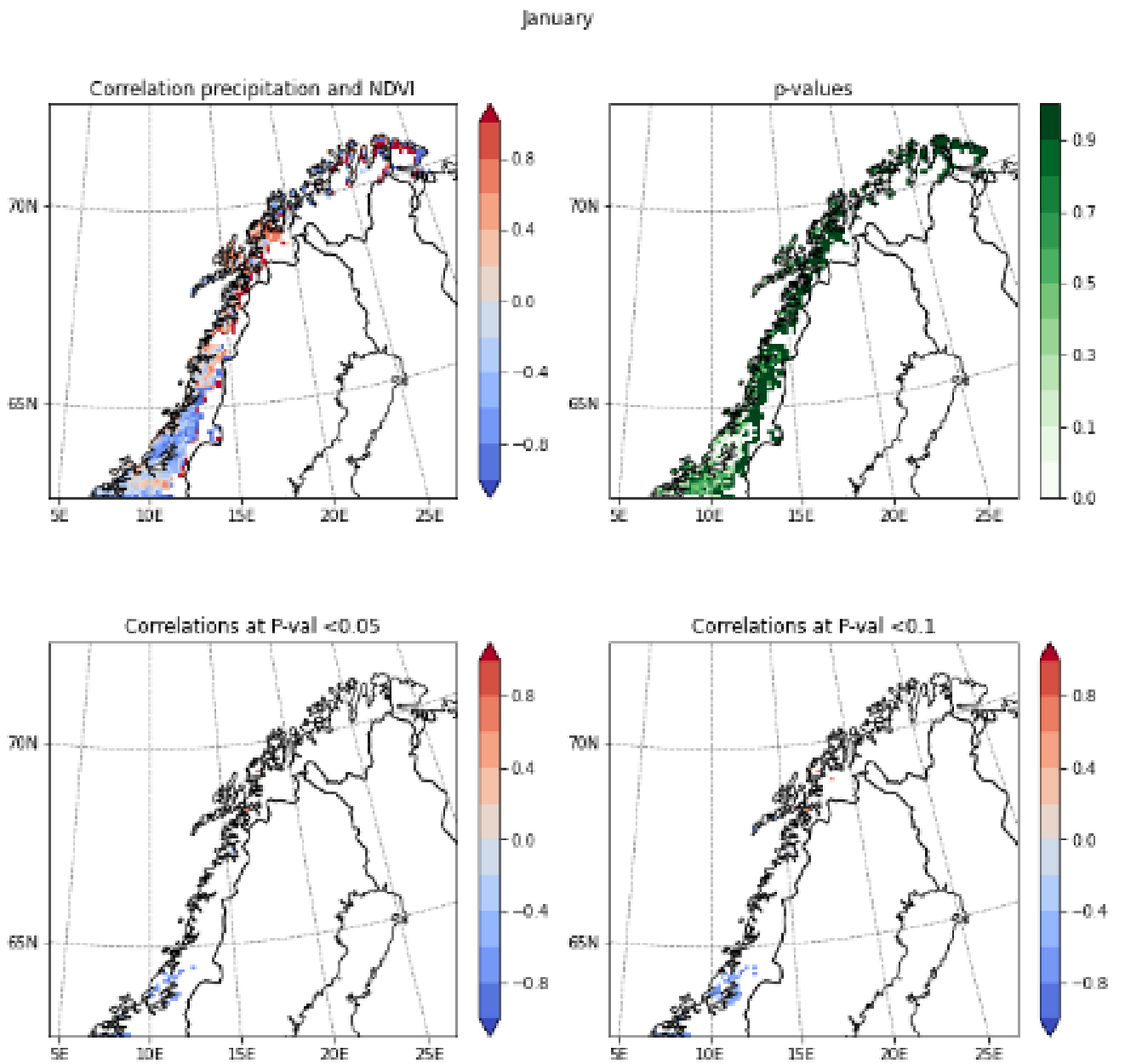


Figure 3.26 (b) Maps showing correlations of mean summer NDVI with mean rainfall of January

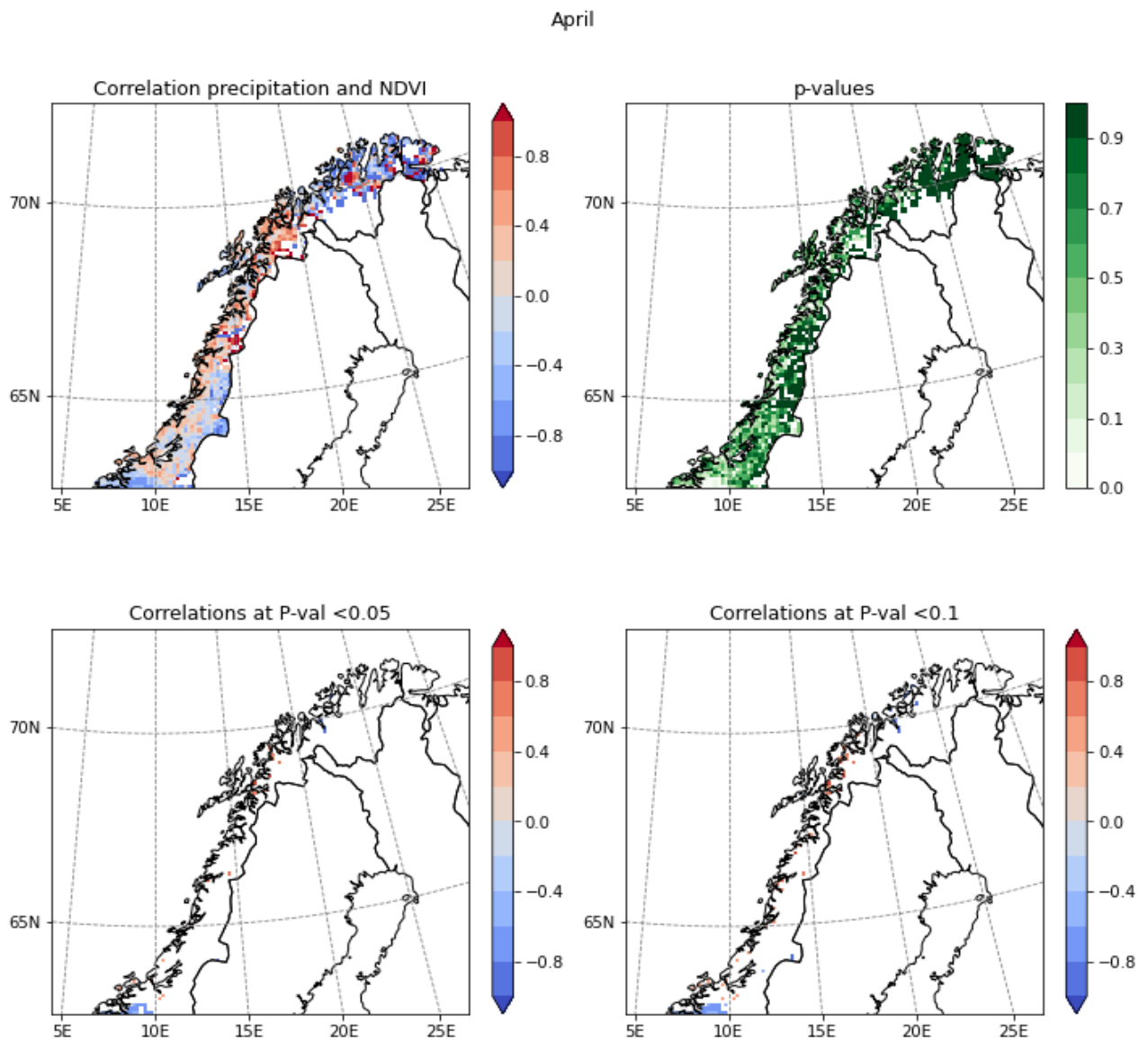


Figure 3.26 (c) Maps showing correlations of mean summer NDVI with mean rainfall of April

Only a few correlations were significant for early, mid and late winter. The months with the highest number of significantly correlated grid boxes were December, January and April, respectively. Where significant, NDVI was positively correlated with precipitation in early and late winter months and *vice versa* for mid-winter. These correlations were scattered around model grid boxes in the counties Trøndelag and Nordland, both under 69°N.

In general, there is mixed evidence related to the NDVI – rainfall relationship. While some studies have shown that NDVI is rather weakly related to rainfall, especially in colder areas (Vicente-Serrano et al.,

2013), others found a negative or no relationship between the two variables over a range of landscapes (Guo et al., 2014).

3.3.3.6 Rain-on-Snow (ROS) and NDVI

ROS and summer NDVI had mixed correlations overall. Large homogenous areas of negative correlations were observed for December, whereas positive correlations were found for April. Out of the three months shown in Figure 3.27 ((a)-(c)), mainly December had a substantial number of model grid boxes with significant correlations. In contrast to the positive correlations between liquid precipitation and NDVI for December, ROS and NDVI were moderately negatively (0.4 – 0.6) correlated for December throughout Nordland County.

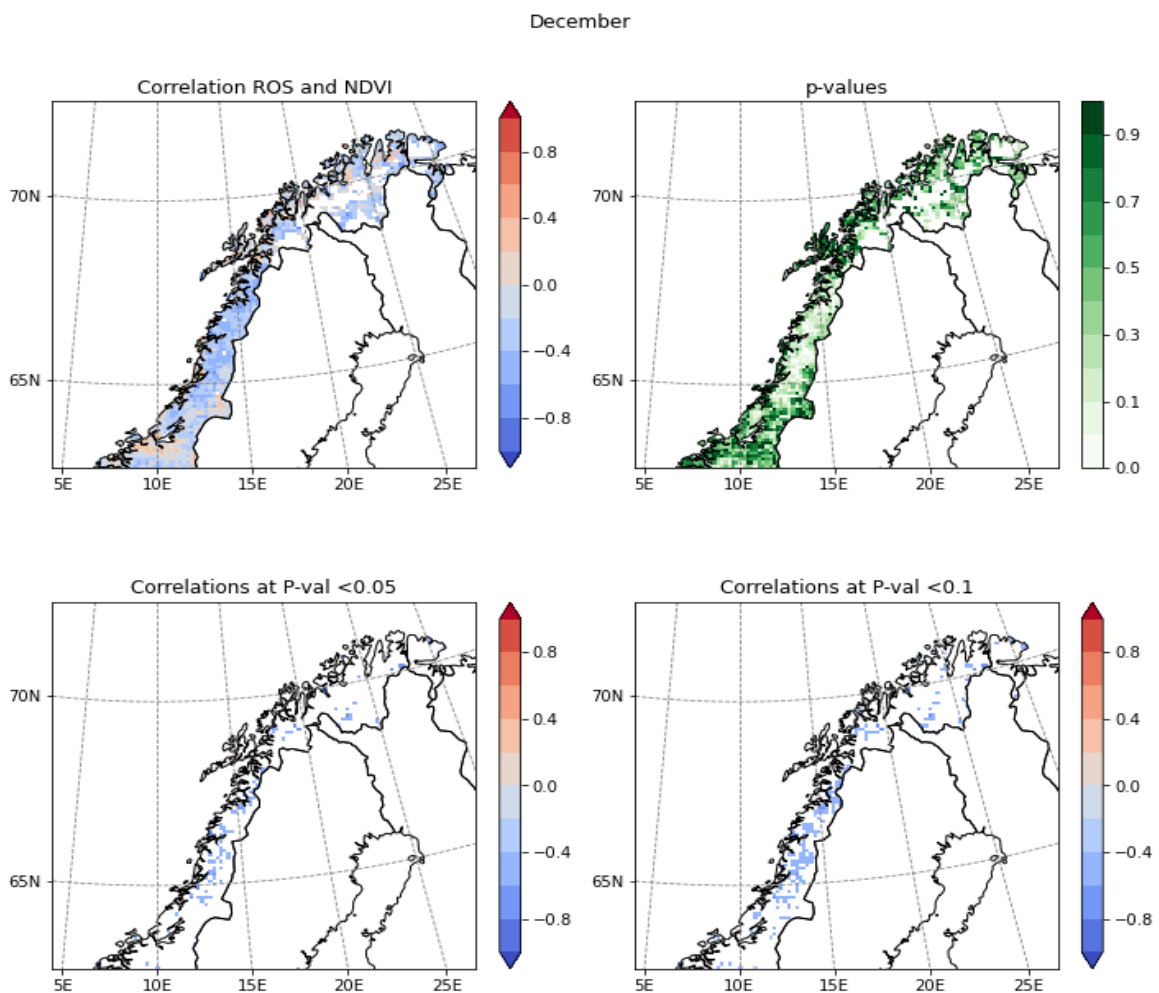


Figure 3.27 (a) Maps showing correlations of mean summer NDVI with ROS day counts of December

January

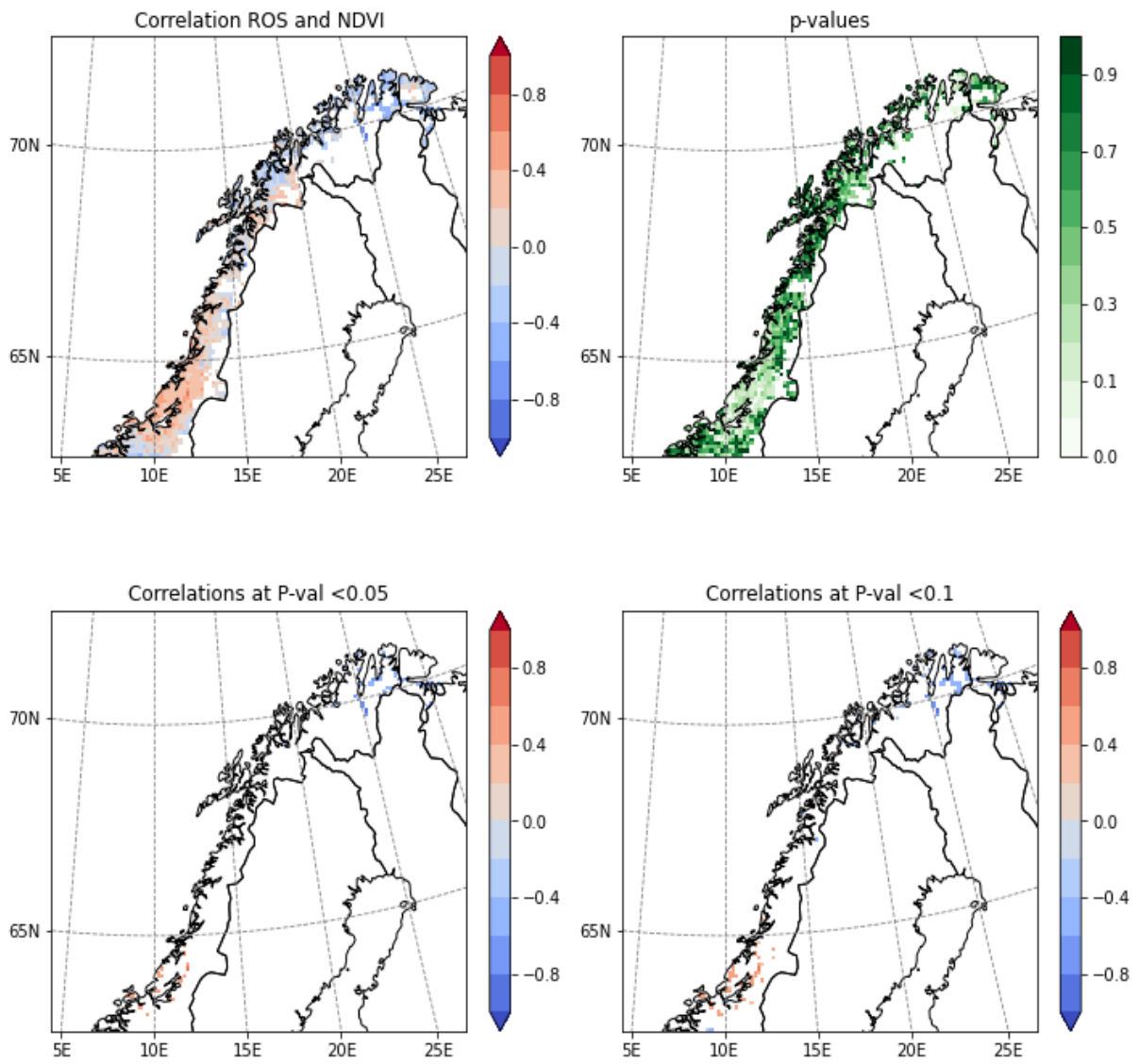


Figure 3.27 (b) Maps showing correlations of mean summer NDVI with ROS day counts of January

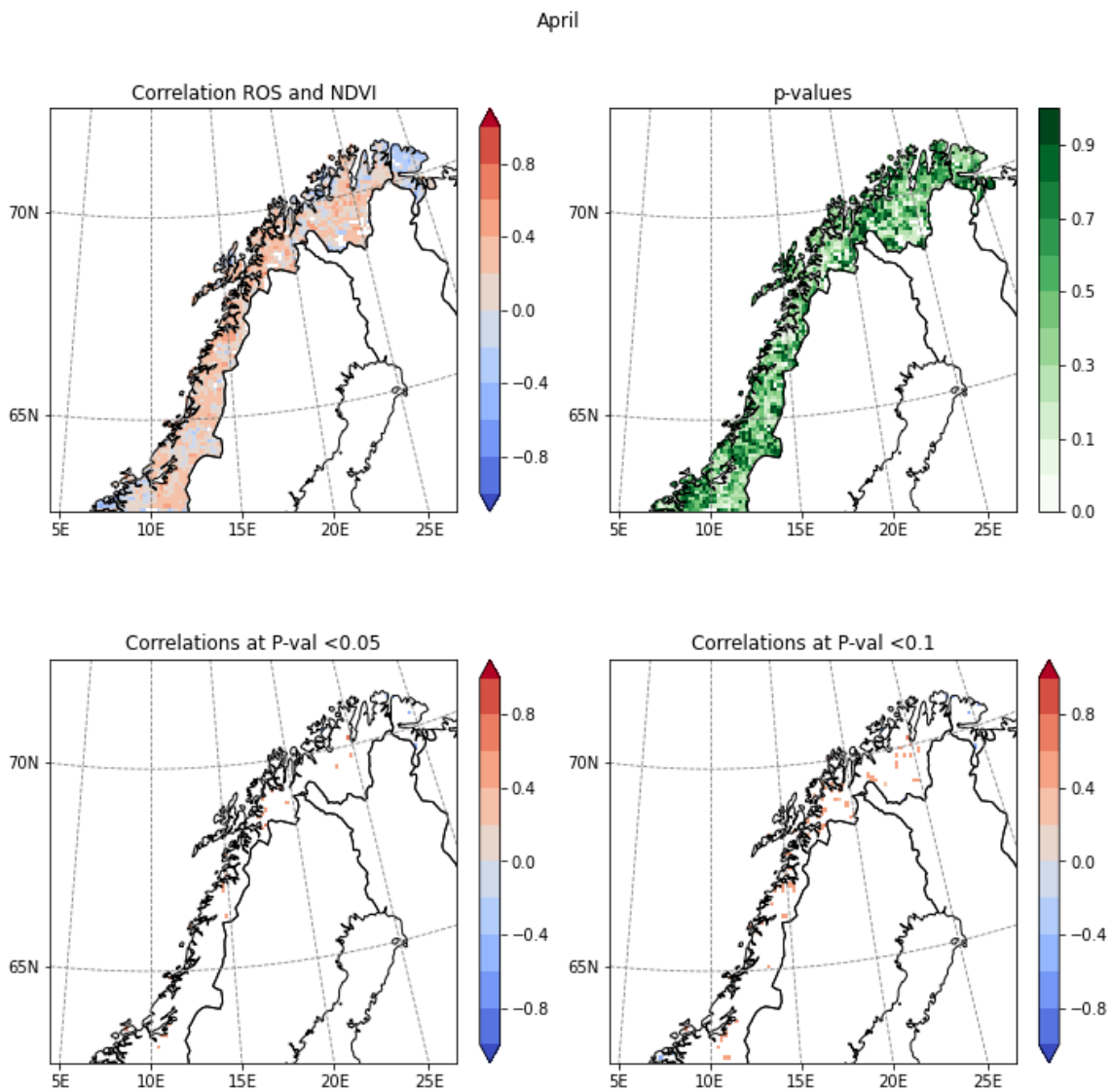


Figure 3.27 (c) Maps showing correlations of mean summer NDVI with ROS day counts of April.

It is worth noting that the number of grid boxes with significant ROS - NDVI correlations was markedly higher in December compared to those of rainfall - NDVI correlations, suggesting that this relationship could be more important in terms of affecting vegetation productivity.

There is established evidence of ROS led vegetation damage in the Arctic (Bjerke et al., 2014). Thus, the absence of significant correlations between ROS and NDVI is likely to be related to WRF's skill at simulating precipitation and snow depth, especially in the mountainous regions of Norway. In addition, because ROS events typically occur at high latitudes and/or altitude regions, are quite localized in nature (Pall et al., 2019), and given that NWP models generally struggle to robustly simulate weather in regions of steep orography, as Norway has, it was not surprising that the number of significant

correlations was limited. Another reason may be simply the limited number of ROS events over the simulated time period 2000 - 2020.

About 30% of precipitation falls as snow in Norway (Dyrrdal et al., 2013). Since WRF's precipitation output in this research represented the total precipitation, both liquid and solid, a temperature threshold of 1.5 °C was applied for the rain-snowfall phase separation (Jennings et al., 2018). Because WRF's simulated temperature had an overall cold bias, it is likely that this temperature threshold would be lower for the precipitation phase separation in WRF, which would lead to more precipitation falling as rain. A systematic bias correction of WRF's meteorological parameters over the full study area could have helped to improve the correlations analysis. However, such a detailed analysis was beyond the scope of this PhD research.

The results of the correlation analysis conducted in the above sections are summarised in Table 3.12. This table presents the statistically significant correlations, on a county level. These results informed the multivariate regressions analysis (results of which are presented in Section 3.3.3).

Table 3.12 A summary of the winter meteorological parameters which showed significant correlations with the average summer MODIS NDVI

County	November	December	January	February	March	April
Trøndelag	T	P, SC10, MDW	P, MDW	T, P	MDW	WWE, MDW
Nordland	T	P, SC10, SC20, ROS, MDW	S	S	S, T	S, T, MDW
Troms og Finnmark	T	S, T, WWE, MDW	S, T, MDW		S, T	S, T

3.3.3 Multivariate regression analysis

The statistically significant relationships between winter metrics and summer NDVI were not linear, and it was found that a quadratic model fitted better. This was consistent across the study sites. The following sections present the results of the multivariate regressions analysis for each case study site. For conciseness, only the statistically significant ($p < 0.05$) model results are presented.

3.3.3.1 Flatanger

For the southern maritime site of Flatanger, the March MDW index explained 30% of the variation in summer NDVI ($F = 3.72$, $p < 0.05$, $R^2 = 0.30$). Figure 3.28 (a) shows the scatterplot of mean summer NDVI and March MDW over the time period 2001-2020.

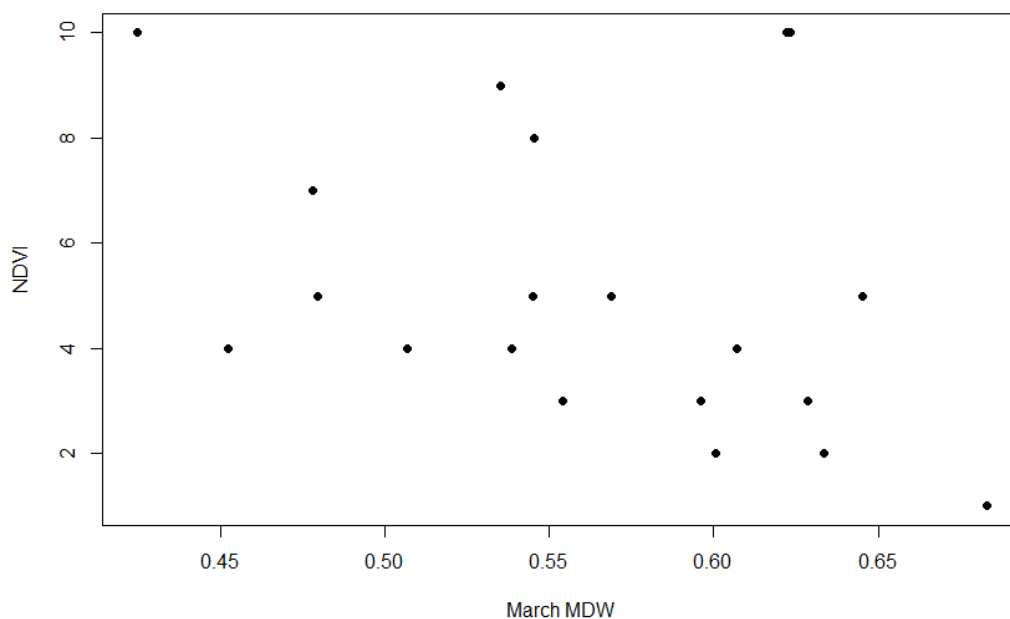


Figure 3.28 (a) Scatter plot of NDVI against March MDW and at the Flatanger study site, over the 2001-2020 time period.

The correlations between summer NDVI and March MDW were not presented in section 3.3.2.3 since the model grid boxes over which the correlations were significant ($p < 0.05$) were quite limited. The maps are presented here to help with interpretation (Figure 3.28 (b)).

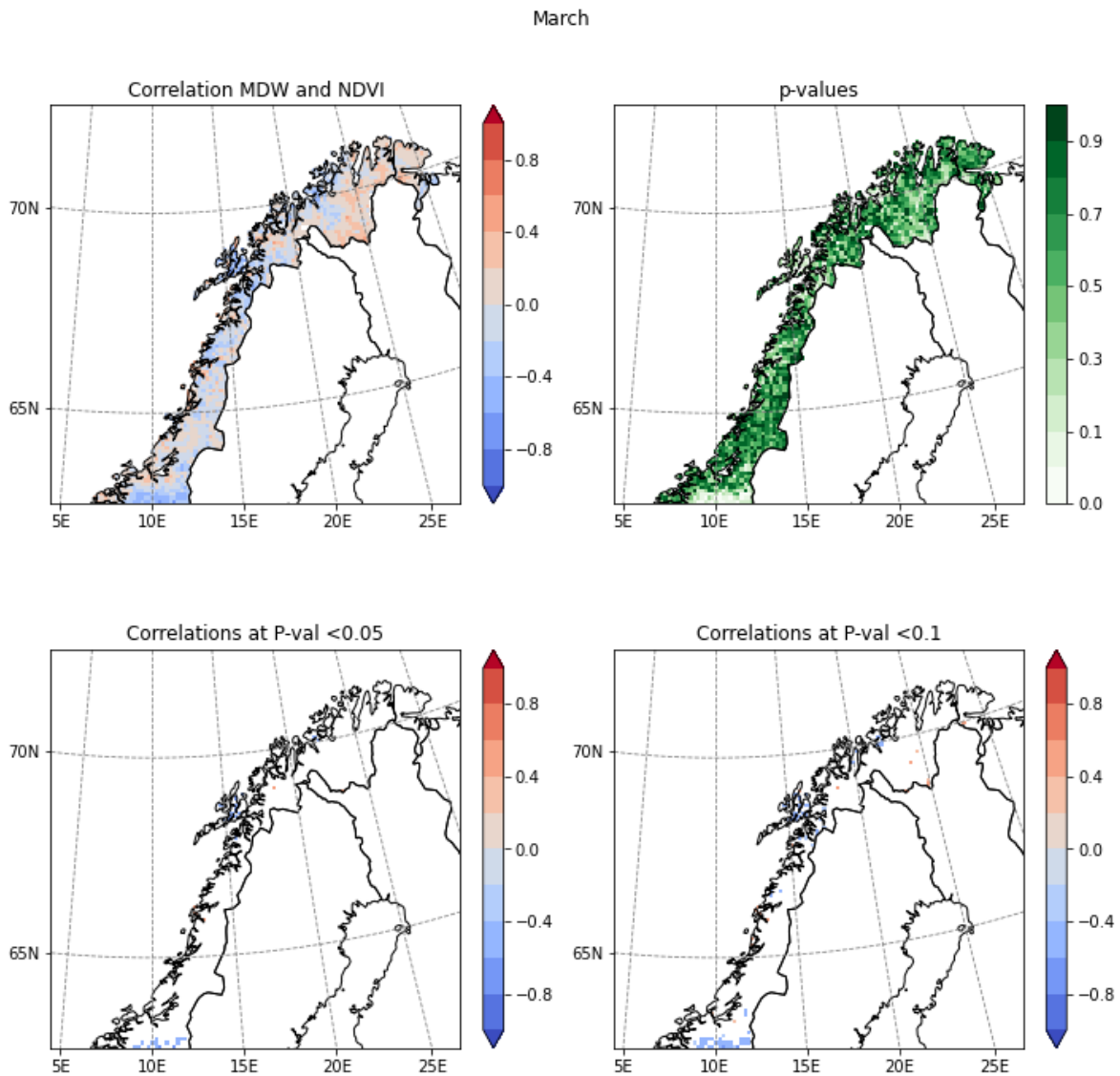


Figure 3.28 (b) Maps showing the correlations of mean summer NDVI with March MDW over the time period 2001 – 2020

The correlations provide insights into the linear relationship between mean summer NDVI and March MDW, which is negative at those grid boxes with significant correlations. The absence of a statistically significant correlation at this site reinforces the results of a statistically significant higher-order, quadratic relationship between summer NDVI and March MDW. Findings of Treharne (2018) showed no correlation between the duration of the longest warming event and time-integrated MODIS NDVI over their study domain, which covered the Nordland County. Although her research did not include Flatanger, these findings are mentioned as they are relevant to northern Norway. It is important to note

that the relationships in the work of Treharne (2018) were based on datasets at a 4 km-resolution and the real extreme weather conditions that occurred over the winter 2013/14, whereas the results of this work are based on datasets at a 10 km-resolution and the time span is twenty winter seasons. Therefore, an absolute comparison of the results is not possible.

3.3.3.2 Lofoten

For the Lofoten study site located in Nordland, the December SC20 index explained almost 50% of the variation in summer NDVI ($F = 7.32$, $p < 0.05$, $R^2 = 0.46$). Figure 3.29 shows the scatterplot of the December SC20 and average growing season NDVI for the time period 2001-2020. The scatterplot indicates a higher summer NDVI with an increased December SC20. The scatterplot also indicated a linear relationship between the variables, however, the regression analysis revealed that a linear relationship was not statistically significant (at $p < 0.05$). This result led exploring higher order model fits and a quadratic model was found to be statistically significant for the December SC20 and summer NDVI relationship.

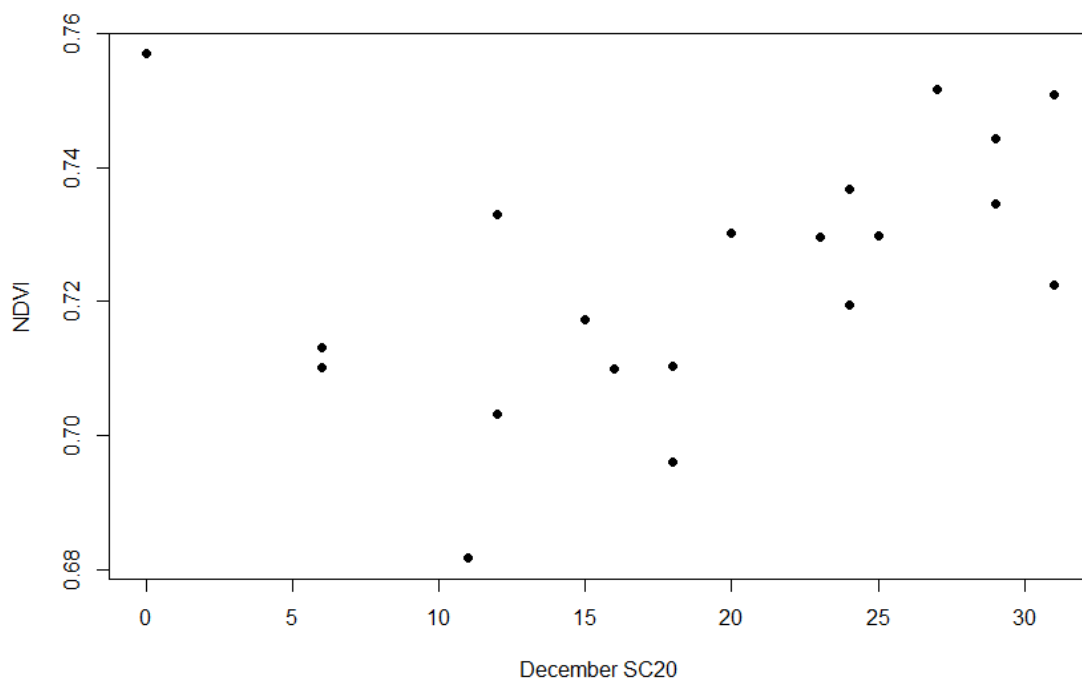


Figure 3.29 Scatter plot of summer NDVI against December SC20 at the Lofoten study site for the 2000-2020 time period.

The quadratic relationship between December SC20 and mean summer NDVI, at Lofoten islands, agrees with the findings of Pedersen et al. (2018) in that they also found non-linear relationships between MODIS derived summer NDVI and snow metrics for heathlands in the Arctic. Although their variables and study area are different from this PhD research, their results showed a statistically significant quadratic relationship between maximum NDVI and snow-water equivalent (SWE) over northeast Greenland for the 2000 – 2015 time period. They have attributed the non-linearity of the relationship between snow and NDVI, partly, to the large spatial variability in SWE over their study region. However, the non-linear relationship between the December SC20 and NDVI at Lofoten was just for a point location. Therefore, in this case (the location being stationary), it is likely that the nonlinearity either arises from the temporal variability of NDVI and snow variables, and/or is reflective of the impacts of low-snow day counts on NDVI in this area of Lofoten.

3.3.3.3 Storfjord

For the northernmost case study Storfjord the statistically significant NDVI predictors included mean December temperature, December MDW index and mean January temperature. Individually these metrics explained 31%, 31% and 29% of the variation in the summer NDVI. In a multivariate model the December MDW and the mean January temperature together explained the highest variance, almost 40% , in the summer NDVI ($F = 4.6$, $p < 0.05$, $R^2 = 0.38$). Figure 3.30 (a) and (b) present the scatterplots of NDVI against December MDW and mean January temperature, respectively.

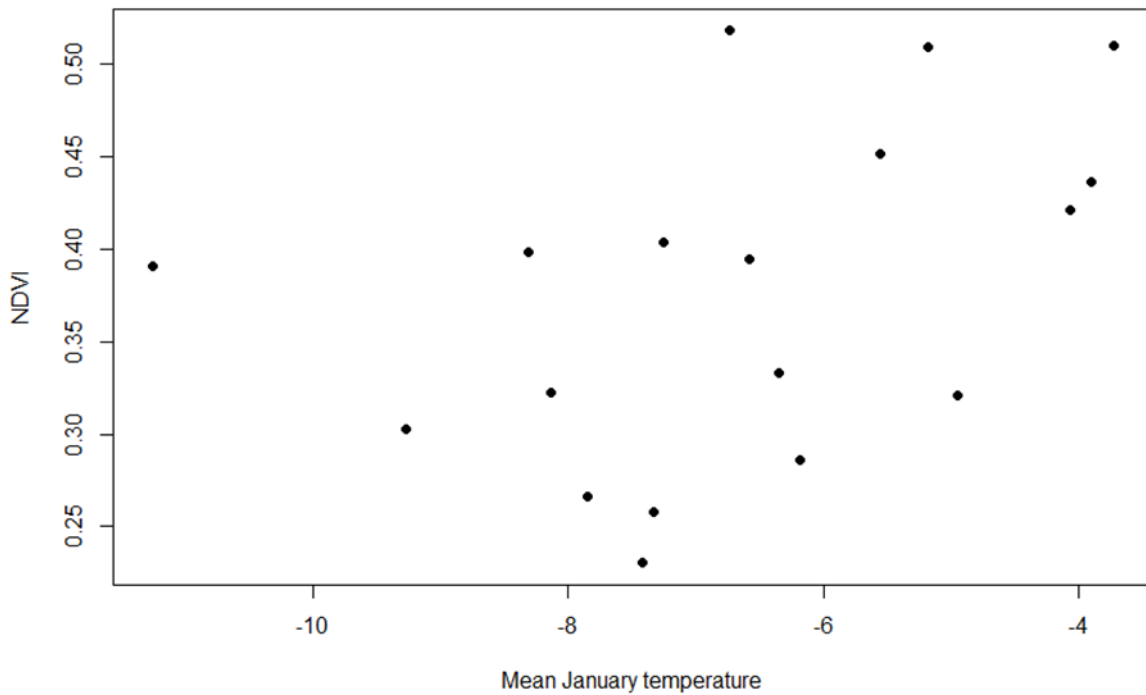


Figure 3.30 (a) Scatter plot of NDVI against mean January 2m surface temperature at the Storjford study site for the 2000-2020 time period.

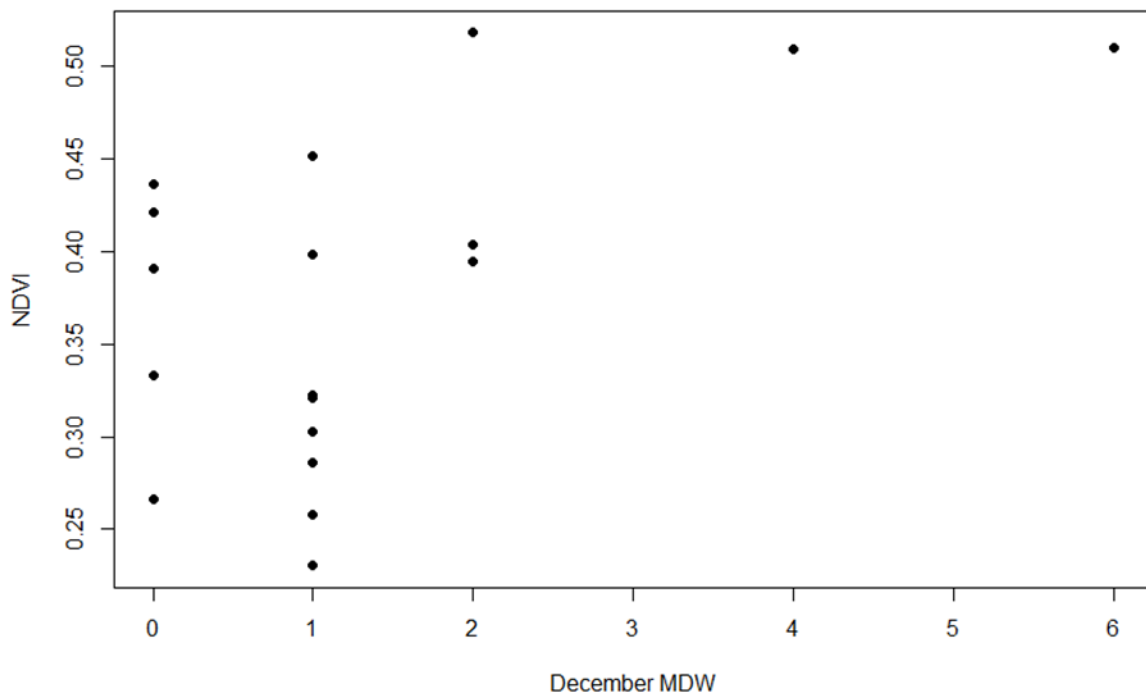


Figure 3.30 (b) Scatter plot of NDVI against December MDW at the Storjford study site for the 2000-2020 time period.

To summarise the results of the multivariate regressions analyses, the mean growing-season MODIS NDVI was moderately linked to a few of the WRF-based winter meteorological parameters. The predictor variables/indices varied across the case study sites. The statistical models performed better at the Lofoten and Storfjord sites compared to Flatanger. The statistically significant summer NDVI - winter variable relationships were better represented by a quadratic rather than linear relationship across the three sites. The influence of the interaction between the predictors, on the statistical models was minimal as the levels of multicollinearity between the predictors was assessed using the VIF method. The higher order of the statistical models here represent the underlying complexity of interactions between the NDVI and, the meteorological variables and indices. It is also worth remembering that the statistical modelling performed here was restricted by the small number of observations, mainly due to the NDVI availability on a temporal scale (2001 – 2020). This limiting factor may be responsible for cases where meteorological variables/indices that have previously been shown to cause vegetation damage did not show a statistically meaningful relationship with NDVI in this analysis.

3.4 Discussion

3.4.1 WRF's skill to reproduce winter meteorological conditions in northern Norway

Reproducibility of anomalous weather events is an important criteria for assessing the performance of NWP models (Heikkilä et al., 2011). One of the components of this research was to examine the skill of high-resolution WRF simulations at reproducing the extreme winter conditions in the Norwegian Arctic and sub-Arctic areas, which led to various vegetation damage events. Overall WRF was able to reproduce the real extreme weather conditions at the study sites fairly well, after bias corrections (based on a comparison with local observations) were applied to the daily mean temperature and snow depth simulations.

Norway being a long country with a complex landform has substantial spatial temperature variability (Solbakken et al., 2021). The three case study sites in this analysis were located at different latitudes. Flatanger is significantly different from Lofoten and Storfjord, as it is located below the Arctic Circle. Moreover, it was the most productive vegetation site as it has comparatively milder winters due to being in the maritime region. A cold bias was found in the WRF simulations across all the three sites, with Storfjord having the coldest bias, 2.5 °C. The model validation measure, RMSE, ranged between 3 - 4.7 across the sites, with Storfjord scoring the largest RMSE compared to the closest meteorological station. These results agree with Heikkilä et al. (2011), who also found that WRF's temperature simulations performed better around the region in which Flatanger was located as compared to the Storfjord region.

Both the Storfjord and Lofoten regions are mountainous. Interestingly the SC5 index (count of days with snow depth <5cm) was higher at the lower elevations for both the study sites during the extreme winter conditions of 2011/12 and 2013/14, respectively. Although the SC5 results here are related to extreme weather events, they are reflective of the findings of Dyrddal and Vikhamar-Schuler (2009) about long-term negative trends in both snow depth and count of snow days for lower elevations in Norway, starting in the 1960s.

It was comparatively straightforward to analyse the winter warming event at the Flatanger site, compared to understanding the frost drought conditions at the Storfjord and Lofoten sites. The process of quantifying these two different climatic drivers of Arctic browning reflects the fact that extreme weather events governed by a single variable, such as mean temperature, are simpler to assess and interpret. In contrast, assessing frost drought is a complex task because currently it is a poorly understood climatic driver of Arctic browning, and can result from multiple conditions such as ROS, winter warming and/or variable snow conditions. The results of this research showed that the meteorological conditions which lead to frost drought were different at Storfjord and Lofoten. While low snow conditions during December, January and February, and resulting exposure to freezing temperatures throughout the winter months, were the main drivers of vegetation damage at Storfjord, multiple winter warming events and variable/low snow conditions during mid-late winter (January, February and March) were the major drivers at Lofoten. Since the known extreme winter conditions driving browning events were rare over the study time period in this research, and that different meteorological processes at different times during winter occurred across the three study sites, there was not enough data to robustly conclude the significance of each winter month with regards to its vegetation damage potential.

'Winter warming' in this research was used for events where surface temperature stays at or above 2 °C for at least three consecutive days. However, previous research e.g., Treharne (2018) and Bjerke et al. (2012), have referred to winter warming also in the cases where snow melt occurred at a patch scale and led to localised warming of the soils and atmospheric boundary layer, rather than landscape-scale temperature increase. This variation in terminologies due to different study disciplines, the previous research being dominantly ecology versus this research being more ecological climatology oriented (Bonan, 2002), can sometimes affect the clarity of vegetation damage attribution.

Extreme weather events that affect ecosystems are a construction of multiple meteorological processes occurring simultaneously (Treharne et al., 2018). In general, extreme meteorological conditions are not well simulated by NWP models (Heikkilä et al., 2011). For example, severely cold winter temperatures

in Norway, due to strong temperature inversions, are not robustly simulated by models (Mölders and Kramm, 2010). In Norway's case the complex landform and a long coastline are added difficulties for NWP models in producing reliable simulations that capture extreme meteorological conditions (Solbakken et al., 2021).

It is possible that the regional landform complexity played a role in the simulations here as well, since WRF could not be run at a higher resolution than 5 km at Storfjord and 3 km at Flatanger, with the default settings. Storfjord is in the fjord region of Norway, surrounded with peninsulas and mountains ranging from sea level up to 1800 m a.s.l. This region presented a much steeper and more heavily dissected orography than the comparatively lower-altitude region of Flatanger. The analysis conducted here implies that simulation of vegetation-damaging extreme winter weather events in the fjord regions is a challenging process, therefore so is generating future projections.

In contrast to temperatures, the validation statistics of the simulated snow depth in the WRF simulations compared with the nearest meteorological station observations were poorer. The statistics were poor for both EWRP and CWRP simulated snow depth, which were at a 10 km grid resolution. Both sets of WRF simulations overestimated the snow depth at the majority of the meteorological stations. Since snow depth can vary considerably over very small distances so this result is not surprising. WRF's exaggeration of the snow depth parameter seems to be a consistent issue across other studies as well. For example, ERA-interim driven WRF simulations were found to overestimate both the snow depth and snow extent, as well as the solid precipitation, for the month of March in the Tibetan Plateau. Moreover, this was true across six different WRF experiments (Liu et al., 2019). Furthermore, WRF's snow depth and snow extent were overestimated for the South Korean peninsulas, with an increased model error for the areas with higher snow depth on the ground (Lee et al., 2022).

It was interesting to note that the performance of WRF's different land and physics schemes varies depending on the region. For example, the Noah LSM and the Lin scheme produced better snowfall simulations for north-eastern China, as compared to the Thompson and RUC schemes (Yu, 2013). Whereas the Thompson and Mellor-Yamada-Janjic scheme was found to be the most efficient in

simulations of precipitation and snow variables over the Castilla and León regions of Spain (Fernández-González et al., 2015). The WRF simulations in this PhD research incorporated the default land and physics scheme, similar to another WRF based study over Norway, Heikkila et al. (2011). Although the authors have not verified WRF's snow depth projections, the precipitation simulations in their study had a lower bias as compared to the driving ERA-40. It also performed well overall at a 10 km horizontal grid, when compared with both the ENSEMBLES mean and meteorological station observations. To what extent the snow depth parameter is controlled by the precipitation in the WRF model is an important question and can help to better determine the reliability of the snow depth simulations, in addition to using statistical measures such as RMSE while validating against the meteorological observations. The snow depth simulations in this research were compared with observations at the nearest meteorological stations as no simulations based studies were found related to WRF snow depth over Norway. Hence it is recommended that different land surface and microphysics schemes, along with different initial and boundary conditions, at differing grid resolutions, should be tested over Norway, as has been carried out in the cases of other regions mentioned above. This would help to determine the optimum settings for running WRF for solid and liquid precipitation, and snow depth simulations over the highly complex terrain of Norway.

One of the objectives of this research was to understand the climatic drivers of browning, hence snow depth was selected as the appropriate meteorological parameter. It is the most suitable parameter in the context of vegetation, rather than solid precipitation (snowfall). However, for accurate projections of the snow depth parameter, it is necessary to have robust modelling of the solid precipitation variable within the NWP models. Newer versions of WRF offer an option for separating liquid and solid precipitations. This needs to be set up during the model compilation process. However, due to time and computational resources constraints such model customizations could not be performed within this PhD research.

Simulating precipitation is generally compounded by various uncertainties. These include inadequate model validation due to an irregular network of precipitation gauges (Barstad and Smith, 2005) and low

resolution NWP models which struggle to simulate orographic precipitation in complex and steep terrains (Gowan et al., 2018). Along with challenges in precipitation modelling, measurement systems of precipitation, specifically for snow, are also widely known to be faced with different uncertainties. These consist of inaccurate gauge measurements due to interferences by blowing surface snow at high wind speeds (Kochendorfer et al., 2017) and unrealistically high snow depth variability between meteorological stations resulting from localised snowfall characteristics (Ibid). Various statistical techniques can be applied to NWP simulations during the post-processing stages to increase the accuracy of the projections. For example, multiple linear regression consisting of meteorological station and WRF precipitation, helped to significantly reduce the model error associated with total precipitation and snow variables over a study area in Spain (Fernán-dez-González et al. 2015). To improve the current understanding of relationships between WRF-simulated rainfall and satellite NDVI and the projections of precipitation related drivers of Arctic Browning, e.g., ROS, it is suggested that future studies use post-processing techniques which have been shown to reduce errors associated with WRF's simulated precipitation over complex terrains as Norway.

3.4.2 Linking winter climate and growing-season NDVI

The correlation analysis in this chapter was conducted on a model grid box level. In order to facilitate a concise discussion of the results, the correlation findings are discussed on a regional, county level.

The winter meteorological parameters and extreme weather indices with which the growing season NDVI showed significant correlations were different for each county. These parameters also varied depending on the winter month. Among the meteorological variables, mean monthly rainfall and temperature were found to be important NDVI controls in Trøndelag County, with the SC10, MDW and WWE indices similarly influential. Interestingly, mean monthly snow depth was not an important parameter for NDVI in this region. For the Nordland region, mean monthly snow depth, rainfall and temperature, and the SC20, SC10, ROS and MDW indices were observed to be the important controls

of NDVI. Lastly for the northernmost Troms og Finnmark County, mean monthly snow depth and temperature, and the WWE and MDW indices were found to be important for growing season mean NDVI. Predictably, rainfall was not significant for the overall NDVI in the Troms og Finnmark region as snowfall is currently the main form of regional precipitation in winter (Dyrrdal et al., 2013).

It was interesting that the NDVI – MDW relationship evolved from a mix of weakly negative/positive in March to moderately positive in April, for the Trøndelag and Nordland regions. A similar transition was observed for the NDVI – WWE March/April relationship, which evolved from moderately negative to moderately positive at most inland areas in Trøndelag and Nordland. Although the statistically significant correlations were limited for March, there were quite a few model grid boxes for April with near-significant ($p < 0.01$) correlations. When considered together, the aforementioned similar patterns for the WWE and MDW indices, which represent aspects of winter warming events (frequency and intensity), emphasize the positive role of warming events towards the end of the winter season with regards to mean summer NDVI, at the model grid boxes with significant and near significant correlations.

Summer NDVI being significantly positively correlated with the frequency of winter warming events in late winter, April, over the maritime region of Trøndelag, and also over a few model grid boxes in the Nordland and Troms og Finnmark regions, disagree with Bokhorst et al. (2010) and Treharne (2018). Treharne (2018) found warming events in late winter caused the highest reductions in time integrated-NDVI. The positive correlations between WWE, MDW and NDVI in this research imply that winter warming events in April aid with snow melt and can provide essential nutrients and soil moisture for the vegetation at beginning of spring when vegetation starts to de-harden accompanied by an increase in sunlight availability (Rixen et al., 2022).

December was the month that showed the highest number of meteorological parameters and extreme weather indices significantly correlated with NDVI, across all three counties examined in detail.

To better understand the relationships between winter climate and summer NDVI, a vegetation classification map (Solberg et al., 2008), (Figure 3.31), and an online interactive relief map of Norway

(TessaDEM, 2022) were examined. This helped to highlight the dominant vegetation types and the role of elevation at the model grid boxes that showed significant correlations. Table 3.13 presents a summary of the vegetation types associated with the different climate variables - NDVI correlations.

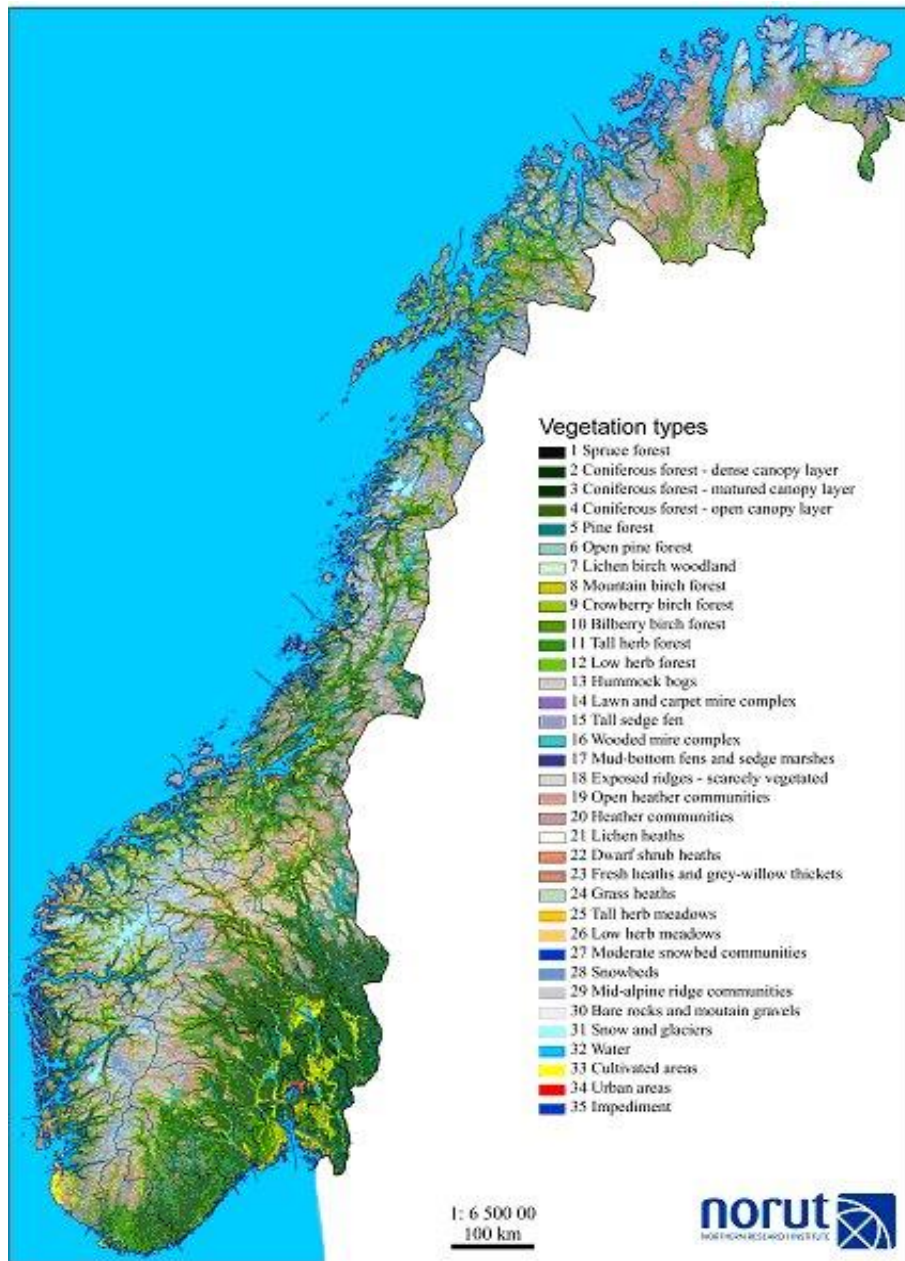


Figure 3.31 Map showing Norway's vegetation classification (Solberg et al., 2008)

Table 3.13 A summary of the vegetation types associated with different correlations. The numbers represent vegetation types based on the vegetation map (Figure 3.31) The colours red and blue represent positive and negative correlations, respectively.

Variables	Months with the highest number of model grid boxes that showed significant correlations and the associated vegetation types					
Snow depth, NDVI	January		February		April	
	11, 10	15	10	15,12	11,12	15
Temperature, NDVI	November		March		April	
	8, 9, 18, 10, 12		15, 24, 20		23, 14, 24, 15, 19, 26	
Liquid precipitation, NDVI	December		January		April	
	20, 10		8, 11, 4		20, 9	15, 12

Interestingly, most of the negative correlations between snow depth and NDVI occurred at higher altitudes, 600 m a.s.l. This could be due to positive trends in winter precipitation and snow depth, observed over 1961-2010 in these regions. Despite recent warming trends over most of Norway, the mountainous and northern areas have continued to experience cold winters with snowfall as the principal form of winter precipitation (Dyrrdal et al., 2013). Hence increased precipitation in winter causes deeper snow accumulation, which takes longer to melt in the spring season. The link with the vegetation productivity (NDVI) here is that depending on the spring and summer temperatures, deeper snow can take longer to melt, causing the growing season duration and soil warmth to decrease. This can result in decreased vegetation productivity of some plant species in higher elevation areas.

It was also observed that for areas with significant negative snow depth-NDVI correlations, tall sedge fen (15) (as referred to in Figure 3.31) was a consistent vegetation type. In contrast to the negative snow depth-NDVI correlations, positive correlations were mostly found at low lying areas, 100-500 m a.s.l.

In the context of temperature – NDVI and rainfall – NDVI correlations, several vegetation types showed significant correlations across the study domain. A clear homogenous pattern with regards to elevation and the sign of the aforementioned correlations was not observed for the study area.

The findings of this research about variation in the sign of the relationship between NDVI and meteorological parameters based on factors such as season stage and vegetation type is not unusual and has been found across other biomes as well. For example Piedallu et al. (2019) modelled the relationship between various environmental factors and MODIS NDVI for a mountainous region in France. They found positive links between NDVI and temperature in spring for mountain coniferous and deciduous vegetation, but negative correlations with increasing temperatures for Mediterranean garrigue or maquis and coniferous stands.

3.4.3 Linking winter climate and Arctic browning

The recent decline in vegetation across several Arctic areas has two temporal perspectives. It can be a longer-term climate trend induced browning or an extreme weather event driven browning, or a combination of both (Phoenix and Bjerke, 2016). The analysis in the previous sections was aimed at systematically quantifying the meteorological causes of both trend and event browning. The correlation analysis conducted over Northern Norway provides a semi-quantitative understanding of: (i) Trend browning through relationships of summer NDVI and winter meteorological parameters (temperature, snow depth and rainfall); (ii) Event browning through relationships of summer NDVI and extreme event meteorological indices (WWE, MDW, ROS, SC20 and SC10).

One of the most relevant previous pieces of work to the analysis of winter meteorology and growing season NDVI conducted in this PhD research is by Treharne (2018, chapter 5). Her main findings about the relationship between extreme winter weather events and satellite NDVI on a regional level were based on an in-depth analysis of one extreme winter season. One of her main findings was that exposure to severely cold temperatures in the absence of snow cover in early winter, e.g., December, had the greatest negative impact on MODIS NDVI in 2014. The findings of this chapter with regards to

the correlation of MODIS NDVI with SC10 and SC20 indices are broadly similar to Treharne (2018). These indices represented low snow depth conditions with respect to dwarf vegetation. The results found here are similar in the way that most of the significant correlations between low snow depth conditions and NDVI in this research were negative, as well as occurred in December, for both Trøndelag and Nordland counties. However, the negative snow depth-NDVI correlations in this research were not verified for the co-occurrence of freezing temperatures in terms of the entire study area, which is most of Northern Norway. Although, in this regard, the findings of the Storfjord case study, where low snow depth conditions were accompanied by freezing temperatures, agreed with Treharne (2018).

The other main finding of Treharne (2018) was that a higher mean temperature during the warming events in late winter i.e., March-April, was the most damaging for MODIS NDVI change in 2014. The results of this research contrast with Treharne (2018), albeit for a different region of sub-Arctic Norway, which was not included in her analysis. NDVI was significantly positively correlated with winter warming events in late winter, April, over the maritime region of Trøndelag, and over a few model grid boxes in the Nordland and Troms og Finnmark counties as well.

It is worth noting that Arctic Browning resulting from extreme winter weather events and/or changing climate trends is a comparatively recent topic of research within Arctic ecological studies. Therefore, the few existing studies related to Arctic Browning have taken quite different approaches to assess relationships between the meteorological drivers and vegetation damage on a regional scale. While Treharne (2018) regressed meteorological station data and the 2014 MODIS NDVI change (calculated w.r.t 2005-2010 NDVI), as the satellite measure of reduced productivity; this research correlated the average of each subsequent growing season NDVI to the preceding winter WRF monthly climatology, and on a model grid box level. The results derived from such different approaches are inherently difficult to compare due to differing datasets, as well as spatial and temporal scales of analyses.

The correlation analysis between meteorological variables and the summer NDVI helped to identify a range of parameters which were significantly correlated with NDVI, both positively and negatively.

However, this research demonstrated that linking these relationships with Arctic browning is not straightforward. The direction/nature of the relationship between meteorological parameters and NDVI does not determine greening or browning in the absolute sense. For example, in the case of NDVI being negatively correlated with December MDW, an increase in the MDW index implies a reduction in the subsequent summer NDVI and *vice versa*. Moreover, the meteorological parameters – NDVI relationships varied temporally across the winter months and spatially as well. Therefore, separating the correlations in terms of an increase and decrease in vegetation productivity is challenging. In this context the multivariate regressions approach was helpful to identify the most important meteorological parameters w.r.t NDVI in general rather than separating the NDVI between greening or browning.

The results of the multivariate regressions in this research showed differences in terms of the winter metrics that explained the highest variance in summer NDVI ($p < 0.05$) across the three case-study sites. This is reflective of the role of spatial heterogeneity, micro to meso-scale meteorological processes and local vegetation characteristics, affecting the MODIS NDVI variability. In addition, the relationships between NDVI and winter metrics were generally of higher order across the study sites. The role of aforementioned factors in explaining the nonlinearity of satellite NDVI-environment relationships, derived using regression models, has been explained in detail within other research e.g. Zhao et al. (2015). Correlations and Ordinary Least Squares (OLS) based regression is usually the first step in understanding NDVI-environment relationships. However, several studies have shown the relationship to be non-linear and exhibit complex features such as spatial nonstationarity on a landscape scale (Ibid). An additional way to understand the potential of winter metrics to cause browning at the study sites is to compare the results of the 20-years based regression analysis with the actual browning events that occurred at these sites. Based on the high-resolution WRF simulations, the 2014 vegetation damage at Flatanger was concluded to be caused by extreme December winter warming led snowmelt. Whereas based on the regression analysis the March MDW index best explained the NDVI variance at this site. At Lofoten, low snow depth conditions and recurrent winter warming events occurring over mid-

December 2013 to mid-March 2014 were the leading meteorological processes associated with the vegetation damage in 2014. The regression analysis indicated that the December SC20 index best explained the NDVI variation at this site, which partly agrees with the WRF high resolution based analysis for Lofoten. Lastly for the high-Arctic Storfjord site, the high-resolution WRF runs showed that a combination of severely low snow conditions in December and January, and consequent exposure of vegetation to the freezing mid-winter temperatures, caused the browning at this site. Results of the multivariate regressions partly agree with the previous, as December MDW and mean January temperature explained the highest variance in NDVI at this site. These comparisons highlight the complexities involved in isolating the climatic drivers of greening and browning across different temporal scales.

The findings of the multivariate regression analysis within this chapter inform the analysis related to the predictions of vegetation damaging events at the end of the 20th century, (ahead in chapter 4). Therefore, it is important to note that the correlation and multivariate regression analyses conducted here were based on the current frequency and intensity of extreme winter weather events over the study domain. Such events are indeed limited in their occurrence and spatial scale (Treharne, 2018), which in turn influences the strength and nature of the relationships between the meteorological parameters and NDVI.

It is also worth noting that the initial focus of the analysis under RO2 was to understand the climate-NDVI relationships related to dwarf, low-stature vegetation in Norway; however, filtering the vegetation in this way proved to be very time consuming and computationally intensive at a spatial resolution of 10 km. Therefore, such categorisation of vegetation was not conducted for the analysis. The discussions here were based on the NDVI of the overall vegetation within each model grid box.

Despite the vast literature on NDVI, the current understanding related to the drivers of NDVI patterns and trends is relatively poor (Piedallu et al., 2019). This work has reduced the gap by providing in-depth

analysis on the role of winter climate in impacting the growing season NDVI patterns over the complex terrain of Norway.

3.4.4 Research limitations

The limitations of the correlation and multivariate regression analysis in this chapter arise from two main sources. Firstly, the spatial resolution of both the NDVI and WRF simulations. While in the context of regional climate modelling a 10 km grid is considered as relatively high resolution, in the world of vegetation remote sensing 10 km is still a coarse resolution. In continuation of this work, it is recommended that future climate - vegetation modelling should be conducted at a higher spatial resolution and at local scale. One might lose the spatial extent of the study area owing to computational and time limitations; however, the potential insights that could be gained at higher resolutions such as 1 – 3 km would immensely improve the current understanding about the nuanced relationships between meteorology and vegetation productivity in the Arctic. This would also ultimately increase the robustness of future vegetation projections in response to a changing climate. The second major source of uncertainty in the analysis here is related to the limited number of NDVI observations per growing season. MODIS NDVI is the most widely used and effective satellite vegetation dataset for the Arctic region. However, for the analysis here the 16-day temporal resolution presented a challenge in terms of the number of observations for robust statistical analysis. While WRF was run on a daily temporal resolution to produce meteorological parameters, these were then necessarily aggregated to monthly averages in many instances in order to generate equal timesteps for paired statistical analyses such as the multivariate regressions.

3.5 Conclusions

This chapter addressed RO2 of this PhD, which is to determine the main meteorological drivers of satellite-based observations of vegetation decline in the Norwegian Arctic and sub-Arctic. To achieve this the relationships between MODIS NDVI and WRF-simulated meteorological variables were examined. This chapter also assessed the skill of ERA5-driven WRF at reproducing real extreme winter weather conditions, which lead to the browning events at the case-study sites. The high resolution simulations (1-5 km) helped to realize the spatial extent and variability of the warming events and frost drought conditions which caused the vegetation damage. Based on the results of the high-resolution simulations it is suggested that there are two principal challenges in predicting browning events on a regional scale, first due to the spatial variability in the frequency and duration of the same event, e.g., over the areas near to the coast vs more inland; and second, due to Arctic vegetation being quite heterogeneous and that previous research has shown species-dependent responses to extreme weather conditions.

The results of the correlation-based analysis for examining the links between extreme winter weather events and summer NDVI revealed large spatial variability in the variables that were important for NDVI in the following summer. Most of the correlations (both negative and positive) were in the range of 0.2 - 0.6 (weak to moderate). The highest number of meteorological parameters and extreme weather indices significantly correlated with summer NDVI were in December. The results of a significant positive relationship between the frequency of winter warming events in April and summer NDVI over the maritime region of Trøndelag, and also over a few model grid boxes in the Nordland and Troms og Finnmark counties, disagree with previous research; which found winter warming events in late winter caused the highest reductions in time integrated-NDVI.

Multivariate regression analysis was conducted for the three case-study sites to determine the best model fit between summer NDVI and winter meteorological variables. These models are used ahead in chapter four for the future projections of changes in NDVI. The results of the regression analysis showed

that quadratic relationships better explained the variance in summer NDVI. The findings about higher order based model fits for the relationships between meteorological variables and NDVI are similar to previous research.

The work in this chapter has provided useful insights in understanding the current relationship (for 2000 – 2020) between winter meteorology and summer NDVI for northern Norway. Moreover, this work is one of the first to test a methodology/approach to examine Arctic browning, based on satellite vegetation indices and regional climate modelling.

3.6 Supplementary data

Appendix 3.1

Table 3.14 Details of the WRF trial runs for estimating real time vs model time for the simulations

Study site	Model resolution	No. of cores HPC	Model time	Real time (hrs)	Estimated time for a 10 year run (All 12 months in a year)
1. Flatanger	45, 15, 5 km	2	1 month	18	3 months
2. Flatanger	45, 15, 5 km	2	1 week	2	1.4 months
3. Flatanger	25, 5, 1 km	2	1 week	28	20.22 months
4. Flatanger	25, 5, 1 km	3	1 week	22	15.88 months
5. Lofoten	45, 15, 5 km	2	1 week	1	0.72 month
6. Lofoten	25, 5, 1 km	2	1 week	33	23.83 months
7. Flatanger and Lofoten	45, 15, 5km	2	1 week	6	4.33 months
8. Flatanger and Lofoten	25, 5, 1 km	2	1 week	Failed	-
9. Flatanger, Lofoten and Storfjord	25, 5, 1 km	3	1 day	Failed	-
10. Storfjord	25, 5, 1 km	3	1 week	53	38.27
11. Flatanger and Lofoten	30,10, 3 km	3	1day	2 hours	
12. All 3 sites	30,10, 3 km	3	1 day	3 hours	8.5 months
13. The whole Norway	30, 10, 3 km	3	1 day	5.5 hours	13.9 months
14. CESM 1979 run	30,10 km	4	10.5 months	168 hours	2.6 months
15. Era5 1979 run	30,10 km	6	5 months	139 hours	For 30 years. It would take 420 days

Chapter 4

Climate change and Arctic Browning: Future Projections

4.1 Introduction

The complexities of assessing vegetation browning events retrospectively, and of providing projections of future occurrences of such events in the light of a changing climate has been discussed within recent literature. For example, Phoenix and Bjerke (2016), have explained how the sporadic nature and localised-scale of browning events makes it challenging to differentiate them from the widespread Arctic greening. Treharne (2018) has highlighted how the Arctic vegetation, which is currently a carbon sink, could turn into a net carbon source if browning events become increasingly frequent at a landscape scale. There are also huge uncertainties about browning events becoming a browning trend and possibly reversing the Arctic greening trend (Myers-Smith et al., 2020). With numerous studies predicting an increase in the frequency, intensity and scale of extreme winter weather for the Arctic region (Vikhamar-Schuler, 2016; Landrum and Holland, 2020), it is crucially important to investigate how Arctic vegetation could respond to such environmental stressors. There is however a significant research gap around the topic of the impacts of extreme winter weather events on Arctic vegetation productivity, especially under different emissions scenarios (as discussed in the literature review presented in Chapter 1, section 1.3). The third research objective of this PhD is aimed at reducing this research gap by examining how frequent and intense the climatic drivers of Arctic browning could become by the end of this century.

This chapter is focused on achieving RO3 of this PhD research through examination of the climatic drivers of both 'trend browning' and 'event browning' under the three Representative Concentration Pathways (RCPs) 4.5, 6.0 and 8.5. This chapter builds upon the findings of Chapter 3 in way that the statistical relationships between vegetation productivity and meteorological parameters (as modelled in Chapter 3), form the basis of future projections of vegetation change in the Norwegian Arctic and sub-Arctic. Chapter Three's findings related to the nature and significance of various climatic drivers of Arctic browning, thus informs the analysis here.

Along with the vegetation and future climate change linkages explored under RO3, this chapter also offers an independent perspective on projections of future climate in Norway. By producing high resolution meteorological projections for Norway at the end of this century, this chapter also addresses the requirement for local scale meteorological projections to drive climate impact related modelling experiments (Pall et al., 2019).

4.2 Methodology

To achieve RO3 of this PhD research a number of steps were followed. Broadly these steps fall under five main components. The first component consisted of generating meteorological projections under different emissions scenarios for the future time period, which was 2090 – 2100. The second component was focused on calculating the metrics which represent extreme weather conditions in this research from these projections. The third stage of the analysis involved comparison of future and historic climatic drivers of vegetation decline. The final component consisted of generating projections of future NDVI under different emissions scenarios and determining the browning changes for 2090–2100.

Each of the analysis stages above is explained in detail in the following sections.

4.2.1 Future climate simulations

WRF was forced with global bias-corrected CESM1 output to produce high resolution (10 km) meteorological simulations for the time period 2090 – 2100. As for the historical simulations in Chapter 3, the future simulations in this chapter were conducted for the winter season, considered as November – April. CESM1 simulations using RCP scenarios provided the entire set of variables required for the initial and boundary conditions for the WRF simulations. Additional CESM1 details have already been explained in Chapter 3. Three different RCPs were selected for future climate simulations so that the potential intensity and frequency of meteorological drivers of Arctic browning could be compared under different emission scenarios for the end of the 21st Century. The scenarios included are RCPs 4.5, 6.0 and 8.5. RCP 4.5 signifies a world with effective greenhouse gas (GHGs) control measures, a

mediocre rise in global air temperatures and a long-term, stabilised anthropogenic radiative forcing of 4.5 Wm^{-2} post 2100 (Riahi et al., 2015). RCP 6.0 is a scenario driven by climate policies, without which it is certain that the radiative forcing would exceed 6.0 Wm^{-2} by the year 2100. This scenario sees GHG emissions peak in the year 2060 and reduce afterwards, with the possibility of a global mean temperature increase of up to $4.9 \text{ }^{\circ}\text{C}$ (Masui et al., 2011). Whereas the RCP 8.5 scenario exhibits continuously increasing GHGs and extreme global warming (Ibid). These scenarios are summarised in Table 4.1. The domain setup for future WRF simulations is presented in Figure 4.1.



Figure 4.1 Domain setup for future WRF simulations

Table 4.1 Summary of RCP scenarios (Source: Moss et al. (2010))

Name	Radiative forcing	Concentration (p.p.m.)	Pathway
RCP8.5	$>8.5 \text{ W m}^{-2}$ in 2100	$>1,370 \text{ CO}_2\text{-equiv.}$ in 2100	Rising
RCP6.0	$\sim 6 \text{ W m}^{-2}$ at stabilization after 2100	$\sim 850 \text{ CO}_2\text{-equiv.}$ (at stabilization after 2100)	Stabilization without overshoot
RCP4.5	$\sim 4.5 \text{ W m}^{-2}$ at stabilization after 2100	$\sim 650 \text{ CO}_2\text{-equiv.}$ (at stabilization after 2100)	Stabilization without overshoot
RCP2.6	Peak at $\sim 3 \text{ W m}^{-2}$ before 2100 and then declines	Peak at $\sim 490 \text{ CO}_2\text{-equiv.}$ before 2100 and then declines	Peak and decline

4.2.2 Quantifying the meteorological drivers of Arctic Browning 2090 – 2100

Arctic warming has intensified since the early 21st Century (Walsh et al., 2011). Therefore, the decade preceding the early 21st Century, 1990-2000, was selected as the baseline time period, against which the future climate projections were compared. It is worth noting that browning events have not been reported for the baseline time period within the scientific literature. Therefore, this comparison helped to develop an overall understanding of potential changes in occurrence and intensity of the climatic drivers of browning at the end of this century; as anthropogenic climate change forcings increasingly continue to affect the Arctic's winter climate.

Since the 1990 – 2000 baseline simulations also served as the WRF-validation simulations (under Chapter 3), sections 3.2.4.1 and 3.2.4.3 provide the model and setup details for the baseline simulations.

The analysis in this chapter builds upon the findings related to the various meteorological drivers of vegetation decline in the Norwegian Arctic and sub-Arctic (as discussed in Chapter 3). These drivers varied regionally as discussed in section 3.4.2.1. The potential future occurrence of vegetation decline over the study domain is dependent on the changes in these drivers. Therefore, changes in meteorological drivers, with which the summer NDVI did not show significant correlations, are also explored within the analysis of future changes.

The meteorological indices explored in Chapter 3 were calculated for the three RCP scenarios using the WRF simulations of 2090 – 2100. These indices are summarised in Table 4.2.

Table 4.2 A summary of the meteorological indices used in this chapter

Extreme weather event metric	Explanation
a. Winter warming event frequency (WWE)	Count of events with daily mean near-surface air temperature (T ₂) > 2 °C, for at least 3 consecutive days
b. Maximum duration warm event (MDW)	Maximum number of days where T ₂ > 2 °C
c. Mean monthly temperature (T)	
d. Rain-on-Snow event (ROS)	Count of days where rainfall > 1 mm and snow depth > 1 cm
e. Mean monthly snow depth	
f. Snow count 10 (SC10)	Count of days where snow depth < 10 cm
g. Snow count 20 (SC20)	Count of day where snow depth < 20 cm

4.2.3 Future NDVI projections

RO3 of this PhD is focused on examining the links between future climate change and Arctic Browning. Therefore, following the analysis of projections related to the various climatic drivers of browning, the next step consisted of producing projections of NDVI. The NDVI projections were generated for the future time period, 2090-2100, under the three RCPs 4.5, 6.0 and 8.5.

The NDVI projections were conducted for the three case study sites, Flatanger, Lofoten and Storfjord. The NDVI projections were based on a polynomial regression-led modelling approach (as detailed in Chapter 3, section 3.2.6.2). As a brief reminder of the methodology, for each case-study site MODIS NDVI (MOD13Q1, as also used in Chapter 3) was regressed against each relevant predictor separately. Next it was examined whether different predictors complemented each other using multivariate

regression analysis. For each set of future NDVI projections, the model used was the one which explained the highest variance in MODIS NDVI (highest R^2 value, at $p < 0.05$), over the time period 2000 – 2020.

It is worth remembering that the models which were found to be statistically significant were not linear. This was consistent across the case study sites. The statistically significant models were of order ≥ 2 . For the purposes of this research, and consistent with ecological knowledge the statistical models were limited to a quadratic level (order = 2) (Piedallu et al., 2019). Therefore, the NDVI projections for all study sites were based on quadratic relationships.

The NDVI projections step was followed by calculations of percentage change between the future and historic NDVI. The NDVI over the time period 2001 – 2020 formed the baseline for the percentage change calculation. A negative percent change indicated a decrease in NDVI (browning) and *vice versa*. It is worth noting that for calculating the change in future NDVI, the past MODIS NDVI dataset used was site-specific, rather than a general baseline NDVI. Hence the analysis was based on three NDVI datasets, the NDVI at Flatanger, Lofoten and Storfjord study sites. This ensured that site-level vegetation composition and other ecological processes were reflected within the NDVI. The NDVI datasets were at the same spatial resolution, 10 km, as the WRF meteorological variables and indices. The statistical analyses were conducted using RStudio software.

One of the factors for selecting the browning sites in Chapter 2 and 3, as case study sites for future NDVI projections was that the current vegetation composition at these sites is known (details provided in Chapter 2). These sites dominantly consist of low lying dwarf vegetation such as heathlands, and thin to no tree cover. Because such vegetation is the focus of this PhD research, these three browning sites offered the optimum conditions for the statistical modelling based NDVI projections. Another reason for selecting these sites was that the analysis in Chapter 2 has provided in-depth knowledge of how field observations of vegetation damage and disturbance translate into satellite-based quantification of

these phenomena. Hence, this background understanding of the ground – satellite browning equivalency helped to better interpret the future NDVI changes.

4.2.3.1 Limitations of the NDVI projections

A large number of dataset observations are required for reliable projections of the dependent variable when using polynomial regression models. One of the limitations of the NDVI projections in this chapter was that the statistical models used for prediction were based on datasets with a small number of observations. This was due to the MODIS NDVI dataset availability 2000 – 2020. However, it is fair to state that this analysis has made the maximum benefit from the MODIS and WRF datasets by systematically generating projections of potential vegetation decline over the Norwegian Arctic and sub-Arctic areas, because such analyses are currently very limited.

4.3. Results

This section first presents the results of the projections of various extreme winter weather events under the three RCPs over the time period 2090 – 2100, compared to the baseline time period 1990 – 2000. The extreme winter weather indices included WWE, WMD, SC10, SC20 and ROS. This is followed by the results of projections related to changes in meteorological parameters; temperature, snow depth and rainfall. It is worth noting that the extreme event indices consider event browning, and the parameters consider trend browning. The future projections of meteorological variables are followed by the results of future changes in the vegetation productivity.

4.3.1. Extreme winter weather events under different RCPs

4.3.1.1 Winter warming event frequency (WWE)

Winter warming events for this research were defined as a time period with at least three consecutive days when the near-surface air temperature stays at or above 2°C.

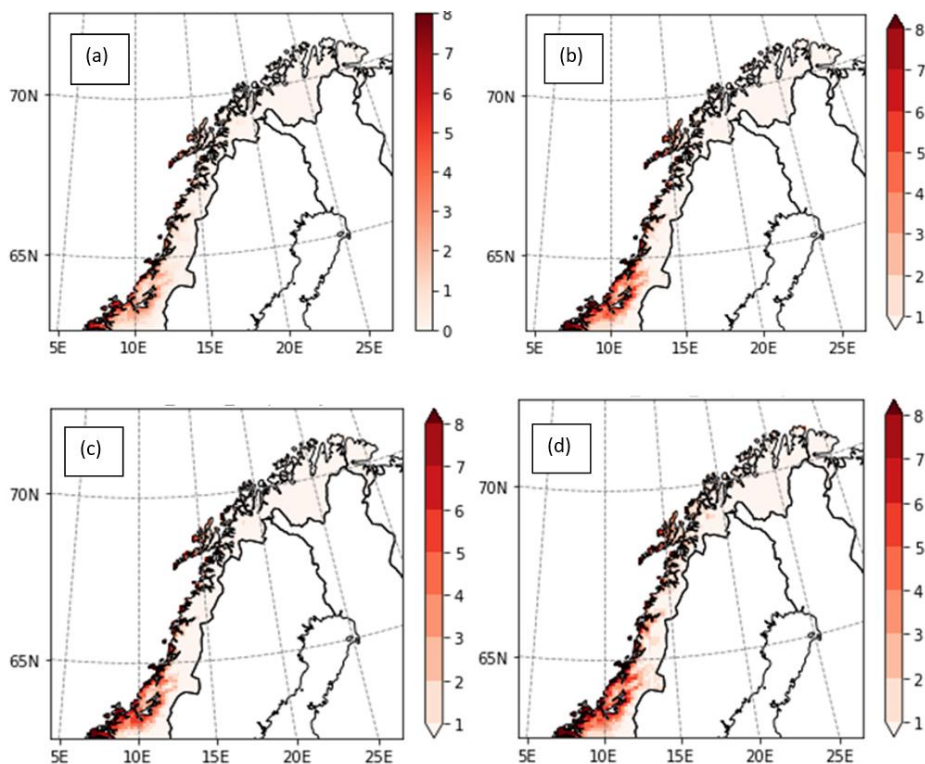


Figure 4.2 Average winter warming event frequency for (a) Historic baseline 1990-2000, (b) RCP 4.5, (c) RCP 6.0 and (d) RCP 8.5 2090-2100 respectively

Figure 4.2 shows maps of the average winter warming event frequency per scenario. For all the RCP scenarios over 2090 - 2100 as well as the baseline time period, the western coastal areas south of 65°N and the Lofoten islands were found to be most exposed to winter warming events. The projections for RCPs 4.5 and 6.0 were similar. RCP 8.5, as expected, showed the highest frequency of winter warming events. Similar to the other RCPs as well as the baseline time period, the warming events under RCP 8.5 are mainly concentrated around the coastal areas under 65°N in the Trøndelag County. However, under RCP 8.5 these events occur at higher latitude coastal areas as well. For example, under this scenario, up to 4 more and 1 more warming event per winter season are projected for the Lofoten islands and for a few areas above 69°N, respectively. Compared to other scenarios, RCP 8.5 could see 2-3 more warming events per winter for a few inland areas as well in the Trøndelag and Nordland counties.

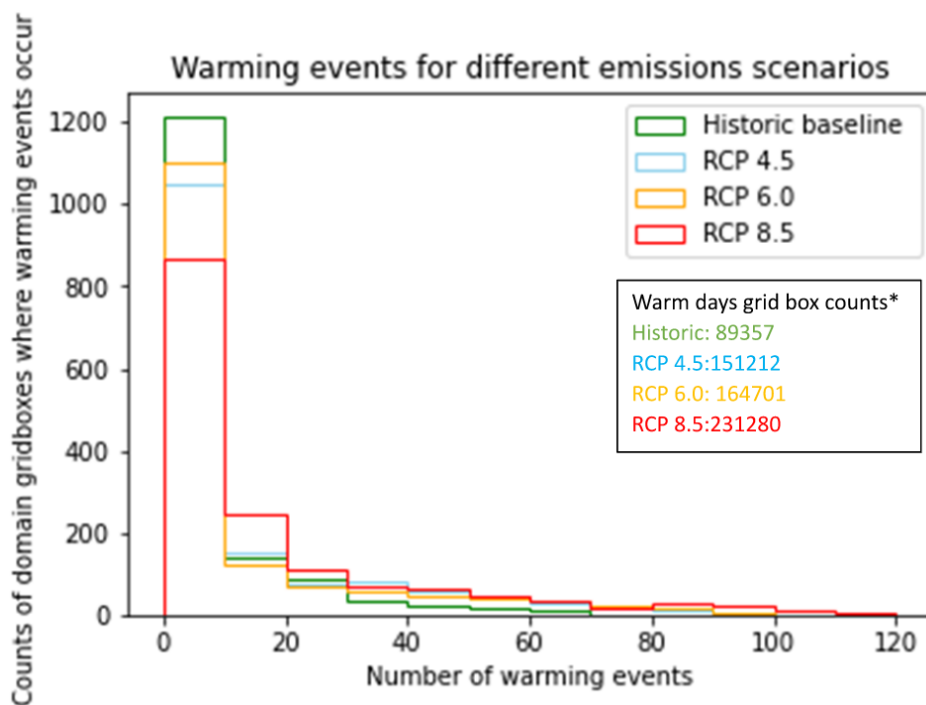


Figure 4.3 Frequency of winter warming events under the different RCP emissions scenarios 2090-2100, as compared to the baseline time period 1990-2000. *The warm days grid box count refers to the total number of model grid boxes where near-surface air temperature > 0 °C, under each scenario respectively.

Figure 4.3 provides a condensed version of Figure 4.2. It compares the counts of model grid boxes with respect to the frequency of winter warming events, for each scenario. Overall RCP 8.5 is the most different scenario compared with the historical baseline. A noticeable shift can be seen towards the right side of the graph, which implies an increase in the number of domain grid boxes with a higher frequency of warm events. For example, there were no areas with 80 – 120 winter warming events under the historic baseline 1990 – 2000, whereas for RCP 8.5 there could be a few of these. Also, important to note was the combined count of days and model grid boxes with near-surface temperature > 0°C, under each scenario (box on Figure 4.3). This count represents a general spatio-temporal view of warmer temperatures in the Norwegian Arctic and sub-Arctic areas. As compared to the baseline, RCP 8.5's projected instances of warming events was greater than double. In this context it is also worth remembering that WRF's validation simulations in this research had shown a cold bias with an average value of 2.6 °C. Therefore, it is quite likely that this temperature related estimate is an under estimation of potential warmer conditions in the future.

Seasonal changes in future WWE

In order to evaluate which winter months could see the strongest increase in warming events at the end of this century, difference maps of the future and baseline WWE index were produced. Figure 4.4 shows the mean WWE index for different winter months.

For all the three months considered here, one more warming event per month is predicted under the three RCPs (2090 – 2100), as compared to the 1990 - 2000 time period. The strongest mean monthly increase in the WWE index is predicted in December for the maritime region of Trøndelag county, which could experience up to two more warming events. Surprisingly RCP 8.5 was not different from RCPs 4.5 and 6.0. In the context of pan-Arctic winter warming, currently the North Pole is increasingly experiencing at least one extreme winter warming during December (Graham et al., 2017). On the other hand, the warming events are not increasing in intensity based on the temperature increase of the event (Ibid).

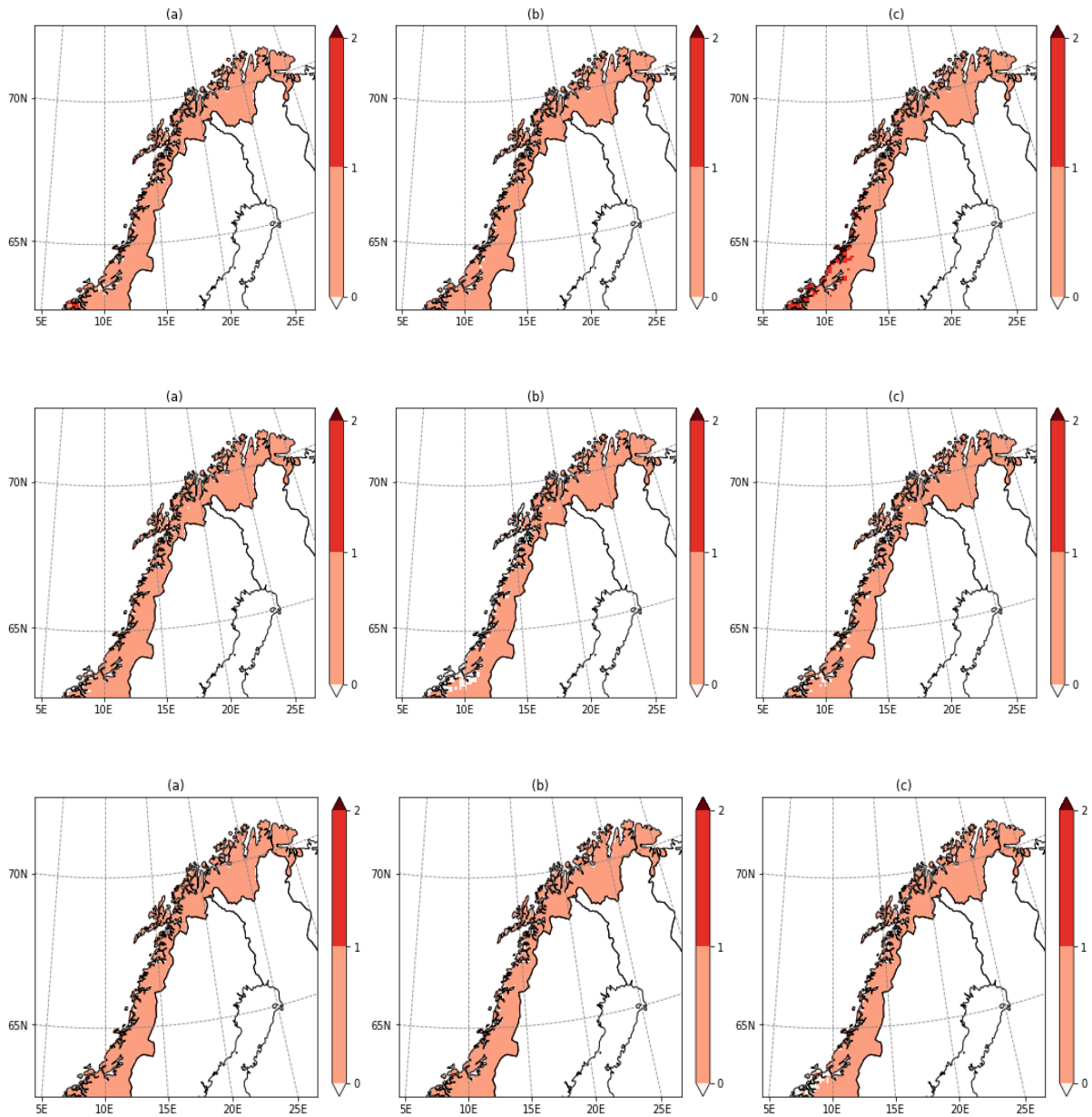


Figure 4.4 Change in the mean monthly WWE index for the months of December, January and February (top to bottom row-wise), under three RCPs (a) 4.5, (b) 6.0 and (c) 8.5, over 2090-2100. The change was calculated w.r.t the baseline time period 1990-2000. The mean monthly WWE refers to the average number of warming events in the respective month for the time period 2090 – 2100.

4.3.1.2 Maximum duration warm event (MDW)

The maximum duration warm event index represents the longest lasting winter warming event, per winter season. This index reflects the significance of the intensity of a warming event, in terms of duration, in the context of vegetation disturbance. Figure 4.5 presents the mean of the highest duration warming event per winter season for each scenario.

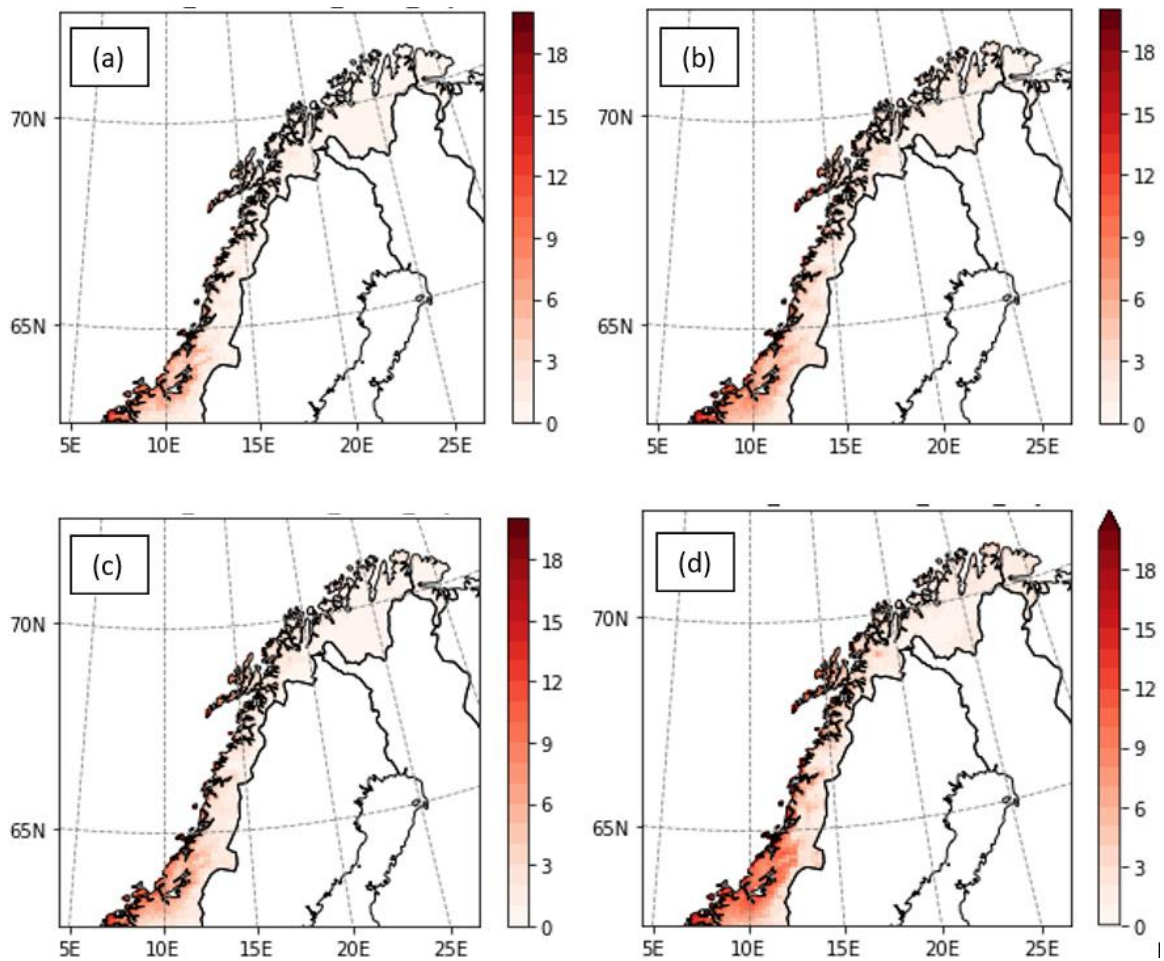


Figure 4.5 Average 'maximum duration winter warming event (*days*)' (MDW) per winter season for (a) Historic baseline 1990-2000, (b) RCP 4.5, (c) RCP 6.0 and (d) RCP 8.5 2090-2100 respectively

For all scenarios, the higher duration warming events were observed for the coastal areas. For example, under RCP 6.0 the Lofoten islands could experience a warming event lasting for 9-12 days, whereas this is 0-3 days for the more inland areas at the same latitude. The spatial pattern of more pronounced events around the coastal areas as compared to the inland regions is similar to the results for the WWE index (Figure 4.2). With reference to the historic baseline 1990-2000, all three RCPs could see longer duration warming events in the winters of 2090-2100. For example, for RCP 8.5, a larger area can be seen along the western coast south of 65°N, where surface temperatures could stay at or higher than 2°C for as long as 9-18 consecutive days, as compared to lasting for 3-6 days under the baseline time period.

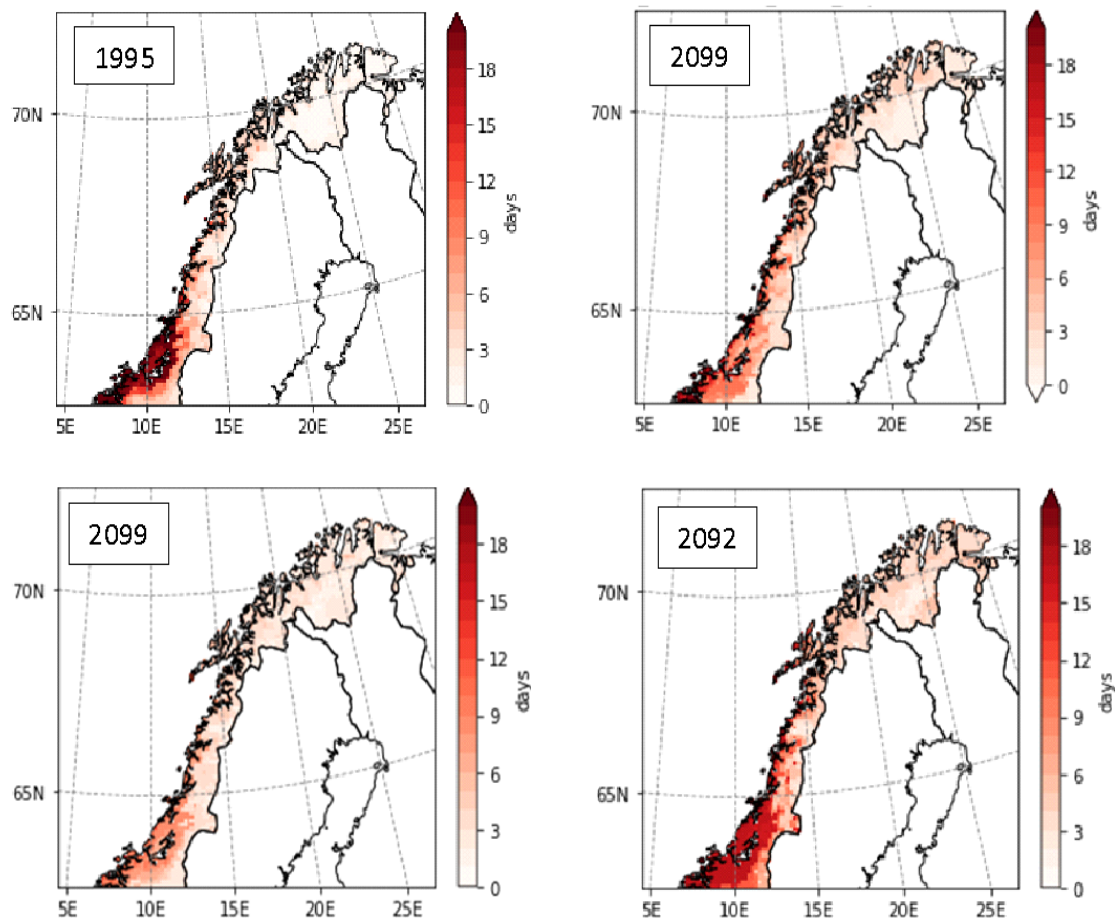


Figure 4.6 The years with the highest MDW under the baseline time period (1990-2000) and RCPs 4.5, 6.0 and 8.5

Figure 4.6 presents the warmest year under each scenario w.r.t to the maximum duration winter warming events. The warmest baseline year was 1995, with the longest lasting warming event over 15-18 days, in the maritime region of Trøndelag. However, as it would not be expected that the timing of events in the CESM driven WRF simulation would match real world timing, as the CESM simulation is driven by external forcings, and not reanalysis. Hence the magnitude, but not the timing, should be considered. It is also worth noting that under the baseline, for the majority of the eastern inland regions of Norway, the longest lasting warming event was 0 – 3 days. Whereas under RCP 8.5 these areas are projected to experience a 6 – 9 days long events.

4.3.1.3 Count of days with snow depth < 10 cm (SC10)

Low snow conditions, such as snow depth < 10 - 20 cm, can be damaging for low-lying Arctic vegetation such as *Empetrum nigrum*, *Vaccinium myrtillus* and *Calluna vulgaris*. These plant species comprise a fair percentage of the current vegetation cover and abundance in Arctic dwarf shrub heathlands. The SC10 index represents the day count where snow depth < 10 cm. Figure 4.7 show the maps of average SC10 count per winter season, for the baseline 1990-2000, and the three RCPs. An increase is projected in SC10 along the coastal areas, under all three RCP scenarios. The increase is pronounced for the maritime region of the southernmost Trøndelag county and the Lofoten islands. Overall, the SC10 projections were similar for the three RCPs. The largest increase in the index was seen for RCP 8.5, under which average SC10 per winter can increase by 60 days in the Trøndelag County and Lofoten islands compared to the baseline time period. In contrast, the SC10 index is projected to stay the same as the baseline for almost all inland regions of Nordland and Troms og Finnmark.

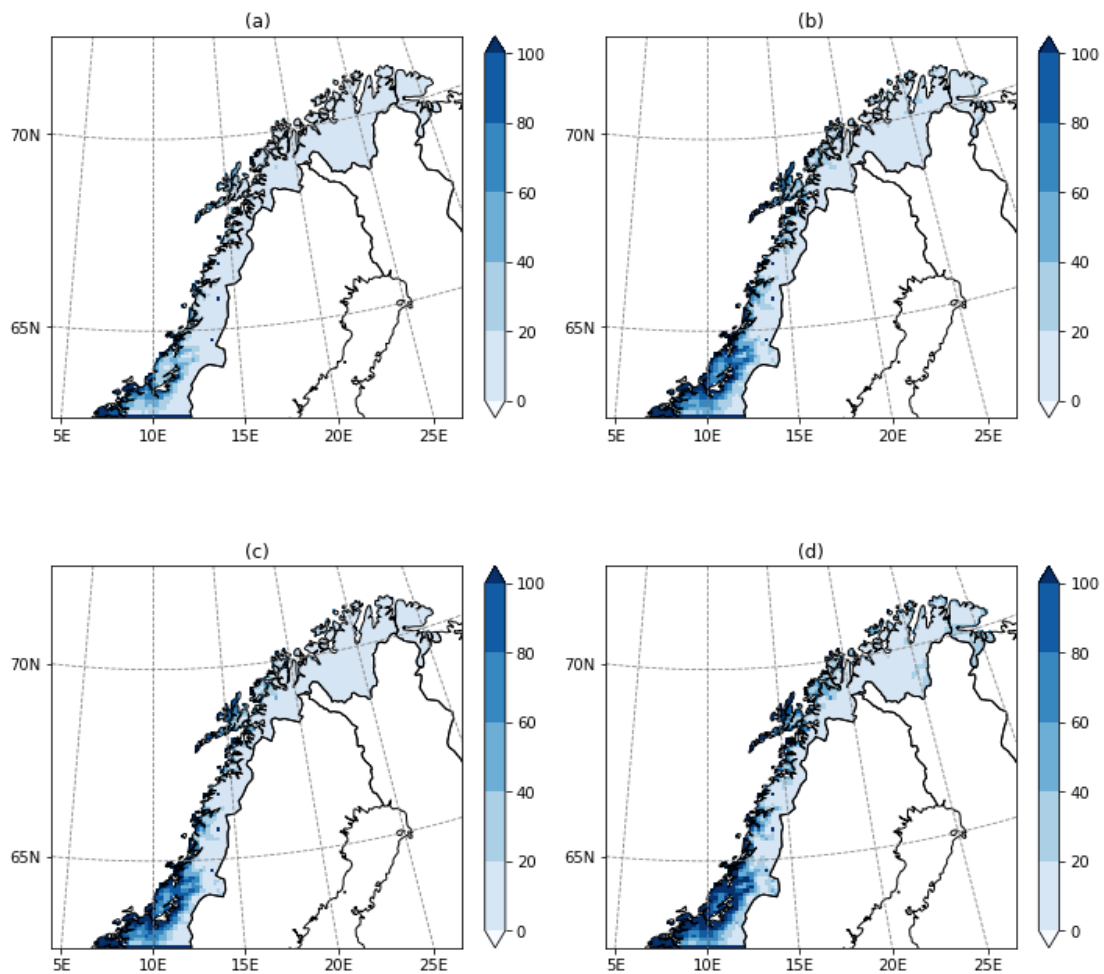


Figure 4.7 Maps showing the mean SC10 index per winter under (a) the baseline time period (1990-2000), (b) RCP 4.5, (c) RCP 6.0 and (d) RCP 8.5

4.3.1.4 Count of days with snow depth < 20 cm (SC20)

The maps of SC20 index (Figure 4.8) represent the average count of days per winter, where the snow depth is < 20 cm.

An increase in the SC20 index across the study area was observed for all three scenarios compared to the baseline. Overall, across the three RCPs, the strongest increase in SC20 was observed for areas along the coast. Trøndelag is projected to experience the most pronounced rise in SC20 as some inland areas in the county also see a marked increase, up to 60-80 SC20 days, compared to the baseline. Among the scenarios, RCP 8.5 showed the highest increase in the SC20 frequency and spatial extent. Up to 80 – 100 more days could be expected in Trøndelag, 20 – 60 more for Nordland, and most notably,

the SC20 index could double for the lower elevation areas located well above the Arctic Circle, in the north-eastern parts of Troms og Finnmark.

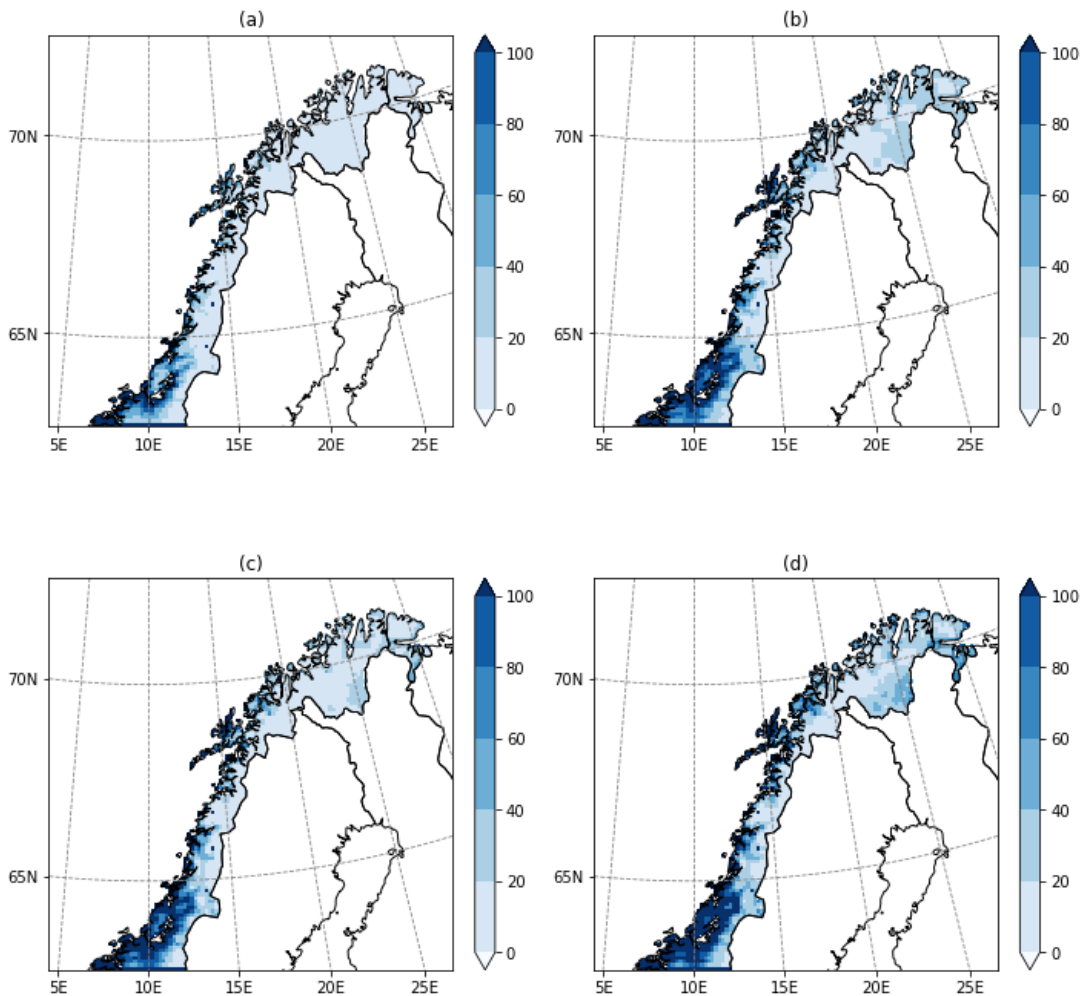


Figure 4.8 Maps showing the mean SC20 index for each winter season under (a) the baseline time period (1990-2000), (b) RCP 4.5, (c) RCP 6.0 and (d) RCP 8.5

Frost drought was one of the common meteorological drivers of browning events at the case study sites (as explained in Chapter 3, section 3.3.1.2). It was also found to be a complex phenomenon to quantify in terms of indices and variables since it can be caused as a result of both winter warming events and/or exposure to freezing temperatures during low snow conditions.

The SC10 and SC20 indices represent low snow conditions and changes in these indices were strongest under RCP 8.5. These results prompted an examination of whether the potential low snow projections

under RCP 8.5 could also be accompanied by sub-zero temperatures, and thus cause frost drought conditions as were found at the Storfjord browning event site. Hence RCP 8.5 was selected here as a case study scenario to assess potential frost drought conditions on a monthly basis.

Figure 4.9 presents the average number of days per month where snow depth < 10 cm and the near-surface temperature < 1 °C, for the months of (a) December, (b) January, (c) February and (d) March over the time period 2090-2100. Thus, these meteorological conditions represent cold exposure days during low-snow conditions.

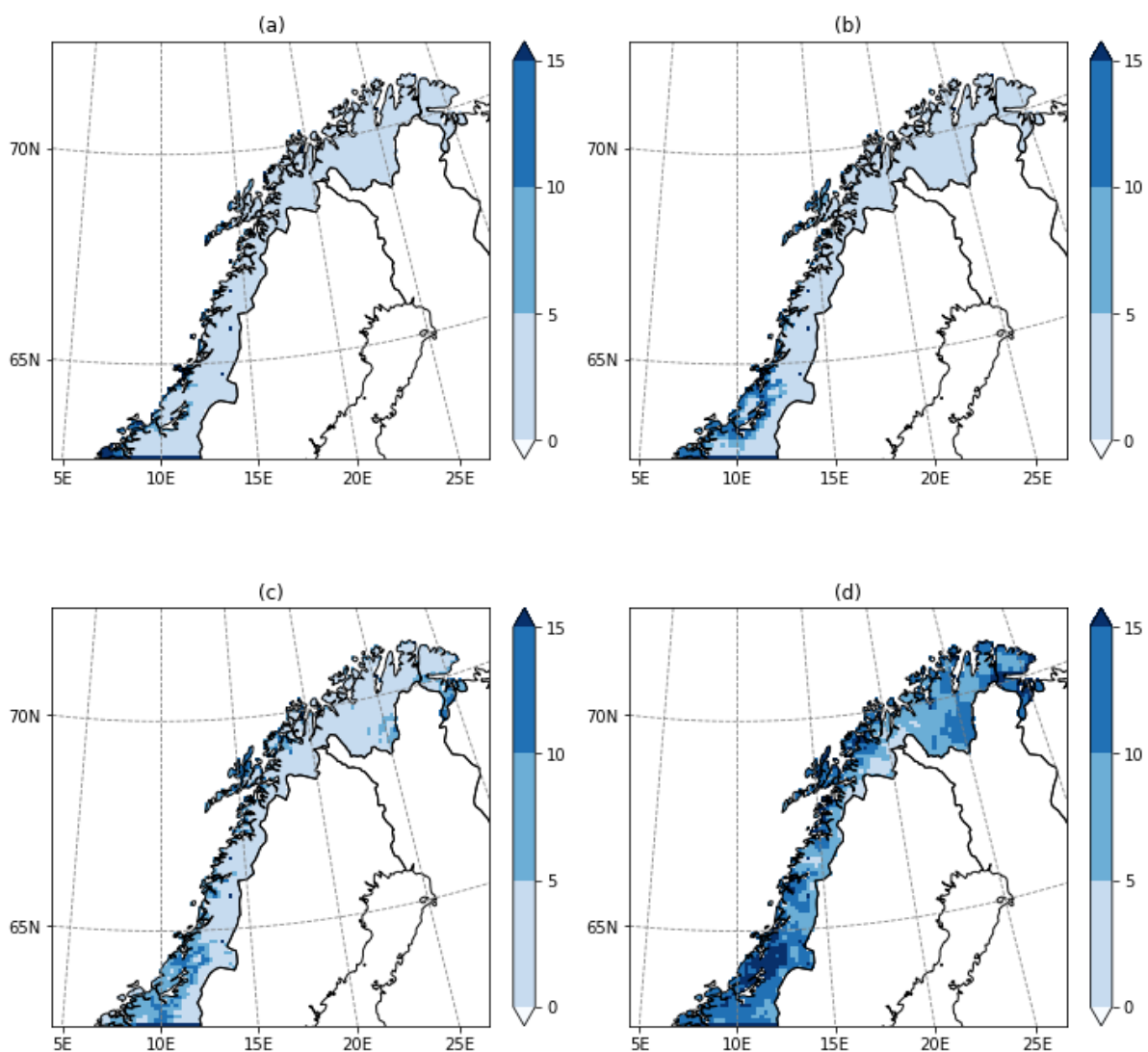


Figure 4.9 Maps showing the average number of days per month where snow depth < 10 cm and the near-surface temperature < 1 °C, for the months of (a) December, (b) January, (c) February and (d) March, over the time period 2090-2100, under RCP 8.5.

Under RCP 8.5, March is predicted to experience the highest number of days per month with frost drought conditions. Major differences were seen between March and the other three months. For December, January and February, most of the domain areas showed 0-5 days per month, whereas for March it was up to 10-15 such days across many regions. Thus, low lying vegetation across the Norwegian Arctic and boreal regions could be at substantial risk of experiencing frost drought conditions during the late winter month of March. It was beyond the scope of this thesis to explore the meteorological mechanisms causing higher days of frost drought conditions in March.

4.3.1.5 ROS events

Rain-on-Snow days (ROS) were estimated for the historic baseline 1990-2000 and the three RCPs. Figure 4.10 presents the average ROS days count per winter season under each scenario. With regards to low-lying Arctic vegetation, it is concerning that as compared to the baseline, not only could ROS days increase at the end of this century under all three RCPs, but as well as ROS occurrence could spatially extend up to the entire northern western coast.

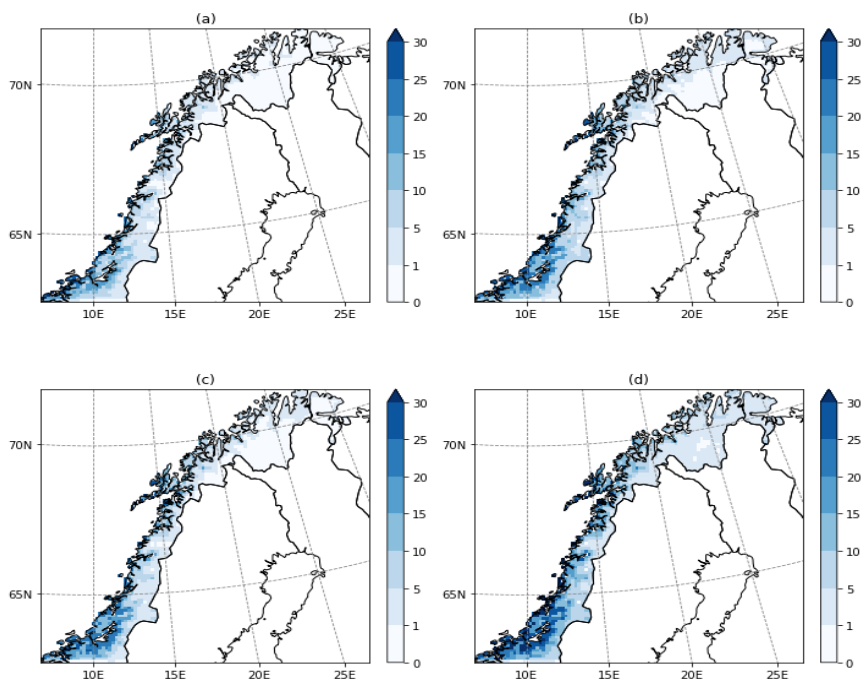


Figure 4.10 Average ROS days per winter season under (a) Historic baseline 1990-2000, (b) RCP 4.5, (c) RCP 6.0 and (d) RCP 8.5 (over 2090-2100 respectively)

Under all RCPs, the strongest increase is projected for Trøndelag, with 10 or more ROS days per winter for both RCPs 4.5 and 6.0 and up to 20 more under RCP 8.5. Under RCP 8.5, ROS could also occur over the northernmost (above 68 °N) inland areas of the Troms og Finnmark county, which currently experiences dry and cold continental winters (Dyrrdal et al., 2013). For this region 1-5 more ROS days are projected per winter season over 2090 – 2100 as compared to 1990 – 2000. The projections of increased ROS events along the western parts of Norway revealed in this research, agree with NCSS (2017), who have also predicted higher precipitation for these regions throughout and until the end of this century.

Figure 4.11 compares the RCPs with the baseline in terms of decadal count for ROS days. The baseline time period 1990-2000 consists of a large number of domain grid boxes where the number of ROS days lie in the range of 0-20. While some areas under the RCPs 4.5 and 6.0 could see a moderate increase in the ROS frequency, a pronounced increase in the ROS day count could occur under RCP 8.5. For example, some areas could experience up to 280 - 340 ROS days over 2090-2100, which is not observed for any other scenario.

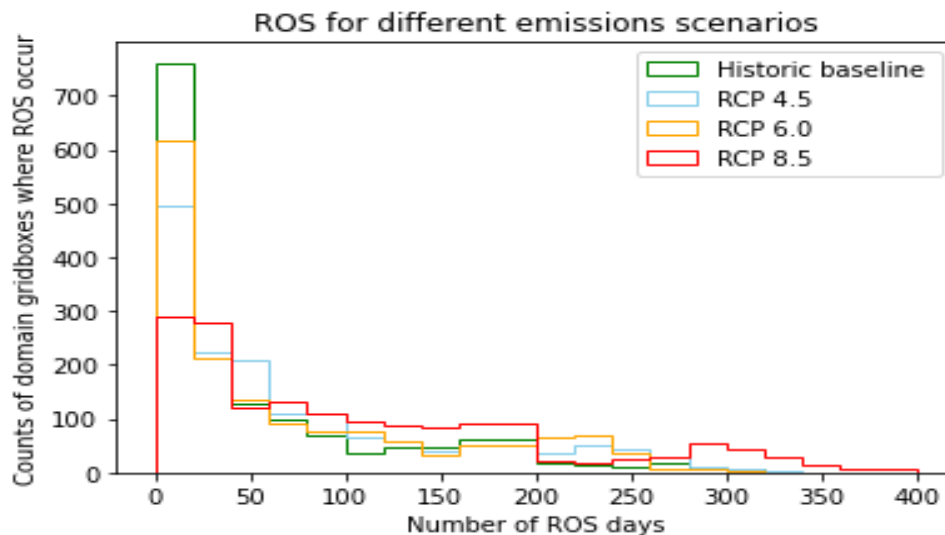


Figure 4.11 A comparison of ROS days for the different scenarios over the time period 2090 – 2100. The counts of model grid boxes with respect to the frequency of ROS. This count represents a general spatio-temporal view of ROS days.

Temperature is the main control for ROS, and upper level circulations are a lesser influence (Rennert et al., 2009). For December and March, under all the RCPs, the change in the mean monthly temperature with regard to the baseline, is above 0°C for the entire study area, and similarly for January albeit for the majority of the study area (Figures 4.14 presented ahead). This means that the mean monthly temperatures in mid and late winter can be above 0°C, explaining the increased probability of ROS in these peak winter months as precipitation would fall as rain.

Seasonal changes in future ROS

Figure 4.12 presents the change in the mean monthly ROS, under RCPs, 4.5, 6.0 and 8.5 during 2090-2100, w.r.t 1990 - 2000. The winter months presented are December, January, February and March. These months are the typical months of ROS in the Arctic, mainly based on the criteria of snow accumulation. For most of the months and study area, an increase of one ROS event per month is projected, under all the RCPs. Specifically, under RCP 4.5, a uniform change for the entire study area, across all the months is projected. It was surprising that, other than a few instances, there was not a major difference between the RCPs. These included the maritime areas of Trøndelag and the Lofoten islands, for the months of January, February and March under both RCPs 6.0 and 8.5. For these instances the ROS days could increase by 2-5 per month w.r.t the mean of these months under the baseline 1990-2000. Table 4.3 presents a summary of the highest changes in mean ROS per month; scenario, winter month and area wise.

Table 4.3 A summary of the mean highest changes in ROS (month and area wise)

Strongest changes in ROS 2090-2100 w.r.t baseline time period 1990-2000		
Scenario	Winter month	Areas
1. RCP 4.5	Equal change in all months	Same change across the study area
2. RCP 6.0	January and February	Maritime Trøndelag and Lofoten islands
3. RCP 8.5	March	Maritime Trøndelag and Lofoten islands

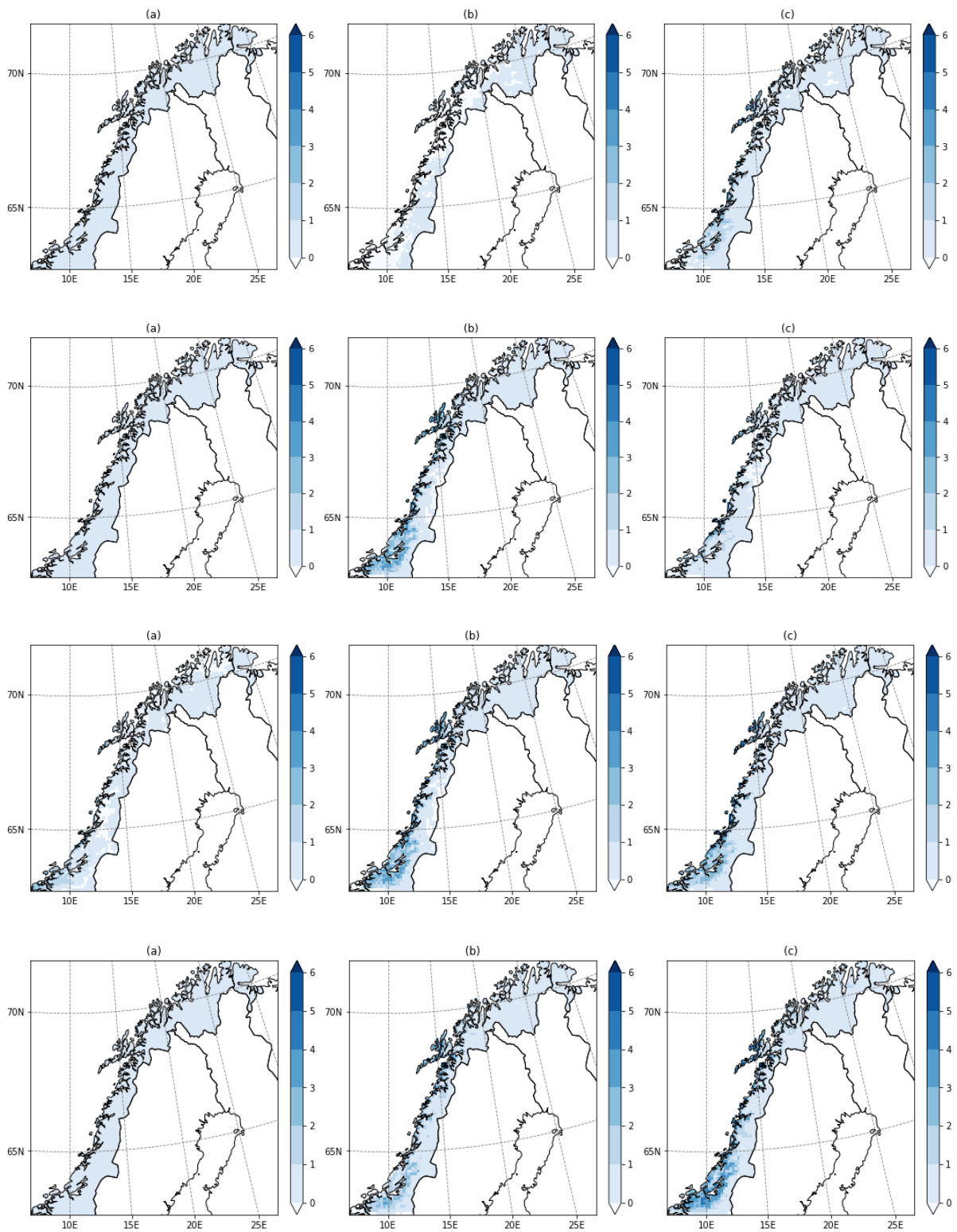


Figure 4.12 Change in the mean monthly ROS, for the months of December, January, February and March (row-wise, top to bottom), under three RCPs, (a) 4.5, (b) 6.0 and (c) 8.5. The change is calculated for 2090 - 2100, w.r.t 1990 - 2000.

4.3.2 Future change in winter meteorological variables under different RCPs

4.3.2.1 Temperature

The mean winter near-surface air temperature is projected to increase under all RCPs for northern Norway. The projected temperature rise is spatially and RCP dependent. However, a pronounced increase for the northernmost and eastern regions of Norway (above 68°N) is a common characteristic across all the RCPs. Figure 4.13 presents the change in the mean winter temperature for 2090 – 2100, under each emission scenario w.r.t the baseline time period.

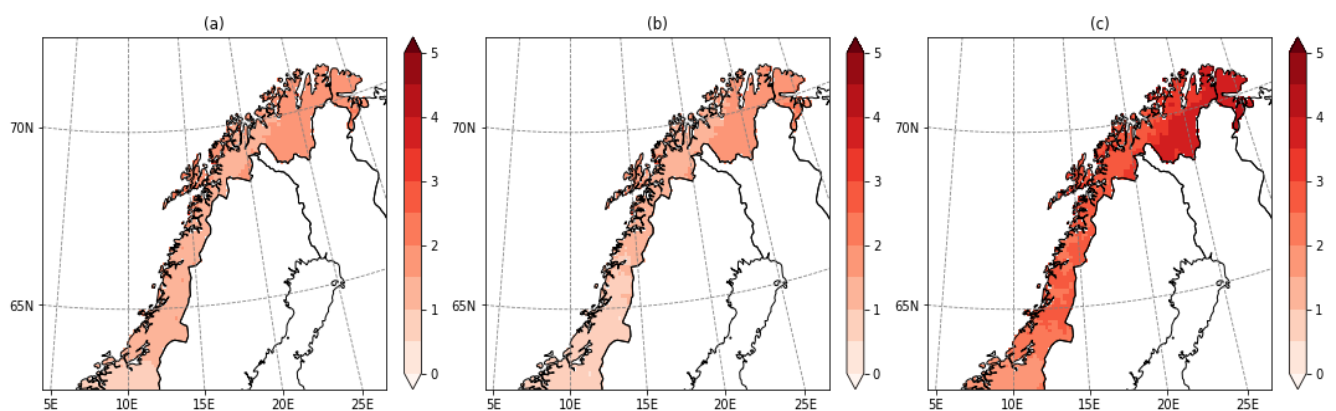


Figure 4.13 Maps showing the change in the mean winter temperature for 2090-2100; (a) RCP 4.5 (b) RCP 6.0 and (c) RCP 8.5. The change was calculated w.r.t the baseline time period 1990-2000.

Under RCPs 4.5 and 6.0 the mean winter temperature rises by 0.5 - 2.5 °C across the study region, whereas it is projected to rise by 2 - 5 °C under RCP 8.5. The strongest increase under the high emission RCP 8.5 is projected for the Lofoten islands and Troms og Finnmark county.

Seasonal changes in future temperature

This section presents the future change in the mean monthly temperature of those winter months with which summer NDVI was found to be significantly negatively correlated in Chapter 3. These months included December, January and March, shown in Figure 4.14. The change for each RCP scenario was calculated w.r.t to the baseline 1990 – 2000.

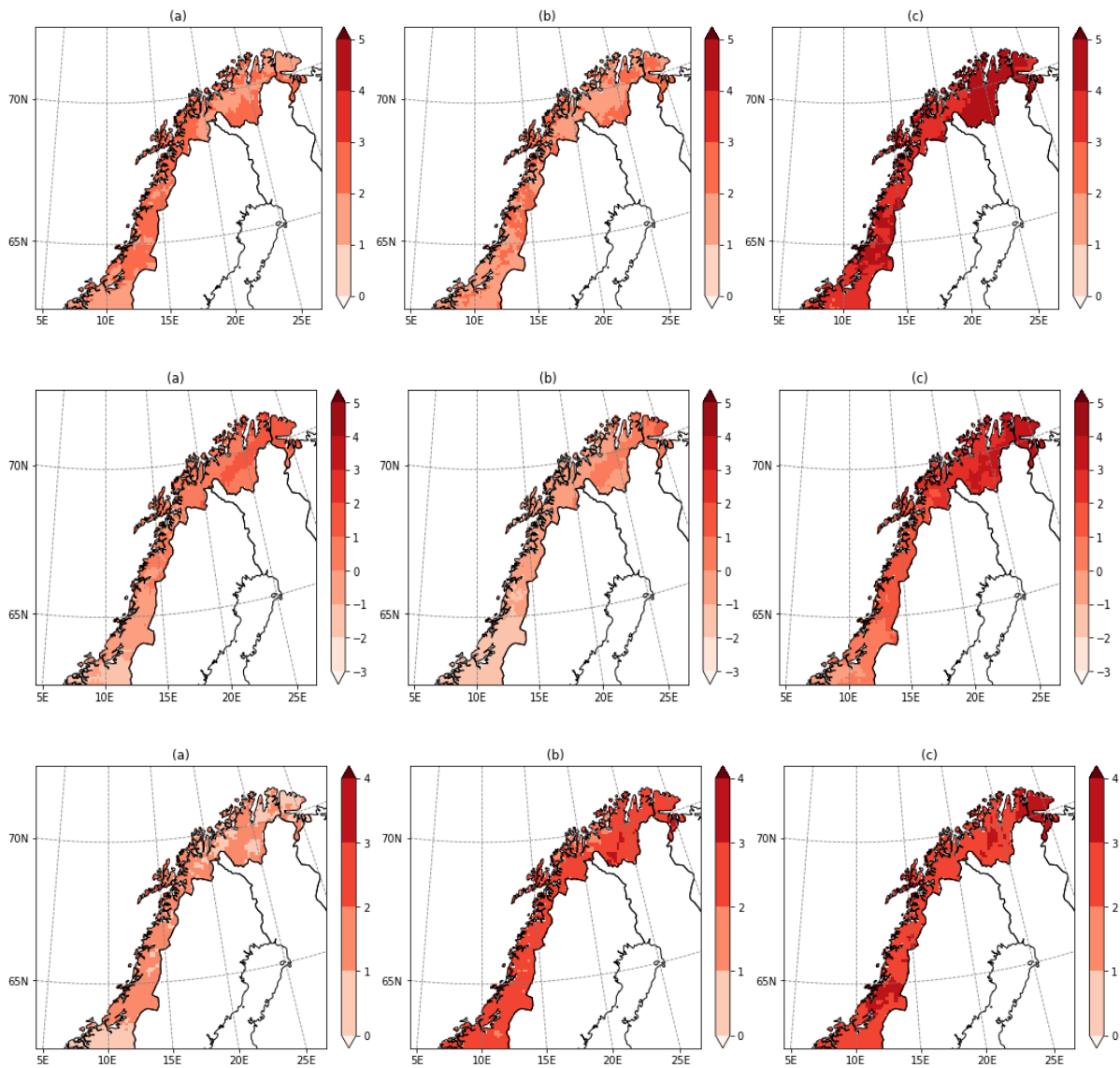


Figure 4.14 Maps showing the change in the mean temperature for the months December, January and March (row wise top to bottom), 2090-2100; under the emissions scenarios (a) RCP 4.5 (b) RCP 6.0 and (c) RCP 8.5. Not the different scale for January.

Examining the change in mean monthly temperature for these months was important because the current warming trends in Norway are generally expected to continue (Dyrdall et al., 2013). The higher the frequency of temperatures staying above 0°C in winter, the higher the possibility of vegetation bud burst and loss of freeze tolerance, which then results in vegetation damage/browning with returning freezing temperatures.

Overall, for the study area, the mean December temperature is projected to be 1-3 °C, 1-3 °C and 3-5 °C higher for RCPs 4.5, 6.0 and 8.5 respectively, as compared to the baseline.

The temperature change is projected to be strongest under RCP 8.5 across the study domain. The change is more pronounced for a few areas of Nordland and for most areas in the northernmost Troms og Finnmark region, above the Arctic Circle. The mean December temperature in these areas could increase by approximately 4-5° C.

In contrast to December, some areas can get colder in January under the RCPs 4.5 and 6.0. The mean January temperature can decrease by 2 - 3 °C in these areas, which are mainly located in the southern Trøndelag county. The results of negative temperature change in January at the end of this century, under RCP 4.5, partly agree with Nilsen et al. (2020). They have also projected a decrease in days with 0° C crossings (DZCs), albeit for the entire western coast of Norway in winter, under RCP 4.5. It is important to note that they project a decrease over December – February (2071 – 2100) compared to 1971 – 2000; whereas this research projects the decrease only for January, in the Trøndelag region, over 2090 – 2100 compared to 1990 – 2000. The difference in these results highlights the significance of selection of a baseline time period. On the other hand, their results of significant increase in DZCs in winter in the Finnmark region, under RCP 8.5, agree with the strong temperature increase projections for the said region under this research. While the variable of interest in this research is mean monthly temperature change, the results of Nilsen et al. (2020) about DZCs are still comparable in a sense that changes in DZCs reflects the magnitude and direction of temperature change

Although this study did not include Svalbard within the WRF simulations, the temperature projections of the northernmost areas of Norway can still be compared with projections of Svalbard. This research's projections of a 1 – 2° C increase in the mean mid-winter (January) temperature over the Troms og Finnmark county, under RCP 4.5, agree with Hansen et al. (2014); who have suggested that if RCP4.5 holds, Svalbard's mean mid-winter temperature could be above 0 °C starting as early as 2050.

As in December, the temperature projections of March showed an increase under all RCPs in this research. The projections were similar for RCPs 6.0 and 8.5. Overall, the study area in March is likely to experience up to 1-2 °C, 2-3 °C and 2-3 °C higher temperatures under RCPs 4.5, 6.0 and 8.5 respectively.

Table 4.4 provides a simple summary of the overall study area’s mean temperature change for different winter months under each RCP.

Table 4.4 A summary of the mean temperature change for various winter months under the RCPs over the study domain

Scenario	Range and median of temperature change (°C)		
	December	January	March
RCP 4.5	1 – 3 (2)	-3 – 2 (-0.5)	0 – 2 (1)
RCP 6.0	1 – 3 (2)	-2 – 1 (-0.5)	2 – 3 (2.5)
RCP 8.5	3 – 5 (4)	-2 – 5 (0.5)	2 – 3 (2.5)

While the future and baseline difference maps show that the mean temperature of the early, mid and late winter months (December, January and March respectively) could be above 0°C (warming), there is an aspect of uncertainty in the context of which winter month could be the warmest. This is because there was variation within the scenarios. March under RCP 6.0 and December under both RCPs 4.5 and 8.5 are projected to be the warmest months.

In terms of spatial patterns, there is little difference between the temperature changes of coastal and inland areas. This is in contrast to NCCS (2017), who have projected a stronger warming for the inland areas for the future time period 2045 and 2085. A pattern was however observed with regards to the north and south. Under the majority of RCP/month combinations, the northern areas (above 65 °N) of Nordland and Troms og Finnmark counties, could see more pronounced warming compared to that in the southern Trøndelag region. These findings agree with NCCS (2017).

Currently the mean annual temperature for the Norwegian mainland is 1.3 °C and continues to experience positive trends since the early 1970s. The strongest increase in temperature has been observed for the Trøndelag and Nordland counties (NCCS, 2017). The WRF projections here showed

that this spatial pattern in the warming trend could change in the future as Troms og Finnmark could be the region with the strongest temperature increase.

4.3.2.2 Snow depth

Seasonal changes in future snow depth

The mean snow depth for the mid-winter months, January and February, and late winter month, March were found to be the most critical for vegetation, based on the detailed analyses of the case study browning events in Chapter 3. Moreover, these are the typical winter months when snow depth is the deepest in Norway (NCCS, 2017). Therefore, these months are the focus for estimating future change in the mean snow depth projections.

Figure 4.15 presents maps of the mean snow depth projections for the mid-winter months, January and February combined, for the baseline time period 1990-2000 and for each RCP scenario 2090-2100.

Figure 4.16 presents the same for the late winter month of March.

The largest changes in the future mid-winter mean snow depth were observed for RCP 8.5. With regards to Arctic vegetation, it is concerning that the mid-winter mean snow depth could be zero for several areas in Trøndelag, under RCP 8.5. Moreover, the mean mid-winter snow depth in the eastern areas of Troms og Finnmark could decrease by 20 cm w.r.t the baseline time period.

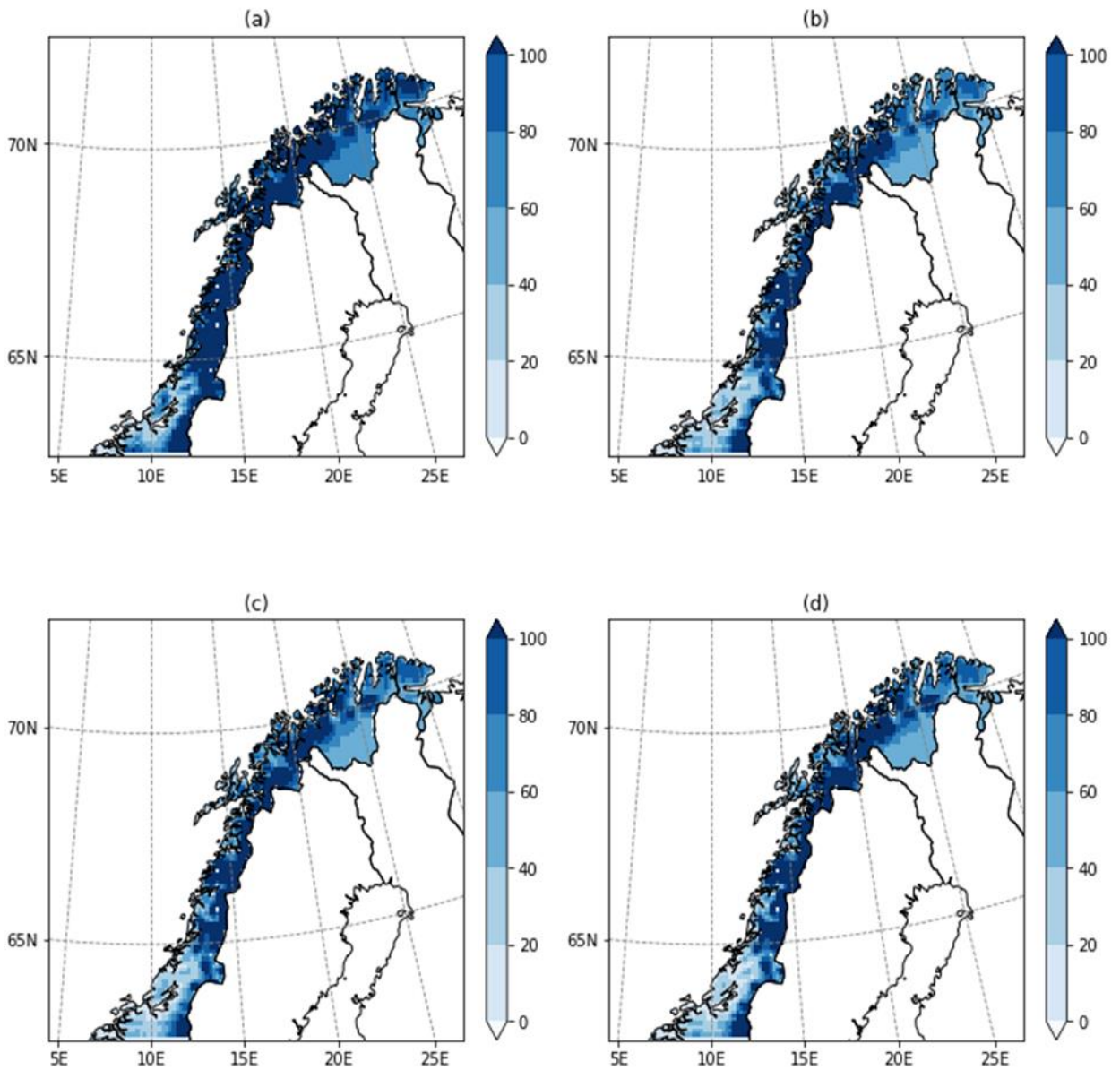


Figure 4.15 Maps of the mean snow depth for the mid-winter months, January and February combined, for (a) baseline time period 1990-2000, (b) RCP 4.5, (c) RCP 6.0 and (d) RCP 8.5

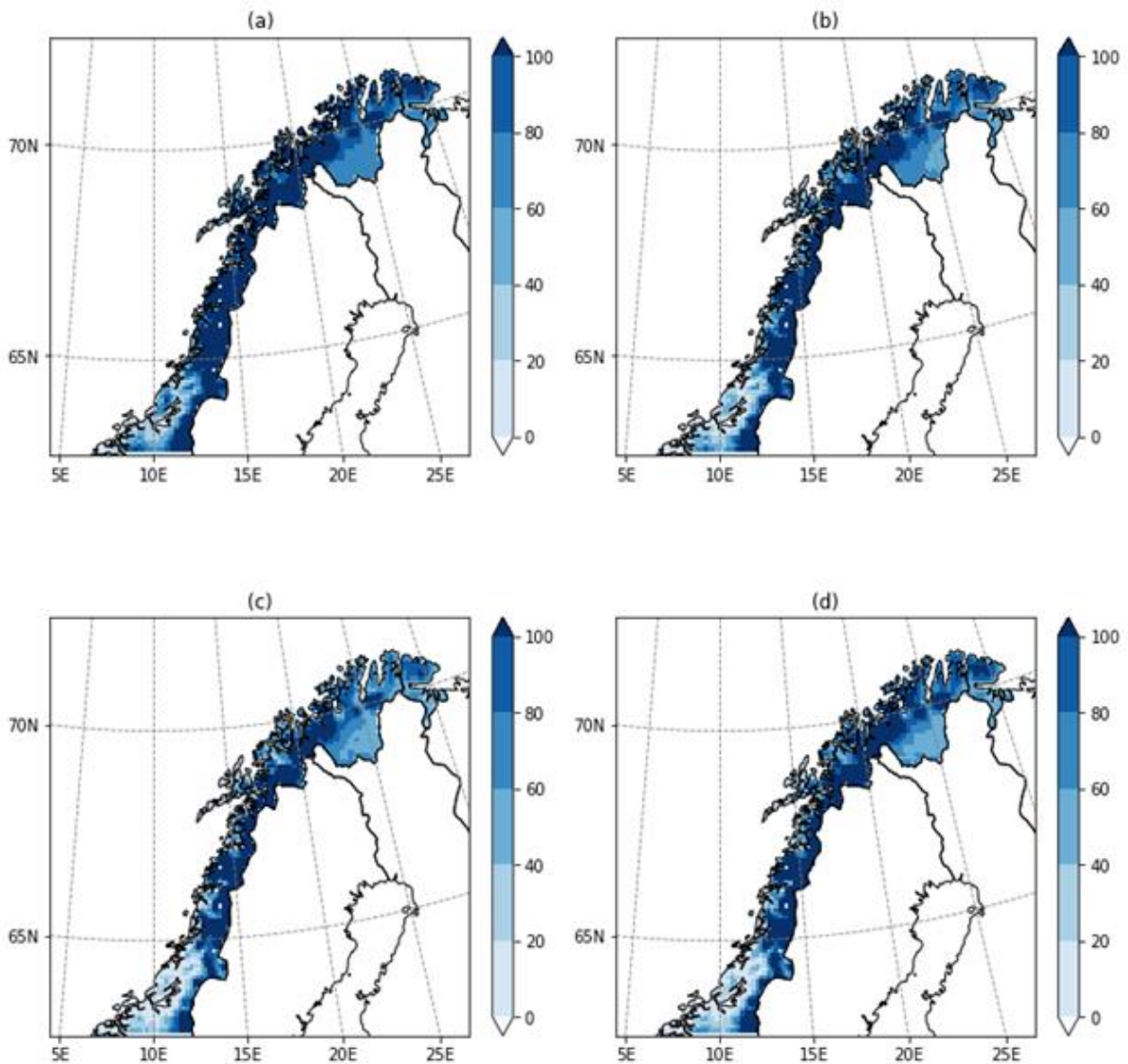


Figure 4.16 Maps of the mean snow depth for the late winter month March, under (a) baseline time period 1990-2000, (b) RCP 4.5, (c) RCP 6.0 and (d) RCP 8.5

In the context of the spatial patterns associated with the change in mean snow depth, overall there was not a major difference between the RCPs. This was true for both mid and late winter stages. The lowest mean snow depth conditions were observed for most of the coastal areas of Trøndelag, and a few coastal areas of Nordland, including the Lofoten Islands. These findings were consistent across the RCPs.

Spatial variability was observed in terms of which winter stage could be the most critical for vegetation to experience lowest mean snow depth conditions. For the southern Trøndelag region, late winter is projected to experience the lowest mean snow depth, whereas for the north-eastern areas above the Arctic Circle this is projected to occur in mid-winter.

4.3.3 Future NDVI-change projections under different RCPs

This section presents the results of future changes in NDVI at each case study site, under the RCPs 4.5, 6.0 and 8.5, respectively, calculated using the regression models outlined in section 3.3.3. The change was calculated for the time period 2090 -2100 w.r.t the 2001 – 2020 baseline NDVI. A positive change reflects greening, whereas a negative change means browning. The statistical relationships between mean summer NDVI and winter metrics for each case study site (in Chapter 3, section 3.3.3) were based on the winter seasons over the time period 2000 – 2020. Given that extreme winter weather events were still rare during this time period, the modelled relationships likely captured gradual greening/browning. Therefore, the projections and the subsequent percentage change calculations of NDVI likely reflect ‘trend browning’ rather than ‘event browning’.

4.3.3.1 Flatanger

The Flatanger study site is predicted to experience a mix of greening and browning, under each RCP scenario, at the end of this century.

The statistically significant model with the highest score ($R^2 = 0.30$, $p < 0.05$) for Flatanger consisted of the MDW index in March (as discussed in chapter 3, section 3.3.3). Therefore, this model was used to predict NDVI at Flatanger, under the different RCPs.

Table 4.5 presents the average of the percentage change in NDVI over 2091-2100 w.r.t the average summer NDVI 2001-2020, under the RCPs 4.5, 6.0 and 8.5. The change in each year is presented in Figure 4.17.

Table 4.5 Mean of the projected percentage change in NDVI at Flatanger, for 2091 – 2100, under different RCPs. The change was calculated w.r.t the average summer NDVI 2001-2020.

RCP	Mean of the projected percentage change in NDVI over 2091 – 2100
4.5	1.52 %
6.0	9.0 %
8.5	57.12 %

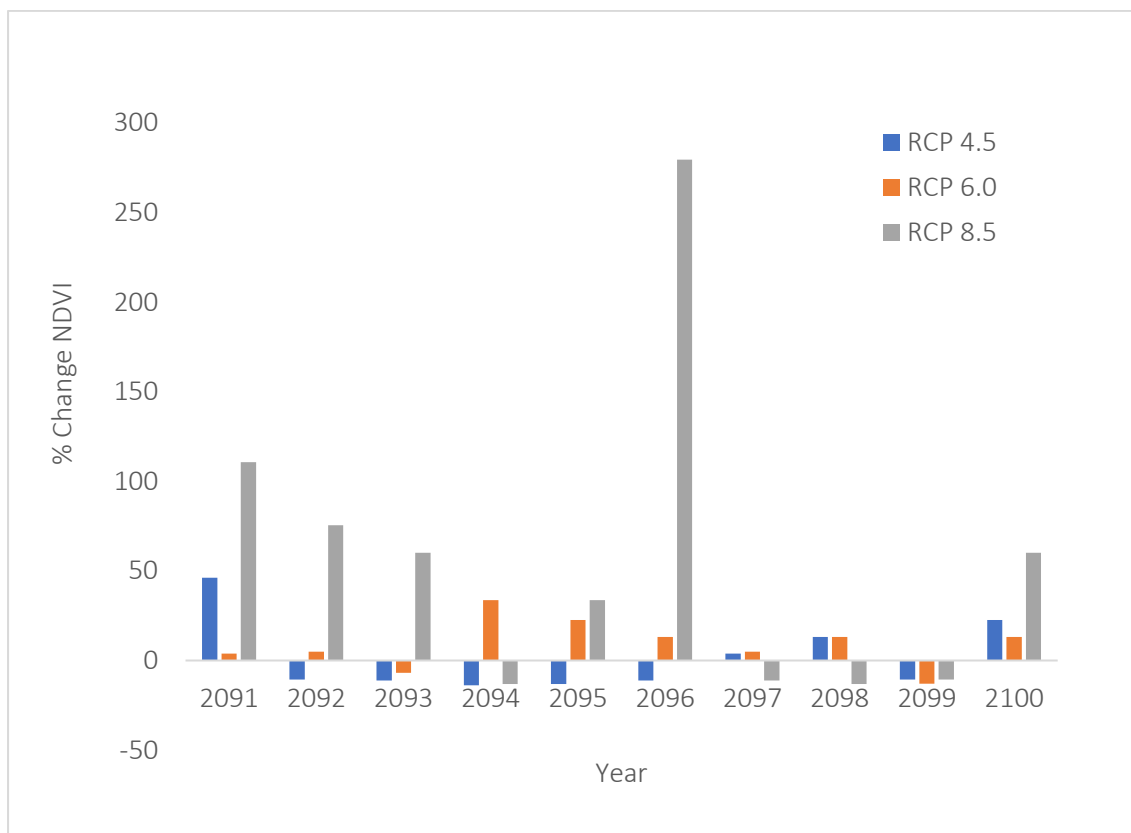


Figure 4.17 Projected change in NDVI at Flatanger for 2090-2100, w.r.t the average NDVI 2001-2020, under different RCPs

The mean percentage change in NDVI over 2091 – 2100 showed greening for the Flatanger study site, under all RCPs. The highest mean percentage greening, 10.3% is projected under RCP 8.5. Under RCP 4.5 the highest percentage change was for the year 2091, for which a 46% increase in the average summer NDVI is predicted. This is a substantial increase in terms of NDVI. Moreover, under RCP 8.5, a 279% increase in the average summer NDVI is predicted for 2096. It is also worth noting that almost all

the greening years are predicted to experience a large increase in NDVI (> 50%). For all the RCPs at the Flatanger study site, the negative percentage changes were < 15. This means that for the years with browning projections, the predicted decrease is not huge.

The strongest increases in the MDW index are projected under RCP 8.5, as presented in section 4.3.1.2. Consequently, the highest positive changes in NDVI at Flatanger, projected w.r.t March MDW, emphasizes that the occurrence of longer warming events towards the end of winter is beneficial for vegetation in this area. The intensity of a warming event is dependent on the duration and temperature of the event (Treharne et al., 2020). In the case of Flatanger, the March MDW index represents the intensity of the longest lasting warming event in March in terms of its duration and a 2° C temperature threshold. It would have been interesting to examine the NDVI projections based on the MDW index in early and peak winter months, such as December and January, in order to further understand the distinct relationships between various stages of winter meteorology and summer NDVI. However, the lack of statistically significant relationships, based on the historic observations (as discussed in section 3.3.3), limited the NDVI projections only to March MDW.

4.3.3.2 Lofoten

Greening was the major projected change in vegetation at the Lofoten study site under all RCP scenarios for the end of this century. For this site, the December SC20 index explained the highest variance ($R^2 = 0.46$, $p < 0.05$) in the subsequent summer NDVI (As discussed in Chapter 3, Section 3.3.3).

Table 4.6 presents the mean of the projected percentage change in both NDVI and December SC20 (2090 – 2100) w.r.t their averages over 2000 – 2020, at the Lofoten study site, under the RCPs 4.5, 6.0 and 8.5. A positive percentage change in each year over 2090-2100, under all the RCPs, is projected as well (Figure 4.18). It was worth noting that the change in NDVI for all instances was small (< 10%), except 2095 under RCP 8.5; for which the highest change, a 47% increase in the average summer NDVI is predicted.

Table 4.6 Mean of the projected change in NDVI and December SC20 at the Lofoten study site, under different RCPs.

RCP	Mean of the projected percent change in NDVI over 2091 – 2100	Mean of the projected percent change in December SC20 over 2090 – 2099
4.5	5.0 %	41 %
6.0	4.7 %	16.8 %
8.5	10.3 %	72.6 %

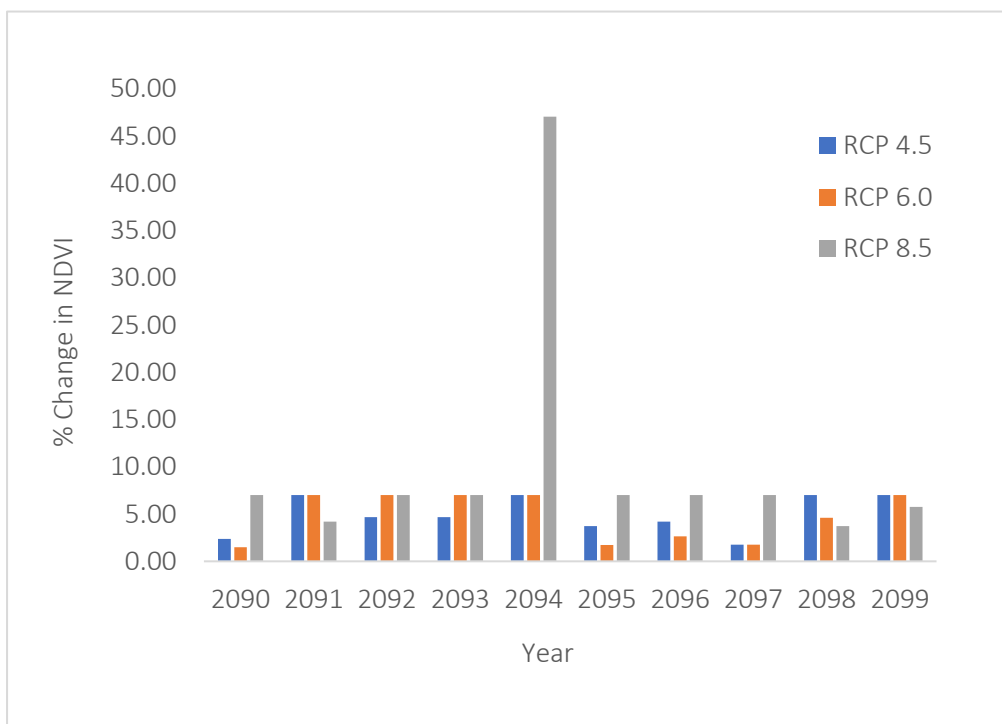


Figure 4.18 Projected change in NDVI at Lofoten for 2090-2100, w.r.t the average NDVI 2001-2020, under different RCPs

The results here highlight the complexity of understanding non-linear relationships between environmental controls and vegetation productivity in the physical world. For an explanation of the projected greening at Lofoten under all RCP scenarios, a closer look at the correlation analysis in Section 3.3.2.4 revealed that the relationship between December SC20 and average summer NDVI is largely positive across the islands. However, the correlation was significant only at a few domain grid boxes ($p < 0.01$). The absence of statistically strong correlations across majority of the grid boxes, representing

the Lofoten islands, is likely due to the non-linear nature of the relationship at those locations. It is also worth remembering here that during previous browning events, such as discussed in section 3.3.1.2, damage to vegetation resulted from low snow conditions accompanied by exposure to freezing temperatures (frost drought). The NDVI projections for Lofoten study site here are based on December SC20 independently due to reasons of model statistical significance. Therefore, the greening projections here, based solely on the December SC20 index, are statistically sound, bearing in mind the correlation results of section 3.3.2.4. It is also worth remembering that the December SC20 index explained 46% variance in the mean summer NDVI, while the rest is unexplained.

4.3.3.3 Storfjord

Browning is projected to be the major future vegetation change at the Storfjord study site under the three RCP scenarios considered here. For Storfjord, the December MDW index and mean January near-surface temperature, together better explained the variation in the subsequent summer NDVI ($R^2 = 0.38$, $p < 0.05$) (As discussed in Chapter 3, Section 3.3.3.3).

Table 4.7 presents the mean percentage change in NDVI, December MDW and mean January temperature over 2090 – 2100, w.r.t their averages over 2000 – 2020, at the Storfjord study site. The changes are presented for RCPs 4.5, 6.0 and 8.5. Figure 4.19 presents the projected change in NDVI over 2091 – 2100.

Table 4.7 Mean of the projected change in NDVI, December MDW and January mean surface temperature at Storfjord study site, under different RCPs.

RCP	Mean of the projected percent change in NDVI over 2091 – 2100	Mean of the projected percent change in December MDW over 2090 – 2099	Mean of the projected percent change in mean January temperature over 2091 – 2100
4.5	-11.2 %	40 %	17.2 %
6.0	-7.5 %	200 %	29 %
8.5	-5%	50 %	-9.5 %

Under both RCPs 4.5 and 6.0, the majority of the growing seasons across 2091 – 2100 are projected to see a decrease in the average NDVI. It was worth noting that under RCP 4.5 for the two years with projected greening, the increase was quite low, 0.68% and 1.84%. Similar to RCP 4.5 and 6.0, browning is projected to dominate under RCP 8.5 at the Storfjord site. However, the decrease in NDVI under RCP 8.5 were smaller overall. The largest change was a 14% decrease observed for the year 2095. Similar to RCP 4.5, where greening is projected it is not very high, i.e., 3.6% and 5.9%.

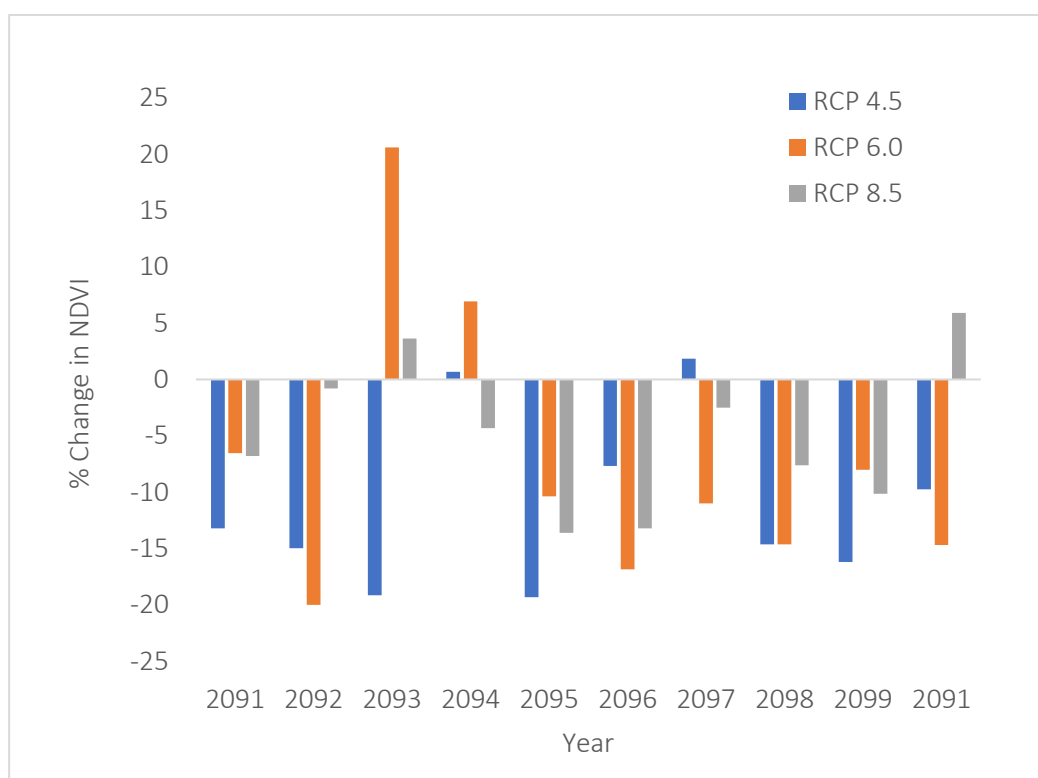


Figure 4.19 Projected change in NDVI at the Storfjord study site for 2090-2100, w.r.t the average NDVI 2001-2020, under different RCPs

Browning (negative change) is projected as the mean change in NDVI at the Storfjord study site at the end of this century, under the three RCPs considered here.

The December MDW index represents the duration (number of days) of the longest winter warming event per December and in that sense also measures the intensity of the warming event. For the Storfjord site, the December MDW index is projected to increase for the majority of the years over 2090 – 2100 (Section 4.6, Appendix 2). The mean January temperature (Section 4.6, Appendix 3) is projected

to increase for almost all years under the RCPs 4.5 and 6.0. In contrast, it is projected to decrease for the majority of the years under RCP 8.5.

The correlation analysis (Chapter 3, section 3.3.2) is referred to better understand how the projected changes in the December MDW and January mean temperature relate with the changes in the future NDVI at Storfjord. The NDVI was negatively correlated with both December MDW ($r = -0.6 - -0.8$) (Figure 3.23 (a)) and mean January temperature ($r = 0 - -0.2$) (Figure 4.20, Appendix 4.4); however statistically significant ($p < 0.05$) only for the former. The December MDW had a relatively stronger relationship with the NDVI as well. Therefore, it is likely that the duration of the warming event plays a larger role in the evolution of summer NDVI at this site, compared to the mean January temperature. Since these two variables together explained less than 50% of the variation in NDVI, it implies that a larger role is played by other environmental and meteorological variable/s. Treharne (2018) studied the relationships of both plot-scale NDVI and MODIS NDVI with the different winter metrics and have indicated that regional scale NDVI (in terms of detection of browning) is influenced by a wide range of ecological processes.

It was interesting that an increase in the December MDW index at Storfjord at the end of this century under all RCPs, resulted in browning projections for the site, whereas an increase in the March MDW at Flatanger drove greening projections at this site. These differences highlight the role of the timing of event occurrence during winter as well as spatial variability, when it comes to ecological impacts of extreme weather events.

In summary for all the sites presented above, a variation was observed in terms of the projected vegetation changes in response to the different meteorological drivers. Table 4.8 presents a simple summary of the overall vegetation change at the case study sites under each scenario.

Table 4.8 A simple summary of the NDVI change for each case study site, under each RCP scenario

Study site	Scenario	Greening / Browning
1. Flatanger	RCP 4.5	G
	RCP 6.0	G
	RCP 8.5	G
2. Lofoten	RCP 4.5	G
	RCP 6.0	G
	RCP 8.5	G
3. Storfjord	RCP 4.5	B
	RCP 6.0	B
	RCP 8.5	B

In the context of NDVI projections under different climate change scenarios, Lara et al. (2018) was the only study found (explained in Chapter 1, Section 1.5). In the absolute sense, it is not most suitable to compare the results of this PhD research with the aforementioned study due to several differences such as the study area, time period of projections and the difference in the seasonal range of the climate datasets. However, a few commonalities and the drivers of the decline in NDVI are still comparable. The projections of the potential drivers of Arctic Browning in this research showed marked spatial variability across the Norwegian Arctic and sub-Arctic areas, with highest increases along the

coastal regions. These findings agree with Lara et al. (2018) in that their browning trends were most pronounced along the Chukchi coast.

It was interesting that while RCP 8.5 consisted of the overall largest increases in the drivers of vegetation decline, this did not necessarily translate into the largest browning at the case study sites. For example, the browning at the Storfjord site was slightly weaker under RCP 8.5 as compared to RCP 4.5. These findings are similar in nature to Lara et al. (2018). Their NDVI projections for 2020-29 presented a mixed picture w.r.t the emission scenario - browning dynamics. This means that based on some model outputs, RCP 4.5 consisted of stronger browning trends than RCP 8.5. Moreover, Lara et al. (2018) found increased temperature and rainfall to be significantly related with browning trends. While mean January temperature and the temperature-based MDW index best explained the variance at Storfjord and Flatanger sites respectively, rainfall was not a statistically important parameter in explaining the browning in this research.

Lara et al. (2018) have not considered the role of winter/spring snow depth in determining the Alaskan Tundra vegetation productivity trends; this research provides evidence of statistically significant relationships between winter low snow depth conditions and summer NDVI over Norwegian Arctic areas. For example, at the Lofoten study site, the December SC20 metric explained 46% of the variation in NDVI (at $p < 0.05$).

4.4 Discussion

4.4.1 Extreme winter weather conditions under different RCPs

The Arctic is now warming three times greater compared to the world (AMAP, 2021). However, winter warming events in the Arctic region are not unprecedented (Bokhorst et al., 2009). The North Pole experiences 10 warming events per winter (Graham et al., 2017). What is concerning is that the trends in these events are getting stronger based on higher frequency, intensity and longer-duration events (AMAP, 2021). Based on the results of this research as well, an increase is projected in the duration, frequency and spatial extent of winter warming events for the Norwegian Arctic and sub-Arctic regions, at the end of this century under all three RCPs studied here. The strongest rise is projected for the coastal areas under RCP 8.5.

What is quite concerning is that the coastal areas generally have higher vegetation productivity as compared to the inland areas in Norway. Therefore, a stronger increase in the frequency of extreme warming events in these areas imply higher cumulative disturbance and damage to the overall vegetation productivity in Norway and subsequently in the Arctic region. However, the relationship between winter warming events and NDVI is not straightforward to quantify across the study domain. This is because in the case of Flatanger an increase in the duration of the longest lasting warming event, towards the end of winter, was a driver of greening projections, under all RCPs, at the end of this century. This is a caveat to previous work regarding damaging impacts of higher intensity winter warming events.

In the context of the relative importance of the different meteorological conditions of different winter months in affecting the growing season NDVI, the results of this research have shown large spatial variability across northern Norway. This is stated based on the largest projected changes in climatic drivers of browning occurring in different months in different regions of the study domain. Overall, on the average it is suggested that changes in the mid to late winter, December – March, extreme weather

conditions are the most important to consider when studying future NDVI trends in Norwegian Arctic and boreal areas.

It is interesting to note that although the highest rise in the mean winter temperatures is projected to occur over the northernmost eastern areas, the strongest increase in the mean winter warming event frequency and duration is predicted for the southern maritime areas of Trøndelag. Such differences in the trends of mean temperature compared to a temperature-based index representing an extreme weather event, highlights the underlying complexity of vegetation damage associated with changes in the regional meteorology. What is meant by this is that the potential impacts on vegetation arising from an increase in mean winter temperatures could be different as compared to those arising from an increase in the longevity of short and sporadic extreme temperature conditions. Moreover, the level and type of vegetation damage arising from these (stress, damage, mortality) would likely vary depending on the plant species.

The results of changes in the WWE, WMD and mean temperature under the three RCPs studied here, have demonstrated that the largest changes in the future w.r.t the baseline are for the mean temperature and in the north-eastern parts of Troms og Finnmark, north of the Arctic Circle. Based on these results it is quite likely that the mean temperature of winter months would play a comparatively higher role than the winter warming events in determining the future browning in the north-eastern parts of Norway.

The projections of mean temperature staying above 0° C in majority of the winter months, under this chapter, broadly agree with Nilsen et al. (2021). Their study used an ensemble of ten different RCMs. Despite different RCMs, the similar results of winter temperatures crossing the 0° C threshold in various areas of Norway, increases the robustness of the warming projections. Although temperature fluctuations around 0° C might not cause browning events as such, it causes damage to plant roots (Kreyling and Henry, 2011) and fruit trees in spring (Rigby and Porporato, 2008).

Flatanger, which was one of the browning event case-study sites in previous chapters, is located in the maritime region of Trøndelag. This area was the most productive vegetation site amongst the case study sites. Low snow depth conditions at this site in January – March 2014 winter was one of the meteorological drivers which caused the vegetation browning event during the 2014 growing season.

The SC20 maps (Figure 4.8) show that on average during the 1990-2000 baseline period, most of the coastal areas in Trøndelag experienced 20-40 days where snow depth < 20 cm. Whereas these areas can experience approximately 60 to above 100 such days per winter under the RCPs 6.0 and 8.5. Moreover, as compared to the baseline, under RCP 8.5, the SC20 index could double for the lower elevation areas in the north-eastern county of Troms og Finnmark. The region with the least change in all three measures of snow depth is projected to be the Scandinavian Mountains in the Nordland region. The projections in this research about the comparative increase in low depth conditions, along most of Norway's coast as compared to the inland areas, agree with NCCS (2017).

The results of this research have also showed that low and/or absent snow cover and snow melt after an initial snow cover time period, were common characteristics across the browning-events case study sites. The SC10 and SC20 indices represent low snow conditions w.r.t vegetation in the Arctic. Although the importance of snow depth thresholds, w.r.t vegetation exposure to either warming events or severe freezing temperatures, vary species-wise. However, on a general basis a snow depth < 20 cm is detrimental to many species of Arctic vegetation. Therefore, such a strong increase in the SC20 index could mean increased exposure to winter warming events, especially at the lower altitudes.

The impacts of low snow depth conditions and consequent cold exposure are discussed with regards to the real browning event at Storfjord in 2012 (Chapter 3, Section 3.3.1.2). In contrast to this, the projections of increased December SC20 index (which means higher number of days with low-snow conditions) at the end of this century under all RCPs, resulted in greening projections at this site. The different findings under Chapter 3 and this chapter, highlight the significance of the cumulative effects

of different meteorological conditions, such as low snow depth conditions accompanied by freezing conditions, on vegetation as compared to only low snow conditions.

In the context of future ROS projections in the Arctic, studies exist on rainfall projections e.g. Bintanja and Andry (2017) and McCrystall et al. (2021). However only two studies, Hansen et al. (2014) and Rennert et al. (2009), assess future ROS occurrence. The former have qualitatively commented on the future occurrence of ROS under RCP 4.5, based on projected above-zero temperature changes only. The research in this thesis is the first to provide quantitative and winter monthly-based projections about future ROS frequency, while considering all three meteorological parameters relevant to ROS events, which are snow depth, rainfall and temperature. These projections are the first for the Norwegian Arctic and sub-Arctic regions, and under three different RCP scenarios.

Based on WRF's projections in this research, ROS is projected to increase throughout the Norwegian coastal region over the 2090-2100 time period. The study of Rennert et al. (2009) although focused on a different time period in the future, 2040-59, have predicted decrease in ROS for the Norwegian coastline, under the IPCC's A1B scenario (For details of this scenario refer to Meehl et al. (2006)). The projected decrease in ROS in their study arises from a reduced snowpack rather than reductions in rainfall. It is worth noting that ROS has been calculated via different parameters across studies. For example, (i) using snow depth or snow water equivalent (SWE) as a measure of the snow; (ii) using model generated rainfall or a temperature threshold to separate precipitation into rainfall and snow during post processing of model output, etc. It would have been interesting to compare the results of SWE-derived ROS with snow depth-derived ROS. However, it was beyond the time limitations of this research. Moreover, the ROS projections here were based on a single GCM (CESM1) and a single RCM (WRF). It is recommended that ensembles of different models should be utilised to increase the robustness of ROS projections since ROS events are inherently complex due to the number of variables involved, in particular the rainfall-snow distinction by NWP models.

Temperature projections of RCMs are generally more reliable compared to precipitation (Heikkilä et al., 2011). The frequency of ROS events in the Arctic has been found to be more strongly linked with temperature than the upper-level circulation (Rennert et al., 2009; Pall et al., 2019). The mean temperature of December, January and March under the three RCPs studied here, is projected to stay above 0 °C across most of the study domain. These warm temperature projections imply an increased frequency of ROS since the likelihood of crossing the temperature threshold above which the precipitation falls as rain rather than snow increases. The mean annual precipitation for mainland Norway was 1600 mm based on the 1971 - 2000 time period (NCCS, 2017). Currently 30% of the total precipitation falls as snow in Norway (Dyrrdall et al., 2013). There are uncertainties related to the fraction of total precipitation that would continue to fall as snow in the future. An important factor in estimating the ROS is the temperature threshold above which precipitation falls as rain, rather than snow. This research used a 1.5 °C threshold. Since the WRF baseline simulations showed a cold bias (as discussed in the previous chapter), it is most likely that the future simulations would also consist of a cold bias. That implies that the rainfall - snow threshold would have caused an underestimation of ROS here. It is recommended that future research related to ROS projections should use ensembles of different models to assess the uncertainty arising from the rain-snow temperature threshold. A systematic comparison of the driving GCM and WRF with meteorological station observations could have helped to understand the source of the cold bias in the WRF simulations in this research. However, such analyses could not be conducted here firstly due to the time limitations and second because the focus of this research was to assess climate change and browning linkages, rather than assessing the performance of WRF and the driving GCM.

Despite the limited number of significant correlations between NDVI and ROS due to various factors, (as discussed in chapter 3), it is an established understanding that ROS causes severe vegetation damage in the Arctic (Bjerke et al., 2014). Therefore, it is important to know which types of vegetation are at the highest risk of getting damaged due to an increase in ROS. The highest ROS projections under all the RCPs within this research, were observed to be for the coastal areas of Trøndelag, located south

of the Arctic Circle. Based on vegetation classification (Solberg et al., 2008), currently the common vegetation areas in this region consist of bilberry birch forest, mid alpine ridge, scant vegetation areas, tall and low herb forests.

4.4.2 Future climate change and Arctic Browning

Initially one of the hypotheses in this PhD research was that Arctic Browning can be described in terms of a threshold-based definition. For example, if the NDVI decreased by a certain percentage as compared to a 10 or 20 year NDVI average, it means a browning event has occurred. However, because the average NDVI of each site was different, due to various factors such as the differences in vegetation types, local geomorphology, CO₂ concentrations (Piedallu et al., 2019), meant that a single/general threshold could not be defined against which to measure a possible browning-year NDVI decline.

The aim of this chapter was to analyse how frequent and intense the climatic drivers of Arctic browning could become at the end of this century. Prediction of Arctic Browning in response to changes in the climatic drivers at the end of this century was a complex process. It is important to note here that browning is not a physical quantity in itself. For the purposes of this research, it was considered as both a sudden/sharp decrease or gradual reduction in satellite NDVI. Therefore, this implies NDVI projections need to be compared with a baseline NDVI to measure the percentage change and thus conclude whether vegetation at a given location is greening or browning in the future. Ideally this required RCP-based WRF future simulations on an annual basis i.e., covering all months of a year because growing season NDVI is essentially affected by both, the preceding winter and on-going growing season (typically June-September in the Arctic). The future RCP-based WRF simulations in this research consisted of the winter season i.e., November - April, owing to time and HPC resource limitations. Hence the NDVI projections here were based on winter meteorology-NDVI relationships, which were sufficiently strong that they can be used as predictors for NDVI in the subsequent growing season.

In the context of NDVI changes at the case study sites the future greening/browning projections varied; first temporally over the years 2090 – 2100, second RCP-wise and third spatially, according to the study

site. The mechanisms underlying the projected vegetation productivity changes are not clear in all instances. An important point in the case of Storfjord site's NDVI predictors is that while December MDW and mean January temperature together explained the highest variance in NDVI, these predictors also occur in succession; which implies a higher potential for recurring vegetation disturbance at the study site and the surrounding vegetated areas (Bokhorst et al., 2012). Current knowledge about impacts of multiple extreme weather events on vegetation productivity in the Arctic is fairly limited. However, there is evidence of higher, more pronounced vegetation damage, such as extensive shoot mortality, resulting from multiple winter warming events as compared to altered timings of flowering and berry production resulting from a single warming event (Bokhorst et al., 2009). These impacts were observed for similar vegetation composition and latitude as at Storfjord (Ibid).

The possibility of browning drivers such as December MDW and January temperature fluctuations, occurring as a series of events in the future at Storfjord is similar to the meteorological patterns observed at the Lofoten study site during December - March 2013/14 (discussed in detail in chapter 3, section 3.3.1.3). The recurring warm temperatures, ranging from 0 – 5 °C, with intermittent return to freezing temperatures (-5.0 to -7.5 °C) in between, led to vegetation browning at Lofoten. Measurements of Gross Primary Productivity (GPP) of vegetation at the study site, two years after the reported browning event, still showed a 37% reduction in GPP as compared to undamaged surrounding vegetation (field observations in 2016, Treharne, 2018). This means that if the GPP measurements had been carried out in 2014, it is most likely that the GPP decrease would be larger. On the other hand, the MODIS NDVI (250m spatial resolution) at the site showed only a 10% decrease in 2014's early season NDVI (w.r.t 2001-2019 early season NDVI) (Chapter 2 of this thesis). The challenges of satellite vs field browning observations have been discussed in detail in chapter 2. The main point here is that with major browning changes predicted in NDVI for the Storfjord site arising from a possible cascade of events in the months of December and January 2090-2100, the 10-20% reductions in NDVI could translate into quite a high decrease in vegetation GPP on the ground.

Net ecosystem CO₂ exchange (NEE600) is a key indicator of ecosystem carbon balance (Heliasz et al., 2011). Mean NEE600 has been shown to decrease by 50% in the growing season in stressed vegetation in the aftermath of extreme winter weather events in the Arctic (Treharne et al., 2019). Such level of reduction in the NEE600 is reflective of major impacts on the carbon sequestration capacity of an ecosystem on a plot scale (Ibid). Based on the findings of Treharne et al. this research's projections of a combined increase in the frequency and intensity of winter warming events, frequency of rain-on-snow days and low snow conditions for the Trøndelag, Lofoten islands and the coastal areas, especially under RCP 8.5, is quite concerning. Even if browning events (physical damage to vegetation) do not occur, repeated stress in vegetation can lead to major reductions in NEE. It is important to remember however that the indices of extreme winter events showed contrasting relationships at the study sites in this PhD research. Therefore, more research is required in terms of assessing the role of spatial variability in quantifying and projecting browning impacts on ecosystems.

Until recently, the majority of ecosystem and earth system models predict vegetation productivity to increase in northern latitudes, as summer temperatures continue to rise. However, based on this research's projections related to an increased frequency and spatial extent of winter warming events, ROS, frost drought and above-zero mid-winter temperatures in Norway, especially if the world enters an RCP 8.5 scenario, it is predicted that vegetation in the Norwegian Arctic and sub-Arctic areas will be hugely exposed to winter disturbance. The level of damage resulting from the repeated exposure of vegetation to these various events on a decadal scale still needs to be statistically examined and is suggested as a priority future research. However, based on previous field-based evidence of vegetation exposure to consecutive events (Bokhorst et al., 2009), that the carbon balance of the Arctic ecosystems could be significantly disrupted.

It is important to note here that while this research has conducted projections of future changes in winter meteorological parameters and extreme weather events, it does not consider changes that could occur in the vegetation distribution, abundance and composition, over Norway by the end of this

century as a result of climate change. The analysis here was conducted based on the current vegetation distribution in Norway. Major bio-geographical shifts in species distribution of Arctic vegetation have been predicted in response to a changing climate. For example, several high-latitude vascular plant species are predicted to occupy higher slopes over the 2070-2099 time period, in order to continue their current range (Niskanen et al., 2019). Moreover, various shrubs and grasses are projected to become more productive as a result of the CO₂ fertilisation effect, under both RCPs 2.5 and 8.5 (Gustafson et al., 2021). However, projections of changes in plant species distribution and abundance are highly uncertain and interestingly, Scandinavia is currently exhibiting resistance to drastic vegetation changes. Nevertheless, it is still important to assess whether an increased frequency of extreme winter weather events such as ROS and frost drought can affect vegetation distribution changes in the Arctic. Consequently, knowledge of the aforementioned factors would increase the robustness of studies related to the role of extreme weather events in vegetation productivity, such as this PhD research.

It is worth remembering that the susceptibility of vegetation to different durations of winter warming events is highly species-dependent. While it was beyond the scope of this research to project the browning trends for different vegetation types over the 2090-2100 time period, the projections related to the extreme winter weather events generated through this research can be utilised to spatially relate/correspond the vegetation types most at risk by linking the dominant vegetation types in areas such as the coastal maritime region of Trøndelag which is projected to experience the highest frequency of winter warming events.

In the context of future research related to Arctic browning, and to increase the accuracy of NDVI projections, it is strongly proposed to incorporate the complex interactions between meteorological parameters and other important environmental controls of NDVI. For example, soil water availability, geomorphology type, elevation, dominant vegetation type should be considered along with the meteorological variables examined in this research, such as temperature, rainfall and snow depth.

Factors such as projected changes in the landform and soil characteristics arising from permafrost thawing should also be considered while predicting NDVI. This is suggested because research in the Alaskan coastal tundra has provided evidence of browning trends linked with the combined effects of geomorphic types, and, both changes and anomalies of temperature and precipitation (Lara et al., 2018).

The projections of greening/browning in this research should be interpreted with some caution, owing to the large uncertainties related to both climate change and vegetation's response to climate change. For example, how are the drivers of browning going to change between the analysis time period of this research and 2090. Could repeated exposure to extreme winter weather events between now and 2090 cause enhanced adaptation responses in Arctic vegetation to browning events, by 2090? What are the possible recovery ways and trends of Arctic vegetation to the potential damage occurring between now and 2090?

Although the study area in this research was focused on the Norwegian Arctic and boreal areas, it serves as a baseline for conceptual frameworks of future studies in the area of Arctic climate change - vegetation modelling. This research provides essential information on issues such as scale mismatch between climate model and satellite datasets, complexities of quantifying extreme weather events from climate model output in a way that statistically meaningful relationships could be developed to predict future impacts of such events on vegetation in the Arctic.

This work also provides the potential for in-depth insights into Norway's future climate, based on high-resolution regional climate change simulations. In this sense the relevance of this work goes beyond the Arctic ecological discipline. The meteorological projections generated here about ROS and winter warming events can be useful for a wide range of socio-economic sectors such as the indigenous Sámi reindeer herders and the snow-based tourism industry.

4.5 Conclusions

This research provides the first detailed assessment of the role of extreme winter weather events on Arctic Browning for the end of this century, under different climate change scenarios. The findings of this work can be viewed in a threefold-perspective; spatial context, seasonal winter meteorology and climate change scenarios based.

In the spatial context the main findings included; the vegetation most at risk of damage is predicted to be in Trøndelag based on a cumulative increase in projections of all the drivers of browning studied in this work. Another key finding from the projections obtained in this research about increased exposure of Norway's coastal areas to higher intensity warming events (duration-based), as compared to the inland regions, agrees with previous studies.

In the context of emission scenarios, the most drastic changes at the end of this century, w.r.t to the 1990 – 2000, are projected under RCP 8.5. These include the strongest increases in the average duration and frequency of warming events, and frequency of low snow depth (< 20 cm) conditions. Moreover, under this scenario a few ROS days are projected to occur in the northernmost areas of Troms og Finnmark, which currently experiences snowfall as the main form of winter precipitation. An index representing frost drought conditions was explored as a case study under RCP 8.5, and more research is recommended to examine the effectiveness of this index with regards to dwarf Arctic vegetation.

With regards to the seasonal scale changes in winter meteorology which could affect vegetation productivity, the strongest changes in ROS and frost drought conditions are projected for March under RCP 8.5. On the other hand, December is projected to experience the highest temperature changes under RCP 8.5; with mean December temperature rising by 4-5^o C in some areas north of the Arctic Circle, at the end of this century compared with 1990 – 2000.

The projections of strong browning at one of the case study sites, located well inside the Arctic Circle, are reflective of the pronounced negative impacts arising from multiple extreme winter weather events

and conditions. Whereas the projections of greening at two of the study sites, calculated in response to low snow conditions in early winter and maximum duration of warming event in late winter, respectively, presented contrasting results w.r.t previous studies. Therefore, the role of spatial variability in assessing future changes in vegetation productivity due to climatic change, is suggested as a priority topic for future work.

4.6 Supplemental material

Appendix 4.1

Table 4.9 Projected change in the SC20 index at Lofoten for 2090-2100, under different RCPs, w.r.t the average SC20 index (2001-2020)

Year	% Change RCP 4.5 December SC20	% Change RCP 6.0 December SC20	% Change RCP 8.5 December SC20
2090	10.53	-26.32	63.16
2091	63.16	63.16	36.84
2092	42.11	63.16	63.16
2093	42.11	63.16	63.16
2094	63.16	63.16	226.32
2095	31.58	-42.11	63.16
2096	36.84	15.79	63.16
2097	-5.26	-5.26	63.16
2098	63.16	-89.47	31.58
2099	63.16	63.16	52.63

Appendix 4.2

Table 4.10 Change in mean December MDW index (2090-2100) for the Storffjord study site, under various RCPs, w.r.t the mean December MDW index (2000-2019)

Year	%Change RCP 4.5 December MDW	%Change RCP 6.0 December MDW	%Change RCP 8.5 December MDW
2091	200	300	0
2092	-100	-100	200
2093	100	700	100
2094	100	500	100
2095	-100	100	-100
2096	100	100	0
2097	100	0	100
2098	-100	-100	0
2099	-100	200	0
2100	200	300	100

Appendix 4.3

Table 4.11 Change in the mean January temperature (2090-2100) for the Storffjord study site, under various RCPs, w.r.t the mean January temperature (2001-2020)

Year	% Change RCP 4.5 Jan T	% Change RCP 6.0 Jan T	% Change RCP 8.5 Jan T
2091	43.33	30.99	-12.93
2092	7.81	55.02	-2.26
2093	70.21	20.95	-29.56
2094	-21.48	21.65	-6.32
2095	42.70	15.70	0.47
2096	5.15	49.51	13.47
2097	-24.74	3.38	-12.13
2098	5.84	5.84	-9.93
2099	15.12	21.41	-0.18
2100	28.06	65.92	-35.49

Appendix 4.4

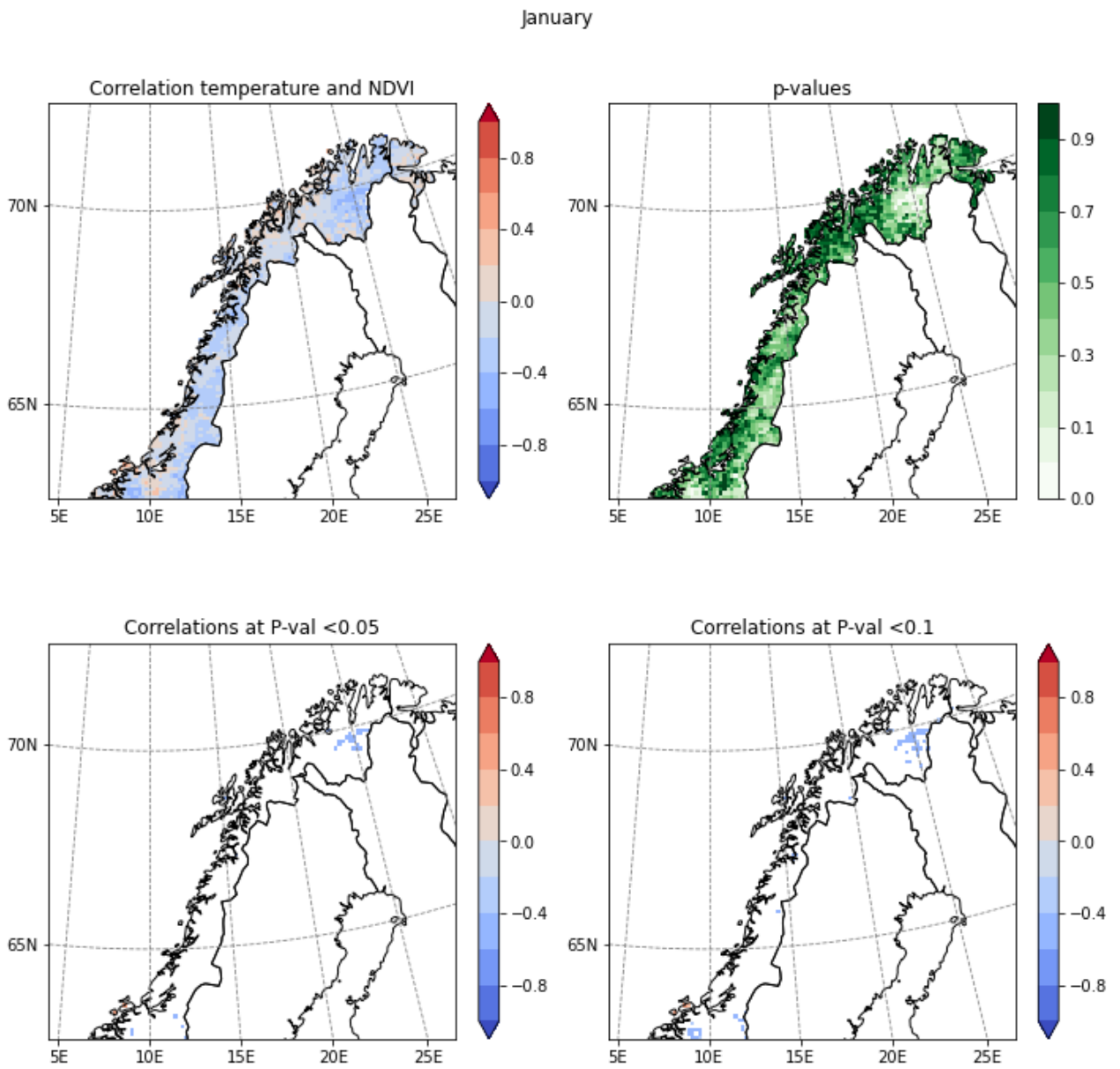


Figure 4.20 Maps showing correlations of mean summer NDVI and mean January temperature for the 2001 – 2020 time period

Chapter 5

Conclusions and Future Recommendations

5.1 Conclusions

Extreme winter weather events in the Arctic are now known to cause acute declines in vegetation biomass and productivity. This phenomenon is known as Arctic browning. Damaged vegetation due to warming events and frost drought conditions in the winter has been shown to change from a sink to a net CO₂ source at the peak of the growing season. Moreover, vegetation disturbance at landscape scales leads to knock-on effects on the wider Arctic ecosystems including trophic interactions. Currently the extreme winter weather events in the Arctic analyzed in this research are relatively rare. However, there is a general consensus within the climate change literature that these will increase in frequency and intensity. Therefore, it is crucial to examine and better understand the changes in frequency, intensity and spatial extent of anomalous winter weather conditions that can lead to vegetation damage and mortality in the Arctic. While most of the work related to Arctic browning has been conducted in-field, this research is the first based on satellite vegetation indices and regional climate modelling. The main aim of this thesis was to understand the current and future significance of extreme winter weather conditions which cause Arctic browning. To achieve this, three research objectives (ROs) were addressed, which are as follows.

1. To understand the satellite-based signature of browning events caused by extreme winter weather conditions.
2. To determine the main meteorological drivers of satellite-based observations of vegetation decline in the Norwegian Arctic and sub-Arctic.
3. Assess the frequency and intensity of climatic drivers of Arctic browning at the end of this century.

Chapter two of this thesis addressed RO1. For RO1 three on-record browning events were selected as case studies. The browning events occurred at Flatanger (Trøndelag County) 2013/1, Lofoten (Nordland County) and Storfjord (Troms og Finnmark County), respectively. Two types of satellite vegetation indices were used to examine the spectral signal for the browning events. A MODIS-derived pigment-

based index, the Chlorophyll Carotenoid Index (CCI), was used, for the first time to study damage in low-lying Arctic vegetation. The effectiveness of the most widely used vegetation index, the Normalized Vegetation Difference Index (NDVI), was assessed as well to detect fine-scale vegetation damage. The results showed that the CCI and the NDVI captured the on-ground decrease in GPP differently. While the spectral browning signal for CCI was observed at the start of the growing season and was short-lived, NDVI was able to detect decreased productivity signals across the start, peak and end of the growing season. The results also highlighted major issues of spatial disparity in that such sporadic vegetation damage and mortality is challenging to detect using medium to coarse resolution (1-10 km) satellite vegetation indices independently. Comparisons of field-based GPP reductions (from other research) with the reductions in the satellite vegetation indices of this research underscore the challenges of understanding the equivalency between on-ground and spectral browning. This raises questions about the robustness of previous pan-Arctic based assessments of greening trends which used coarse-resolution NDVI. Based on the results of chapter two it is suggested that medium-coarse satellite vegetation indices cannot detect browning events on a regional scale independently and that meteorological information should be used in conjunction to provide evidence of the occurrence of extreme winter weather events.

The second RO of this PhD research was addressed in chapter three. The majority of research on responses of Arctic vegetation to a changing climate has been focused on understanding the links between greening trends and warmer temperatures in summer. The work in chapter three has reduced the gap on understandings of relationships between winter meteorological processes, in particular extreme winter weather events, and summer vegetation productivity (as represented by satellite NDVI) in the Arctic region. The results showed large spatial variability in the winter meteorological variables that were important for mean NDVI in the following growing season. Moreover, the multivariate regression analysis revealed a predominant non-linear relationship between different variables of winter climate and the NDVI at the three case study sites. These results agreed with previous research.

The work in chapter three also examined the skill of ERA5-driven WRF at reproducing the real extreme winter weather conditions, which lead to the browning events at the study sites. These high-resolution simulations helped to realize the spatial extent of the warming events and frost drought conditions that caused the vegetation damage. WRF's simulated 2m near-surface temperature had a cold bias and the snow depth was over-estimated across the study sites. However, simple bias corrections of the WRF simulations showed that it was able to reproduce the real extreme winter warming and low snow depth conditions across the case study sites in the Norwegian Arctic and boreal regions.

Chapter four of this thesis was focused on RO3 of the PhD. The future occurrence of climatic drivers of Arctic browning was examined under three emissions scenarios, Representative Concentration Pathways (RCPs) 4.5, 6.0 and 8.5. While the findings about increased projections of extreme winter weather conditions, under all three RCPs are concerning for vegetation productivity, unsurprisingly, RCP 8.5 in particular exhibited the strongest increases at the end of this century. Under this scenario, a notable increase is projected for the frequency and intensity of winter warming events, frequency of rain-on-snow days (ROS) and low snow conditions for the Trøndelag County, Lofoten islands and the coastal areas overall. While the work does not account for the possibility that vegetation in the future might be better adapted to warmer winter climates in the southern areas of research (Trøndelag County), a combined rise in all of these metrics implies a cumulative effect of these extreme winter weather conditions; thus, the vegetation is at unprecedented risk of damage and mortality on large spatial scales in these areas.

The work in chapter four also included projections of future changes in NDVI based on the modelled relationships between NDVI and meteorological variables at the three case study sites derived in chapter three. The NDVI projections for the growing seasons across the 2090 – 2100 time period were compared against a historic baseline (2001 – 2020) to determine the relative change in NDVI at these sites. The results were different across the study sites, with greening projected at Flatanger and Lofoten, and browning projected at Storfjord. It is important to remember, however, that the

projections are based on a certain percentage of the explained seasonal variance in NDVI and more than 50% of the variance in the NDVI at the three sites remains unexplained by the regression relationships.

Along with implications for vegetation productivity, the findings of chapter four regarding overall changes in winter meteorology are useful for the snow-based tourism industry and indigenous reindeer herders in Norway. In addition, the WRF projections in chapter four can be compared against those of other regional climate models (RCMs), especially for regions with complex orography and landforms as Norway, to better understand the local performance of such models.

It is worth noting that a significant component of this work has helped to develop and test methodologies to investigate Arctic browning on larger spatial scales (i.e. county and national levels). The approach used here serves as foundational work to investigate browning events in a multi-disciplinary context, which is required to robustly identify and examine this phenomena. Because browning events are comparatively recent and occur at finer scale as compared to Arctic greening trends, limited research exists in this regard. This made it challenging to compare the results of this research with the wider literature.

The definitions of Arctic browning vary slightly within the remote sensing and ecological literatures. ‘Spectral browning’ is the terminology associated with satellite-based decrease in vegetation productivity, whereas ‘vegetation browning’ is linked with field-based measurements of decreased biomass or productivity. It was not straightforward to consider each definition separately within this thesis because these definitions overlapped at many instances. For example, comparisons of a decrease in satellite NDVI/CCI (‘spectral browning’) with the field-based decrease in GPP (‘vegetation browning’) in chapter two, and while examining the relationships between meteorological variables and vegetation productivity in chapter three.

5.2 Future recommendations

The CCI is a robust indicator of vegetation productivity dynamics. However, it presented mixed results with regards to detecting vegetation damage under this research. It exhibited a clear signal for vegetation damage at the start of the growing season at only one of the study sites (Flatanger), despite the level of vegetation damage being similar across the three sites. It is quite likely that CCI's signature is dependent on the dominant vegetation type. Therefore, more research is required to understand the links between ground productivity and satellite CCI of dominant vegetation types in the Arctic. This should be conducted considering the contribution of other factors within a satellite pixel. These include different landform, proximity to water bodies and soil moisture levels at the site.

NDVI at two of the study sites showed clear vegetation recovery by a continuous increase in the two-three growing seasons, following the extreme winter weather events. Besides the damage intensity and species type, vegetation recovery is dependent on the seasonal meteorological conditions as well. This is because phenology on the seasonal scale is a function of various environmental controls such as temperature, snowmelt times and precipitation. Therefore, it is suggested that future studies examine meteorological variables within the recovery growing seasons, to better understand the phenological effects of browning events.

This research used two different MODIS-based VIs to understand the spectral signature of on-ground GPP decrease. However, it is quite likely that the spectral signature would also vary depending on the sensor. Therefore, it is recommended to analyse the hypotheses in chapter two of this work using other sensors which are available for the study time period considered in this research. For example, Landsat NDVI can be used to examine browning events.

Few studies have shown a lagged response of NDVI to extreme weather conditions, beyond annual time scales. The work in this thesis examined the relationships between the preceding winter meteorology and the summer NDVI. However, it is possible that the effects of browning events last for more than

one growing season. Therefore, it is suggested that future research examines the possibility of lagged relationships between satellite NDVI and damaged Arctic vegetation.

Polar WRF (PWRF) offers polar-specialized configurations, which better represent processes related to ice and snow covered surfaces. For example, it accounts for fractional sea ice cover, which is an important variable for regional simulations in the Arctic. This is especially important with regards to browning events because reduced sea ice in autumn has been linked with anomalous warmth in winters, in the Arctic. PWRF has also demonstrated more accurate temperature simulations over polar regions. Therefore, it is proposed to evaluate PWRF's relative skill at reproducing the extreme winter weather conditions associated with the case study browning events of this research.

Quantification of extreme weather events that damage Arctic ecosystems is a challenging task. This research used meteorological indices mainly representing winter warming events, ROS and low-snow conditions, respectively. While an index representing cold exposure (related to frost drought) was briefly applied as a case study in chapter four, a comprehensive evaluation of this index is recommended under future studies on Arctic browning. Moreover, considering that strong temperature fluctuations was one of the drivers of browning at Lofoten Islands it is recommended to develop a metric which captures temperature fluctuations in the light of damaging effects on Arctic vegetation.

References

- AMAP 2021. *AMAP Arctic Climate Change Update 2021: Key Trends and Impacts* [Online]. Available from: <https://www.amap.no/documents/download/6759/inline>.
- Barkman, J.J. 1990. Ecological differences between *Calluna*- and *Empetrum*-dominated dry heath communities in Drenthe, The Netherlands. *Acta Botanica Neerlandica*. **39**(1), pp.75–92.
- Barstad, I. and Smith, R.B. 2005. Evaluation of an orographic precipitation model. *Journal of Hydrometeorology*. **6**(1), pp.85–99.
- Beamish, A., Reynolds, M.K., Epstein, H., Frost, G. V., Macander, M.J., Bergstedt, H., Bartsch, A., Kruse, S., Miles, V., Tanis, C.M., Heim, B., Fuchs, M., Chabrillat, S., Shevtsova, I., Verdonen, M. and Wagner, J. 2020. Recent trends and remaining challenges for optical remote sensing of Arctic tundra vegetation: A review and outlook. *Remote Sensing of Environment*. [Online]. **246**(October 2019), p.111872. Available from: <https://doi.org/10.1016/j.rse.2020.111872>.
- Beamish, A.L., Coops, N.C., Hermosilla, T., Chabrillat, S. and Heim, B. 2018. Monitoring pigment-driven vegetation changes in a low-Arctic tundra ecosystem using digital cameras: *Ecosphere*. **9**(2).
- Beck, H.E., Zimmermann, N.E., McVicar, T.R., Vergopolan, N., Berg, A. and Wood, E.F. 2018. Present and future köppen-geiger climate classification maps at 1-km resolution. *Scientific Data*. **5**, pp.1–12.
- Berner, L.T., Massey, R., Jantz, P., Forbes, B.C., Macias-Fauria, M., Myers-Smith, I., Kumpula, T., Gauthier, G., Andreu-Hayles, L., Gaglioti, B. V., Burns, P., Zetterberg, P., D'Arrigo, R. and Goetz, S.J. 2020. Summer warming explains widespread but not uniform greening in the Arctic tundra biome. *Nature Communications*. [Online]. **11**(1), pp.1–12. Available from: <http://dx.doi.org/10.1038/s41467-020-18479-5>.
- Bhatt, U.S., Walker, D.A., Reynolds, M.K., Bieniek, P.A., Epstein, H.E., Comiso, J.C., Pinzon, J.E., Tucker, C.J. and Polyakov, I. V. 2013. Recent declines in warming and vegetation greening trends over pan-arctic tundra. *Remote Sensing*. **5**(9), pp.4229–4254.
- Bhatt, U.S., Walker, D.A., Reynolds, M.K., Bieniek, P.A., Epstein, H.E., Comiso, J.C., Pinzon, J.E., Tucker, C.J., Steele, M., Ermold, W. and Zhang, J. 2017. Changing seasonality of panarctic tundra vegetation in relationship to climatic variables. *Environmental Research Letters*. **12**(5).
- Bhatt, U.S., Walker, D.A., Reynolds, M.K., Comiso, J.C., Epstein, H.E., Jia, G., Gens, R., Pinzon, J.E., Tucker, C.J., Tweedie, C.E. and Webber, P.J. 2010. Circumpolar Arctic tundra vegetation change is linked to sea ice decline. *Earth Interactions*. **14**(8).
- Bieniek, P.A., Bhatt, U.S., Walker, D.A., Reynolds, M.K., Comiso, J.C., Epstein, H.E., Pinzon, J.E., Tucker, C.J., Thoman, R.L., Tran, H., Mölders, N., Steele, M., Zhang, J. and Ermold, W. 2015. Climate drivers linked to changing seasonality of Alaska Coastal tundra vegetation productivity. *Earth Interactions*. **19**(19).
- Bintanja, R. and Andry, O. 2017. Towards a rain-dominated Arctic. *Nature Climate Change*. **7**(4), pp.263–267.
- Bjerke, J.W. 2011. Winter climate change: Ice encapsulation at mild subfreezing temperatures kills freeze-tolerant lichens. *Environmental and Experimental Botany*. **72**(3), pp.404–408.
- Bjerke, J.W., Bokhorst, S., Zielke, M., Callaghan, T. V., Bowles, F.W. and Phoenix, G.K. 2011. Contrasting sensitivity to extreme winter warming events of dominant sub-Arctic heathland

- bryophyte and lichen species. *Journal of Ecology*. **99**(6), pp.1481–1488.
- Bjerke, J.W., Rune Karlsen, S., Arild Hogda, K., Malnes, E., Jepsen, J.U., Lovibond, S., Vikhamar-Schuler, D. and Tommervik, H. 2014. Record-low primary productivity and high plant damage in the Nordic Arctic Region in 2012 caused by multiple weather events and pest outbreaks. *Environmental Research Letters*. **9**(8).
- Bjerke, J.W., Treharne, R., Vikhamar-Schuler, D., Karlsen, S.R., Ravolainen, V., Bokhorst, S., Phoenix, G.K., Bochenek, Z. and Tømmervik, H. 2017. Understanding the drivers of extensive plant damage in boreal and Arctic ecosystems: Insights from field surveys in the aftermath of damage. *Science of The Total Environment*. [Online]. **599–600**, pp.1965–1976. [Accessed 23 September 2018]. Available from: <https://linkinghub.elsevier.com/retrieve/pii/S0048969717311506>.
- Boisvert, L.N. and Stroeve, J.C. 2015. The Arctic is becoming warmer and wetter as revealed by the Atmospheric Infrared Sounder. *Geophysical Research Letters*., pp.4439–4446.
- Bokhorst, S., Bjerke, J.W., Bowles, F.W., Melillo, J., Callaghan, T. V. and Phoenix, G.K. 2008. Impacts of extreme winter warming in the sub-Arctic: Growing season responses of dwarf shrub heathland. *Global Change Biology*. **14**(11), pp.2603–2612.
- Bokhorst, S., Bjerke, J.W., Street, L.E., Callaghan, T. V. and Phoenix, G.K. 2011. Impacts of multiple extreme winter warming events on sub-Arctic heathland: Phenology, reproduction, growth, and CO₂ flux responses. *Global Change Biology*. **17**(9), pp.2817–2830.
- Bokhorst, Stef, Bjerke, J.W., Tømmervik, H., Preece, C. and Phoenix, G.K. 2012. Ecosystem response to climatic change: The importance of the cold season. *Ambio*. **41**(SUPPL.3), pp.246–255.
- Bokhorst, S., Phoenix, G.K., Berg, M.P., Callaghan, T. V., Kirby-Lambert, C. and Bjerke, J.W. 2015. Climatic and biotic extreme events moderate long-term responses of above- and belowground sub-Arctic heathland communities to climate change. *Global Change Biology*. **21**(11), pp.4063–4075.
- Bokhorst, S., Tømmervik, H., Callaghan, T. V., Phoenix, G.K. and Bjerke, J.W. 2012. Vegetation recovery following extreme winter warming events in the sub-Arctic estimated using NDVI from remote sensing and handheld passive proximal sensors. *Environmental and Experimental Botany*. [Online]. **81**(December 2007), pp.18–25. Available from: <http://dx.doi.org/10.1016/j.envexpbot.2012.02.011>.
- Bokhorst, S.F., Bjerke, J.W., Tømmervik, H., Callaghan, T. V. and Phoenix, G.K. 2009. Winter warming events damage sub-Arctic vegetation: Consistent evidence from an experimental manipulation and a natural event. *Journal of Ecology*. **97**(6), pp.1408–1415.
- Bonan, G.B. 2002. Ecological climatology: concepts and applications. *Choice Reviews Online*. **40**(07), pp.40-3988-40–3988.
- Bret-Harte, M.S., Mack, M.C., Shaver, G.R., Huebner, D.C., Johnston, M., Mojica, C.A., Pizano, C. and Reiskind, J.A. 2013. The response of Arctic vegetation and soils following an unusually severe tundra fire. *Philosophical transactions of the Royal Society of London. Series B, Biological sciences*. **368**(1624), p.20120490.
- Bruyere, C.L., Monaghan, A.J., Steinhoff, D.F. and Yates, D. 2015. *Bias-Corrected CMIP5 CESM Data in WRF / MPAS Intermediate File Format NCAR / TN 515 + STR*.
- Callaghan, T. V., Bergholm, F., Christensen, T.R., Jonasson, C., Kokfelt, U. and Johansson, M. 2010. A new climate era in the sub-Arctic: Accelerating climate changes and multiple impacts. *Geophysical Research Letters*. **37**(14), pp.1–6.

- Callaghan, T. V., Johansson, M., Brown, R.D., Groisman, P.Y., Labba, N., Radionov, V., Bradley, R.S., Blangy, S., Bulygina, O.N., Christensen, T.R., Colman, J.E., Essery, R.L.H., Forbes, B.C., Forchhammer, M.C., Golubev, V.N., Honrath, R.E., Juday, G.P., Meshcherskaya, A. V., Phoenix, G.K., Pomeroy, J., Rautio, A., Robinson, D.A., Schmidt, N.M., Serreze, M.C., Shevchenko, V.P., Shiklomanov, A.I., Shmakin, A.B., Skořd, P., Sturm, M., Woo, M.K. and Wood, E.F. 2011. Multiple effects of changes in arctic snow cover. *Ambio*. **40**(SUPPL. 1), pp.32–45.
- Christensen, T.R., Lund, M., Skov, K., Abermann, J., López-Blanco, E., Scheller, J., Scheel, M., Jackowicz-Korczynski, M., Langley, K., Murphy, M.J. and Mastepanov, M. 2021. Multiple Ecosystem Effects of Extreme Weather Events in the Arctic. *Ecosystems*. **24**(1), pp.122–136.
- Cullather, R.I., Lim, Y.K., Boisvert, L.N., Brucker, L., Lee, J.N. and Nowicki, S.M.J. 2016. Analysis of the warmest Arctic winter, 2015–2016. *Geophysical Research Letters*. **43**(20), 10,808-10,816.
- Drolet, G.G., Huemmrich, K.F., Hall, F.G., Middleton, E.M., Black, T.A., Barr, A.G. and Margolis, H.A. 2005. A MODIS-derived photochemical reflectance index to detect inter-annual variations in the photosynthetic light-use efficiency of a boreal deciduous forest. *Remote Sensing of Environment*. **98**(2–3), pp.212–224.
- Dyrddal, A.V., Isaksen, K. and Hygen, H.O. 2011. Author (s) . . (03).
- Dyrddal, A.V., Saloranta, T., Skaugen, T. and Stranden, H.B. 2013. Changes in snow depth in Norway during the period 1961-2010. *Hydrology Research*. **44**(1), pp.169–179.
- Eklundh, L. and Jöhnsson, P. 2017. TIMESAT 3.3 Software Manual. , pp.1–92.
- Fensholt, R., Langanke, T., Rasmussen, K., Reenberg, A., Prince, S.D., Tucker, C., Scholes, R.J., Le, Q.B., Bondeau, A., Eastman, R., Epstein, H., Gaughan, A.E., Hellden, U., Mbow, C., Olsson, L., Paruelo, J., Schweitzer, C., Seaquist, J. and Wessels, K. 2012. Greenness in semi-arid areas across the globe 1981-2007 - an Earth Observing Satellite based analysis of trends and drivers. *Remote Sensing of Environment*. [Online]. **121**, pp.144–158. Available from: <http://dx.doi.org/10.1016/j.rse.2012.01.017>.
- Fernández-González, S., Valero, F., Sánchez, J.L., Gascón, E., López, L., García-Ortega, E. and Merino, A. 2015. Numerical simulations of snowfall events: Sensitivity analysis of physical parameterizations. *Journal of Geophysical Research*. **120**(19), pp.10130–10148.
- Filella, I., Porcar-Castell, A., Munné-Bosch, S., Bäck, J., Garbulsky, M.F. and Peñuelas, J. 2009. PRI assessment of long-term changes in carotenoids/chlorophyll ratio and short-term changes in de-epoxidation state of the xanthophyll cycle. *International Journal of Remote Sensing*. **30**(17), pp.4443–4455.
- Friend, A.D., Lucht, W., Rademacher, T.T., Keribin, R., Betts, R., Cadule, P., Ciais, P., Clark, D.B., Dankers, R., Falloon, P.D., Ito, A., Kahana, R., Kleidon, A., Lomas, M.R., Nishina, K., Ostberg, S., Pavlick, R., Peylin, P., Schaphoff, S., Vuichard, N., Warszawski, L., Wiltshire, A. and Woodward, F.I. 2014. Carbon residence time dominates uncertainty in terrestrial vegetation responses to future climate and atmospheric CO₂. *Proceedings of the National Academy of Sciences of the United States of America*. **111**(9), pp.3280–3285.
- Gadian, A.M., Blyth, A.M., Bruyere, C.L., Burton, R.R., Done, J.M., Groves, J., Holland, G., Mobbs, S.D., Pozo, J.T. del, Tye, M.R. and Warner, J.L. 2018. A case study of possible future summer convective precipitation over the UK and Europe from a regional climate projection. *International Journal of Climatology*. **38**(5), pp.2314–2324.
- Gamon, J.A., Huemmrich, K.F., Stone, R.S. and Tweedie, C.E. 2013. Spatial and temporal variation in primary productivity (NDVI) of coastal Alaskan tundra: Decreased vegetation growth following

- earlier snowmelt. *Remote Sensing of Environment*. [Online]. **129**, pp.144–153. Available from: <http://dx.doi.org/10.1016/j.rse.2012.10.030>.
- Gamon, J.A., Huemmrich, K.F., Wong, C.Y.S., Ensminger, I., Garrity, S., Hollinger, D.Y., Noormets, A. and Peñuelask, J. 2016. A remotely sensed pigment index reveals photosynthetic phenology in evergreen conifers. *Proceedings of the National Academy of Sciences of the United States of America*. **113**(46), pp.13087–13092.
- Gamon, J.A., Kovalchuck, O., Wong, C.Y.S., Harris, A. and Garrity, S.R. 2015. Monitoring seasonal and diurnal changes in photosynthetic pigments with automated PRI and NDVI sensors. *Biogeosciences*. **12**(13), pp.4149–4159.
- Gamon, J.A., Serrano, L. and Surfus, J.S. 1997. The photochemical reflectance index: An optical indicator of photosynthetic radiation use efficiency across species, functional types, and nutrient levels. *Oecologia*. **112**(4), pp.492–501.
- Gillespie, T.W., Ostermann-Kelm, S., Dong, C., Willis, K.S., Okin, G.S. and MacDonald, G.M. 2018. Monitoring changes of NDVI in protected areas of southern California. *Ecological Indicators*. [Online]. **88**(February), pp.485–494. Available from: <https://doi.org/10.1016/j.ecolind.2018.01.031>.
- Goerner, A., Reichstein, M. and Rambal, S. 2009. Tracking seasonal drought effects on ecosystem light use efficiency with satellite-based PRI in a Mediterranean forest. *Remote Sensing of Environment*. [Online]. **113**(5), pp.1101–1111. Available from: <http://dx.doi.org/10.1016/j.rse.2009.02.001>.
- Goerner, A., Reichstein, M., Tomelleri, E., Hanan, N., Rambal, S., Papale, D., Dragoni, D. and Schullius, C. 2011. Remote sensing of ecosystem light use efficiency with MODIS-based PRI. *Biogeosciences*. **8**(1), pp.189–202.
- Gowan, T.M., Steenburgh, W.J. and Schwartz, C.S. 2018. Validation of mountain precipitation forecasts from the convection-permitting NCAR ensemble and operational forecast systems over the western United States. *Weather and Forecasting*. **33**(3), pp.739–765.
- Graham, R.M., Cohen, L., Petty, A., Boisvert, L.N., Rinke, A., Hudson, S.R., Nicolaus, M. and Granskog, M.A. 2017. Increasing frequency and duration of Arctic winter warming events.
- Guo, L., Wu, S., Zhao, D., Yunhe, Y., Leng, G. and Zhang, Q. 2014. NDVI-Based Vegetation Change in Inner Mongolia from 1982 to 2006 and Its Relationship to Climate at the Biome Scale Linghui. *Advances in Meteorology*. **2014**, p.12.
- Gustafson, A., Miller, P.A., Björk, R.G., Olin, S. and Smith, B. 2021. Nitrogen restricts future sub-Arctic treeline advance in an individual-based dynamic vegetation model. *Biogeosciences*. **18**(23), pp.6329–6347.
- Hansen, B.B., Isaksen, K., Benestad, R.E., Kohler, J., Pedersen, Å., Loe, L.E., Coulson, S.J., Larsen, J.O. and Varpe, Ø. 2014. Warmer and wetter winters: Characteristics and implications of an extreme weather event in the High Arctic. *Environmental Research Letters*. **9**(11).
- Hawbecker, P. 2013. *A Comparison of 1-Way and 2-Way Nesting in the WRF-LES Framework* No Title. Texas Tech University.
- Heikkilä, U., Sandvik, A. and Sorteberg, A. 2011. Dynamical downscaling of ERA-40 in complex terrain using the WRF regional climate model. *Climate Dynamics*. **37**(7–8), pp.1551–1564.
- Heliasz, M., Johansson, T., Lindroth, A., Mölder, M., Mastepanov, M., Friborg, T., Callaghan, T. V. and Christensen, T.R. 2011. Quantification of C uptake in subarctic birch forest after setback by an

extreme insect outbreak. *Geophysical Research Letters*. **38**(1), pp.1–5.

- Hersbach, H., Bell, B., Berrisford, P., Hirahara, S., Horányi, A., Muñoz-Sabater, J., Nicolas, J., Peubey, C., Radu, R., Schepers, D., Simmons, A., Soci, C., Abdalla, S., Abellan, X., Balsamo, G., Bechtold, P., Biavati, G., Bidlot, J., Bonavita, M., De Chiara, G., Dahlgren, P., Dee, D., Diamantakis, M., Dragani, R., Flemming, J., Forbes, R., Fuentes, M., Geer, A., Haimberger, L., Healy, S., Hogan, R.J., Hólm, E., Janisková, M., Keeley, S., Laloyaux, P., Lopez, P., Lupu, C., Radnoti, G., de Rosnay, P., Rozum, I., Vamborg, F., Villaume, S. and Thépaut, J.N. 2020. The ERA5 global reanalysis. *Quarterly Journal of the Royal Meteorological Society*. **146**(730), pp.1999–2049.
- Horstkotte, T., Utsi, T.A., Larsson-Blind, Å., Burgess, P., Johansen, B., Käyhkö, J., Oksanen, L. and Forbes, B.C. 2017. Human-animal agency in reindeer management: Sámi herders' perspectives on vegetation dynamics under climate change. *Ecosphere*. [Online]. **8**(9), p.e01931. [Accessed 23 September 2018]. Available from: <http://doi.wiley.com/10.1002/ecs2.1931>.
- Huete, A., Didan, K., Miura, T., Rodriguez, E., Gao, X. and Ferreira, L. 2002. Overview of the radiometric and biophysical performance of the MODIS vegetation indices. *Remote Sensing of Environment*. **83**, pp.195–213.
- Jennings, K.S., Winchell, T.S., Livneh, B. and Molotch, N.P. 2018. Spatial variation of the rain-snow temperature threshold across the Northern Hemisphere. *Nature Communications*. [Online]. **9**(1), pp.1–9. Available from: <http://dx.doi.org/10.1038/s41467-018-03629-7>.
- Jentsch, A., Kreyling, J. and Beierkuhnlein, C. 2007. A new generation of climate-change experiments: Events, not trends. *Frontiers in Ecology and the Environment*. **5**(7), pp.365–374.
- Jeong, S.J., Schimel, D., Frankenberg, C., Drewry, D.T., Fisher, J.B., Verma, M., Berry, J.A., Lee, J.E. and Joiner, J. 2017. Application of satellite solar-induced chlorophyll fluorescence to understanding large-scale variations in vegetation phenology and function over northern high latitude forests. *Remote Sensing of Environment*. [Online]. **190**, pp.178–187. Available from: <http://dx.doi.org/10.1016/j.rse.2016.11.021>.
- Ji, L., Wylie, B., Ramachandran, B. and Jenkerson, C. 2010. A comparative analysis of three different MODIS NDVI datasets for Alaska and adjacent Canada. *Canadian Journal of Remote Sensing*. **36**, pp.S149–S167.
- Johansson, M., Callaghan, T. V., Bosiö, J., Åkerman, H.J., Jackowicz-Korczynski, M. and Christensen, T.R. 2013. Rapid responses of permafrost and vegetation to experimentally increased snow cover in sub-arctic Sweden. *Environmental Research Letters*. **8**(3).
- Jönsson, P. and Eklundh, L. 2004. TIMESAT - A program for analyzing time-series of satellite sensor data. *Computers and Geosciences*. **30**(8), pp.833–845.
- Karlsen, S.R., Anderson, H.B., Van Der Wal, R. and Hansen, B.B. 2018. A new NDVI measure that overcomes data sparsity in cloud-covered regions predicts annual variation in ground-based estimates of high arctic plant productivity. *Environmental Research Letters*. **13**(2).
- Kerguillec, R. 2015. Seasonal distribution and variability of atmospheric freeze/thaw cycles in Norway over the last six decades (1950-2013). *Boreas*. **44**(3), pp.526–542.
- Kochendorfer, J., Nitu, R., Wolff, M., Mekis, E., Rasmussen, R., Baker, B., Earle, M.E., Reverdin, A., Wong, K., Smith, C.D., Yang, D., Roulet, Y.A., Buisan, S., Laine, T., Lee, G., Aceituno, J.L.C., Alastrué, J., Isaksen, K., Meyers, T., Brækkan, R., Landolt, S., Jachcik, A. and Poikonen, A. 2017. Analysis of single-Alter-shielded and unshielded measurements of mixed and solid precipitation from WMO-SPICE. *Hydrology and Earth System Sciences*. **21**(7), pp.3525–3542.
- Kreyling, J. and Henry, H.A.L. 2011. Vanishing winters in Germany: Soil frost dynamics and snow

- cover trends, and ecological implications. *Climate Research*. **46**(3), pp.269–276.
- Landrum, L. and Holland, M.M. 2020. Extremes become routine in an emerging new Arctic. *Nature Climate Change*. [Online]. **10**(12), pp.1108–1115. Available from: <http://dx.doi.org/10.1038/s41558-020-0892-z>.
- Lara, B. and Gandini, M. 2016. Assessing the performance of smoothing functions to estimate land surface phenology on temperate grassland. *International Journal of Remote Sensing*. [Online]. **37**(8), pp.1801–1813. Available from: <http://dx.doi.org/10.1080/2150704X.2016.1168945>.
- Lara, M.J., Nitze, I., Grosse, G., Martin, P. and David McGuire, A. 2018. Reduced arctic tundra productivity linked with landform and climate change interactions. *Scientific Reports*. **8**(1), pp.1–10.
- Lee, J., Lee, S.-M. and Lee, S.-J. 2022. Ground- and Satellite-Based Evaluation of WRF Snowfall Prediction. *Sola*. **18**(0), pp.173–180.
- Li, L. and Pomeroy, J.W. 1997. Estimates of threshold wind speeds for snow transport using meteorological data. *Journal of Applied Meteorology*. **36**(3), pp.205–213.
- Liang-Liang, L., Jian, L. and Ru-Cong, Y. 2022. Evaluation of CMIP6 HighResMIP models in simulating precipitation over Central Asia. *Advances in Climate Change Research*. [Online]. **13**(1), pp.1–13. Available from: <https://doi.org/10.1016/j.accre.2021.09.009>.
- Liu, L., Ma, Y., Menenti, M., Zhang, X. and Ma, W. 2019. Evaluation of WRF Modeling in Relation to Different Land Surface Schemes and Initial and Boundary Conditions: A Snow Event Simulation Over the Tibetan Plateau. *Journal of Geophysical Research: Atmospheres*. **124**(1), pp.209–226.
- Maguire, A.J., Eitel, J.U.H., Magney, T.S., Frankenberg, C., Köhler, P., Orcutt, E.L., Parazoo, N.C., Pavlick, R. and Pierrat, Z.A. 2021. Spatial covariation between solar-induced fluorescence and vegetation indices from Arctic-Boreal landscapes. *Environmental Research Letters*. **16**(9).
- Maraun, D. 2016. Bias Correcting Climate Change Simulations - a Critical Review. *Current Climate Change Reports*. [Online], pp.211–220. Available from: <http://dx.doi.org/10.1007/s40641-016-0050-x>.
- Marshall, G.J., Kivinen, S., Jylhä, K., Vignols, R.M. and Rees, W.G. 2018. The accuracy of climate variability and trends across Arctic Fennoscandia in four reanalyses. *International Journal of Climatology*. **38**(10), pp.3878–3895.
- Masui, T., Matsumoto, K., Hijioka, Y. and Kinoshita, T. 2011. An emission pathway for stabilization at 6 Wm – 2 radiative forcing. , pp.59–76.
- May, J.L., Parker, T., Unger, S. and Oberbauer, S.F. 2018. Short term changes in moisture content drive strong changes in Normalized Difference Vegetation Index and gross primary productivity in four Arctic moss communities. *Remote Sensing of Environment*. [Online]. **212**(March), pp.114–120. Available from: <https://doi.org/10.1016/j.rse.2018.04.041>.
- McCrystall, M.R., Stroeve, J., Serreze, M., Forbes, B.C. and Screen, J.A. 2021. New climate models reveal faster and larger increases in Arctic precipitation than previously projected. *Nature Communications*. **12**(1), pp.1–12.
- Mcdonnell, J., Lambkin, K. and Fealy, R. 2018. Verification and bias correction of ECMWF forecasts for Irish weather stations. . **301**(November 2017), pp.292–301.
- McGuire, A.D., Anderson, L.G., Christensen, T.R., Scott, D., Laodong, G., Hayes, D.J., Martin, H., Lorenson, T.D., Macdonald, R.W. and Nigel, R. 2009. Sensitivity of the carbon cycle in the Arctic to climate change. *Ecological Monographs*. **79**(4), pp.523–555.

- Meehl, G.A., Washington, W.M., Santer, B.D., Collins, W.D., Arblaster, J.M., Hu, A., Lawrence, D.M., Teng, H., Buja, L.E. and Strand, W.G. 2006. Climate change projections for the twenty-first century and climate change commitment in the CCSM3. *Journal of Climate*. **19**(11), pp.2597–2616.
- Merzlyak, M.N., Gitelson, A.A., Chivkunova, O.B., Solovchenko, A.E. and Pogosyan, S.I. 2003. Merzlyak2003_Article_ApplicationOfReflectanceSpectr. . **50**(5), pp.704–710.
- Mölders, N. and Kramm, G. 2010. A case study on wintertime inversions in Interior Alaska with WRF. *Atmospheric Research*. [Online]. **95**(2–3), pp.314–332. Available from: <http://dx.doi.org/10.1016/j.atmosres.2009.06.002>.
- Moss, R.H., Edmonds, J.A., Hibbard, K.A., Manning, M.R., Rose, S.K., Vuuren, D.P. Van, Carter, T.R., Emori, S., Kainuma, M., Kram, T., Meehl, G.A., Mitchell, J.F.B., Nakicenovic, N., Riahi, K., Smith, S.J., Stouffer, R.J., Thomson, A.M., Weyant, J.P. and Wilbanks, T.J. 2010. The next generation of scenarios for climate change research and assessment. *Nature*. **463**(February), pp.747–756.
- Myers-Smith, I.H., Kerby, J.T., Phoenix, G.K., Bjerke, J.W., Epstein, H.E., Assmann, J.J., John, C., Andreu-Hayles, L., Angers-Blondin, S., Beck, P.S.A., Berner, L.T., Bhatt, U.S., Bjorkman, A.D., Blok, D., Bryn, A., Christiansen, C.T., Cornelissen, J.H.C., Cunliffe, A.M., Elmendorf, S.C., Forbes, B.C., Goetz, S.J., Hollister, R.D., de Jong, R., Loranty, M.M., Macias-Fauria, M., Maseyk, K., Normand, S., Olofsson, J., Parker, T.C., Parmentier, F.J.W., Post, E., Schaepman-Strub, G., Stordal, F., Sullivan, P.F., Thomas, H.J.D., Tømmervik, H., Treharne, R., Tweedie, C.E., Walker, D.A., Wilmking, M. and Wipf, S. 2020. Complexity revealed in the greening of the Arctic. *Nature Climate Change*. [Online]. **10**(2), pp.106–117. Available from: <http://dx.doi.org/10.1038/s41558-019-0688-1>.
- Nilsen, I.B., Hanssen-Bauer, I., Tveito, O.E. and Wong, W.K. 2021. Projected changes in days with zero-crossings for Norway. *International Journal of Climatology*. **41**(4), pp.2173–2188.
- Niskanen, A.K.J., Niittynen, P., Aalto, J., Väre, H. and Luoto, M. 2019. Lost at high latitudes: Arctic and endemic plants under threat as climate warms. *Diversity and Distributions*. **25**(5), pp.809–821.
- Overland, J.E. and Wang, M. 2016. Recent extreme arctic temperatures are due to a split polar vortex. *Journal of Climate*. **29**(15), pp.5609–5616.
- Pall, P., Tallaksen, L.M. and Stordal, F. 2019. A climatology of rain-on-snow events for Norway. *Journal of Climate*. **32**(20), pp.6995–7016.
- Pedersen, S.H., Liston, G.E., Tamstorf, M.P., Abermann, J., Lund, M. and Schmidt, N.M. 2018. Quantifying snow controls on vegetation greenness. *Ecosphere*. **9**(6).
- Peñuelas, J., Garbulsky, M.F. and Filella, I. 2011. Photochemical reflectance index (PRI) and remote sensing of plant CO₂ uptake. *New Phytologist*. **191**(3), pp.596–599.
- Phoenix, G.K. and Bjerke, J.W. 2016. Arctic browning: extreme events and trends reversing arctic greening. *Global change biology*. **22**(9), pp.2960–2962.
- Phoenix, G.K. and Lee, J.A. 2004. Predicting impacts of Arctic climate change: past lessons and future challenges. *Ecological Research*. [Online]. **19**(1), pp.65–74. Available from: <http://www.springerlink.com/index/906BLL9F5NC4AH6Q.pdf>.
- Phoenix, Gareth K. and Lee, J.A. 2004. Predicting impacts of Arctic climate change: Past lessons and future challenges. *Ecological Research*. **19**(1), pp.65–74.
- Piedallu, C., Chéret, V., Denux, J.P., Perez, V., Azcona, J.S., Seynave, I. and Gégout, J.C. 2019. Soil and climate differently impact NDVI patterns according to the season and the stand type. *Science of*

the Total Environment. [Online]. **651**, pp.2874–2885. Available from:
<http://dx.doi.org/10.1016/j.scitotenv.2018.10.052>.

- Powers, J.G., Klemp, J.B., Skamarock, W.C., Davis, C.A., Dudhia, J., Gill, D.O., Coen, J.L., Gochis, D.J., Ahmadov, R., Peckham, S.E., Grell, G.A., Michalakes, J., Trahan, S., Benjamin, S.G., Alexander, C.R., Dimego, G.J., Wang, W., Schwartz, C.S., Romine, G.S., Liu, Z., Snyder, C., Chen, F., Barlage, M.J., Yu, W. and Duda, M.G. 2017. The weather research and forecasting model: Overview, system efforts, and future directions. *Bulletin of the American Meteorological Society*. **98**(8), pp.1717–1737.
- Preece, C. and Phoenix, G.K. 2014. Impact of early and late winter icing events on sub-arctic dwarf shrubs. *Plant Biology*. **16**(1), pp.125–132.
- Rahman, A.F., Cordova, V.D., Gamon, J.A., Schmid, H.P. and Sims, D.A. 2004. Potential of MODIS Ocean Bands for Estimating CO₂ Flux from Terrestrial Vegetation : A Novel Approach Potential of MODIS ocean bands for estimating CO₂ flux from terrestrial vegetation : A novel approach. . (March 2016), pp.2–6.
- Raynolds, M.K. and Walker, D.A. 2016. Increased wetness confounds Landsat-derived NDVI trends in the central Alaska North Slope region, 1985-2011. *Environmental Research Letters*. [Online]. **11**(8), pp.1–13. Available from: <http://dx.doi.org/10.1088/1748-9326/11/8/085004>.
- Rennert, K.J., Roe, G., Putkonen, J. and Bitz, C.M. 2009. Soil thermal and ecological impacts of rain on snow events in the circumpolar arctic. *Journal of Climate*. **22**(9), pp.2302–2315.
- Riahi, K., Kriegler, E., Johnson, N., Bertram, C., den Elzen, M., Eom, J., Schaeffer, M., Edmonds, J., Isaac, M., Krey, V., Longden, T., Luderer, G., Méjean, A., McCollum, D.L., Mima, S., Turton, H., van Vuuren, D.P., Wada, K., Bosetti, V., Capros, P., Criqui, P., Hamdi-Cherif, M., Kainuma, M. and Edenhofer, O. 2015. Locked into Copenhagen pledges - Implications of short-term emission targets for the cost and feasibility of long-term climate goals. *Technological Forecasting and Social Change*. [Online]. **90**(PA), pp.8–23. Available from:
<http://dx.doi.org/10.1016/j.techfore.2013.09.016>.
- Rigby, J.R. and Porporato, A. 2008. Spring frost risk in a changing climate. *Geophysical Research Letters*. **35**(12), pp.1–5.
- Rixen, C., Høye, T.T., Macek, P., Aerts, R., Alatalo, J.M., Anderson, J.T., Arnold, P.A., Barrio, I.C., Bjerke, J.W., Björkman, M.P., Blok, D., Blume-Werry, G., Boike, J., Bokhorst, S., Carbognani, M., Christiansen, C.T., Convey, P., Cooper, E.J., Cornelissen, J.H.C., Coulson, S.J., Dorrepaal, E., Elberling, B., Elmendorf, S.C., Elphinstone, C., Forte, T.G.W., Frei, E.R., Geange, S.R., Gehrman, F., Gibson, C., Grogan, P., Halbritter, A.H., Harte, J., Henry, G.H.R., Inouye, D.W., Irwin, R.E., Jespersen, G., Jónsdóttir, I.S., Jung, J.Y., Klings, D.H., Kudo, G., Lämsä, J., Lee, H., Lembrechts, J.J., Lett, S., Lynn, J.S., Mann, H.M.R., Mastepanov, M., Morse, J., Myers-Smith, I.H., Olofsson, J., Paavola, R., Petraglia, A., Phoenix, G.K., Semenchuk, P., Siewert, M.B., Slatyer, R., Spasojevic, M.J., Suding, K., Sullivan, P., Thompson, K.L., Väisänen, M., Vandvik, V., Venn, S., Walz, J., Way, R., Welker, J.M., Wipf, S. and Zong, S. 2022. Winters are changing: snow effects on Arctic and alpine tundra ecosystems. *Arctic Science*. **37**(February), pp.1–37.
- Rossini, M., Cogliati, S., Meroni, M., Migliavacca, M., Galvagno, M., Busetto, L., Cremonese, E., Julitta, T., Siniscalco, C., Morra Di Cella, U. and Colombo, R. 2012. Remote sensing-based estimation of gross primary production in a subalpine grassland. *Biogeosciences*. **9**(7), pp.2565–2584.
- Sakai, A. and Larcher, W. 1987. Low Temperature and Frost as Environmental Factors. , pp.1–20.
- Salathe Jr., E.P., Steed, R., Mass, C. and Zahn, P.H. 2008. A High-Resolution Climate Model for the U .

- S. Pacific Northwest : Mesoscale Feedbacks and Local Responses to Climate Change *. *Journal of Climate.*, pp.5708–5726.
- Semenchuk, P.R., Elberling, B. and Cooper, E.J. 2013. Snow cover and extreme winter warming events control flower abundance of some, but not all species in high arctic svalbard. *Ecology and Evolution*. **3**(8), pp.2586–2599.
- Serreze, M.C., Gustafson, J., Barrett, A.P., Druckenmiller, M.L., Fox, S., Voveris, J., Stroeve, J., Sheffield, B., Forbes, B.C., Rasmus, S., Laptander, R., Brook, M., Brubaker, M., Temte, J., McCrystall, M.R. and Bartsch, A. 2021. Arctic rain on snow events: Bridging observations to understand environmental and livelihood impacts. *Environmental Research Letters*. **16**(10).
- Skamarock, W.C. 2004. Evaluating mesoscale NWP models using kinetic energy spectra. *Monthly Weather Review*. **132**(12), pp.3019–3032.
- Skamarock, W.C., Klemp, J.B., Dudhia, J., Gill, D.O., Zhiquan, L., Berner, J., Wang, W., Powers, J.G., Duda, M.G., Barker, D.M. and Huang, X.-Y. 2019. A Description of the Advanced Research WRF Model Version 4. *NCAR Technical Note NCAR/TN-475+STR*. [Online], p.145. Available from: <http://library.ucar.edu/research/publish-technote>.
- Smith, M.D. 2011. An ecological perspective on extreme climatic events: A synthetic definition and framework to guide future research. *Journal of Ecology*. **99**(3), pp.656–663.
- Solbakken, K., Birkelund, Y. and Samuelsen, E.M. 2021. Evaluation of surface wind using WRF in complex terrain: Atmospheric input data and grid spacing. *Environmental Modelling and Software*. [Online]. **145**(September), p.105182. Available from: <https://doi.org/10.1016/j.envsoft.2021.105182>.
- Solberg, R., Malnes, E., Amlien, J., Danks, F., Haarpaintner, J., Høgda, K.A., Johansen, B.E., Karlsen, S.R. and Koren, H. 2008. *State of the art for tropical forest monitoring by remote sensing* [Online]. Available from: http://publications.nr.no/4870/Solberg_-_State_of_the_art_for_tropical_forest_monitoring_by.pdf.
- Treharne, R. 2018. *Arctic browning: impacts of extreme events on vegetation and carbon balance in high latitude ecosystems*. [Online] The University of Sheffield. Available from: <http://etheses.whiterose.ac.uk/22784/>.
- Treharne, R., Bjerke, J.W., Tømmervik, H. and Phoenix, G.K. 2020. Development of new metrics to assess and quantify climatic drivers of extreme event driven Arctic browning. *Remote Sensing of Environment*. **243**(March).
- Treharne, R., Bjerke, J.W., Tømmervik, H., Stendardi, L. and Phoenix, G.K. 2019. Arctic browning: Impacts of extreme climatic events on heathland ecosystem CO₂ fluxes. *Global Change Biology*. **25**(2), pp.489–503.
- Tucker, C.J. 1979. Red and photographic infrared linear combinations for monitoring vegetation. *Remote Sensing of Environment*. **8**(2), pp.127–150.
- Tucker, C.J., Slayback, D.A., Pinzon, J.E., Sietse, L.O., Myneni, R.B. and Taylor, M.G. 2001. Higher northern latitude normalized difference vegetation index and growing season trends from 1982 to 1999. *International Journal of Biometeorology*. **45**, pp.184–190.
- Vicente-Serrano, S.M., Gouveia, C., Camarero, J.J., Beguería, S., Trigo, R., López-Moreno, J.I., Azorín-Molina, C., Pasho, E., Lorenzo-Lacruz, J., Revuelto, J., Morán-Tejeda, E. and Sanchez-Lorenzo, A. 2013. Response of vegetation to drought time-scales across global land biomes. *Proceedings of the National Academy of Sciences of the United States of America*. **110**(1), pp.52–57.

- Vickers, H., Høgdal, K.A., Solbø, S., Karlsen, S.R., Tømmervik, H., Aanes, R. and Hansen, B.B. 2016. Changes in greening in the high Arctic: Insights from a 30 year AVHRR max NDVI dataset for Svalbard. *Environmental Research Letters*. [Online]. **11**(10), pp.1–9. Available from: <http://dx.doi.org/10.1088/1748-9326/11/10/105004>.
- Vikhmar-Schuler, D., Isaksen, K., Haugen, J.E., Tømmervik, H., Luks, B., Schuler, T.V. and Bjerke, J.W. 2016. Changes in Winter Warming Events in the Nordic Arctic Region. *Journal of Climate*. [Online]. **29**(17), pp.6223–6244. [Accessed 23 September 2018]. Available from: <http://journals.ametsoc.org/doi/10.1175/JCLI-D-15-0763.1>.
- Walsh, J.E., Overland, J.E., Groisman, P.Y. and Rudolf, B. 2011. Ongoing climate change in the arctic. *Ambio*. **40**(SUPPL. 1), pp.6–16.
- Wang, R., Gamon, J.A., Emmerton, C.A., Springer, K.R., Yu, R. and Hmimina, G. 2020. Detecting intra- and inter-annual variability in gross primary productivity of a North American grassland using MODIS MAIAC data. *Agricultural and Forest Meteorology*. **281**(November 2019).
- Wang, S., Lu, X., Cheng, X., Li, X., Peichl, M. and Mammarella, I. 2018. Limitations and challenges of MODIS-derived phenological metrics across different landscapes in pan-Arctic regions. *Remote Sensing*. **10**(11), pp.1–21.
- Wipf, S., Gottfried, M. and Nagy, L. 2013. Climate change and extreme events - their impacts on alpine and arctic ecosystem structure and function. *Plant Ecology and Diversity*. **6**(3–4), pp.303–306.
- Wong, C.Y.S., D’Odorico, P., Bhatena, Y., Arain, M.A. and Ensminger, I. 2019. Carotenoid based vegetation indices for accurate monitoring of the phenology of photosynthesis at the leaf-scale in deciduous and evergreen trees. *Remote Sensing of Environment*. [Online]. **233**(August), p.111407. Available from: <https://doi.org/10.1016/j.rse.2019.111407>.
- Wong, C.Y.S. and Gamon, J.A. 2015. Three causes of variation in the photochemical reflectance index (PRI) in evergreen conifers. *New Phytologist*. **206**(1), pp.187–195.
- Yu, E.T. 2013. High-resolution seasonal snowfall simulation over Northeast China. *Chinese Science Bulletin*. **58**(12), pp.1412–1419.
- Zhang, X., A., M., Tan, B., D., M. and Yu, Y. 2012. Long-Term Detection of Global Vegetation Phenology from Satellite Instruments. *Phenology and Climate Change*. (May 2014).
- Zhang, X., Jayavelu, S., Liu, L., Friedl, M.A., Henebry, G.M., Liu, Y., Schaaf, C.B., Richardson, A.D. and Gray, J. 2018. Evaluation of land surface phenology from VIIRS data using time series of PhenoCam imagery. *Agricultural and Forest Meteorology*. **256–257**(November 2017), pp.137–149.
- Zhao, Z., Gao, J., Wang, Y., Liu, J. and Li, S. 2015. Exploring spatially variable relationships between NDVI and climatic factors in a transition zone using geographically weighted regression. *Theoretical and Applied Climatology*. **120**(3–4), pp.507–519.